Supramolecular Chemistry of Thiazole Based Urea/Thiourea and Imine/Amine Derivatives: Polymorphism, Molecular/ion recognition

A Dissertation submitted to the
Indian Institute of Technology Guwahati as
partial fulfillment for the Degree of
Doctor of Philosophy in Chemistry

Submitted by
Nithi Phukan

Department of Chemistry
Indian Institute of Technology Guwahati
August 2016

Dedicated to My Father

Statement

I hereby declare that this thesis entitled "**Supramolecular Chemistry of Thiazole Based Urea/Thiourea and Imine/Amine Derivatives: Polymorphism, Molecular/ion recognition**" is the outcome ofresearch work carried out by me under the supervision of Prof. Jubaraj B. Baruah, at the Department of Chemistry, Indian Institute of Technology Guwahati, India.

In keeping with the general practice of reporting scientific observations, due acknowledgement has been made whenever work described here has been based on the findings of other investigators.

IIT Guwahati Nithi Phukan

September, 2016

Certificate

This is to certify that Nithi Phukan has been working under my supervision since August, 2011 as a regular registered Ph. D. student. I am forwarding his thesis entitled "**Supramolecular Chemistry of Thiazole Based Urea/Thiourea and Imine/Amine Derivatives: Polymorphism, Molecular/ion recognition**" being submitted for the Ph. D. (Science) Degree of thisInstitute.

I certify that she has fulfilled all the requirements according to the rules of this institute regarding the investigations embodied in her thesis and this work has not been submitted elsewhere for a degree.

IIT Guwahati
September, 2016

Prof. Jubaraj B. Baruah

Acknowledgements

This thesis might not have seen through its completion unless I had the support and encouragement of numerous people around me. Today, when I bring it to an end, I would like to express few words of appreciation to the people who actually made this thesis a reality and an unforgettable experience for me.

First and foremost, with a deepest sense of gratitude, I wish to express my sincere thanks to my supervisors, Prof. Jubaraj B. Baruah whose timely help during my crucial phase of my career has made possible to achieve this target. The enlightening experience of doing science under his guidance can hardly be described in words. The numerous discussions and interactions I had with him expanded my horizons to hitherto unknown frontiers of science and knowledge. I am in debt to this wonderful person for all that hehas given me and above all for motivating me towards scientific research. Myeverlasting gratitude goes towards him.

I would like to acknowledge my sincere gratitude to all my doctoral committee members for their insightful advices and valuable suggestions. I am also grateful to the entire faculty and staff in the Department of Chemistry, Indian Institute of Technology Guwahati for providing wonderful work atmosphere throughout this period.

I would like to thank my lab mates Dr. Rupam Sarma, Dr. Devendra Singh, Dr. Dipjyoti Kalita, Dr. Babulal Das, Dr. Bhaskar Nath, Dr. Bigyan R. Jali, Dr. Jayanta Nath, Dr. Prithiviraj Khakhlary, Krapa, Arup and Munindra whom I had an opportunity to work with. No words can express my thankfulness for giving me their time and companionship, which made the time spent in the laboratory and outside pleasant and memorable. I would like to give my special thanks to my friends Nabajit, Barnali, Tulsi, Pojul da, Suchendra, Kameli and all my batch mates for their timely help, support and for the wonderful time we shared during this period.

The financial support from University grant commission (CSIR), New Delhi for the research fellowship is duly acknowledged.

I would also like to acknowledge all my teachers for their love and blessings and motivation.

Finally, my Ph. D. endeavor could not be completed without the endless love, unending support, tolerance and blessings from my parents, my brother and my sister.

They are the main soul and inspiration for each and every step that I achieve in my life.

Nithi Phukan

Preview

This thesis deals with studies on synthesis, characterization of various polymorphs and ion/s recognition properties of thiazole derivatives. The content of the thesis is divided into six chapters.

Chapter 1: Introduction

The content of this chapter is on a general introduction of thiazole derivatives to bring out the necessity for study of supramolecular aspects of them. To bring a general outlook on pharmaceutical applications, molecular and ion recognition properties associated with thiazole derivatives are discussed. Scope of the work with thiazole derivatives is presented as the last part of this particular chapter.

Chapter 2:

Polymorphs and anion-assisted assemblies of thiourea tethered thiazole

This chapter deals with the polymorphic behavior as well as various anion assisted assemblies formed by thiourea group containing two positional isomeric thiazole derivatives **2.1** and **2.2**.

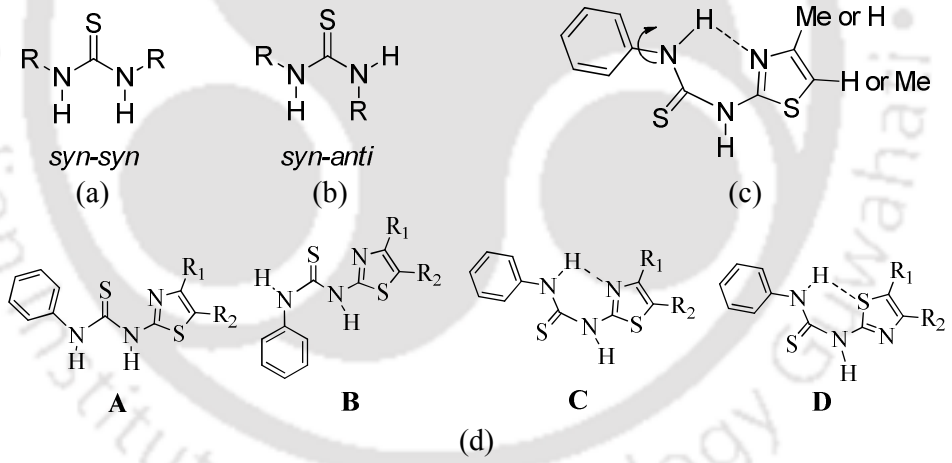

*Figure 2.1: Two different geometries of a symmetric thiourea (a) syn-syn and (b) syn-anti; (c) Showing the rotation of the phenyl group in **2.1** and **2.2;** (d) Some conformers of **2.1** and **2.2**.*

Based on the orientation of phenyl-group over intramolecular hydrogen-bonded six-membered synthon (Figure 2.1c), we isolated three polymorphs of **2.1** named as polymorph **I**, polymorph **II** and polymorph **III.** These three polymorphs belong to $P2_1/c$, $P\bar{1}$ and $C2/c$ respectively. Self-assembly of each polymorph is comprised of hydrogen-bonded dimeric synthons held together in head to tail arrangement but are

packed in different manners. The positional isomer **2.2** is monomorphic as there is an intermolecular C-H**…**S hydrogen bond between a C-H bond of phenyl-ring with sulphur atom of neighboring thiocarbonyl moiety, which locks the orientation of phenyl group in solid state.

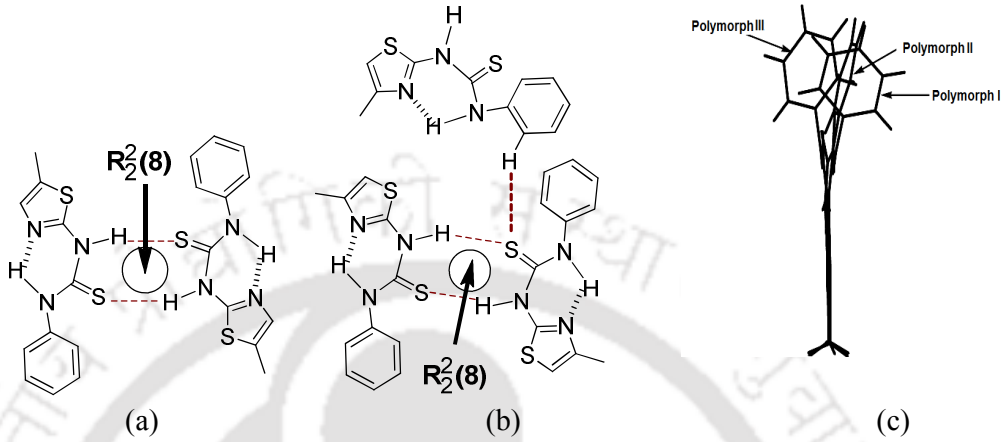

*Figure 2.2: (a) Dimeric assembly within the three polymorphs of **2.1**, (b) assembly of **2.2** showing intermolecular C-H**…**S hydrogen bonds. (c) Overlay diagram showing orientations of the phenyl group of three polymorphs of **2.1** (drawn by fixing the 5-methylthiazole planes in one direction).*

A series of inorganic salts are prepared by treating **2.1** and **2.2** with different mineral acids as shown in Scheme 2.2. It is found that the structure of these salts are influenced by type of host and mainly dependent on the shape and charge on the anions.

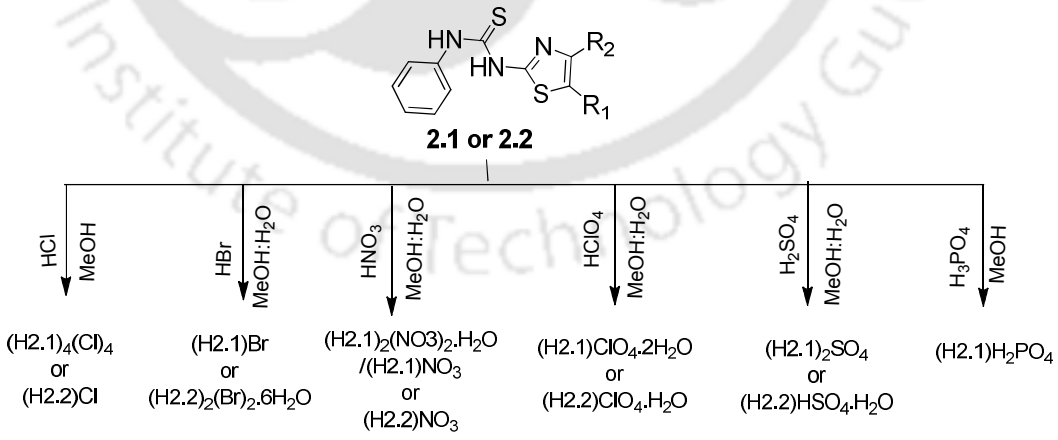

Scheme 2.2: Schematic diagram showing the synthesis of different salts.

Here, each salt is composed of cationic host/s that protonated at the nitrogen atom of methylthiazole unit and corresponding hydrated or anhydrous anion/s. The *syn-anti* conformation across the thiourea group originally present in the positional isomers **2.1** and **2.2** are invariably transformed to *syn-syn* conformation in their salts.

The anhydrous chloride salt of **2.1** has large difference in packing patterns with corresponding anhydrous chloride salt of **2.2**; they also differ in the numbers of symmetry non-equivalent molecules in their respective unit cells. The bromide salt **2.1b** is a one-dimensional polymeric chain, while **2.2b** provided platform for stabilization of a bromide-water cluster having composition $\{H(\mathbf{2.2})\}_2(Br)_2.6H_2O$ as shown in Figure. 2.3a.

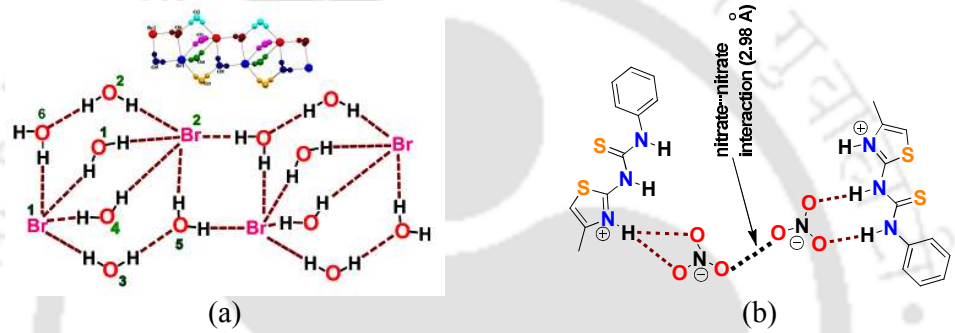

(a) (b)

*Figure 2.3: (a) Two units of bromide-water cluster present in **2.2b**, (b) hydrogen-bonds in the anhydrous nitrate salts **2.2c***

We have isolated hydrated and anhydrous form of nitrate salts of **2.1**, namely, $\{H(\mathbf{2.1})_2\}(NO_3)_2{\cdot}H_2O$ (**2.1c**) and $\{H(\mathbf{2.1})\}NO_3$ (**2.1.1c**). Anhydrous form $\{H(\mathbf{2.2})\}NO_3$ (**2.2c**) is isolated in case of **2.2**. The anhydrous nitrate salts **2.1.1c** and **2.2c** have structural similarities by having nitrate**…**nitrate interactions (Figure 2.3b), which is lost in hydrated form **2.1c** by an intervening water molecule of hydration. The ability to abstract proton from sulphuric acid to form crystalline salts by the **2.1** and **2.2** differs. The sulphate salt $\{H(\mathbf{2.1})\}_2(SO_4)$ (**2.1e**) is formed by reaction of sulphuric acid with **2.1**, but **2.2** forms bisulphate salt $\{H(\mathbf{2.2})\}HSO_4{\cdot}H_2O$ (**2.2e**).The lattice water molecules bridges the bisulphate ions and form a $R_4^4(12)$ hydrogen-bonded synthons in **2.2e** as shown in Figure 2.4a. Compound **2.1** forms corresponding dihydrogenphosphate salt, namely $\{H(\mathbf{2.1})\}H_2PO_4$ (**2.1f**), on reaction with orthophosphoric acid. The dihydrogenphosphate anions are held together in the form of cyclic hexameric hydrogen-bonded assemblies in the lattice of salt **2.1f** as shown in

Figure 2.4b. To the best of our knowledge, it is a new type of hexameric assembly of dihydrogenphosphate. Whereas, we could not obtain crystalline salt from the reaction of orthophosphoric acid with compound **2.2**.

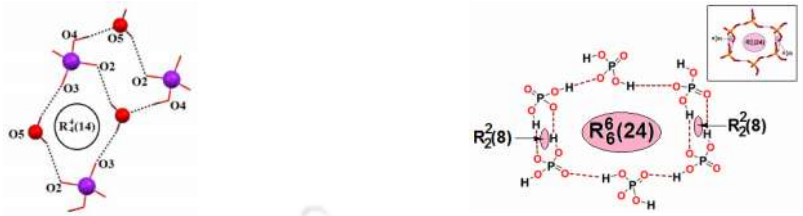

(a) (b)

Figure 2.4: (a) $R_4^4(12)$ hydrogen-bond motif inbisulphate-(water)$_2$-bisulphate assembly formed within ***2.2e*** *(b) Cyclic-hexameric assembly of the dihydrogenphosphate ion of* ***2.1f****.*

The detail synthetic procedure, spectroscopic characterization and thermal analysis of polymorphs and salts are available in the experimental section which is included at the end of the chapter.

Cryst. Growth Des. 2014, **14**, 2640

Chapter 3:

Conformational adjustments over hydrogen bonded synthons of thiourea/urea tethered thiazole.

In this chapter, conformational adjustments of rotatable group acting like a top over hydrogen bonded synthon are studied in multi-component crystals.

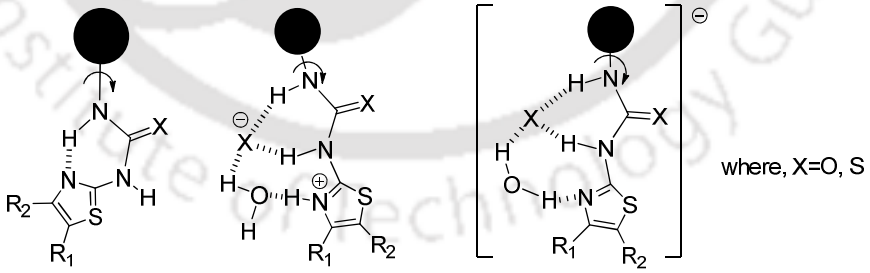

(a) (b) (c)

Figure 3.1: Models to show rotation of a top over (a) thiazole derived six-membered intramolecular hydrogen bonded hetero synthon, (b) Protonated thiazole locked by anion and water, (c) Neutral thiazole derived thiourea/urea derivative holding an anion and water.

We have chosen a set of molecules shown in chart 3.1 to understand generality of conformational adjustment across hydrogen bonded cyclic synthons. Polymorphs of compound **3**.**1** are designated as **3**.**1a** and **3.1b** while **3.2a** and **3.2b** for compound **3.2**. Due to the presence of intramolecular hydrogen bonds all the polymorphic forms adopt *syn-anti* orientation across the thiourea unit. In each case, homodimeric hydrogen bonded sub-assemblies are observed.

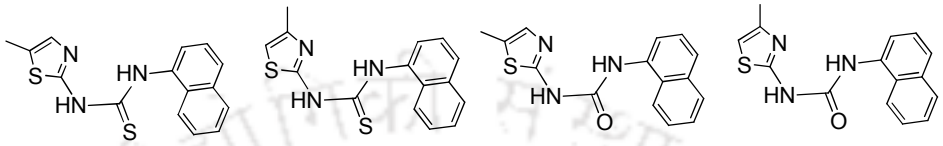

3.1 **3.2** **3.3** **3.4**

Chart 3.1: Different n-methylthiazole (n=5,4) containing positional isomers of thiourea and urea derivatives.

Crystallization of **3.3** and **3.4** from various solvents did not yield polymorphs of any of these compounds. Structures elucidation of **3.3** and **3.4** has showed similar conformations across the urea moiety as that found in the corresponding thiourea derivatives. The packing patterns of the compounds **3.3** and **3.4** showed that one -NH of urea is involved in intramolecular N-H**…**N with N-atom of the methylthiazole unit.

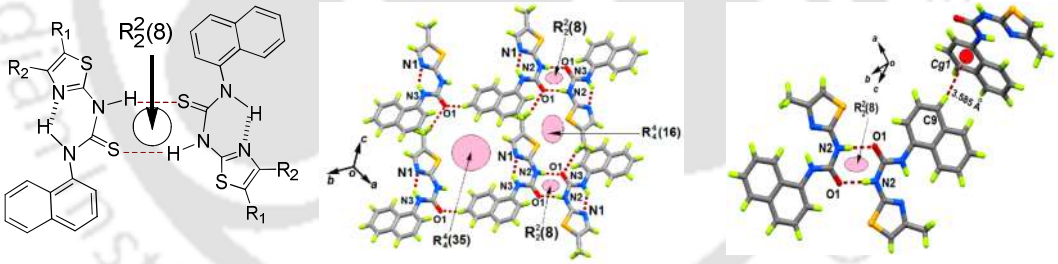

(a) (b) (c)

*Figure 3.2: (a) Homodimeric assemblies of polymorphs of **3.1** and **3.2.** Hydrogen-bonded assemblies within the crystal lattice of (b) **3.3** and(c) **3.4.***

Compound **3.1**underwent cyclization reaction in presence of different acid such as HCl, HBr, HNO_3, $HClO_4$, and H_3PO_4. In each case the compound **3.5** (Equation 3.1) was formed.

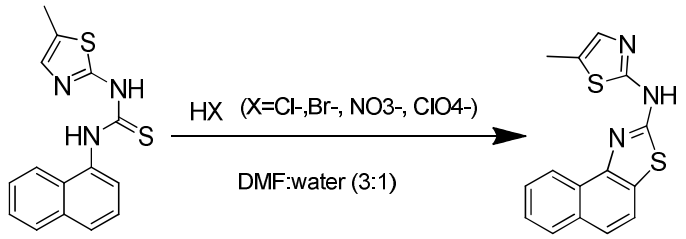

3.1 **3.5**

*Equation 3.1: Acid catalysed cyclization of compound **3.1***

Two crystalline salts of urea derivatives **3.1** were prepared by reacting **3.1** with hydrochloric or perchloric acid as shown in Equation 3.2. Chloride salt **3.3a** and perchlorate salt **3.3b** were obtained as hydrate.

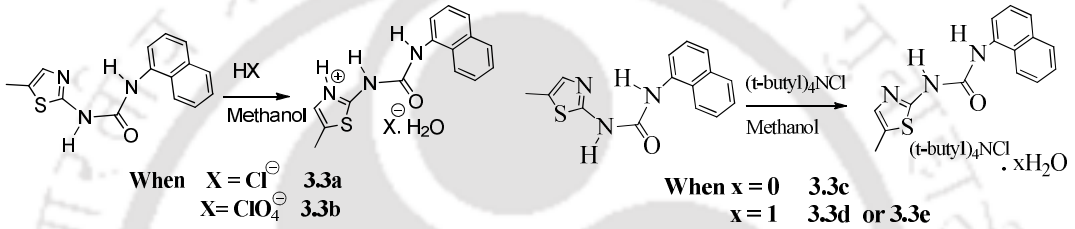

(a) (b)

*Equation 3.2: (a) Crystalline salts of urea derivative **3.3;** (b) Cocrystllization of **3.3** with tetrabutylammonium chloride.*

Two salts **3.3a** and **3.3b** have different bifurcated synthons, hence not suitable to make direct comparison on conformational adjustments across two independent synthon formed by aid of anions. Neutral multi-component crystals of urea derivative **3.3** with tetrabutylammonium chloride were isolated as shown in equation 3.2b. In multi-component crystals the conformational adjustment over hetero synthons took place due to local environment change and through interplay of weak supramolecular interactions.

Thus, a general approach on polymorphism by rotation over intramolecular hydrogen bonded synthon of thiourea derivatives has been established.

CrystEngComm., 2016, DOI: 10.1039/C6CE01326K

Chapter 4:

Imine-tautomers of aminothiazole derivatives: intriguing aspects of chemical reactivities

Several solvent and ion guided crystallization and signal transduction processes of 1-(5-methylthiazol-2-yl)-3-(4-nitrophenyl) thiourea (**4.1**) and 1-(4-methylthiazol-2-yl)-3-(4-nitrophenyl) thiourea (**4.2**) are presented in this chapter. Structural elucidation shows that **4.1** and **4.2** adopt imine form in solid state (Figure 4.1c) reflected in the bond parameters of C4-N1 and C4=N2.

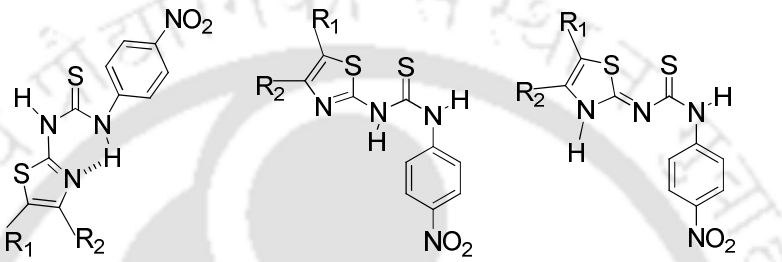

*Figure 4.1: (a-b) Conformers of amine form and (c) imine form of **4.1** or **4.2**.*

Solvent play a crucial role in catalytic reactions of thiourea derivatives. With such an anticipation we attempted preparation of solvates of compound **4.1** and **4.2** with dimethylformamide or dimethylacetamide having C=O as acceptor for hydrogen bond and dimethylsulfoxide which has S=O as the acceptor to form hydrogen bond. But, we find that the isomers **4.1**and **4.2** showed distinguishable reactivities in solution as illustrated in Scheme 4.1. Solvate **4.1b** has $R_2^2(8)$ and $R_2^2(24)$ type dimeric sub-assembly of host molecules formed through N-H**…**S and N-H**…**O hydrogen bonds as shown in Figure 4.2a. The metastable form **4.1.1b** has only one type of cyclic hydrogen bonded synthons that is $R_2^2(8)$, guided by N-H**…**S hydrogen bonds. In this case the dimethylformamide molecules are present as discrete unit (Figure 4.2b) but in a disordered manner by sharing of the carbon atoms as well as the nitrogen atoms at two equivalent positions.

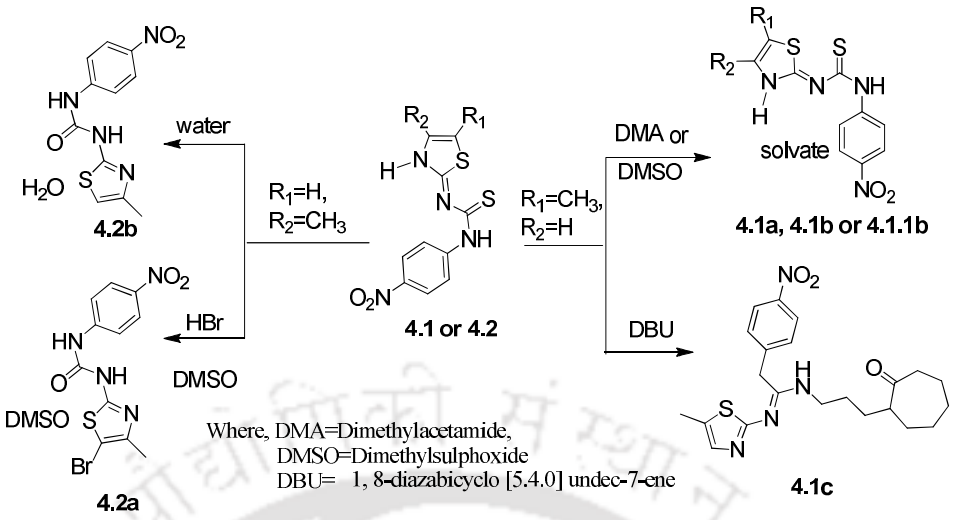

*Scheme 4.1: Reactivity of the **4.1** and **4.2** towards different solvents.*

Upon heating the mixture of the two forms (**4.1b** and **4.1.1b**) under mild condition at 50 ºC for about 10 minutes the metastable form **4.1.1b** transforms to stable form **4.1b**, which was confirmed by comparing the mixture samples before heating and after heating as illustrated in Figure 4.2c.

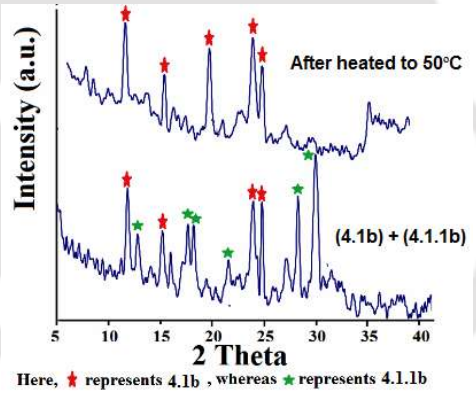

*Figure 4.2: Powder X-ray diffraction patterns of a mixture of **2a** and **2.1a** (i) as obtained, (ii) after heating mixed crystal of **2a** and **2.1a** at 50 ºC for 10 mins.*

The compound **4.1** reacted with 1,8-diazabicyclo [5.4.0] undec-7-ene (DBU) to give ring opened product (**4.1c**) illustrated in Scheme 4.2.This observation is significant from the point that it cautions on the limitation of using DBU as a solvent while performing a reaction with a thiourea derivative.

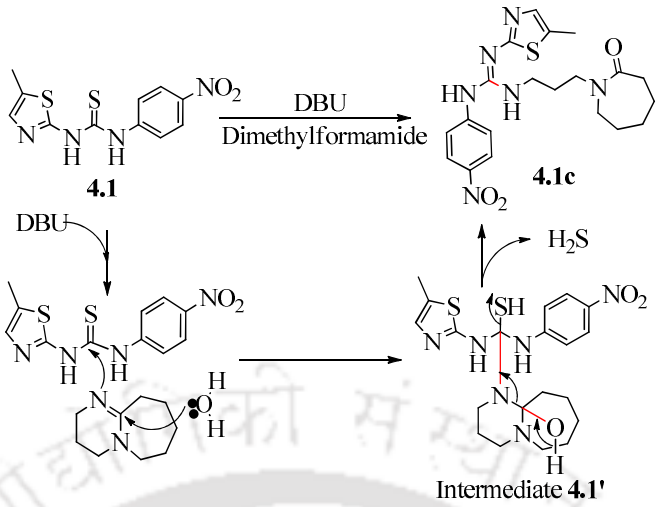

*Scheme 4.2: A plausible mechanism on formation of **4.1c**.*

Small heterocyclic organic molecules are useful for selective detection of ions. Selective interactions of compound **4.1**and **4.2** were checked with chloride salts of various metal ions. Only interactions of Hg^{2+} ions with **4.1**and **4.2** resulted in characteristic colorimetric change.

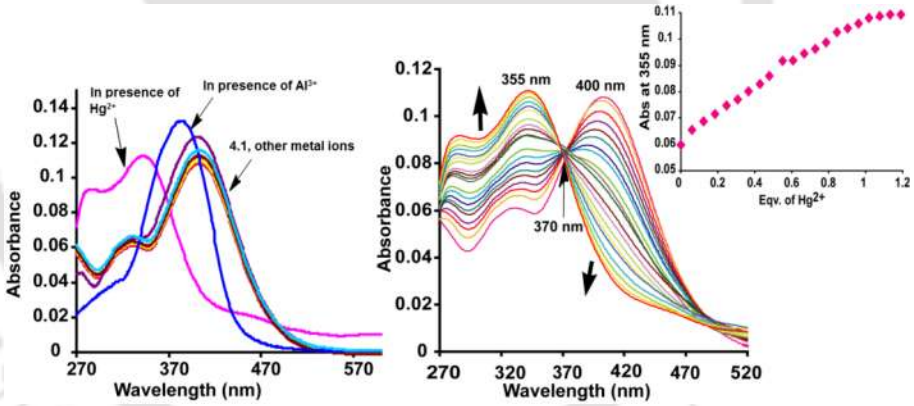

(a) (b)

*Figure 4.3: UV-Visible spectra of (a) **4.1** (5 μM) in the presence of 10 equivalents of various metal ions in dimethylformamide solution. (b) **4.1** (5 μM, 4.0 mL) with incremental addition of the Hg^{2+}in dimethylformamide solution. inset: change in absorbance at 355 nm with the equivalents of Hg^{2+}added into the solution.*

The selective colorimetric change induced by Hg^{2+} ions is attributed to easy hydrolysis of thiourea to urea. Incremental addition of Hg^{2+} to **4.1** rendered a

systematic growth of the absorbance maxima at 355 nm with a simultaneous decrease of the peak at 400 nm.

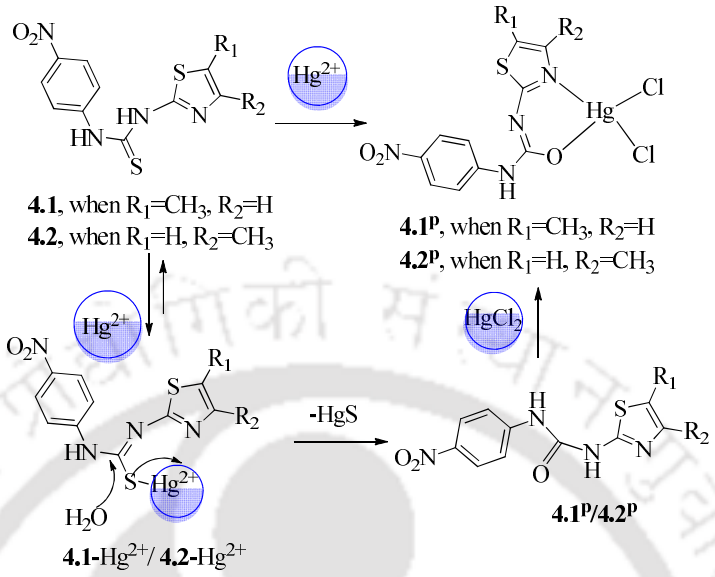

*Figure 4.4: Schematic representation of mechanism of hydrolysis of **4.1** and **4.2** leading complexation with Hg^{2+}.*

The binding selectivity of **4.1** and **4.2** was checked with various anions such as, F^-, Br^-, Cl^-, I^-, SO_4^{2-}, HSO_4^-, PF_6^-, NO_3^-, HPO_4^-, $H_2PO_4^-$, OAc^-, ClO_4^-etc by taking the respective tetrabutylammonium salts. Only tetrabutylammonium fluoride was able to induce a significant colorimetric response in dimethylformamide as well as in dimethylsulphoxide. These changes caused visual color change from yellow to orange red (Figure 4.5a inset).

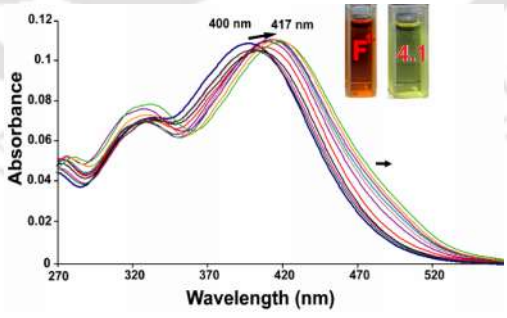

*Figure 4.5: (a) Absorption spectra of **4.1** (5 µM) in DMF.*

We found that between the two positional isomers, **4.2** reacted with hydrobromic acid and it yielded a very selective bromo derivative **4.2a** as illustrated in Scheme 4.3.

Though this reaction was slow and yet this was an interesting reaction as it was specific to compound **4.2**. The compound **4.2** underwent hydrolysis and reacted with hydrobromic acid to form the brominated product **4.2a**.

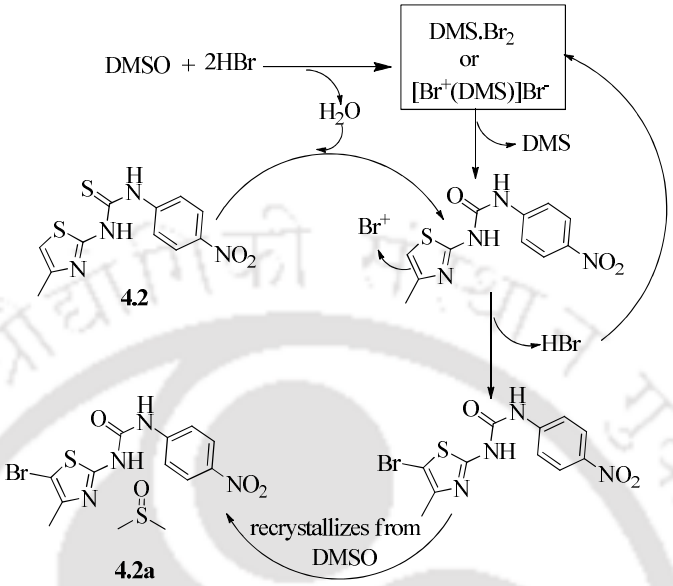

*Scheme 4.3: Proposed mechanistic path on the formation of **4.2a**.*

We addressed here the need for a robust and holistic approach to investigate the intrinsic reactivities of two positional isomers.

CrystEngComm, 2016, **18**, 3877.

Chapter 5: Part A:

Polymorphs of thiazole-derived imines tethered hydroxyaromatics.

This chapter deals with the role of intramolecular and self-assembling properties of thioazole derivatives connected to aromatic hydroxy compounds. For this purpose, we synthesized two thiazole tethered imine derivatives namely(E)-2-(((5-methylthiazol-2-yl)imino)methyl)phenol (**5.1**) and (E)-1-(((5-methylthiazol-2-yl)imino)methyl)naphthalen-2-ol (**5.2**).Thioimidazole has N- and S-atoms in a five-membered planar ring separated by an intervening carbon; thus, the orientation of such a planar unit across an unsymmetrical planar unit, like **5.1** and **5.2** in Figure 5.1b, would lead to polymorphs. Presence of a methyl group at 5-positions of thiazole in these compounds would contribute a steric factor to stabilize or destabilize a particular conformer(s) generated through C-N rotation.

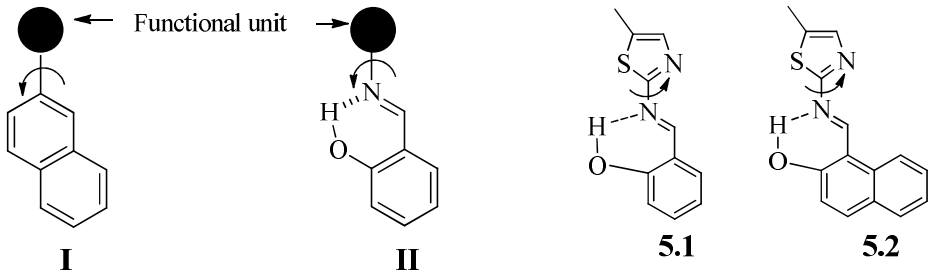

(a) (b)

*Figure 5.1: (a) Possible rotation of functional unit attached to (I) naphthyl ring, (II) intramolecular hydrogen bonded six-member ring above a phenyl ring. (b) thiazole-tethered imines **5.1** and **5.2**, with arrows showing possible rotations.*

A series of crystallization from different solvents were carried out leading to different types of crystals Morphologies of each polymorph was different. The polymorphs are designated as polymorphs **5.1a** and **5.1b** for compound **5.1** whereas **5.2a** and **5.2b** for compound **5.2**.

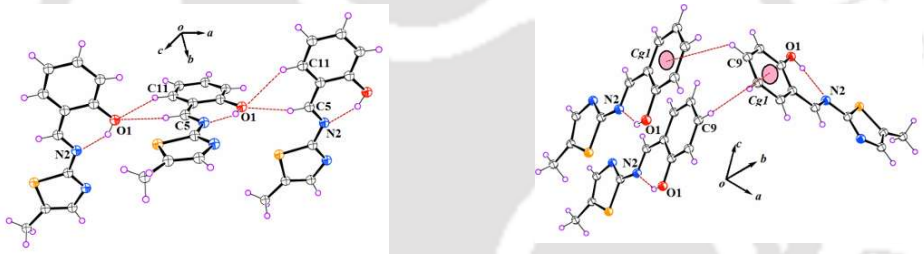

(a) (b)

*Figure 5.2: (a) Hydrogen bonds in polymorph **5.1a**. (b) C-H…π interactions in **5.1b** (d) C9-H…π = 3.531 Å, where π is the centroid of the phenyl ring).*

Polymorph **5.2a** exists as dimeric assemblies in its crystal lattice through very weak C-H···O hydrogen bonds, as shown in Figure 5.3(b). The structure also shows the presence of an intramolecular O-H···N hydrogen bond. Polymorph **5.2b** contains two symmetry-nonequivalent molecules in its asymmetric unit ($Z' = 2$). The two symmetry independent molecules are connected to each other through C-H**…**N hydrogen bonds via a C-H of the naphthyl ring interacting with the N-atom of the thiazole unit of a neighboring molecule of **5.2b**, as shown in Figure 5.3(c).

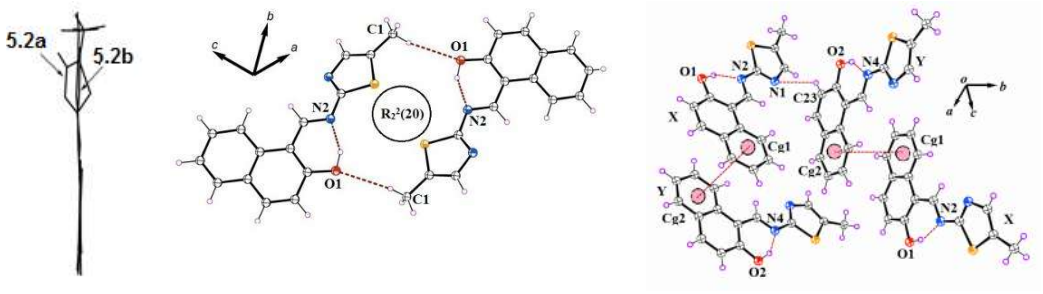

(a) (b) (c)

*Figure 5.3: (a) Overlaid diagram of molecules from polymorphs **5.2a** and **5.2b** shown by fixing hydroxynaphthyl unit in one plane, (b) hydrogen bonds in polymorph **5.2a**, (c) π-π Stacking interactions in lattice of **5.2b**.*

DSC plots of **5.1a**and **5.1b** showed conventional features of melting, with their respective melting points at 118 and 117 °C. However, DSC of polymorphs **5.2a** and **5.2b** revealed several interesting features. Schematic representations of the thermal events occurring in polymorphs **5.2a** and **5.2b** are shown in Schemes 5.1 and 5.2 respectively.

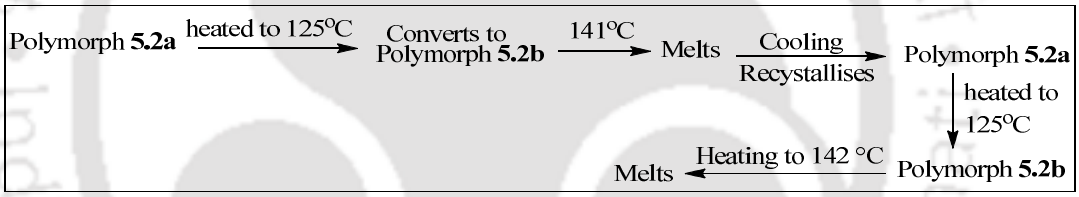

*Scheme **5.1**: Thermal events of Polymorph **5.2a***

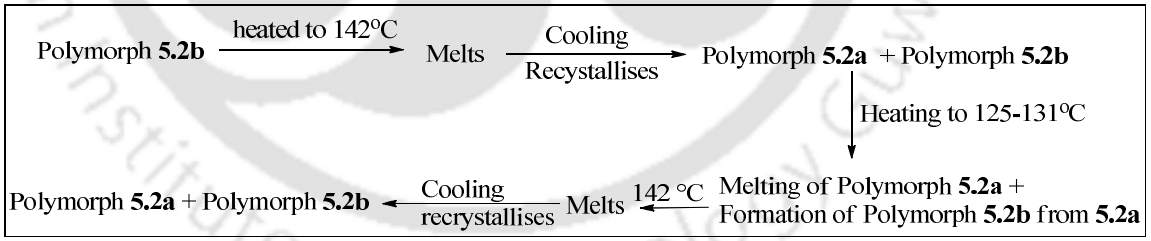

*Scheme **5.2**: Thermal events of polymorph **5.2b***

Thus, conformational polymorphs arising due to different orientations of thiazole ring *via* C-N bond rotation over intramolecular hydrogen bonded six membered ring have been established.

Cryst. Growth Des. 2015, **15**, 1843.

Chapter 5: Part B:

Detection of Al^{3+} and Zn^{2+} ions by 2-(5-methylthiazol-2-yliminomethyl) phenol

In this chapter, we have studied Al^{3+} catalyzed hydrolysis of 2-(5-methylthiazol-2-yliminomethyl) phenol (**5.1**). This reaction can be specifically used for detection of Al^{3+} ions in the presence of various other ions from the characteristic emission at 446 nm (λ_{ex}=365 nm).We have observed that compound **5.1** undergoes fast catalytic hydrolysis by Al^{3+} ions to form 2-hydroxybenzaldehyde and 2-amino-5-methylthiazole which can be monitored by fluorescence spectroscopy. On the other hand, addition of Zn^{2+} ions to a solution of **5.1** leads to a strong emission peak at 490 nm. This peak is attributed to 1:1 complex formation with **5.1**. Such emission peak was not observed with other metal ions. The characteristic emission at 490 nm shown by Zn^{2+} ions with **5.1**, was not interfered by the other metal ions such as Zn^{2+}, Ni^{2+}, Cu^{2+}, Hg^{2+}, In^{3+}, Na^{+}, and Li^{+}. However, Al^{3+} ion is an exception to this, upon addition of catalytic amount of Al^{3+} ions under neutral condition to a solution containing equimolar amount of **5.1** and Zn^{2+} ions, the fluorescence emission at 490 nm decreases and a new emission peak at 446 nm develops. The new emission peak at 446 nm grows due to formation of 2-hydroxybenzaldehyde that interacts with Al^{3+} ions as well as Zn^{2+} ions. The intensity of the new emission peak at 446 nm enhances until the hydrolysis of the **5.1** is complete.

Inorg. Chem. Comm. 2013, **37**, 89.

Chapter 6: Part A:

Anion guided conformational adjustments by protonation leading to conformation reversal

In this chapter, anion guided conformational adjustments of an uncommon conformer of 2-[(5-methylthiazol-2-ylamino)-methyl]-phenol (**6.1**) found in its self-assembly and subsequent protonation leading to reversal of conformer is shown. *Syn* or *anti* forms A and B illustrated in Figure 6.1 of thiazole derivatives. These derivatives are prone towards protonation, hence the protonated forms also can have similar conformers (C and D in Figure 6.1) and one may utilize the hydrogen bonding ability of aminothiazole to stabilize any of such forms by hydrogen bonds.

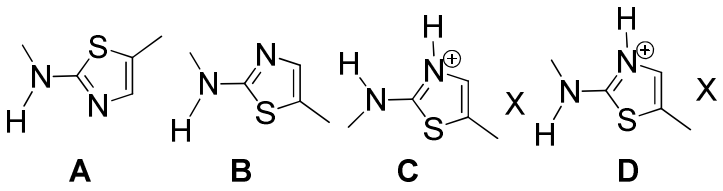

Figure 6.1: Syn and anti-conformers of aminothiazole (A and B) and aminothiazolium salt (C and D).

Structural elucidation of **6.1**showed that, it possesses an overall twisted geometry in which the aminothiazole ring has NH and the sulphur atom of the ring *syn* to each other across the C-N bond (Figure 6.2) to form an *anti*-conformer.

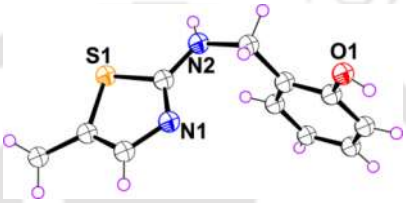

*Figure 6.2: The structure of the compound **6.1** (with 50% thermal ellipsoids)*

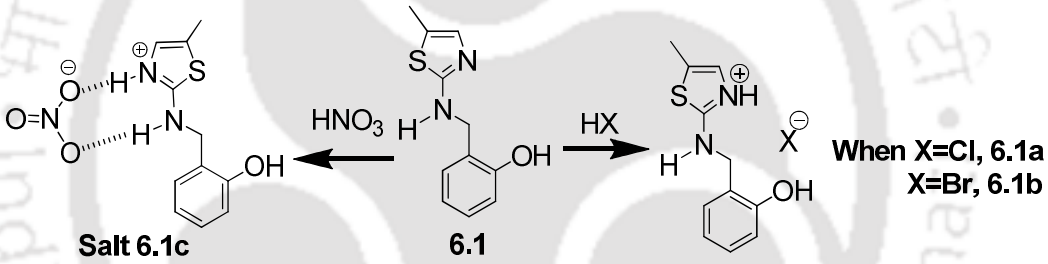

*Scheme 6.1: Synthesis of salts of compound **6.1**.*

Generally self-assembly of a salt is different from the parent compound. Accordingly the chloride (**6.1a**) or bromide (**6.1b**) salt forms self-assembly which has the orientation of the thiazole ring across C-NH bond similar to the parent compound **6.1**. Importantly, the nitrate salt has the opposite conformer of the thiazole across the C-NH bond as that of the one found in the parent compound.

In a nutshell, with an example of thiazole derivative we have shown the importance of conformation adjustments to get reversal of orientations of a functional unit.

ChemistrySelect, 2016, **3**, 440.

Chapter 6: Part B:

Solvent and anion facilitated conformational changes in benzylamine substituted thiazolamine

In this chapter, solvent and anion facilitated conformational adjustments in the solid state structures of *syn-anti-syn* form of N,N'-(1,4-phenylenebis(methylene)-bis(5-methylthiazol-2-amine) (**6.2**) was studied. Crystallization of **6.2** from different solvents resulted in two polymorphic forms abbreviated as **6.2a** and **6.2b**. There are two types of geometrical arrangements of *syn-anti-syn* conformers one resembling ***S***-geometry and another ***l***-geometry leading to the polymorphs. Such orientations arise from the adjustments on rotations through two C-N bonds.

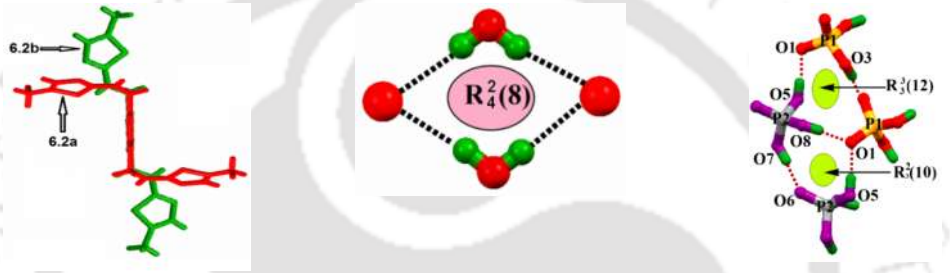

(a) (b) (c)

*Figure 6.1: (a)Overlay diagram showing the **S-** and **l-** types of syn-anti-syn conformation of the 5-methyl aminothiazole unit in the two polymorphs of **6.2** (drawn by fixing the phenylene units in one plane). (b) Bromide-water tetrameric $[(H_2O)_2Br_2]^{2-}$ cluster in **6.2a**. (c) Hydrogen bonded cyclic synthon within the $(H_2PO_4^- \cdot H_3PO_4)_2$ cluster.*

We find that the crystalline salts **6**.**2c**, **6.2d**, and **6.2e** have doubly protonated cationic host. Other than nitrate salt (**6.2d**) in other two salt (**6**.**2c, 6**.**2e**), anions are in the form of assemblies. In the self-assembly of the salt **6.2c**, the spherical Br^- ions were hydrated by forming anionic hydrogen-bonded cluster $[Br_2(H_2O)_2]^{2-}$ (Figure 6.1b). Interestingly, each $H_2PO_4^-$ anion interacts concurrently with another $H_2PO_4^-$ anion and one H_3PO_4 molecule which, in turn, interacts with another H_3PO_4 moiety generating an infinite tetrameric anion-acid $[(H_2PO_4^-.H_3PO_4)_2]_n$ cluster with a tetragonal planar arrangement (Figure 6.1c).

Intriguing aspect of the nitrate salt is the orientation of the amino-thiazolinium cations, which are *anti-anti-anti* as shown in Scheme 6.2. Inter-conversion of *syn-*

anti-syn to *anti-anti-anti* conformation can be done by crystallization from solution with nitric acid and subsequent neutralization.

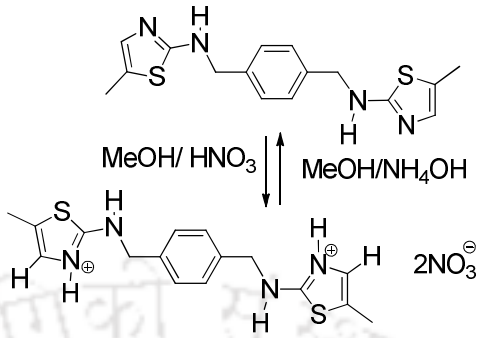

Scheme 6.2: Conformational change from syn-anti-syn to anti-anti-anti of cationic ***6.2***.

In a nutshell, the change from *syn-anti-syn* to *anti-anti-anti* was observed when the nitrate salt was formed whereas *syn-anti-syn* conformer was observed in all other cases.

New J. Chem., 2016, **40**, 6899.

A conclusion section is given at the thesis underlying the major overall findings from the present work; this is done to complement the conclusions that are given at the discussion of each chapter. Relevant literatures and experimental sections of each chapter is compiled after results and discussion in each chapter. The crystallographic parameters are given as an appendix and corresponding crystallographic information files are provided as soft copy attached to the thesis.

Table of Content: Page No.

Chapter 1

Introduction

1.1: Supramolecular chemistry: A general introduction

Supramolecular chemistry has been defined by one of its leading proponents, Jean-Marie Lehn, who won the Nobel Prize for his work in this area in 1987, as the 'chemistry of molecular assemblies and of the intermolecular bond'.[1] While traditional chemistry focuses on the covalent bond and coordinative bond formation, supramolecular chemistry deals with the weaker and reversible non-covalent interactions such as hydrogen bonds, cation-π, anion-π, π-π interactions, Van der Waals forces, hydrophobic effects etc[2] between molecules. Understanding of these non-covalent interactions and exploiting them in a new ways continues to be the essence of the field. Important disciplines that have been demonstrated by supramolecular chemistry include molecular self-assembly, host-guest chemistry etc. Molecular/ion recognition, mechanically-interlocked molecular architectures, dynamic covalent chemistry are some important aspects routinely dealt in supramolecular chemistry. Many biological processes are covered by supramolecular chemistry, which makes the subject indispensable. Supramolecular chemistry also has been used to understand many physical and chemical properties like optical, magnetic and catalysis associated with self assemblies. The assemblies formed by supramolecular system are flexible. Thereby, can be easily reorganized, which provides new avenues to explore new properties associated with such assemblies. In principle, originally supramolecular chemistry was defined in terms of the non-covalent interaction between a 'host' and a 'guest' molecule, where the host is commonly referred to a large molecule or aggregate such as an enzyme or synthetic cyclic and acyclic compounds possessing a sizeable central hole or cavity.[2] whereas a guest may be a cationic or anionic species, an ion pair or a more sophisticated molecule such as hormone, pheromone or neurotransmitter that easily accommodated. Conventionally, host-guest chemistry associated with hydrogen bonds. But, the thermodynamic stability of a supramolecular host-guest complex may be enhanced by additional non-covalent interactions such as chelate effect or macrocyclic effect. The macrocyclic effect plays a crucial role in cyclic hosts such as corands (e.g. crown

ethers) up to a factor of 10^4 times higher than closely related acyclic podands with similar binding sites. Absence of such additional effects in a macrocyclic system makes relatively straightforward understanding of preorganized macrocyclic systems. But the binding processes of acyclic receptors remain more elusive. In order to bind, a host molecule must have binding sites that are of the appropriate electronic character namely polarity, hydrogen bond donor/acceptor ability, hardness or softness etc. to complement the guest. Thus, preorganization of host molecule is a key concept because it represents a major enhancement in the overall free energy of guest complexation.[3]

1.2: Hydrogen Bond (HB) in Supramolecular Chemistry

Hydrogen bond is the most reliable design element for constructing non-covalent assembly of molecules, and as such it is the most important interaction in the areas of supramolecular chemistry.[4-7] Hydrogen bond is defined as a form of association between an electronegative atom and a hydrogen atom attached to a second, relatively electronegative atom.[8,9] It is a particular kind of dipole-dipole interaction in which the hydrogen atom attached to an electronegative atom (or electron withdrawing group) is attracted towards neighboring electronegative atom. Hydrogen bonds are typically designated as D-H**…**A which involve a hydrogen atom attached to an electronegative atom, for example, O or N as the donor (D) and similarly electronegative atom bearing a lone pair of electrons as an acceptor (A). There is also significant hydrogen bond interactions where carbon acts as donor rather than nitrogen or oxygen (electronegativities: C: 2.55, H: 2.20, N: 3.04, O: 3.44).[10-12] Because of its relatively strong and highly directional nature, hydrogen bonding has been described as the 'masterkey interaction in supramolecular chemistry'[2] Typical examples include, the formation of carboxylic acid dimer and Guanine-Cytosine base pair in DNA (Scheme 1.1).

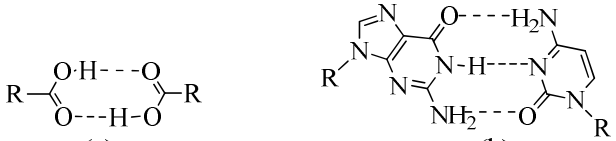

Scheme 1.1: (a) A hydrogen bonded carboxylic acid dimer, (b) base pair in DNA (Guanine-Cytosine) by hydrogen bond.

Hydrogen bond is the major important discriminating cohesive force in directing crystallization and self-assembly of organic molecules.[13] Hydrogen bonds have a wide spread of bond lengths and angles. Accordingly hydrogen bond interactions between hydrogen bond donor D and acceptor A (D-H**…**A), may be classified as strong, moderate and weak.[14] Different parameters used to define the strength of the hydrogen bond can be depicted with the help of Figure 1.1.

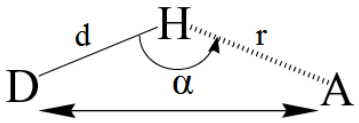

Figure 1.1: Schematic representation of hydrogen bond.

Table 1.1: Donor acceptor distances and angles in hydrogen bonds.

Parameters	Type of hydrogen bonds		
	Strong	Moderate	Weak
Bond energy ($kJmol^{-1}$)	60-120	16-60	Less than 12
H···A (r Å)	1.2-1.5	1.5-2.2	2.2-3.2
D···A (R Å)	2.2-2.5	2.5-3.2	3.2-4.0
<D-H···A (α°)	175-180	130-180	90-150

Orderly assemblies are formed by hydrogen bonds due to its directional properties. Such orderliness has helped in many natural processes and in construction of different assemblies with novel properties. One of the simplified way to analyze a sub-assembly (within a assembly) was put forward by Desiraju, is known as synthon approach.[15] The non-covalent bonds between two molecules in supramolecular assemblies can be thought as supramolecular synthon.[16-21] Identification and understanding of these synthons have provided definite advantage to analyze complicated self-assemblies and helps to construct predesigned assemblies. In general, a hydrogen bonded assembly follows Etter's rule. Etter et al.[22] have studied the preferential hydrogen bond patterns in organic crystals and have presented the following rules.

1. All good proton donors and acceptors are involved in hydrogen bonding.
2. Six-membered-ring intramolecular hydrogen bonds form in preference to intermolecular hydrogen bonds.
3. The best proton donor and acceptor remaining after intramolecular hydrogen bond formation will form intermolecular hydrogen bonds.

It may also be mentioned that, Etter et al. have introduced a language based upon graph-theory for describing and analyzing hydrogen bond synthons in three-dimensional assembly.[23] A generic graph-set descriptor is illustrated in Figure 1.2a. Some of the commonly observed cyclic synthons, with their graph set notations are represented in Figure 1.2b.

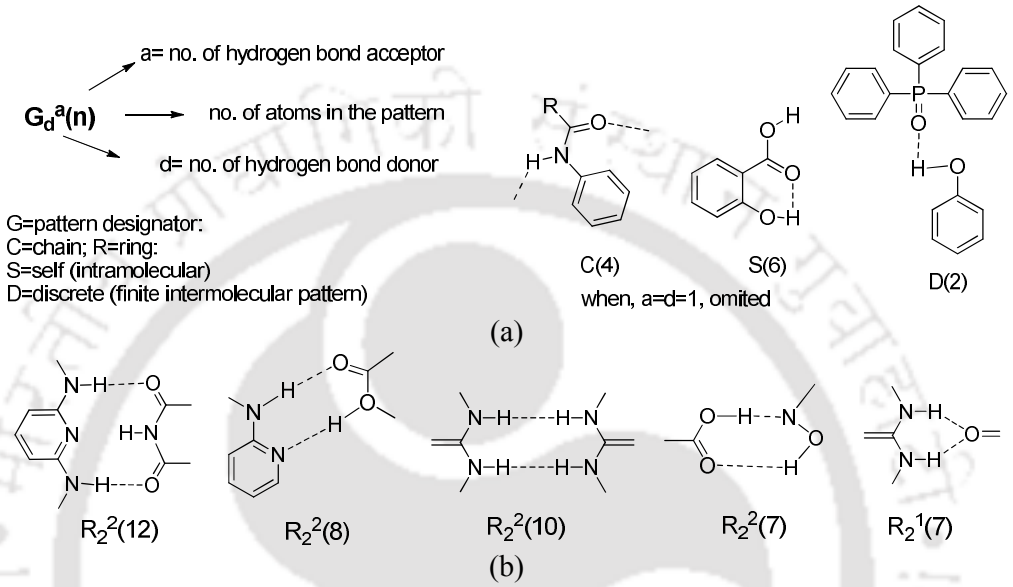

Figure 1.2: (a) Composition of the graph set descriptor with illustrative examples, (b) some cyclic hydrogen bonded synthons.

1.3: Hydrogen bonded assemblies of Heterocyclic molecules

Heterocyclic molecules contain at least two different atoms in one or more rings, and are constituents of many biologically important molecules. Heterocycles are widely employed as useful building blocks to construct supramolecular assemblies that are useful in molecular recognition processes.[24,25] Since, several families of heterocycles exhibits electrochemical activities, photochemical reactivities, characteristics optical properties and other functions, current heterocyclic chemistry offers a robust basis for sophisticated molecular architectures towards molecular recognition and supramolecular assembly. To construct supramolecular assemblies from heterocycles, there are two types of molecular architecture approaches: (a) 'convergent' approach; that mainly target molecular recognition; (b) 'divergent' approach; to construct supramolecular assembly. These two approaches are illustrated schematically in Figure 1.3, by taking the example of oligopyridine derivatives. Namely, Sauvage et al.

have used the convergent approach to metal-templated synthesis of catenane **1.**[26] In this case, two 2,2′-bipyridine subunits cooperatively co-ordinated to one copper (I) center.[26] Divergent approach employed by Fujita et al. using 4,4′-bipyridine derivatives in the synthesis of metallocycle **1.2,** so that each pyridine moiety work independently forming cyclic grid-like structure.[27] Thus, the template effect of metal ion can be used to construct non-covalently linked assemblies or metallocycle by suitably chosen ligands.

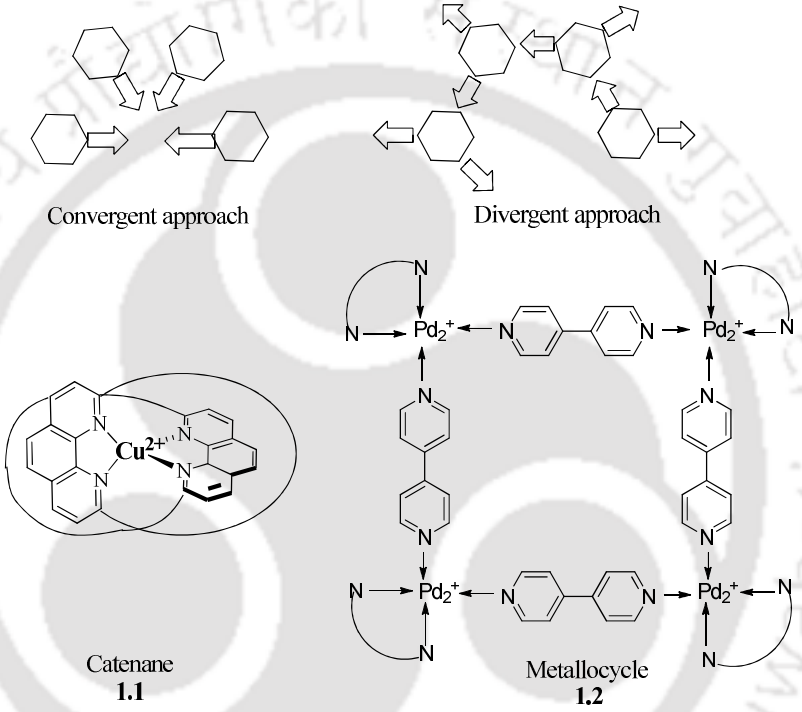

Figure 1.3: Convergent and Divergent approaches to construct supramolecular assemblies based on heterocycles.

In addition to metal co-ordination, hydrogen bond, eletrostatics, π-π interactions play important roles in the construction of supramolecular architecture of heterocyclic compound. Another example of hydrogen-bonded self assembly is Synthetic guanosine derivative **1.3**. It forms hydrogen-bonded quartet structure **1.3a**, which is a self-assembly to recognize metal cations.[28]

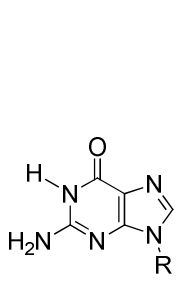

1.3

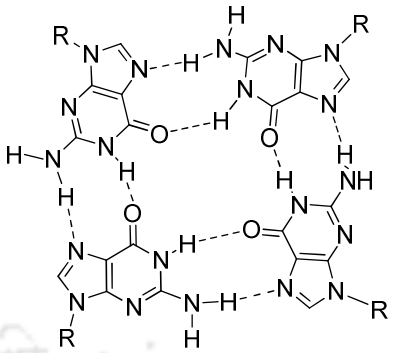

1.3a

Due to the pre-organised structure of 2,7-bis(1H-pyrrol-2-yl)ethynyl-1,8-naphthyridine has complementing hydrogen bonds with octylglucopyranoside (OGU) and it selectively binds to OGU forming the supramolecular host-guest complex **1.4a.** This selective binding has helped it to be an ultra sensitive fluorescent probe for octylglucopyranoside.[29]

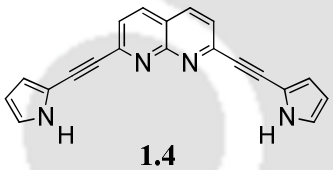

1.4

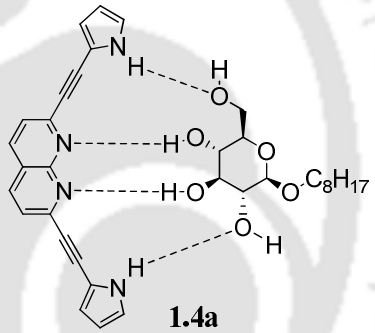

1.4a

The molecule **1.5** has a rigid V-shaped geometry and it contains an active carboxylic acid group that helps it to act as an efficient receptor for adenine. It binds adenine molecule through N-H**…**O and O-H**…**N hydrogen bonds (**1.5a** and **1.5b**).[30]

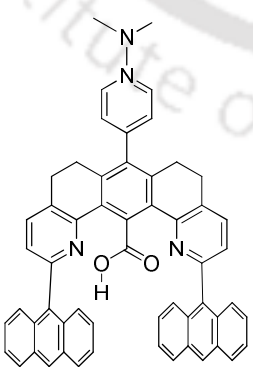

1.5

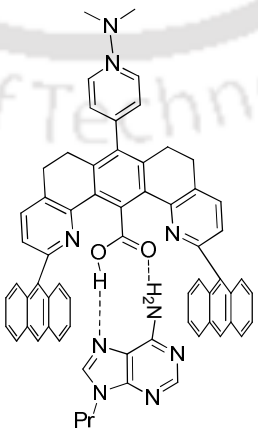

1.5a

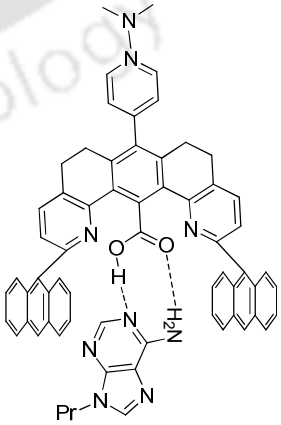

1.5b

Indole-3-acetic acid and indole-2-carboxylic acid forms 1: 2 and 1: 1 cocrystal with 5-nitroquinoline, namely **1.6** and **1.7** respectively. Both the cocrystals involve charge transfer as well as a network of hydrogen-bonding interactions as shown in Figure 1.4. Thin flim of cocrystal **1.7** exhibit a weak second order optical signal.[31]

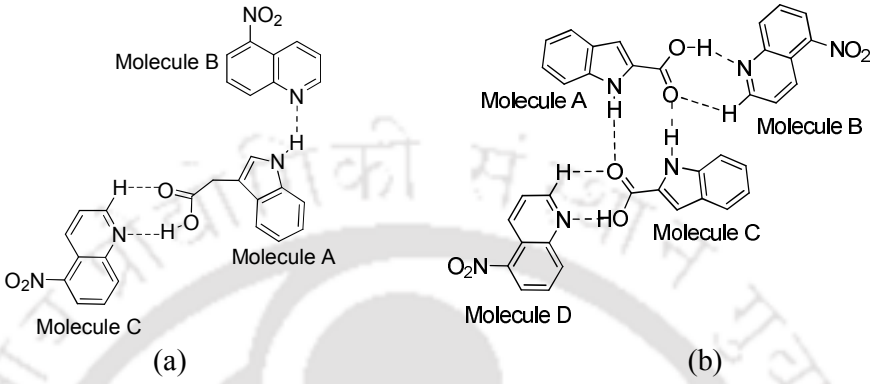

*Figure 1.4: Self-assembly of (a) cocrystal **1.6**, (b) cocrystal **1.7**.*

Thus these discussions have clarified the extensive use of heterocyclic molecules to make varieties of molecular scaffolds which in turn have selectivity to bind or to make new well defined supramolecular architectures.

1.4: General features of Thiazole derivatives

Among heterocyclic molecules, thiazoles are one of the most intensively investigated classes. Thiazoles contain sulfur and nitrogen heteroatom at positions-1 and -3, of the aromatic five-membered ring. Thiazole structure was first described by Hantzsch and Weber in 1887.[32] Thiazole derivatives play a central role in the biochemistry of life, being found as constituent of nutrients like vitamin B_1,[33] also known as thiamine, **1.5**. Thiamine is a water soluble vitamin that helps human body to release energy from carbohydrates during metabolism.

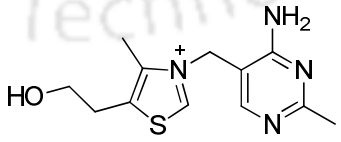

1.5

Thiazoles also found in a diverse range of natural products,[24-38] perhaps the most well known are the epothilones, **1.6-1.11**.[39,40] The epothilones are a class of potential cancer drugs, act as microtubule polymerization promoters and have a similar mechanism of action to drug action of Taxol.[41]

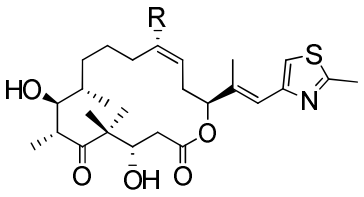

R=H epithilone C **1.8**
R=Me epithilone D **1.9**

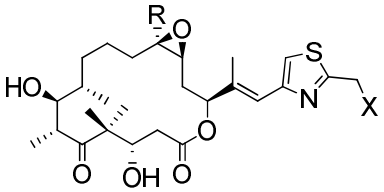

R=H, X=H epithilone A **1.6**
R=Me, X=H epithilone B **1.7**
R=H, X=OH epithilone E **1.10**
R=Me, X=OH epithilone F **1.11**

Thiazoles are increasingly being incorporated into pharmaceutical compounds,[42] thereby can be used as valuable medicine.[43,44] Sulfathiazole (antimicrobial drug) **1.12**, Ritonavir (antiretroviral drug) **1.13**, Abafungin (antifungal drug) **1.14** with trade name Abasol cream and Tiazofurin (antineoplastic drug) **1.15**, are some thiazole derivatives that widely used as medicine.[45]

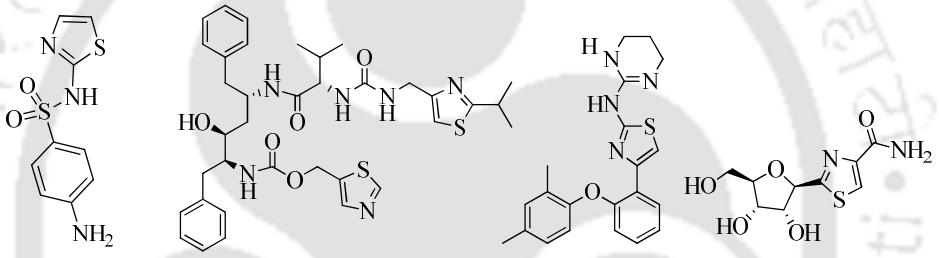

1.12 **1.13** **1.14** **1.15**

Thiazoles have wide use in flavourings and perfume industry.[46] Thiazoles are also present in many agrochemicals.[47] Thiazolic compounds possess interesting electronic and optical properties[48] and as such have received considerable attention from material scientists. Metal complexes of thiazole derivatives are biologically potent.[49-54] Thiazole derivatives are used in inorganic chemistry for building polydentate ligands.[55]

In nature, there is an amazing diversity of organisms including bacteria, fungi, crustaceans, mollusks, fishes and insects that emit light. D-Firefly luciferin **1.16**[56] is a thiazole based compound found within fireflies. Luciferins are oxidised in the presence of the enzyme luciferase producing an excited-state molecule of oxyluciferin. Decay of excited state oxyluciferin to the ground state is the source of the emitted light and differences in luciferin molecules, or changes in the environment of the active site, may result in differences in the color of the emitted light. The generation of the excited state oxyluciferin is thought to proceed by a chemically induced electron exchange luminescence (CIEEL) mechanism.[56] In general, the

reactions catalyzed by enzyme luciferases are special cases of chemiluminescent reactions. The general reaction scheme is as follows:

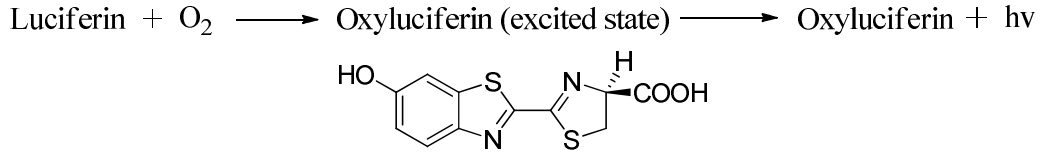

D-Firely luciferin

1.16

1.5: Supramolecular aspects of thiazole derivatives

Thiazole derivatives are no exceptions to contribute towards supramolecular chemistry by showing polymorphism, versatile self assemblies and specific material properties in confined medium. Many thiazole based molecules exhibiting potential drug activity shows polymorphism. Polymorphism was defined by McCrone[57] as the ability of a substance to crystallize in different crystal forms. Polymorphism is very important in those areas of chemical research where full characterization of a material has a pivotal role in determining its ultimate use, for example, in pharmaceutical, pigment, agrochemical, explosive and fine chemical industries. The physical properties of different polymorphs such as solubility, spectroscopic properties, thermal properties and electrical properties differ. Specially, the solubility and drug activities of polymorphic drugs require special attention to make them effective active pharmaceutical ingredient.[58-64] But, the particular advantage of polymorphism is that the chemical identity of the molecule remains unchanged from one polymorph to another, so that a direct correlation between activity and solid state structure may be made.

The antimicrobial drug 4-amino-N- (thiazol-2-ylidene)-benzene sulfonamide **1.12** (trivial name sulfathiazole) is a classic example of polymorphism. Five crystalline polymorphs of unsolvated **1.10** are fully characterized by single crystal X-ray diffraction[65-69] over 100 crystalline solvates.[70] Drug **1.10** can exist as imino and amido tautomers, but in the crystal phase it is exclusively found as the imino tautomeric form. Ritonavir **1.13**, a novel protease inhibitor for Human Immunodeficiency Virus (HIV), the causative agent of Acquired Immune Deficiency Syndrome (AIDS).[71] It is marketed as Norvir and lunched in 1996. From the discovery of ritonavir until the

new drug application (NDA) filing, only one crystalline form was known to exist. Attempts to identify other possible crystal forms were unsuccessful. Two years after the launch of Norvir to the market, some lots of Norvir capsules failed a dissolution specification. Investigation of this phenomena revealed the existence of a crystal form of ritonavir other than the one already known (Form I). This other crystal form was designated as Form II. The two crystal forms are polymorphs and differ substantially in their physical properties such as solubility, drug activity.[72]

Two polymorphic forms of a potential drug, 4-phenylthiazole-2-thiol **1.17**[73] exhibiting fairly interesting human indoleamine 2, 3-dioxygenase (hIDO) inhibition effect was isolated. Compound **1.17** shows thiol-thione tautomerism as Scheme **1.2**.

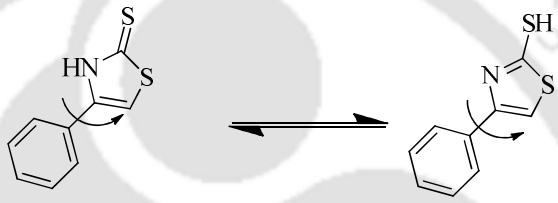

4-phenylthiazole-2(3H)-thione 4-phenylthiazole-2-thiol

*Scheme 1.2: Thiol-thione Tautomerism for Compound **1.17** (Torsion angle is indicated by a curved arrow)*

Thienothiophene tethered thiazolothiazole trimers **1.18** act as organic semiconductor.[74] Compound **2.6** shows dimorphic behaviour. One polymorph was found to be a p-type semiconductor, while the other form behaves as insulator. The different charge-transport behaviour and optical properties of the two polymorphs of **1.16** are strongly related to the topology of their π-stacks. Dasatinib **1.19** is an oral anticancer agent, which is poorly soluble in water. Commercial **1.19** is a monohydrate. The anhydrous phase of **1.19** is better soluble than its commercial hydrate form.[75]

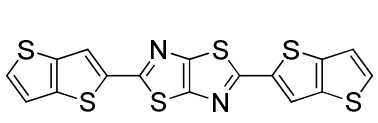

1.18

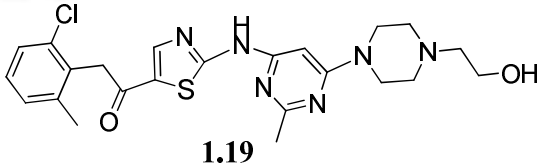

1.19

Febuxostat **1.20** is a nonpurine selective inhibitor of xanthine oxidase, which is used for the management of hyperuricemia in patients with gout.[76] Compound **1.20**, regarded as active pharmaceutical ingredient (API) forms pharmaceutical cocrystals

with another pharmaceutically acceptable molecule, such as urea, acetamide, nicotinamide, p-aminobenzoic acid and saccharin.[77] Nitazoxanide **1.21** is a commercially available nitrothiazolyl-salicylamide ester indicated for the treatment of gastrointestinal diseases caused by protozoa and helminthic parasites.[78] **1.21** forms cocrystals with different acids such as succinic acid, glutaric acid etc.[79] All these cocrystals exhibited faster dissolution rates and good to moderate stability.

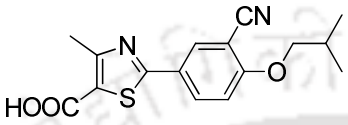

1.20

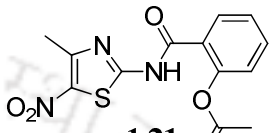

1.21

Meloxicam **1.22** is a nonsteroidal anti-inflammatory drug with low aqueous solubility and high permeability. Pharmaceutical cocrystallization of meloxicam is a promising approach to enhance its aqueous solubility. 1:1 co-crystal of aspirin with meloxicam exhibited superior kinetic solubility and significantly decreases the time required to reach the human therapeutic concentration compared with the parent drug.[80] The supramolecular heterosynthon **1.22a** present in aspirin: meloxicam cocrystal is shown in Figure 1.5.

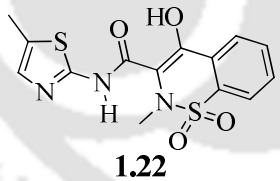

1.22

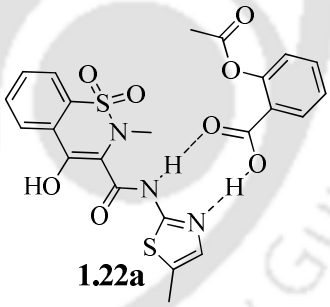

1.22a

*Figure 1.5: Meloxicam **1.22** and its supramolecular synthon with aspirin **1.22a**.*

Meloxicam **1.22** also forms various pharmaceutical cocrystals with different carboxylic acids as shown in Figure 1.6. Meloxicam dimer **1.23** as robust synthon is found in crystal lattice of all these cocrystals (Figure 1.6).[81]

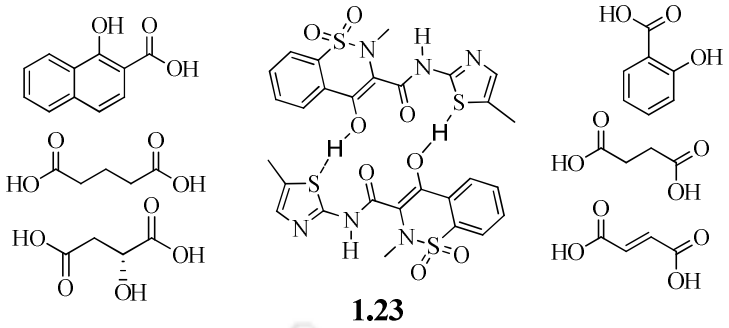

1.23

*Figure 1.6: Meloxicam dimer **1.23** and various carboxylic acids*

Natural as well as synthetic thiazole peptides have shown widespread pharmacological and metal binding properties. Phenylalanine- and tyrosine-derived thiazole-containing cyclic tripeptides **1.24** and **1.25** forms various solvates that revealed strongly divergent supramolecular assemblies in the solid state.[82] All the assemblies are predominantly guided by intermolecular S**…**O interactions of a thiazole and a carbonyl unit of solvent molecule arranged in a coplanar fashion.

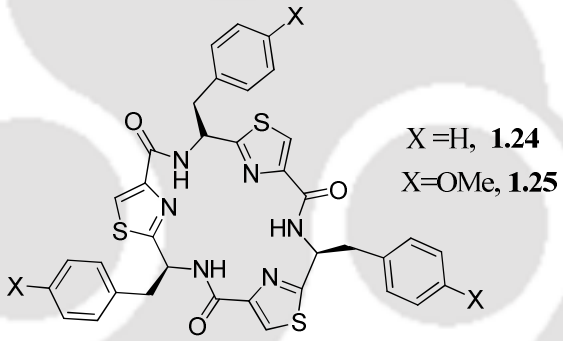

Thiazole moiety, which turned out to be a quite reliable scaffold for organo/hydrogelation.[83] 2-aminothiazole (and its methyl derivatives) forms salts/cocrystals with various dicarboxylic acids.[84] Some of it forms hydrogel. The formation of void along with sufficient hydrophobic interactions may attribute to hydrogelation phenomenon. The different types synthon formed by 2-amino thiazole with different carboxylic acids is shown in Figure 1.7.

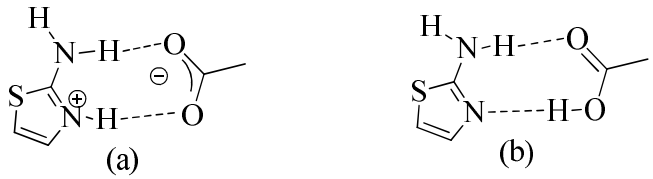

Figure 1.7: R_2^2 (8) synthons present in (a) salt (b) co-crystal

Supramolecular recognition via synthon formation play a key role in the development of new materials.[85] Synthon formation is employed as a methodology in the synthesis of amidophosphine ligands.[86]

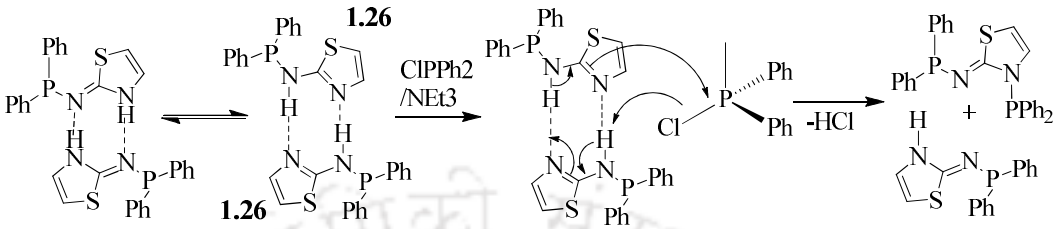

Figure 1.8: Dimerization via synthon formation and Phosphanylation of the dimer.

Dimerization of 2-phosphanylamino-thiazole **1.26** via hydrogen bonding acts as a template to establish the preferred stereochemistry of the second substitution reaction (Figure 1.8).

1.6: Thiazole derivatives in detection of cations

Thiazole derivatives are UV/Vis as well as fluorescence active. The best example is the naturally occurring luciferin **1.16**, the light-emitting dye of fireflies.[56] Thiazole containing colorimetric and ratiometric receptors are very common. Generally design of thiazole based fluorescence receptors shows signal transduction through inhibition of excited-state intramolecular proton transfer (ESIPT), ICT (intramolecular charge transfer) and Fluorescence resonance energy transfer (FRET) mechanisms. To explain these mechanistic processes, we illustrate each case by taking illustrative case of each type.

ESIPT has attracted much attention due to the applications in molecular probes,[88] luminescent materials,[89] and molecular logic gates,[90] etc. Chromophores that show large Stokes shift show ESIPT. ESIPT is a faster process than fluorescence. The basic photophysical process of ESIPT chromophore is illustrated in Figure 1.9, by 2-(2-hydroxyphenyl)-benzothiazole **1.27**.[91] E and E* are ground and excited states of enol form **1.27**. ^{1}K* is the singlet excited state for *cis*-keto form. Besides the radiative decay to K state, ^{1}K* can be deactivated either to triplet excited state ^{3}K* through intersystem crossing (ISC) or isomerizes to the *trans*-keto form K_Z (Figure. 1.9). Another unique feature of the ESIPT chromophores is the transient character of the

ground state of the emissive species of the ESIPT chromophores, i.e. the keto tautomer.[87]

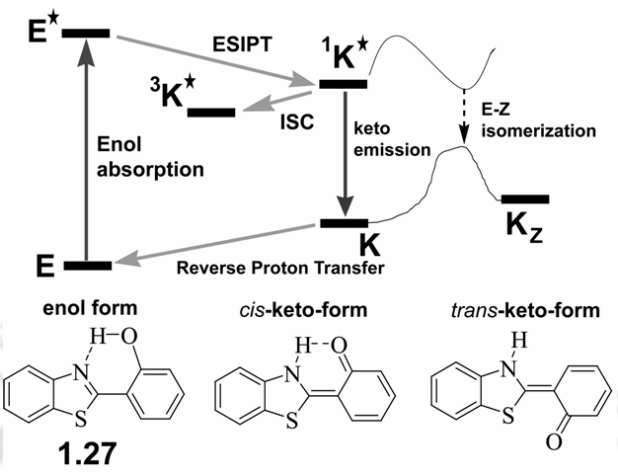

*Figure 1.9: Photophysics of ESIPT, illustrated by 2-(2-hydroxyphenyl)- benzothiazole **1.27**.*

Compound **1.28** has been shown to be a selective fluorescent chemosensor for quantification of Zn^{2+} ions.[92] **1.28** revealed absorption and emission peaks at 390 and 481 nm, respectively. In this detection process, ESIPT shown by the **1.28** was inhibited by coordination with Zn^{2+} ions as shown in Figure 1.10. Coordination of Zn^{2+} with **1.28** causes a red shift in UV-visible absorption and a blue shift in fluorescent spectrum along with enhancement in the degree of intensity.

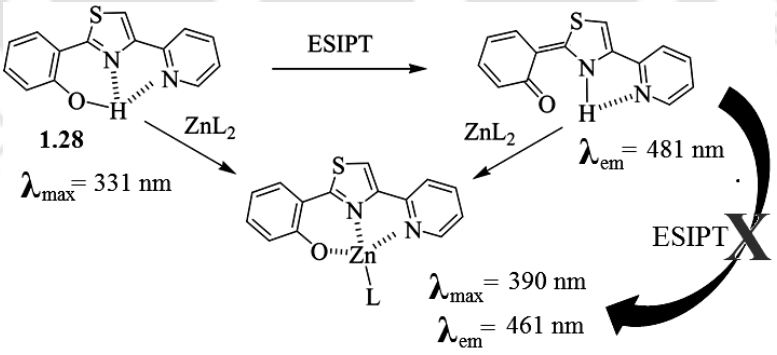

*Figure 1.10: Binding mechanism of Zn^{2+} with **1.28** to inhibit ESIPT.*

Internal charge transfer (ICT) based probes are characterized by an electron-donating unit conjugated to an electron-accepting unit within one molecule that give rise to a ‘‘push–pull’’ π-electron system in the excited state. ICT mechanism can be explained with coumarin–thiazole group containing chemosensor **1.29**[93] as shown in Figure

1.11. **1.29** was employed as a novel fluorescent probe for Cu^{2+} ions. The introduction of the -NEt_2 group linked with the coumarin moiety creates a strong 'push-pull' interaction of π-electrons throughout the receptor **1.29**.

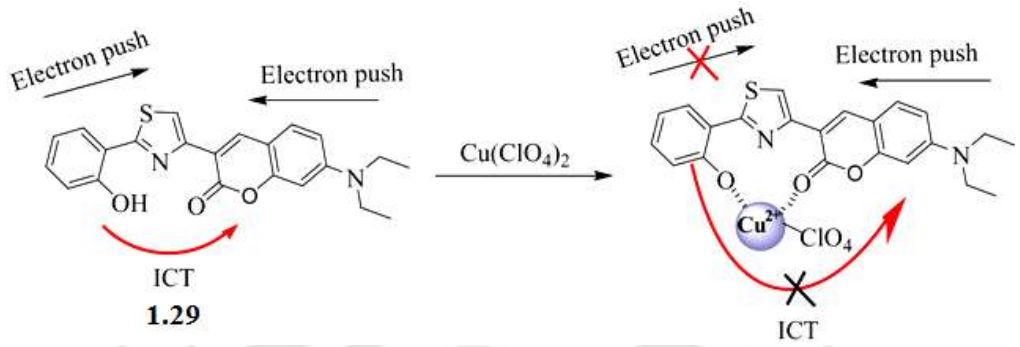

*Figure 1.11: Intramolecular charge transfer mechanism in compound **1.29**.*

Fluorescence resonance energy transfer (FRET) is a widely used sensing mechanism for the design of fluorescence ratiometric probes. This nonradiative process involves the energy transfer between a pair of fluorophores that acts as energy donor and acceptor linked together through a nonconjugated spacer. Following conditions must be satisfied for observing FRET: a) Donor part should have sufficient lifetime for energy transfer. (b) An appropriate distance between the donor and acceptor (~10−100 Å) as the energy transfer occurs through space.[94] (c) The absorption spectrum of the acceptor fluorophore must overlap with fluorescence emission spectrum of the donor fluorophore (at least by 30%).

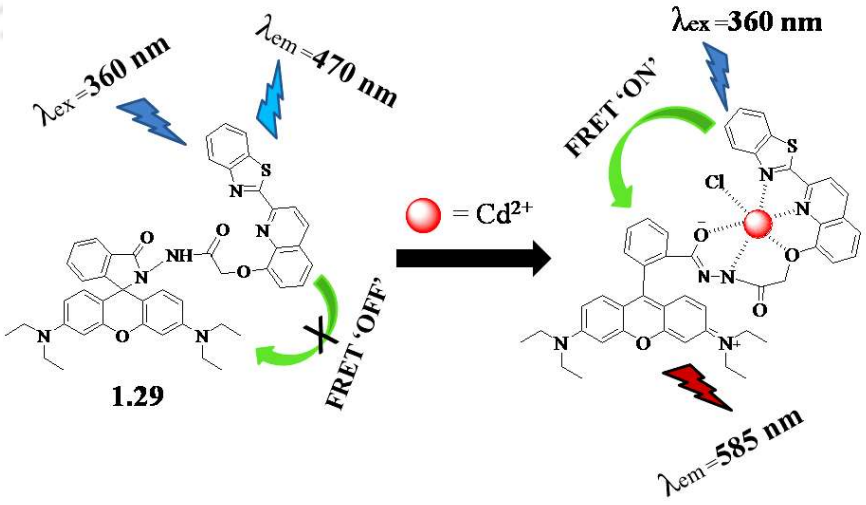

*Figure 1.12: Proposed FRET-Based Sensing Strategy of **1.30** with Cd^{2+}.*

On the basis of the FRET mechanism between rhodamine and quinoline-benzothiazole conjugated dyad, a colorimetric as well as fluorescence ratiometric probe **1.30**[95] was synthesized for the selective detection of Cd^{2+}. Probe **1.30** itself exhibits three absorption bands at 262, 300, and 360 nm. But no peak appears at 565 nm, indicating the probe predominantly exits in spirolactam form (Figure 1.12). On complexation with Cd^{2+} a distinct new peak having the maximum at 565 nm appeared indicating energy transfer. The quantam yield of **1.30** also increases upon complexation with Cd^{2+}. Since FRET is very sensitive to the distance between fluorophores, compound **1.30** on complexation with Fe^{3+} brings the acceptor and donor moiety close and also provides favorable orientation for energy transfer. This shifting of the emission to higher wavelength (360 nm to 585nm) suggested that in this system distance of separation between donor and acceptor changes through coordination hence fluorescence changes may be used to estimate distance between fluorophores.

There are large numbers of examples on thiazole derivatives which have evolved over the years to detect various metal ions. Thus list of some thiazole derivatives used in detection of different metal ions are listed in Table 1.2. Major challenge in this area is to identify water soluble molecules with specific signal response to an analyte. Further understanding on interference of other metal ions prior to development of a new analytical device is essential. Thus, major aspect of this research is directed towards screening of fluorescence responsive molecules and modulation of signals.

Table 1.2: List of compounds with their respective metal ion/s detections.

Compound Structure	Compound no.	Metal cation
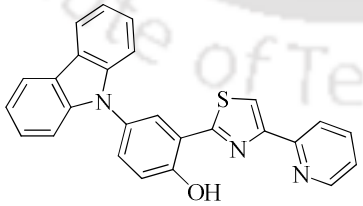	**1.31**	Zinc[96]
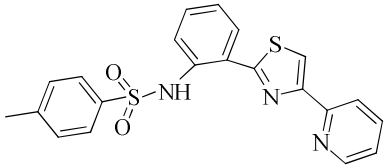	**1.32**	Zinc[97]

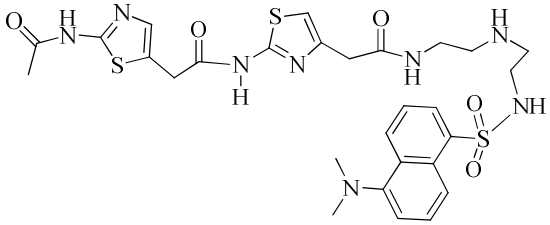

1.33 Copper[98]

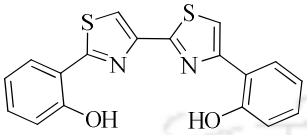

1.34 Zinc and Copper[99]

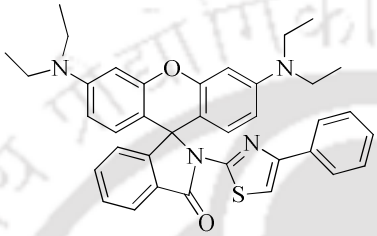

1.35 Iron[100]

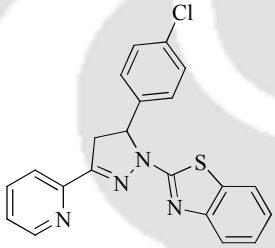

1.36 Iron[101]

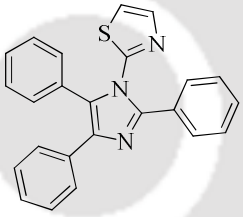

1.37 Chromium[102]

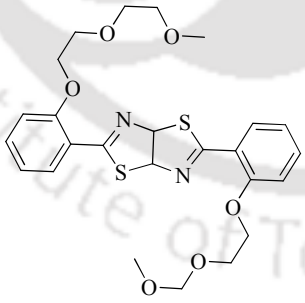

1.38 Chromium[103]

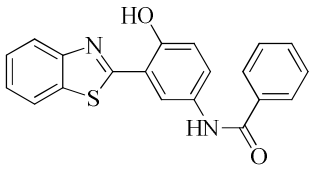

1.39 Palladium[104]

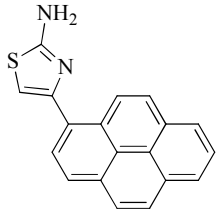	**1.40**	Tin[105]
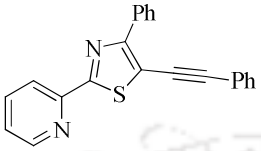	**1.41**	Iron[106]
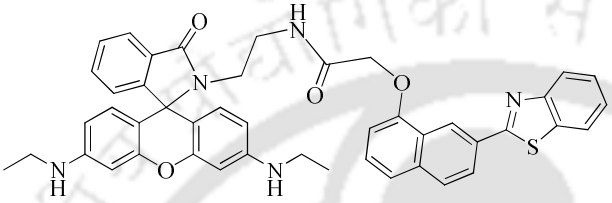	**1.42**	Iron [107]
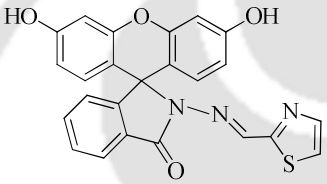	**1.43**	Cobalt and Nickel[108]
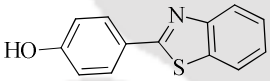	**1.44**	Mercury[109]
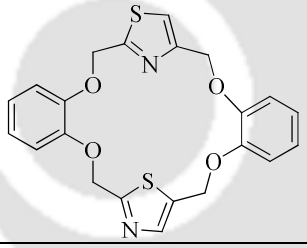	**1.45**	Ammonium Ion[110]

Thiazole based receptors can be used to sense various types of metal cations as listed in Table 1.12. Carbazole incorporated thiazole **1.31**[96] is a chemosensor for Zn^{2+}. **1.31** produce remarkable red shift in emission upon complexation with Zn^{2+}. Peptide based thiazole derivative **1.33**,[98] was reported for the sensing of Cu^{2+} ions in the presence of other competing divalent transition metal ions in water at physiological pH. Such sensors are biocompatible. Hence, can easily bind with proteins or nucleic acids. A bisthiazole chemosensor **1.34**[99] with phenolic substituents at the position 2 of the thiazole rings acts as a dual-function fluorescence chemosensor with Cu^{2+} and Zn^{2+} ions based on cation induced inhibition of EPIST mechanism. The binding of thiazole **1.34** with paramagnetic open-shell d-orbital of Cu^{2+} produced a complete

quenching of fluorescence due to the inhibition of ESIPT, while the closed-shell d-orbital of Zn^{2+} causes inhibition of the ESIPT producing a ratiometric change in emission. A rhodamine-thiazole based probe **1.35**[100] is a chemosensor for Fe^{3+} ions. The sensor **1.35** showed a remarkable enhancement of the fluorescence intensity and a clear color change from colorless to pink upon binding with Fe^{3+} ions. Here transfer of electrons of the phenylthiazole ring to rodamine moiety upon coordination with Fe^{3+} causes opening of the spiro-ring. Pyrazoline-thiazole based probe **1.36**[101] is another chemosenor for Fe^{3+}. This sensor forms a 1:1 complex with Fe^{3+} and displays fluorescent quenching. The imidazole-thiazole based probe **1.37**[102] is a selective sensor for Cr^{3+} ions, **1.37** forms 1:1 complex with Cr^{3+} ions. The thiazolothiazole based probe **1.38**[103] is another selective chemosensor for Cr^{3+} ions. **1.38** displayed a selective fluorescence "*Off-On*" change upon the addition of Cr^{3+}. The benzothiazole derivative **1.39**[104] is a fluorescent probe for Pd^{2+}. The allyl group connected to the phenolic oxygen atom of probe **1.39** undergoes Pd^0 catalysed hydrolysis as shown in Figure 1.13. The resultant enolic form of **1.39** shows two emission maximum at **415** and **555** nm respectively via EPIST mechanism. Here, Pd^0 is oxidized to Pd^{2+}, which binds to **1.39**.

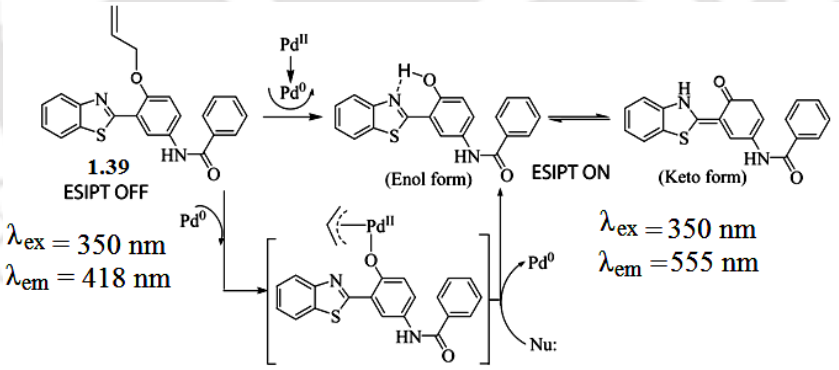

*Figure 1.13: Proposed mechanistic process of fluorescent probe **1.39** activated via Pd species catalytic reaction.*

Tin, is one of the most commonly used heavy metals in agricultural industry[111,112] including food container, food processing equipment, toothpaste, perfumes, soaps, food additives and dyes. But, excess accumulation of tin can cause eye and skin irritation, headaches, stomachaches and dizziness, breathlessness urination problems, liver damage, malfunctioning of immune systems, chromosomal damage and gastrointestinal effects (abdominal cramps, nausea, diarrhoea, vomiting).[113] Pyrene

thiazole conjugate amine **1.40**[105] act as a ratiometric fluorescence probe for Sn^{4+} in aqueous medium. **1.40** also shows tin recognition in live cells. **1.40** shows fluorescence quenched behavior via PET from the amine group to the excited singlet state of pyrene. Upon complexation with Sn^{4+}, large fluorescent enhancement was observed due to chelation-enhanced-fluorescence (CHEF) effect. Metal chelation break-off the PET process as shown in Figure 1.14.

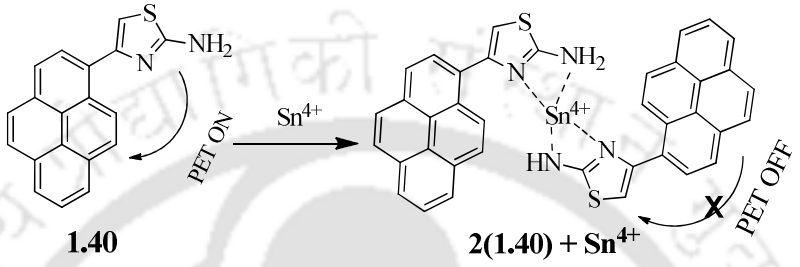

*Figure 1.14: Possible binding of **1.40** with Sn^{4+}.*

1.41[106] is a ratiometric fluorescent sensor for Fe^{3+}. **1.41** exhibits fluorescence emission at 431 nm, and at 517nm after addition of Fe^{3+}. A typical ICT process should be responsible to the fluorescence of the sensor. Benzothiazole conjugated quinoline derivative **1.42**[107] is a FRET-based molecular switch for Fe^{3+} in semi-aqueous medium. **1.42** can discriminate Fe^{3+} from Fe^{2+}.

1.43[108] is a dual sensor for both Co^{2+} and Ni^{2+}. **1.43** shows turn-on fluorescence with paramagnetic ions like Co^{2+} and Ni^{2+}. The mode of binding is shown in Figure 1.15. **1.44**[109] is selective sensor to measure Hg^{2+} in the presence of high concentrations of Cd^{2+} and Zn^{2+}. Hg^{2+} being softer than Cd^{2+} and Zn^{2+} expected to prefer binding to **1.44** through the S and O atoms to form chelate.

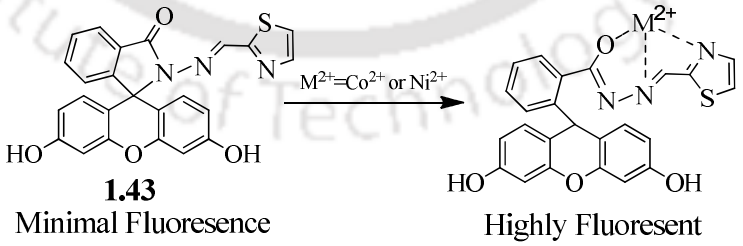

*Figure 1.15: Proposed mechanism for fluorescence changes of **1.43** on addition of Co^{2+} or Ni^{2+}*

Thiazole based Crown ether **1.45**[110] is a highly selective ammonium ionophore, which find important applications in the detection of NH_4^+ in aqueous systems for clinical

and environmental analyses. The observed selectivities of these types of crown ethers containing thiazole units were found to be superior to, or at least comparable to, that of nonactin, a naturally occurring cyclic ionophore.

1.7: Thiazole derivatives as sensors for anions

Thiazole derivatives have provided wide ranges of templates to selectivity bind anions. Fluoride (F-) being an important biological anion, having significance use in clinical treatment for osteoporosis and dental care.[114] but excessive accumulation of fluoride can cause fluorosis, bone cencer.[115] Thiazole attached to phenolic units such as **1.46**[116] and **1.47**[116] were used to detect selectively F^- ions. Interactions of **1.46** and **1.47** with F^- caused a red-shift in UV-visible absorption and a large Stokes shift in fluorescence emission due to the inhibition of Excited state intramolecular proton transfer (ESIPT) induced by the deprotonation of phenolic proton by F^- as shown in Figure 1.16.

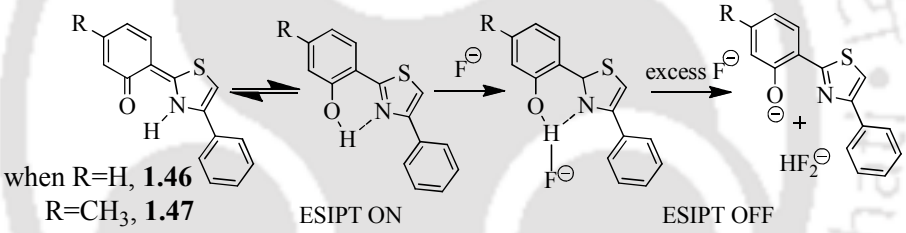

*Figure 1.16: The mechanism of the interaction of F^- with **1.46** and **1.47**.*

Chemosensor **1.48**[117] has been found to shows high selectivity to bind acetate ($CH_3CO_2^{1-}$) ions over other anions. The high selectivity is related to the configuration of the $CH_3CO_2^{1-}$ matching with the chemosensor and also the alkali nature of the anion, as well as the acidity of urea N-H protons in chemosensor. The possible binding mechanism is shown in Figure 1.17.

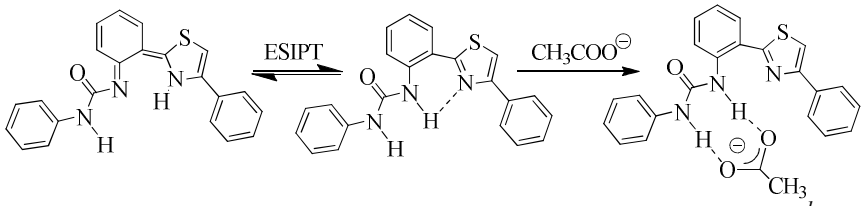

*Figure 1.17: The possible ESIPT in **1.48** and binding of $CH_3CO_2^{1-}$ in a 1:1 stoichiometry.*

Many anion selective compounds have been prepared based on thiazole moieties. Some of such compounds are listed in Table 1.3.

Table 1.3: List of compounds with their respective anion/s detections.

Compound Structure	Compound No.	Anion/s
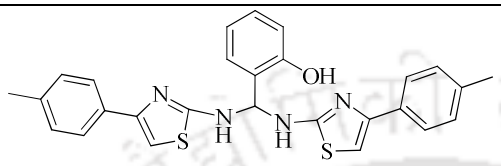	**1.49**	Fluoride[118]
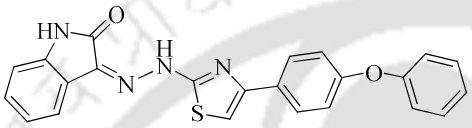	**1.50**	Fluoride [119]
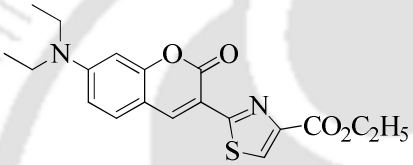	**1.51**	Cyanide[120]
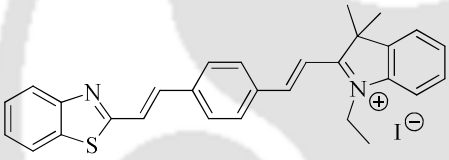	**1.52**	Cyanide [121]
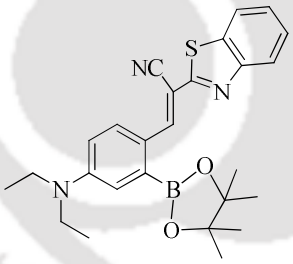	**1.53**	Peroxynitrite[122]
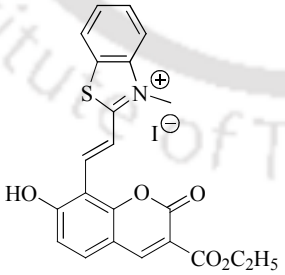	**1.54**	Bisulfite[123]

Compound **1.49**[118] is a "turn on" fluorescent and chromogenic chemosensor for fluoride (F^-) anion. **1.49** shows high selectivity and good sensitivity towards fluoride (F^-) ions. Compound **1.50**[119] is another chemosensor for detection fluoride (F^-) ion through naked eye. Compound **1.50** shows large bathochromic shift in the absorption

spectrum (from yellow to orange). Coumarin thiazole based compound **1.51**[120] is a highly selective and sensitive probe towards cyanide (CN^-) anion over other anions. Cyanide (CN^-) is bind with **1.51** through Michael addition (Figure 1.18) showing color and fluorescence change.

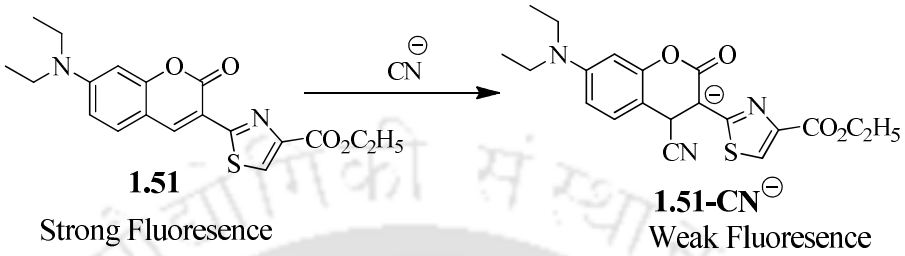

*Figure 1.18: The binding of **1.51** with cyanide (CN^-)*

Compound **1.52**[121] is a near-infrared (NIR) sensor for cyanide (CN^-) ion. Compound **1.52** is a multi-channel detector of cyanide (CN^-) ion. This sensor can selectively detect CN^- either through dual-ratiometric fluorescence or under various absorption and emission channels. The binding mechanism of **1.52** with cyanide (CN^-) ion is shown in Figure 1.19.

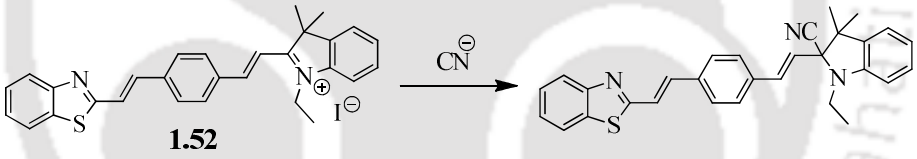

*Figure 1.19: The binding of **1.52** with cyanide (CN^-)*

Arylboronate-based compound **1.53**[122] is selective and sensitive fluorescent probe for peroxynitrite ($ONOO^-$) ion as shown in Figure 1.20. **1.53** can detect with a big fluorescence *off-on* ratio with fast response rate in aqueous medium. The sensing mechanism was proved to be the $ONOO^-$ triggered oxidative hydrolysis of **1.53** followed by an intramolecular cyclization to lead to fluorescent iminocourmarin (Figure 1.20).

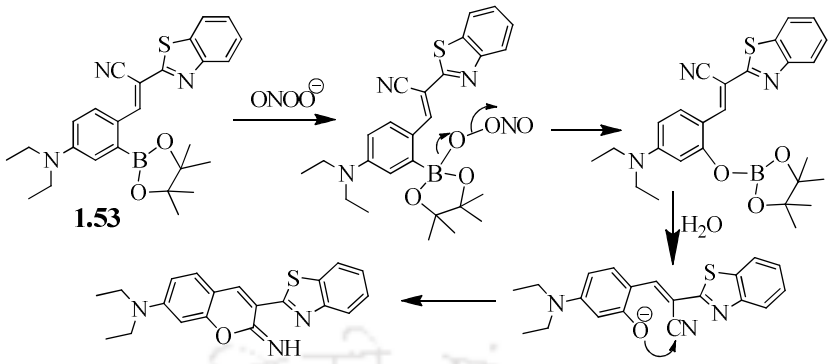

*Figure 1.20: Proposed sensing mechanism of **1.53** for $ONOO^-$.*

The hybrid coumarin-thiazole compound **1.54**[123] ratiometric and colorimetric sensor for bisulfite (HSO_3^-) anions. The detection of bisulfate (HSO_3^-) anions was performed through the Michael addition of the bisulfite anion toward the hybrid coumarin-thiazole sensor **1.54** as shown in Figure 1.21. On additton of bisulfite (HSO_3^-) to fluorescence intensity decrease at 600 nm and to increase at 450 nm and simultaneously yielded a visible color change from purplish red to colorless.

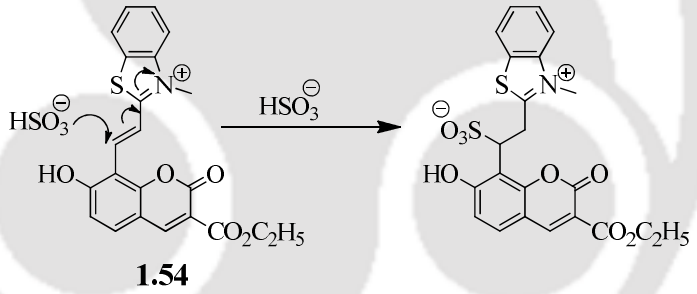

*Figure 1.21: The proposed mechanism of **1.54** with bisulfate (HSO_3^-).*

1.8: Metal complexes/coordination polymers of thiazole derivatives

Thiazole is a multidonor heterocyclic compound containing both nitrogen and sulfur atoms possessing versatile coordination ability toward various transition metal ions. As a result, thiazole have attracted considerable interest, particularly in the synthesis and applications of biomimicking and bioactive coordination compounds.[124] Electron-rich polyfunctional thiazole, isothiazole derivatives assume an exceptional importance on the construction of metal complexes of different types, in particular valuable organometallic frameworks and functional materials. Thiazole based pyridinecarboxylate compound [2-(2-pyridyl)-4-methylthiazole-5-carboxylic acid]

1.55[125], forms three-dimensional metal-organic frameworks (MOF) with manganese $[Mn(L_{1.54})_2](H_2O)_3(DMF)]$ **1.55a** and cadmium. $[Cd(L_{1.54})_2](H_2O)_4(DMF)]$ **1.55b**. MOF **1.55a** shows weak anti-ferromagnetic coupling between the magnetic centres while MOF **1.55b** displays adsorption selectivity for CO_2.

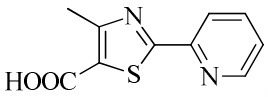

1.55

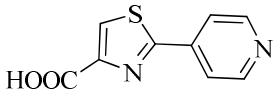

1.56

Cu^{2+} complex of compound [2-(4-pyridyl)-thiazole-4-carboxylic acid] **1.56**[126] affords the neutral 3D coordination polymer $[Cu_3(L_{1.55})_6](H_2O)]_{14}$ **1.56a,** which has the rare moganite topology (Figure 1.22). Moganite is a mineral having topology closely related to quartz topology.

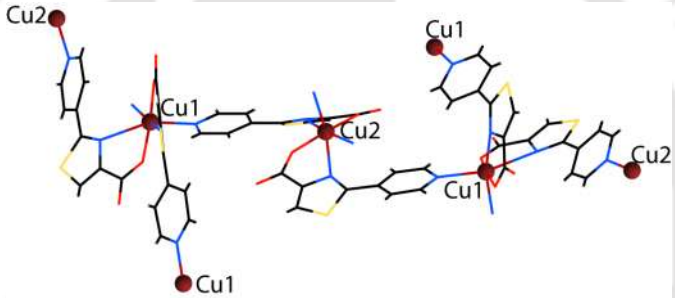

*Figure 1.22: Portion of the extended structure of **1.56a** showing the coordination geometry of the two independent Cu atoms.*

The thiazole based tripodal compound **1.57**[127] itself and its Ca^{2+} complex **1.57a**[127] act as a inhibitor of catalytic hydrolysis by matrix metalloproteinase (MMPs) which are zinc dependent endopeptidases capable of degrading all kinds of extracellular matrix proteins and are involved in the cleavage of cell surface receptors

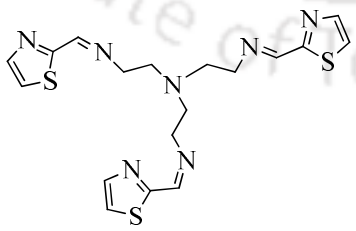

1.57

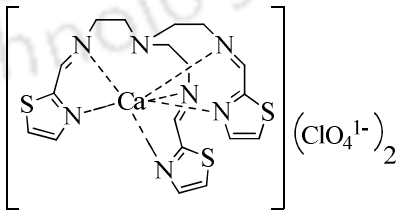

1.57a

The thiazole based compound [2-(pyridine-2-yl)thiazole] **1.58**[128] forms metal complexes $[(\eta^6\text{-}C_6H_6)Ru(L_{1.57})Cl]^+$ **1.58a** and $[(\eta^5\text{-}C_5Me_5)M(L_{1.57})Cl]^+$ **1.58b** where

M=Rh, Ir. These metal complexes shows significant anti-cencer activities when tested in human ovarian cells.

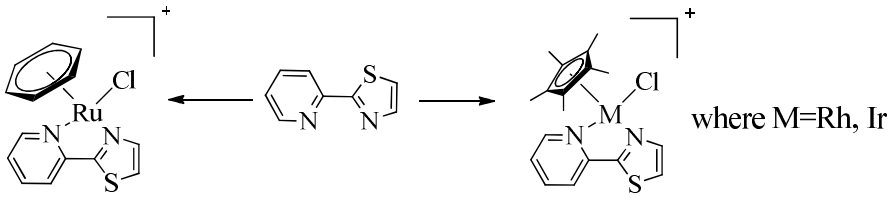

1.58a **1.58** **1.58b**

Ni^{2+} complex of 2-amino-5-methylthiazole $[Ni(i\text{-}MNT)(L_{1.58})_2]$ **1.59**[129] where i-MNT^{2-}= the dianion of 1,1-dicyano-2,2-ethylenedithiolate shows significant binding interactions with calf-thymus DNA (CT-DNA). Platinum complex **1.60**[130] having thiazole ring shows significant anticancer activities. **1.60** obtained by incorporation of planar heterocyclic thiazole nucleus in place of one of the amine in clinically ineffective trans-$[PtCl_2(NH_3)_2]$ (transplatin). The compound **1.60** has a trans geometry and its clinical activity makes new avenues for study of related systems.

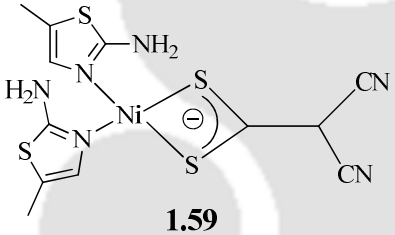

1.59

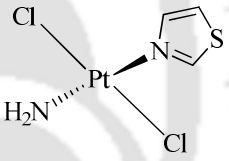

1.60

From the above discussion, it is apparent that there is a huge scope to use thiazole derivative to explore interesting properties. Further, to study biological activity where thiazole has a role.

1.9: Scope of the present work

Foregoing discussion, have suggested the important role of weak interactions in self-assembly of heterocyclic compound, thereby exploring interesting properties. Here, special emphasis is given on thiazole ring containing compounds. The discussions also made it evident that thiazole derivatives could be the choice for many supramolecular studies. Thiazole group contains conjugated π-systems which provide an important contribution in stabilization of the supramolecular assemblies by π-π interactions. Thiazole derived compounds also have great potential in medicinal chemistry. They show anti-Cancer[131], anti-HIV[132] as well as anti-Alzheimer[133] activities. The iridium benzothiazole complexes[134] are efficient phosphors and have

wide applications in optoelectronic devices. Bisthiazole based derivatives[135] can be efficiently used in solar cell devices. Some benzothiazole shows liquid crystalline behavior and act as semiconductor devices.[136] Thiazole derivatives also act as good senors towards environment polluting metal ions.[105,109]

Aminothiazole is one of the important derivatives of thiazole family. Aminothiazoles have supramolecular properties and can act as good hosts.[137] There are several possibilities to cause slight structural modifications in aminothiazoles. Structural changes can be as a result of (a) rotation around the C-N bond, (b) salt formation, (c) amine-imine equilibrium, and (d) binding to metal ions, which are illustrated in Scheme 1.9.

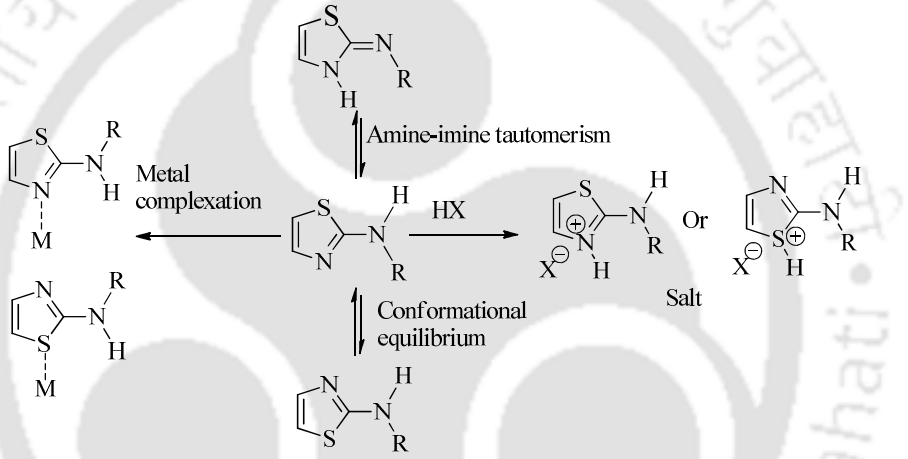

Scheme 1.9: Possibilities to cause structural modification in aminothiazole

5-Methyl-2-[(2-nitrophenyl)amino]-3-thiophenecarbonitrile, known as ROY has various polymorphs based on the rotation of thiophenecarbonitrile unit over a intramolecularly hydrogen bonded ring.[138] Thiazole derivatised with appropriate functionality have provision to form intrmolecular hydrogen bonded synthon bearing an end to rotate, thereby forming various polymorphs. Protonation can be done on the nitrogen and sulpher atom of thiazole moiety to form a salt. Self assembly of a cationic species is different from the neutal one. We may construct various anion guided supramolecular architectures and to study conformational adjustment of the cationic species. It is well known that amino thiazole tautomerizes to imine form. Imines form has different supramolecular assembly bearing different properties. Metal complaxation through either hard nitrogen or soft sulpher show different properties as well as different supramolecular assemblies.

Thus, looking at the potentials of these thiazole derivative in the field of supramolecular assemblies, host-guest interactions, biological activities and the properties of its metal complexes, we have synthesized a number of thiazole derivatives and investigated various aspects including host-guest interactions, polymorphism and molecular/ion recognition properties.

1.10: References

1. J.-M. Lehn, 'Supramolecular chemistry and self-assembly special feature: Toward complex matter: Supramolecular chemistry and self-organization', *Proc. Nat. Acad. Sci.*, *USA*, 2002, **99**, 4763.
2. J. W. Steed, J. L. Atwood, *Supramolecular chemistry*, John Wiley and Sons, Ltd; **1997**, 1-6.
3. D. J. Cram, *Angew. Chem., Int. Ed*., 1986, **25**, 1039.
4. G. A. Jeffrey, *An Introduction to Hydrogen Bonding*, Oxford University Press, London, **1997**.
5. G. R. Desiraju, *Acc. Chem. Res.*, 2002, **35**, 565.
6. T. Steiner, G. R. Desiraju, *Chem. Commun.*, 1998, 891.
7. G. R. Desiraju, *Angew. Chem., Int. Ed. Engl.*, 1995, **34**, 2311.
8. E. Arunan, G. R. Desiraju, R. A. Klein, J. Sadlej, S. Scheiner, I. Alkorta, D. C. Clary, R. H. Crabtree, J. J. Dannenberg, P. Hobza, H. G. Kjaergaard, A. C. Legon, B, Mennucci, D. J. Nesbitt, *Pure Appl. Chem.*, 2011, **83**, 1637.
9. G. R. Desiraju, *Angew. Chem. Int. Ed.*, 2011, **50**, 52.
10. G. R. Desiraju, *Acc. Chem. Res.*, 1991, **24**, 290.
11. G. R. Desiraju, *Acc. Chem. Res.*, 1996, **29**, 441.
12. J. A. R. P. Sarma, G. R. Desiraju, *Acc. Chem. Res.*, 1986, **19**, 222.
13. T. Steiner, Hydrogen Bond in the Solid State. *Angew. Chem., Int. Ed*., 2002, **41**, 48.
14. W. L. Jorgensen , J. Pranata, *J. Am. Chem. Soc.*, 1990, **112**, 2008.
15. G. R. Desiraju, *Angew. Chem., Int. Ed.*, 1995, **34,** 2311.
16. J. W. Steed, J. L. Atwood, *Supramolecular Chemistry*; Wiley: Chichester, 2000.

17. G. R. Desiraju, C. V. K. Sharma, *In The Crystal as a Supramolecular Entity*; G. R. Desiraju, *Ed.;* Wiley: Chichester, 1996;
18. J. A. R. P. Sarma, Gautam R. Desiraju; *Cryst. Growth Des.*, 2002, **2**, 93.
19. K.M. Anderson, A. E. Goeta, J. W. Steed, *Cryst. Growth Des.*, 2008, **8**, 2517.
20. D. S. Reddy, Y. E. Ovchinnikov, O. V. Shishkin, Y. T. Struchkov, G. R. Desiraju, *J. Am. Chem. Soc.*, 1996, **118**, 4085.
21. V. R. Hathwar, T. S. Thakur, R. Dubey, M. S. Pavan, T. N. Guru Row, G. R. Desiraju, *J. Phys. Chem. A*, 2011, **115**, 12852.
22. M. C. Etter, *Acc. Chem. Res.*, 1990, **23**, 120.
23. J. Bernstein, R. E. Davis, L. Shimoni, N.-L. Chang, 'Patterns in hydrogen bonding: functionality and graph set analysis in crystals', *Angew. Chem., Int. Ed. Engl.*, 1995, **34**, 1555.
24. D.N. Reinhoudt, *Reference Module in Chemistry, Molecular Sciences and Chemical Engineering*, 2013.
25. K. Matsumoto, *Topics in heterocyclic chemistry*, Spinger-Verlag Berlin Heidelberg, 2008.
26. C. O. Dietrich-Buchecker, J. P. Sauvage, J. M. Kern, *J. Am. Chem. Soc.*, 1984, **106**, 3043.
27. M. Fujita, J. Yazaki, K. Ogura, *J. Am. Chem. Soc.*, 1990, **112**, 5645.
28. J. R. Williamson, M. K. Raghuraman, T. R. Cech, *Cell*, 1989, **59**, 871.
29. J. -H. Liao, C. -T. Chen, H. -C. Chou, C. -C. Cheng, P. -T. Chou, J. -M. Fang, Z. Slanina, T. J. Chow, *Org. Lett.*, 2002, **18**, 3107.
30. S. C. Zimmerman, W. Wu, *J. Am. Chem. Soc.*, 1989, **111**, 8054.
31. D.E. Lynch, N. Mistry, G. Smith, K.A. Byriel, C.H.L. Kennard, *Aust. J. Chem.*, 1998, **51**. 813.
32. A. R. Hantzsch, H. J. Weber, *Ann. Chem.*, 1888, **1**, 249.
33. A. R. Katritzky, C. W. Rees, E. F. V. Scriven, *Comprehensive Heterocyclic Chemistry 3.*

34. G. R. Pettit, Y. Kamano, C. L. Herald, A. A. Tuinman, F. E. Boettner, H. Kizu, J. M. Schmidt, L. Baczynskyj, K. B. Tomer, R. J. Bontems, *J. Am. Chem. Soc*., 1987, **109**, 6883.
35. V. S. Aulakh, M. A. Ciufolini, *J. Org. Chem*., 2009, **74**, 5750.
36. G. Haberhauer, F. Rominger, *Eur. J. Org. Chem*., 2003, 3209.
37. P. Pornsuriyasak, N. P. Rath, A. V. Demchenko, *Chem. Commun*., 2008, 5633.
38. Z. Jin, Z. Li, R. Huang, *Nat. Prod. Rep.*, 2002, **19**, 454.
39. J. Mann, *Nature*, 1997, **385**, 117.
40. B. Zhu, J. S. Panek, *Org. Lett.*, 2000, **2**, 2575.
41. S. Rosenberg, V. T. DeVita, S. Hellman, *Cancer: Principles & Practice of Oncology* (7th ed.). Hagerstwon, MD: Lippincott Williams & Wilkins. 2005.
42. Z. Jin, *Nat. Prod. Rep.*, 2005, **22**, 196.
43. H. D. Troutman, L. M. Long, *J. Am. Chem. Soc*., 1948, **70**, 3436.
44. V. E. Borisenko, A. Koll, E. E. Kolmakov, A. G. Rjasnyi, *J. Mol. Struct*., 2006, **783**, 101.
45. N. Siddiqui, M. F. Arshad, W. Ahsan, M. S. Alam, *International Journal of Pharmaceutical Sciences and Drug Research*, 2009, **1**, 136.
46. D. Rowe, *Spec. Chem. Mag.*, 2001, **21**, 17.
47. I. Grayson, *Spec. Chem. Mag.*, 2001, **21**, 10.
48. A. Mori, A. Sekiguchi, K. Masui, T. Shimada, M. Horie, K. Osakada, M. Kawamoto, T. Ikeda, *J. Am. Chem. Soc.*, 2003, **125**, 1700.
49. M. V. Beusichem, N. Farrell, *Inorg. Chem.*, 1993, **31**, 634.
50. H. Yu, L. Shao, J. Fang, *J. Organomet. Chem*., 2007, **692**, 991.
51. E. Matczak-Jon, T. Kowalik-Jankowska, K. Slepkura, P. Kafarski, A. Rajewska, *Dalton Trans*., 2010, **39**, 1207.
52. F. Tellez, A. Flores-Parra, N. Barba-Behrens, R. Contreras, *Polyhedron*, 2004, **23**, 2481.
53. A. Giusti, G. Peyronel, *Spectrochim. Acta, Part A*, 1982, **38**, 975.
54. H. D. Yin, S. W. Chen, *J. Organomet. Chem*., 2006**, 691**, 3103.

55. T. Weidner, N. Ballav, M. Zharnikov, A. Priebe, N. J. Lonh, J. Maurer, R. Winter, A. Rothenberger, D. Fenske, D. Rother, C. Bruhn, H. Fink, U. Siemeling, *Chem. Eur. J*., 2008**, 14**, 4346.
56. J. W. Hastings, *J. Mol. Evol.*, 1983, **19**, 309.
57. W. C. McCrone, *Polymorphism.* In *Physics and Chemistry of the Organic Solid State*; D. Fox, M. M. Labes, A. Weissberger Eds.; Wiley-Interscience: New York, 1965, Vol. **2**, pp 725.
58. J. D. Dunitz, *Pure Appl. Chem.*, 1991, **63**, 177.
59. J. D. Dunitz, J. Bernstein, *Acc. Chem. Res.*, 1995, **28**, 193.
60. J. D. Dunitz, *Acta Crystallogr., Sect. B.*, 1995, **51**, 619.
61. J. Bernstein, R. J. Davey, J. -O. Henck, *Angew. Chem. Int. Ed.*, 1999, **38**, 3441.
62. J. Bernstein, *Polymorphism in Molecular Crystals*; Oxford University Press: Oxford, 2002.
63. R. J. Davey, *Chem. Commun.*, 2003, 1463.
64. A. Nangia, *Acc. Chem. Res.*, 2008, **41**, 595.
65. T. Gelbrich, D. S. Hughes, M. B. Hursthouse, T. L. Threlfall, *CrystEngComm***,** 2008, **10**, 1328.
66. G. J. Kruger, G. Gafner, *Acta Crystallogr.*, 1971, **B27**, 326.
67. G. J. Kruger, Gafner, G. *Acta Crystallogr.*, 1972, **B28**, 271.
68. F. C. Chan, J. Anwar, R. Cernik, P. Barnes, R. M. J. Wilson, *Appl. Crystallogr*., 1999, **32**, 436.
69. D. S. Hughes, M. B. Hursthouse, T. S. Threlfall, S. Tavener, *Acta Crystallogr Sect. C*, 1999, **55**, 1831.
70. A. L. Bingham, D. S. Hughes, M. B. Hursthouse, R.W. Lancaster, T. Stewart, T. L. Threlfall, *Chem. Commun.*, 2001, 603.
71. D. J. Kempf, K. C. Marsh, J. F. Denissen, E. McDonald, S. Vasavanonda, C. A. Flentge, B. E. Green, L. Fino, C. H. Park, X. P. Kong, N. E. Wideburg, A. Saldivar, L. Ruitz, W. M. Kati, H. L. Sham, T. Robins, K. D. Stewart, A. Hsu, J. J. Plattner, J. M. Leonard, D. W. Norbeck, *Proc. Natl. Acad. Sci. U.S.A.*, 1995, **92**, 2484.

72. S. R. Chemburkar, J. Bauer, K. Deming, H. Spiwek, K. Patel, J. Morris, R. Henry, S. Spanton, W. Dziki, W. Porter, J. Quick, P. Bauer, J. Donaubauer, B. A. Narayanan, M. Soldani, D. Riley, K. McFarland, *Organic Process Research & Development*, 2000, **4***,* 413.
73. U. F. Röhrig, L. Awad, A. Grosdidier, P. Larrieu, V. Stroobant, D. Colau, V. Cerundolo, A. J. G. Simpson, P. Vogel, B. J. Van den Eynde, V. Zoete, O. Michielin, *J. Med. Chem*., 2010, **53**, 1172.
74. J. A. Schneider, H. Black, H.-P. Lin, D. F. Perepichka, *ChemPhysChem*., 2015, **16**, 1173.
75. S. Roy, R. Quinones, A. J. Matzger*, Cryst. Growth Des*., 2012, **12**, 2122.
76. K. H. Yu, *Recent Pat. Inflamm Allergy Drug Discovery*, 2007, **1**, 69.
77. D. Maddileti, S. K. Jayabun, A. Nangia, *Cryst. Growth Des.*, 2013, **13**, 3188.
78. V. R. Anderson, M. P. Curran, *Drugs*, 2007, **67**, 1947.
79. B. C. Felix-Sonda, J. Rivera-Islas, D. Herrera-Ruiz, H. Morales-Rojas, H. Hopfl, *Cryst. Growth Des*., 2014, **14**, 1086.
80. M. L. Cheney, D. R Weyna, N. Shan, M. Hanna, L. Wojtas, M. J. Zaworotko, *J Pharm Sci.*, 2011, **6**, 2172.
81. M. L. Cheney, D. R Weyna, N. Shan, M. Hanna, L. Wojtas, M. J. Zaworotko, *Cryst. Growth Des*., 2010, **10**, 4401.
82. S. M. Mali, T. F. Schneider, A. Bandyopadhyay, S. V. Jadhav, D. B. Werz, H. N. Gopi, *Cryst. Growth Des.*, 2012, **12**, 5643.
83. P. Yadav, A. Ballabh, *RSC Adv.*, 2014, **4**, 563.
84. P. Yadav, P. Kr. Dutta, A. Ballabh, *Cryst. Growth Des.*, 2014, **14**, 5966.
85. H. W. Roesky, M. Andruh, *Coord. Chem. Re*v., 2003, **236**, 91.
86. O. Kuhl, B. Walfort, T. Ruffer, *Cryst. Growth Des*., 2006, **6**, 366.
87. T. Iijima, A. Momotake, Y. Shinohara, T. Sato, Y. Nishimura , T. Arai, *J. Phys. Chem. A*, 2010, **114**, 1603.
88. J. S.Wu, W. M. Liu, J. C. Ge, H. Y. Zhang, P. F. Wang, *Chem.Soc. Rev*., 2011, **40**, 3483.

89. J. E. Kwon and S. Y. Park, Adv. Mater., 2011, **23**, 3615.
90. V. Luxami, S. Kumar, *New J. Chem*., 2008, **32**, 2074.
91. J. Zhao, S. Ji, Y. Chen, H. Guo, P. Yang, *Phys. Chem. Chem. Phys.,* 2012, **14**, 8803.
92. A. Helal, H.-S. Kim, *Tetrahedron Lett.*, 2009, **50**, 5510.
93. A. Helal, M. H. O. Rashid, C.-H. Choi, H.-S. Kim, *Tetrahedron*, 2011, **67**, 2794.
94. J. Fan, M. Hu, P. Zhan, X. Peng, *Chem. Soc. Rev.*, 2013, **42**, 29.
95. K. Aich, S. Goswami, S. Das, C. Das Mukhopadhyay, C. K. Quah, H.-K. Fun, *Inorg. Chem.*, 2015, **54**, 7309.
96. A. Helal, H.-S. Kim, *Spectrochimica Acta Part A: Molecular and Biomolecular Spectroscopy*, 2013, **105**, 273.
97. A. Helal, S. H. Kim, H.-S. Kim, *Tetrahedron*, 2010, **66**, 9925.
98. S. Bhattacharya, M. Thomas, *Tetrahedron Lett.*, 2000, **41**, 10313.
99. A. Helal, S. H. Lee, S. H. Kim, H.-S. Kim, *Tetrahedron Lett.*, 2010, **51**, 3531.
100. E. Matczak-Jon, T. Kowalik-Jankowska, K. Slepkura, P. Kafarski, A. Rajewska, *Dalton Trans*., 2010, **39**, 1207.
101. S. Hu, S. Zhang, C. Gao, C. Xu, Q. Gao, *Spectrochim. Acta Part A*, 2013, **113**, 325.
102. B. Zhao, Y.-C. Zhou, M.-J. Fan, Z.-Y. Li, L.-Y. Wang, Q.-G. Deng, *Chin. Chem. Lett.*, 2013, **24,** 257.
103. J. Y. Jung, S. J. Han, J. Chun, C. Lee, J. Yoon, *Dyes Pigm.*, 2012, **94**, 423.
104. L. Cui, W. Zhu, Y. Xu, X. Qian, *Anal. Chim. Acta*, 2013, **786**, 139.
105. A K. Mahapatra, S. Mondal, K. Maiti, S. K. Manna, R. Maji, D. Mandal, S. Mandal, S. Goswami, C. K. Quahd, H.-K. Fun, *RSC Adv*., 2014, **4**, 56605.
106. Y. Wang, M.-Y. Yang, M.-H. Zheng, X.-L. Zhao, Y.-Z. Xie, J.-Y. Jin, *Tetrahedron Lett.*, 2016, **57**, 2399.
107. S. Das, K. Aich, S. Goswami, C. K. Quahb**,** H.-K. Fun, *New J. Chem.*, 2016, **40**, 6414.

108. F. A. Abebe, C. S. Eribal, G. Ramakrishna, E. Sinn, *Tetrahedron Lett*., 2011, **52**, 5554.
109. R. Sarma, B. Nath, A. Ghritlahre, J. B. Baruah, *Spectrochim. Acta Part A*, 2010, **77**, 126.
110. M. K. Benson, S. O. Lee, K. D. M. Harris, H.-S. Kim, K.S. Do, K-Il Kim, *Cryst. Growth Des.*, 2002, **2**, 41.
111. A.-M. Florea, D. B¨usselber, *BioMetals*, 2006, **19**, 419.
112. Concise International Chemical Assessment Document 65 by WHO, Geneva, 2006.
113. Agency for Toxic substances and Disease Registry (ATSDR) 2005.
114. M. Kleerekoper, *Endocrinol. Metab. Clin. North Am*, 1998, **27**, 441.
115. Mmmm
116. A. Helal, N. T. T. Thao. S. W. Lee, H.-S. Kim, *J. Incl Phenom Macrocycl Chem*., 2010, **66**, 87.
117. A. Helal, H.-S. Kim, *Tetrahedron*, 2010, **66**, 7097.
118. P. B. Thale, P. N. Borase , G. S. Shankarling , *Inorg. Chem. Front.*, 2016, **3**, 977.
119. A. B. Sarıguney, A. O. Saf, A. Coskun, *Spectrochimica Acta Part A: Molecular and Biomolecular Spectroscopy*, 2014,**128**, 575.
120. S. Park, H.-J Kim, *Sensors and Actuators B* 2012, **161**, 317.
121. P. Xing, Y. Xu, H. Li, S. Liu, A. Lu, S. Sun, *Scientific Reports*, 5:16528, DOI: 10.1038/srep16528.
122. J. Zhanga, Y. Lia, J. Zhaob, W. Guoa, *Sensors and Actuators B*, 2016, **237**,67.
123. M.-J. Peng, X.-F. Yang, B. Yin, Y. Guo, F. Suzenet, D. En, J. Li, C.-W. Li, Y.-W. Duan, *Chem. Asian J*., 2014, **9**, 1817.
124. E.S. Raper, *Coord. Chem. Rev.*, 1996, **153**, 199.
125. X. Zhou, Z. Zhang, B. Li, F. Yang, Y. Peng, G. Li, Z. Shi, S. Feng, J. Li, *New J. Chem.*, 2013, **37**, 425.
126. C.-Y. Su, M. D. Smith, A. M. Goforth, H.-C. Loye, *Inorg. Chem*., 2004, **43**, 6881.

127. H. He, D. P. Linder, K. R. Rodgers, I. Chakraborty, A. M. Arif, *Inorg. Chem*., 2004, **43**, 2392.

128. M. Grasa, B. Therrien, G. Süss-Fink, A. Casini, F. Edafe, P. J. Dyson, *J. Organomet. Chem.*, 2010, **695**, 1119.

129. P. J. Cox, G. Psomas, C. A. Bolos, *Bioorg. Med. Chem.*, 2009, **17,** 6054.

130. M. R. Shiradkar, K. C. Akula, V. Dasari, V. Baru, B. Chiningiri, S. Gandhi, R. Kaur, *Bioorg. Med. Chem.*, 2007, **15**, 2601.

131. E.L. Luzina, A.V. Popov, *Eur J Med Chem.*, 2009, **44**, 4944.

132. R. K. Rawal, R. Tripathi, S. B. Katti, C. Pannecouque, E. D. Clercq, *Bioorg. Med. Chem.*, 2007; **15**: 1725.

133. M.R. Shiradkar, K.C. Akula, V. Dasari, V. Baru, B. Chiningiri, S. Gandhi, R. Kaur, *Bioorg Med Chem.*, 2007, **15**: 2601.

134. C. Fan, L. Zhu, B. Jiang, Y. Li, F. Zhao, D. Ma, J. Qin, C. Yang, *J. Phys. Chem. C*, 2013, **117**, 19134.

135. P. Dutta, W. Yang, S. H. Eom, S.-H. Lee, *Org. Electron.*, 2012, **13**, 273.

136. G. K. Dutta, S. Guha, S. Patil, *Org. Electron.*, 2010, **11**, 1.

137. F. H. Allen, P. R. Raithby, G. P. Shields and R. Taylor, *Chem. Commun.*, 1998, 1043.

138. L. Yu, *Acc. Chem. Res*., 2010, **43**, 1257.

भारतीय प्रौद्योगिकी संस्थान गुवाहाटी
Indian Institute of Technology Guwahati

Chapter 2

Polymorphs and anion-assisted assemblies of thiourea tethered thiazole

As discussed in Chapter 1, the term 'polymorphism' is related to molecular similarity but supramolecular dissimilarity. From crystallographic point of view, polymorphism is divided in to two classes:

a) Conformational polymorphism[1-2] and
b) Packing or orientational polymorphism.[3,4]

Conformational polymorphism is associated with molecular flexibility and related to differences in molecular conformation in crystal phase.[2] Whereas, Packing polymorphism occurs due to packing of molecules in different manners while maintaining the same conformation. Thus, packing polymorphs may arise from different crystal structures in which the unit cells have more than one molecule. Number of symmetry independent molecules per asymmetric unit is described by Z′; higher Z′ value provides more avenues to form Packing polymorphs. In the case of the molecules with flexible structure both the Conformational and the Packing polymorphism may occur. In structurally rigid molecules due to conformational rigidity only packing polymorphism is observed. But, there are also examples of flexible molecules showing only packing polymorphism.[5-7] The strong hydrogen bonds such as O-H**…**O, N-H**…**O or O-H**…**N which have energies in the range of 4-15 kcal mol^{-1} are often the main contributor to different packing patterns. But weak interactions ranging from 1-4 kcal mol^{-1}, such as C-H**…**O, C-H**…**N, and N-H**…**π also have definite importance contributing to stability of a particular packing pattern.[8,9] From theoretical point of view polymorphs can be infinite numbers, but few of them can be isolated or practically feasible.

Polymorphism provides valuable insights to understand crystal packing and structure-property relationships. As discussed in the Chapter 1, different polymorphs of 5-methyl-2-[(2-nitrophenyl)amino]-3-thiophenecarbonitrile, known as ROY (Figure 2.1a) shows different colors such as red, orange, and yellow (Figure 2.1b). ROY has attracted attention of solid-state chemists because it has remarkable diversity as organic solid showing various polymorphic structures.

(a) (b)

Figure 2.1: (a) Structure of 5-methyl-2-[(2-nitrophenyl)amino]-3-thiophenecarbonitrile (ROY) (b) Polymorphs of ROY showing different colors and shape.

ROY is a conformationally flexible molecule. It can adopt different conformations in each polymorph. Conformational difference arises due to the rotation of C-N bond (Figure 2.1a), which ranges from 21 to 104°. Various polymorphs of ROY show characteristic visible absorption due to different conformations of different polymorphs[10] as shown in Figure 2.2.[11] ROY is an ideal small molecule for testing computational models.

Figure 2.2: Overlaid Diagram of different Polymorphs of ROY.[11]

Keeping above discussions in mind, we choose to functionalize thiazole with thiourea, as thiazole based molecules also shows polymorphic behavior, discussed in Chapter 1. Again, thiourea has its own application, like it can form channel-like structures to include various guest molecules like ferrocene.[11-13] Certain biological processes are studied with the aid of thiourea channels.[14] From crystal engineering perspective, polymorphism[15,16] of thiourea based molecules have gained interest.[17] For example, symmetric N,N-disubstituted thiourea derivatives may adopt *trans*, *trans* or *cis*, *trans* geometries (a and b of Figure 2.3) which are documented in literature[18,19]

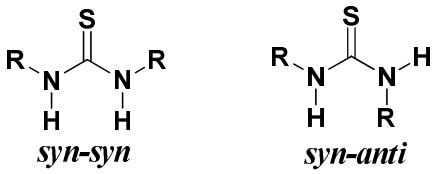

(a) (b)

Figure 2.3: (a) syn-syn, and (b) syn-anti forms of a symmetric thiourea.

However, locking of either geometry through weak interactions may help to generate interesting packing patterns. Subtle changes by electronic and steric effect may generate different self assemblies due to C-C bond rotation. Energy required for conformational change is comparable to weak hydrogen bond.[20-21] Accordingly, two thiourea tethered thiazole derivatives namely, 1-(5-methylthiazol-2-yl)-3-phenylthiourea (**2.1**) and 1-(4-methylthiazol-2-yl)-3-phenylthiourea (**2.2**) as shown in Figure 2.4a were synthesized for structural study. Our anticipation was to obtain different geometries under different conditions such as the ones shown in A-D of Figure 2.4b.

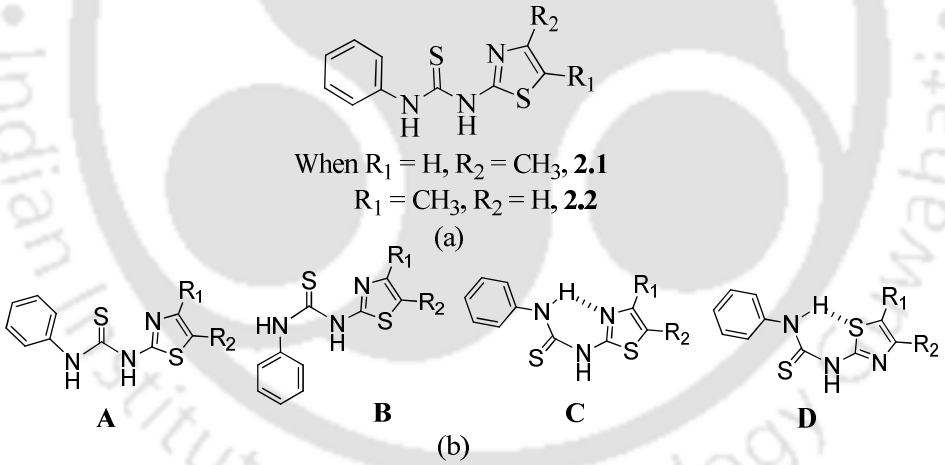

(a)

(b)

*Figure 2.4: (a) Methyl-thiazole functionalized phenyl thiourea derivatives **2.1** and **2.2**, (b) possibilities of different geometries in **2.1** and **2.2**.*

2.1: Synthesis and Characterization of thiazole derivatives 2.1 and 2.2

The derivatives **2.1** and **2.2** were synthesized by the reaction of phenyl isothiocyanate with 5-methylthiazol-2-ylamine and 4-methylthiazol-2-ylamine respectively, following the procedure as discussed in experimental section. These compounds were

characterized by various spectroscopic techniques, such as IR spectroscopy, ^{1}H-NMR and Mass spectrometry. The mass spectrum of **2.1** shows a peak at 250.7944 (Calculated 250.0474), corresponding to [M+1] peak (Figure 2.27). Compound **2.2** shows peak at 250.0490 (Calculated 250.0474), corresponding to [M+1]. (Figure 2.30). In the ^{1}H-NMR, the characteristic thiazolic proton (designated as -a) appear at 6.96 ppm for **2.1** (Figure 2.5a), whereas it appears at 6.37 ppm for **2.2** (Figure 2.5b).

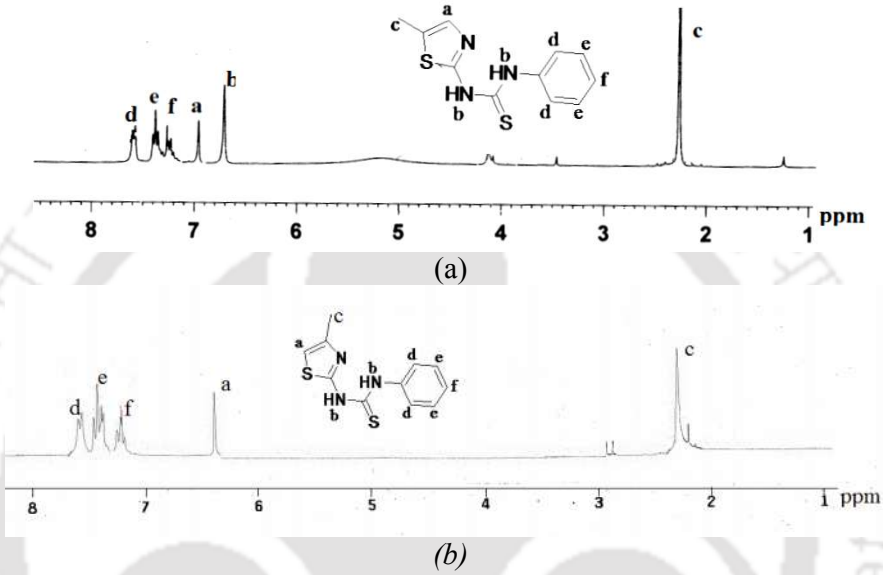

*Figure 2.5: ^{1}H-NMR (400MHz) of (a) **2.1** in $CDCl_3$ and (b) **2.2** in $CDCl_3$.*

2.2: Polymorphs of compound 2.1

Crystallization of compound **2.1**, from series of solvent resulted in crystals with different morphologies. Three types of crystals with different morphologies are shown in Figure 2.6, isolated from three different solvents. Preliminary structural analysis, have revealed that, they belong to different crystallographic space groups, monoclinic $P2_1/c$, triclinic $P\bar{1}$, and monoclinic $C2/c$. These three forms are designated as Polymorph **I**, Polymorph **II** and Polymorph **III** respectively, were obtained independently from methanol (MeOH), Tetrahydrofuran (THF) and Dimethylformamide (DMF) solvents as shown in Scheme 2.1

*Figure 2.6: The optical micrograph of the crystals of the polymorphs of **2.1**.*

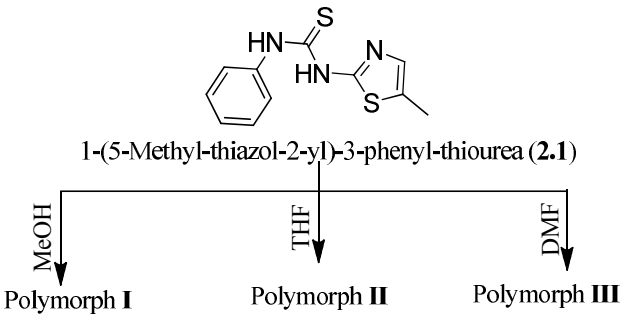

*Scheme 2.1: Three forms of the polymorphs of **2.1**.*

The phase purity of these polymorphs was analyzed by recording their experimentally determined powder X-ray diffraction (PXRD) patterns. The simulated PXRD patterns generated from the CIF files by MERCURY software tally with the experimental diffraction patterns as shown in Figure 2.7a-c. These observations indicated that the solvents guided the crystallization of these polymorphs.

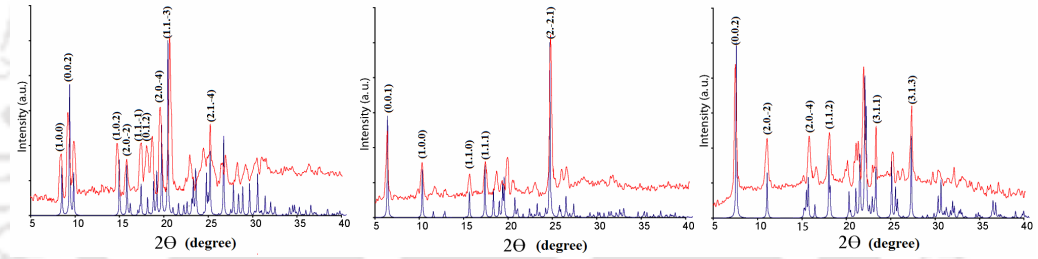

(a) (b) (c)

*Figure 2.7: PXRD patterns of (b) **2.1a,** (c) **2.1b,** (d) **2.1c** (in each case top/red = experimental, bottom/blue = simulated).*

2.2.1: Supramolecular assembly of polymorphs of 2.1

Crystal packing of polymorph **I** shows that the N atom of the 5- methylthiazole unit is engaged in intramolecular N-H**…**N hydrogen bond with the thiourea N-H proton with N**…**N distance 2.70 Å and N-H**…**N bond angle 139° (Table 2.1, Figure 2.8a). This provides a *syn-anti* orientation across the thiourea units (Figure 2.4b-C). Molecules of polymorph **I** form dimeric assemblies, associated through N-H**…**S hydrogen bonds, that can be represented by Etter's $R_2^2(8)$ notation.[22] This $R_2^2(8)$ units being replica of the supramolecular sub-assembly, also called as synthons in the terminology put forwarded by Desiraju.[23]

Polymorph **II** possesses two symmetry-independent molecules (X and Y) in its crystallographic asymmetric unit as shown in Figure 2.8b. Each symmetry-

independent molecule has independent intramolecular N-H**…**N hydrogen bonds (Figure 2.8b): $d_{D\cdots A}$ distances are 2.72 and 2.69 Å and N-H**…**N bond angles are 143° and 144°, respectively (Table 2.1).

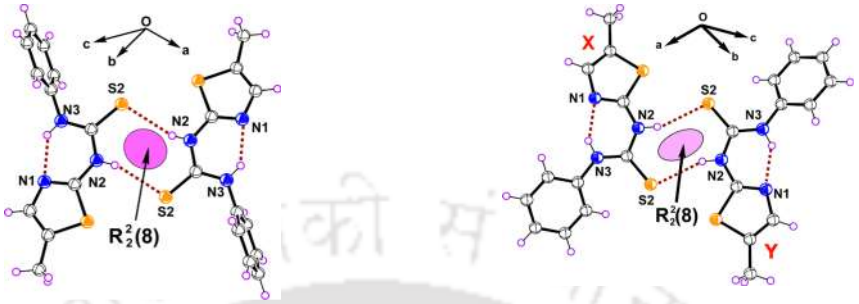

(a) (b)

*Figure 2.8: (a) Assembly of polymorph **I** having intramolecular N-H**…**N and intermolecular N-H**…**S hydrogen bonds, (b) assembly of two symmetry nonequivalent molecules (designated as X and Y) in the crystal lattice of polymorph **II**.*

Polymorphs **I** and **III** have structural similarities. The packing pattern of polymorph **III** is composed of identical hydrogen-bonded synthons, as in polymorph **I**, (Therefore, assembly diagram of polymorph **III** is omitted). But polymorphs **I** and **III** have differences in hydrogen-bond parameters as well as torsion angles (Table 2.1). Polymorph **III** also possesses intramolecular hydrogen bonds, in which the donor-acceptor distance ($d_{D\cdots A}$) is 2.68 Å and N-H**…**N bond angle is 140°. Polymorph **III** has R_2^2 (8) hydrogen-bond synthon containing N-H**…**S hydrogen bonds (Table 2.1).

The common feature of the three polymorphs of **2.1** is the presence of homomeric $R_2^2(8)$ type hydrogen-bonded assemblies (Figure 2.9a). Earlier similar assemblies in benzoyl-carvacryl thiourea derivatives forming planar dimeric chain were reported.[24]

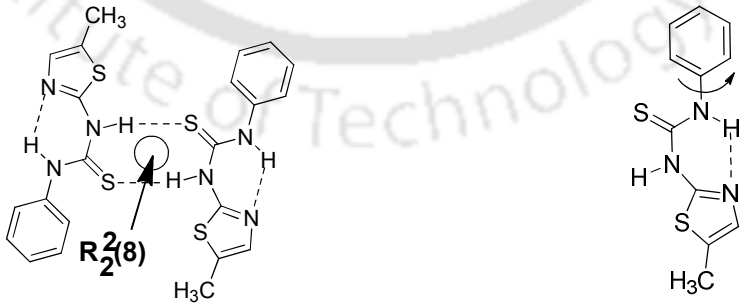

(a) (b)

*Figure 2.9: (a) Schematic Diagram of the homodimeric assembly present within the crystal lattices of polymorphs of **2.1**, (b) rotation of the phenyl ring over the intramolecularly locked hydrogen bonded six membered ring.*

In compound **2.1**, phenyl group connected to the thioamide bond is free to rotate over the intramolecularly hydrogen bonded six-membered ring as shown in Figure 2.9b. This six-membered ring can also be called as synthon having graph set notation S(6) (Figure 1.2a, Chapter 1). Due to this free rotation, there occurs a difference in orientation of the phenyl group with respect to a plane containing the 5-methylthiazole unit in respective polymorphs as illustrated in Figure 2.10b. To explain the orientations, two independent planes may be constructed with dihedral angle C11-C6-N3-C5 (**τ**) as illustrated in Figure 2.10a. The dihedral angle **τ** is 81.91° for Polymorph **I** and 123.06° for Polymorph **III**, whereas Polymorph **II**, with two symmetry-nonequivalent molecules, has dihedral angles 160.11° and 54.04° for the two symmetry-independent molecules. Thus, in each polymorph the phenyl ring lies in a different plane with respect to the thiourea plane, providing characteristic packing patterns.

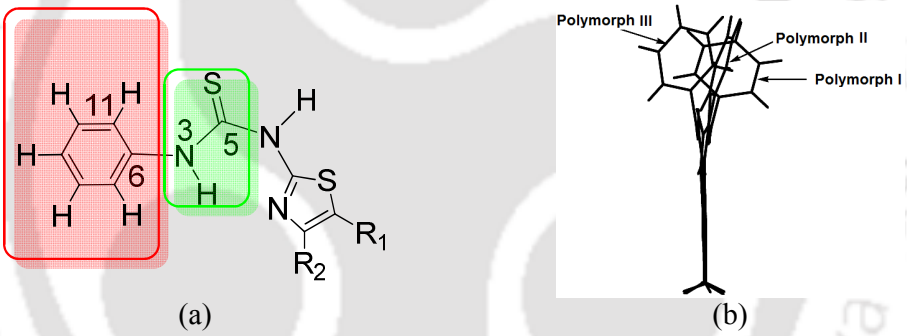

(a) (b)

*Figure 2.10: (a) Representation of the plane of the phenyl ring with respect to the thioamide plane polymorphs of **2.1** and **2.2**, (b) overlaid diagram showing orientations of the phenyl group in three polymorphs of **2.1** (drawn by fixing the 5-methylthiazole unit in one plane).*

We have also observed differences among the arrangements of dimeric assemblies in the respective crystal lattices of the polymorphs. Assemblies of polymorph **I** comprise hydrogen-bonded dimers arranged in such a way that, when viewed along a sequence of linearly placed molecules in the lattice, these are related by a 2_1 screw axis. Thus, phenyl groups present on alternate molecules are oriented toward opposite sides as shown in Figure 2.11a. On the other hand, there are two symmetry independent molecules in the hydrogen-bonded dimer of polymorph **II**. These dimers occur in pairs, forming a sheet-like arrangement, shown in Figure 2.11b. In such an

arrangement, the phenyl groups of molecules in the next layer are placed nearly perpendicular to each other.

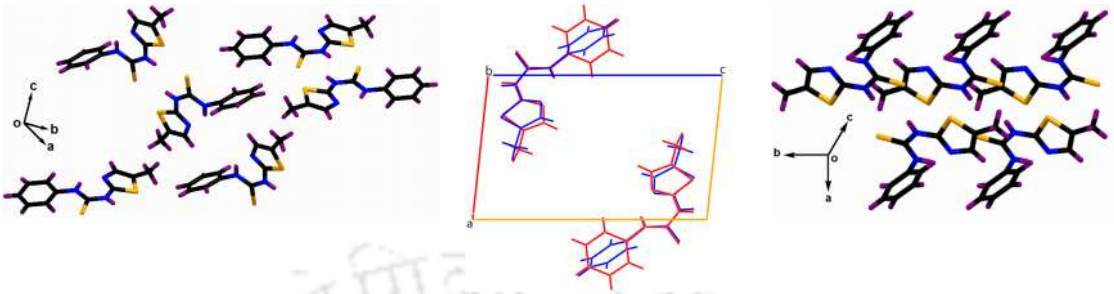

(a) (b) (c)

*Figure 2.11: Packing patterns of (a) Polymorph **I**, (b) Polymorph **II**, and (c) Polymorph **III**.*

In the lattice of polymorph **III** the molecules are positioned in an orderly manner along the *b*-crystallographic axis such that the phenyl rings are present on one side. Such chains occur in pairs, in which two chains are related by a mirror plane of reflection (Figure 2.11c). Thus, it is clear that the three polymorphs are result of differences in the arrangements of their dimeric assemblies within their respective crystal lattices.

Table 2.1: Hydrogen bond parameters for the polymorphs of **2.1** and compound **2.2**.

Compd No.	D-H···A [symmetry]	$d_{D-H(Å)}$	$d_{H\cdots A(Å)}$	$d_{D\cdots A(Å)}$	∠D-H···A(°)
Polymorph I	N(2)-H(2) ···S(2)	0.86	2.48	3.3118(19)	163
	N(3)-H(3) ···N(1) [-x,1-y,-z]	0.86	2.01	2.707(2)	137
Polymorph II	N(2)-H(2) ···S(4) [-x,1-y,-z]	0.86	2.54	3.361(3)	161
	N(3)-H(3) ···N(1)	0.86	1.98	2.716(5)	143
	N(5)-H(5) ···S(2) [-x,1-y,-z]	0.86	2.54	3.355(3)	158
	N(6)-H(6) ···N(4)	0.86	1.95	2.691(6)	144
	C(7)-H(7) ···S(2)	0.93	2.64	3.208(4)	120
	C(18)-H(18) ···S(4)	0.93	2.61	3.214(5)	123
Polymorph III	N(3)-H(2) ···N(1)	0.86	1.97	2.685(3)	140
	N(2)-H(3) ···S(2) [1/2-x,-1/2-y,-z]	0.86	2.54	3.345(2)	155
2.2	N(2)-H(2) ···S(2) [2-x,2-y,1-z]	0.86	2.50	3.330(3)	163
	N(3)-H(3A) ···N(1)	0.86	1.99	2.698(4)	139

2.2.2: Supramolecular assembly of polymorphs of 2.2

The polymorphism exhibited by **2.1** has generated interest in investigating the structural aspects of another positional isomer 1-(4-methylthiazol-2-yl)-3-phenylthiourea (**2.2**) with a methyl group at another position of thiazole unit. Crystallization of **2.2** was pursued from solutions in different solvents such as MeOH, THF, and DMF; however, from all these solutions, we observed crystallization of

only one type of crystals belonging to triclinic $P\bar{1}$ space group. Crystal structure of **2.2** displays an intramolecular N-H**…**N interaction with $d_{D\cdots A}$ 2.69 Å and N-H**…**N bond angle 133° (Table 2.1).

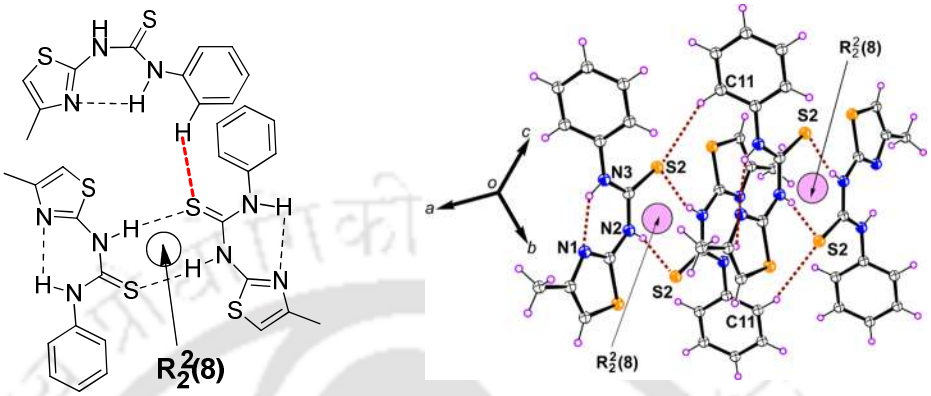

(a) (b)

*Figure 2.12: (a) Homodimeric assembly along with C-H**…**S hydrogrn bond present within the crystal lattice of **2.2**, (b) self-assembly in of **2.2** (drawn with 30% thermal ellipsoids).*

Compound **2.2** also exhibits $R_2^2(8)$ type synthons through N-H**…**S hydrogen bonds. These synthons are similar to form homodimeric assembly that of **2.1** as shown in Figure 2.12a. In addition to these common features, an additional feature observed in the case of **2.2,** is the intermolecular C11-H**…**S2 bond with an aromatic C-H unit (Figure 2.12a). This particular hydrogen bond resulted in the formation of a three-dimensional assembly of dimeric units (Figure 2.12b). The C-H bonds acting as donors are of considerable interest due to their influence on stabilization of conformers and roles in supramolecular chemistry.[25-27] The C-H**…**S hydrogen bonds help in locking of conformation of enantiomer to obtain a selective optical isomer.[28] The dihedral angle **τ** of **2.2** as defined in Figure 2.10a is 125.08°. This shows that the orientation of the phenyl ring in any polymorph of **2.1** as well as in **2.2** is different. But, due to the locking the orientation of the phenyl group through C-H**…**S hydrogen bond, in the case of **2.2**, we observed monomorphism,

2.2.3: Gas phase DFT Calculation

We calculated the energies associated with the conformational polymorphs of **2.1** and with **2.2** in gas phase. B3LYP/6-31++g(d,p)-level calculations to show that the three polymorphs of **2.1** have identical energy, whereas the positional isomer **2.2** is more

stable than **2.1** and the energy difference is 1.374 26 kcal/mol. Polymorph **II** has two symmetry-independent molecules in its asymmetric unit. Thus for energy calculation, both symmetry-independent molecule of Polymorph **II** separately treated to calculate individual energies and took average of the two energy values. Packing effects were ignored as we carried out gas-phase calculations. The Z values for Polymorph **I** and Polymorph **II** are 4, whereas the Z value for Polymorph **III** is 8. On the other hand, the Z′ values of Polymorph **I**, Polymorph **II**, and Polymorph **III** are 1, 2, and 1, respectively. The higher Z′ values are generally associated with metastable states.[29-32] In this case, the polymorph with higher Z′ value is not a metastable state; it also has equal energy with other two polymorphs. The role of solvent in generating different Z′ values was revealed earlier by isolation of different solvates of the same compound with different Z′ values.[33] The present results on selective crystallization of polymorphs from particular solvents has provided support to the role of solvent in stabilization of different conformers.

2.2.4: Differential scanning calorimetry study

Differential scanning calorimetry (DSC) helps to understand thermal behaviors of the different polymorphs.[34-35] Differential scanning calorimetry of the three polymorphs of **2.1** showed similar features by showing melting cum phase transition having two closely spaced endothermic peaks. On cooling none of the polymorph showed exothermic peak that are commonly observed in recrystallization process. This is presumably attributed to the loss of crystallinity upon melting as seen in the additional peak close to melting point. In an earlier case with polymorph of 4-Nitro-N-(quinolin-8-yl) benzamide, two close exothermic point was observed,[36] where one point corresponds to melting of the sample and the other due to liquid crystal like property. The phenomenon was studied by optical microscope to show such phase transition. In the present case, two exothermic peaks of the polymorphs are very close and optical microscopy was not performed. The differences in melting temperature of polymorphs of **2.1** range 170-182 °C shows their comparable stabilities as shown in Figure 2.13.

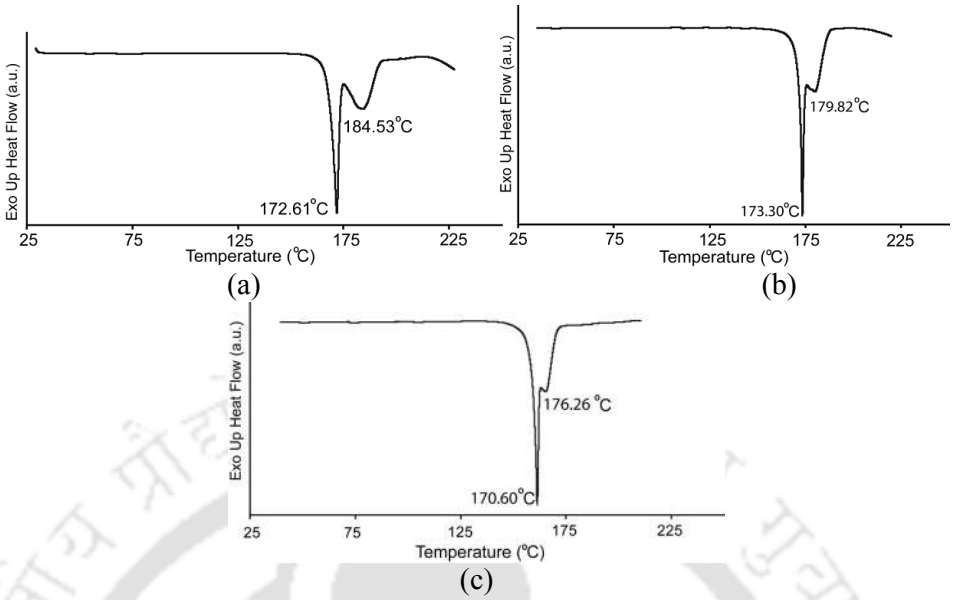

Figure 2.13: DSC plots obtained for heating at a rate of 5 ºC /min of the polymorph (a) ***I****, (b)* ***II*** *and (c)* ***III****.*

2.3: Anion Guided Assemblies of 2.1 and 2.2

Supramolecular chemistry of anions is important in biology,[36-40] medicines, catalysis, ion exchange processes and in environment.[41-44] Generally, neutral or cationic substrates interact with anions through hydrogen bonding. Many host system possesses selective anion binding site to act as host in which interactions are guided by weak dispersive forces.[45-50] As discussed in Chapter 1, Thiazole based molecules act as good host for anion binding purposes. Anions also guided the protonated host to form various supramolecular architectures.[51] Supramolecular architectures assembled from various delicate non-covalent interactions such as hydrogen bonds, π**…**π stacking, C-H**…**π and electrostatic interactions, etc., have attracted intense interest in recent years because of their wide applications for catalysis, material and life sciences.[36,37] Especially, the application of intermolecular hydrogen bonds is a well-known and efficient tool in the field of organic crystal design because of its strength and directional properties.[38]

Deng et al. designed nitrate (NO_3^-) and perchlorate (ClO_4^-) guided supramolecular architectures of N-containing flexible bis(pyridyl)-based organic molecules.[52] Some of the assembly is shown in Figure 2.14. It demonstrates that the conformations of the flexible bis(pyridyl) molecules and the variation of the anions can modulate the

structures of the supramolecular assemblies (Figure 2.14). Since compound **2.1** and **2.2** also posses heterocyclic unit which can be protonated and thiourea moiety can alter structure by adopting different conformations; we have studied the effect of anion binding to influence self-assembly and packing pattern.

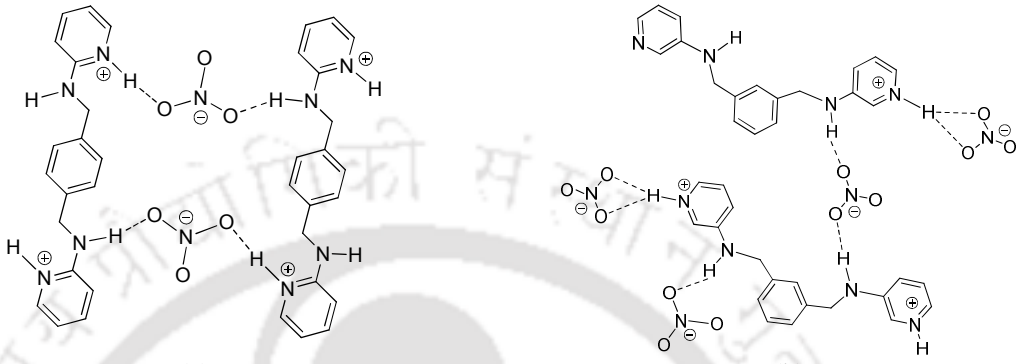

(a) (b)

Figure 2.14: Supramolecular architectures formed by bis(pyridyl)-based organic molecules.

A series of different salts of **2.1** and **2.2** were prepared by reacting them independently with different inorganic acids. The whole results are summarized in the Table 2.2. All the salts were characterized by FT-IR, ^{1}H-NMR and finally by single crystal X-ray diffraction technique. Presence of solvent molecules were also confirmed by thermogravimetric analyses.

Table 2.2: Composition of various salts of **2.1** and **2.2**

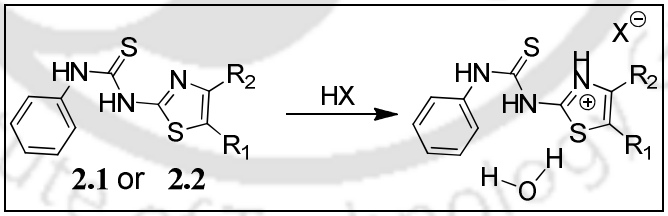

Acid/Anion	Compound **2.1**	Compound **2.2**
HCl/Cl^-	$[H(\mathbf{2.1})]_4(Cl)_4$ (**2.1a**)	**[**H(**2.2**)]Cl (**2.2a**)
HBr/Br^-	[H(**2.1**)] Br (**2.1b**)	$[H(\mathbf{2.2})]_2(Br)_2.6H_2O$(**2.2b**)
HNO_3/NO_3^-	$[H(\mathbf{2.1})]_2(NO_3)_2.H_2O$ (**2.1c**) or $[H(\mathbf{2.1})]NO_3$ (**2.1.1c**)	[H(**2.2**)]NO_3(**2.2c**)
$HClO_4/ClO_4^-$	$[H(\mathbf{2.1})]ClO_4.2H_2O$ (**2.1d**)	$[H(\mathbf{2.2})]ClO_4.H_2O$(**2.2d**)
H_2SO_4/SO_4^{2-} or HSO_4^-	$[H(\mathbf{2.1})]_2SO_4$ (**2.1e**)	[H(**2.2**)]$HSO_4.H_2O$(**2.2e**)
$H_3PO_4/H_2PO_4^-$	$[H(\mathbf{2.1})]H_2PO_4$ (**2.1f**)	No suitable crystal

2.3.1: Chloride assisted assemblies of 2.1 and 2.2

Crystallographic study have revealed that asymmetric unit of chloride salt **2.1a** contains four protonated molecules of **2.1** and four chloride anions (Figure 2.15a); each ion has independent symmetry. Both N^+-H bond of the 5-methylthiazole unit as well as N-H bonds of the thiourea act as hydrogen-bond donors and engage in hydrogen-bond formation with chloride ions. The two N-H bonds of thiourea are hydrogen-bonded to one chloride ion in each case. The assemblies of the salts have a numbers of C-H**…**Cl bonds: C14-H**…**Cl1 ($d_{D\text{-}A}$ = 3.60 Å), C3-H**…**Cl2 ($d_{D–A}$ = 3.59 Å), C43-H**…**Cl3 ($d_{D–A}$ = 3.81 Å), C25-H**…**Cl4, C32-H**…**Cl4 ($d_{D–A}$ = 3.71 Å), etc. The chloride ions are arranged along the *b*-crystallographic axis with a channel-like arrangement of the cations $[\mathbf{(2.1)H}]^+$ (Figure 2.15c) . Hydrogen bond parameters are listed in Table 2.3.

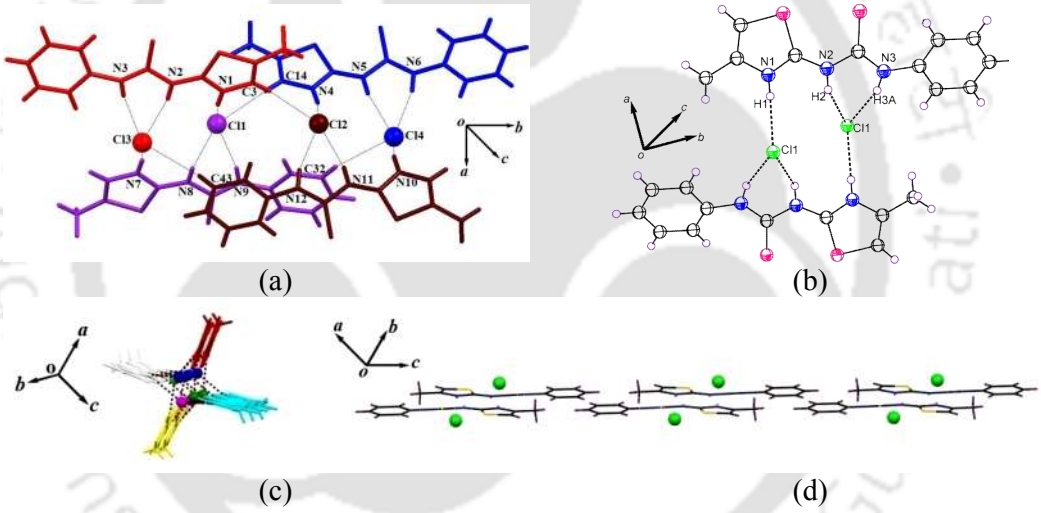

(a) (b)

(c) (d)

*Figure 2.15: Weak interactions in chloride salts (a) 2.1a and (b) 2.2a, (c) chloride ions in channel like structure in **2.1a** viewed along b-crystallographic axis, (d) one dimensional sheet like structure of chloride ions in salt **2.2a**.*

The asymmetric unit of the chloride salt **2.2a** contains one protonated molecule of **2.2** and one chloride anion. Similar to salt **2.1a**, N^+-H of the 4-methylthiazole unit and both N-H bonds of thiourea act as hydrogen-bond donors and engage in hydrogen-bond formation with the chloride ions, forming an end-capped dimeric structure (Figure 2.15b). Although these chloride salts **2.1a** and **2.2a** crystallizes in the same space group, they differ in Z' values. The packing patterns of **2.1a** and **2.2a** are different. Salt **2.2a** also has hydrogen bonds involving the chloride ions to anchor the

[**H(2.2)**]$^+$ ions through N1-H**…**Cl1 ($d_{D\cdots A}$ = 3.06 Å), N2-H**…**Cl1 ($d_{D\cdots A}$ = 3.18 Å), and N3-H**…**Cl1 ($d_{D\cdots A}$ = 3.17Å) bonds. Assembly of the [**H(2.2)**]$^+$ ions forms a one dimensional sheet-like structure (Figure 2.15d). Hydrogen bond parameters are listed in Table 2.3.

Table 2.3: Hydrogen bond parameters of **2.1a** and **2.2a:**

Compd No.	D-H**…**A [symmetry]	$d_{D\cdots H}$ Å	$d_{H\cdots A}$ Å	$d_{D\cdots A}$ Å	∠D-H···A (°)
2.1a	N(1)-H(1) ··· Cl(1)	0.89(3)	2.19(3)	3.034(3)	157(3)
	N(2)- H(2) ··· Cl(3)	0.87(3)	2.32(3)	3.162(3)	163(3)
	N(3)- H(3A) ··· Cl(3)	0.87(4)	2.37(4)	3.195(3)	159(3)
	N(4)-H(4) ··· Cl(2)	0.90(3)	2.20(3)	3.056(3)	161(3)
	N(5)-H(5) ··· Cl(4) [1-x,1-y,1-z]	0.85(3)	2.31(3)	3.124(3)	161(3)
	N(6)- H(6) ··· Cl(4) [1-x,1-y,1-z]	0.90(3)	2.32(3)	3.192(3)	164(3)
	N(7)-H(7A) ··· Cl(3)	0.91(3)	2.22(3)	3.085(3)	157(3)
	N(8)- H(8A) ··· Cl(1)	0.89(3)	2.27(3)	3.113(3)	159(2)
	N(9)- H(9A) ··· Cl(1)	0.92(3)	2.27(3)	3.151(3)	160(3)
	N(10) -H(10A) ··· Cl(2)	0.90(4)	2.34(3)	3.215(3)	164(3)
	N(11)- H(11A) ··· Cl(2)	0.82(4)	2.32(4)	3.121(3)	165(3)
	N(12)- H(12) ··· Cl(4)	0.94(4)	2.17(3)	3.036(3)	154(3)
	C(3)- H(3) ··· Cl(2)	0.94(3)	2.68(3)	3.587(3)	163(2)
	C(7)- H(7) ··· S(2)	0.94(4)	2.58(5)	3.225(5)	126(3)
	C(14) - H(14) ··· Cl(1)	0.91(3)	2.70(3)	3.601(3)	172(2)
	C(18)- H(18) ··· S(4)	0.89(3)	2.60(3)	3.229(5)	129(2)
	C(25)- H(25) ··· Cl(4) [1-x,-y,1-z]	0.94(3)	2.70(3)	3.630(3)	169(2)
	C(29)- H(29) ··· S6	0.95(4)	2.58(5)	3.244(5)	128(3)
	C(43)-H(43) ··· Cl(3)	0.97	2.87	3.806	163
	C(32)-H(32) ···Cl4	0.97	2.85	3.710	148
	C(36)- H(36) ··· Cl(3) [1-x,-y,1-z]	0.87(3)	2.81(3)	3.670(4)	170(2)
2.2a	N(1)-H(1) ···Cl(1) [1-x,1-y,1-z]	0.85(4)	2.24(4)	3.058(3)	161(3)
	N(2)-H(2) ···Cl(1) [1+x,-1+y,z]	0.87(4)	2.40(4)	3.177(3)	148(3)
	N(3)-H(3A) ···Cl(1) [1+x,-1+y,z]	0.84(3)	2.37(3)	3.175(3)	161(3)

2.3.2: Bromide assisted assemblies of 2.1 and 2.2

Crystals of the bromide salt of **2.1b** belong to monoclinic *I2/c* space group. The crystallographic asymmetric unit contains one protonated molecule of **2.1** and one bromide anion. The N^+-H bond of the 5-methylthiazole unit and both N-H bonds of the thiourea unit act as hydrogen bond donor to the bromide anion (Figure 2.16a). Apart from this, the sulfur atom of the thiocarbonyl group participates in a C-H**…**S bond with the methyl proton of methylthiazole. Such interactions lead to one-dimensional polymeric sheet-like structure, where bromide ions are intercalated between two oppositely oriented protonated **2.1** molecules along the *b*-crystallographic axis.

The bromide salt of **2.2b**, is a trihydrate, but it is observed in the form of a dimeric assembly with composition (H**2.2**)$_2$(Br)$_2$·6H$_2$O. The crystals of **2.2b** belong to monoclinic space group $P2_1/n$. The crystallographic asymmetric unit of **2.2b** contains

two protonated molecules of **2.2**, two bromide anions, and six water molecules from crystallization.

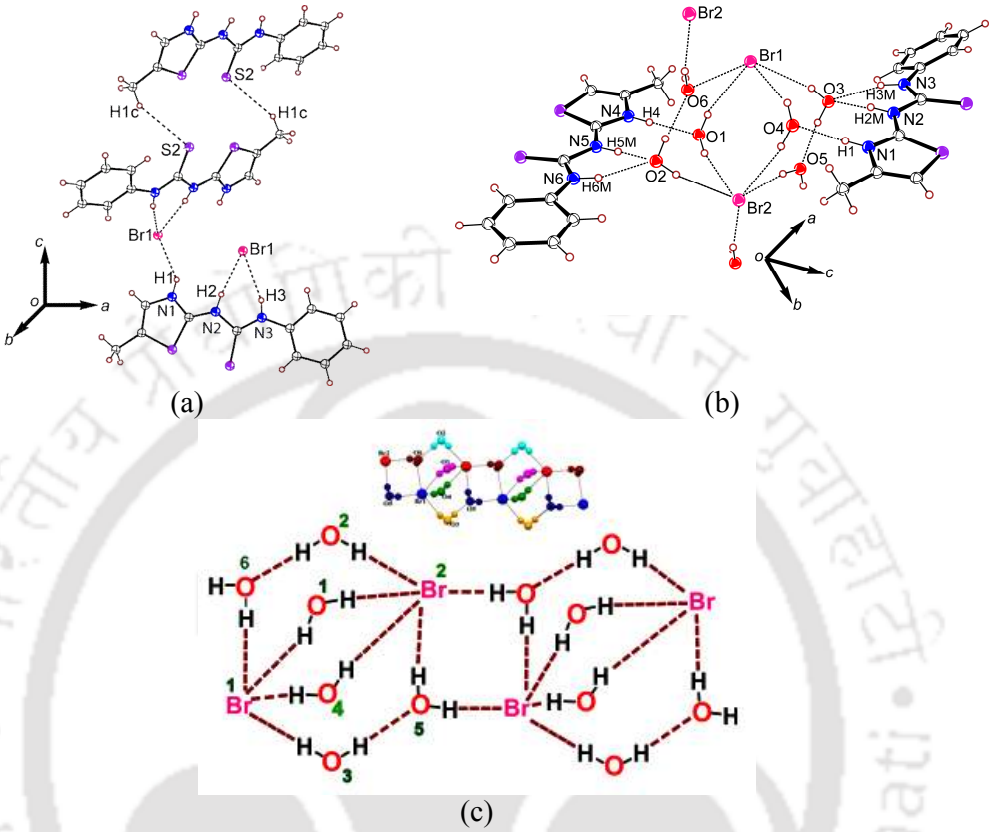

Figure 2.16: Various weak interactions in (a) ***2.1b*** *and (b)* ***2.2****. (c) Schematic diagram of two units of bromide-water clusters present in* ***2.2b****, inset: bromide-water cluster in ball and stick model.*

The cationic host $[\mathbf{H(2.2)}]^{+}$ provides the required platform to accommodate a bromide-water cluster of composition $[(Br)_2(H_2O)_6]^{2-}$. The bromide-water cluster held between the cations is shown in Figure 2.16c. Each octameric cluster consisting of two bromide anions and six water molecules is connected to another similar octameric cluster through O-H**…**Br via $R_2^2(8)$ hydrogen-bond synthon. The cluster looks like an octahedron where bromide ions occupy the opposite vertices. The two different bromide anions are strongly held in the lattice through several O-H**…**Br interactions, as depicted in Figure 2.16c. Hydrogen bond parameters are listed in Table 2.4. Discrete cubane-like bromide-water cluster[53] as well as propeller shape bromide-water cluster[54] were reported earlier as shown in Figure 2.17. We find a new octameric bromide-water cluster added to the database.

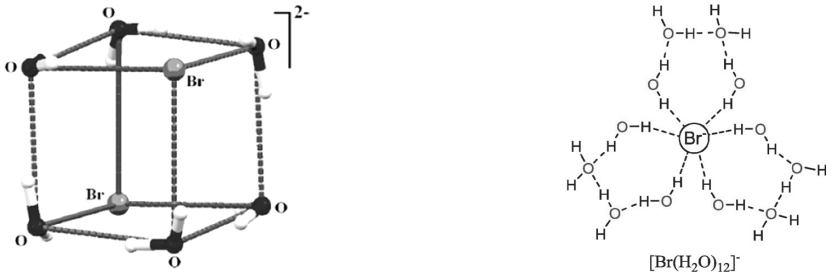

(a) (b)

Figure 2.17: (a) cubane-like bromide-water cluster, (b) propeller shape bromide-water cluster.

Table 2.4: Hydrogen bond parameters of **2.1b** and **2.2b**

Compd No.	D-H…A [symmetry]	$d_{D\cdots H}$ Å	$d_{H\cdots A}$ Å	$d_{D\cdots A}$ Å	∠D-H···A (°)
2.1b	N1-H1 ··· Br1 [x,1+y,z]	0.85(2)	2.59(3)	3.277(3)	138(3)
	N(2) --H(2) ..Br(1) [1/2-x,1/2+y,-z]	0.87(3)	2.35(3)	3.217(3)	173(4)
	N(3) --H(3) ..Br(1) [1/2-x,1/2+y,-z]	0.85(2)	2.66(3)	3.458(3)	158(3)
	C(7) --H(7) ..S(2)	0.91(4)	2.60(4)	3.213(5)	125(3)
2.2b	N(1)-H(1) ···O(4) [-1+x,y,z]	0.86	1.89	2.715(7)	162
	O(1)-H(1P) ···Br(2)	0.85(6)	2.55(6)	3.380(6)	164(5)
	O(1)-H(1Q) ···Br(1)	0.83(5)	2.50(5)	3.311(6)	164(4)
	N(2)-H(2M) ···O(3)	0.86	2.00	2.797(7)	154
	N(3)-H(3M) ···O(3)	0.86	2.07	2.884(7)	158
	O(3)-H(3P) ···Br(1) [-1+x,y,z]	0.83(3)	2.55(4)	3.353(6)	165(4)
	O(3)-H(3Q) ···O(5) [1/2-x,1/2+y,1/2-z]	0.84(4)	1.83(4)	2.660(9)	171(5)
	N(4)-H(4) ···O(1) [1-x,1-y,-z]	0.86	1.87	2.708(7)	165
	O(4)-H(4P) ···Br(1)	0.84(6)	2.60(6)	3.350(6)	150(6)
	O(4)-H(4Q) ···Br(2)	0.83(4)	2.51(5)	3.296(6)	158(5)
	N(5)-H(5M) ···O(2) [1-x,1-y,-z]	0.86	1.97	2.777(7)	156
	O(5)-H(5P) ···Br(2) [3/2-x,-1/2+y,1/2-z]	0.86(6)	2.55(5)	3.393(7)	168(10)
	O(5)-H(5Q) ···Br(1) [3/2-x,1/2+y,1/2-z]	0.82(2)	2.53(3)	3.306(6)	158(4)
	N(6)-H(6M) ···O(2) [1-x,1-y,-z]	0.86	2.05	2.878(8)	160
	O(6)-H(6P) ···Br(2)	0.84(3)	2.48(4)	3.303(7)	170(4)
	O(6)-H(6Q) ···Br(1) [x,1+y,z]	0.85(7)	2.88(7)	3.389(7)	120(5)
	O(2)-H(8P) ···O(6) [x,-1+y,z]	0.84(4)	1.84(4)	2.685(9)	176(4)
	O(2)-H(8Q) ···Br(2	0.83(5)	2.49(5)	3.297(6)	166(5)

2.2.3: Nitrate assisted Assemblies of 2.1 and 2.2

We obtained hydrated and anhydrous form of nitrate salts of **2.1**, namely, $(H\mathbf{2.1})_2(NO_3)_2{\cdot}H_2O$ (**2.1c**) and (H**2.1**)·NO3 (**2.1.1c**). The hydrated form **2.1c** was obtained from reaction in aqueous methanol solution of **2.1** and the crystals belong to triclinic space group $P\bar{1}$, while the crystals of anhydrous form **2.1.1c** were obtained from reaction of **2.1** with nitric acid in dry methanol and crystallize in monoclinic space group $P2_1/n$. Structural analysis of **2.1c** revealed that the primary interactions of one nitrate ion are established through N-H**…**O hydrogen bonds, forming $R_2^2(8)$ synthons between the thiourea moiety of the protonated host and nitrate ion (Figure 2.18a). There are two symmetry-nonequivalent nitrate ions in the asymmetric unit; these ions are bridged by water molecules through O-H**…**O bonds. The oxygen atom

O4 forms two hydrogen bonds, while the O3 atom is involved in three hydrogen bonds. The hydrogen bonds of N6-H**…**O4 and O7-H**…**O4 have $d_{D...A}$ 2.85 and 2.83 Å and ∠D-H**…**A angles 167° and 165°, respectively. The hydrogen bonds associated with O3 to connect N3-H, C11-H, and O7-H have D**…**A distances of 2.816(3)-2.799(4) Å, which are in the range permissible to have weak hydrogen bonds.[9] The asymmetric unit of the anhydrous nitrate salt contains two protonated host molecules and two nitrate ions. As the two NO_3^- ions are symmetrically nonequivalent, only one of the nitrate ions is involved in the $R_2^2(8)$ synthons formed by N-H**…**O hydrogen bonds between the thiourea moiety of the protonated host and nitrate ion (Figure 2.18b). The O1, O2, and O4 atoms are involved in formation of bifurcated hydrogen bonds. Hydrogen bond parameters are listed in Table 2.5.

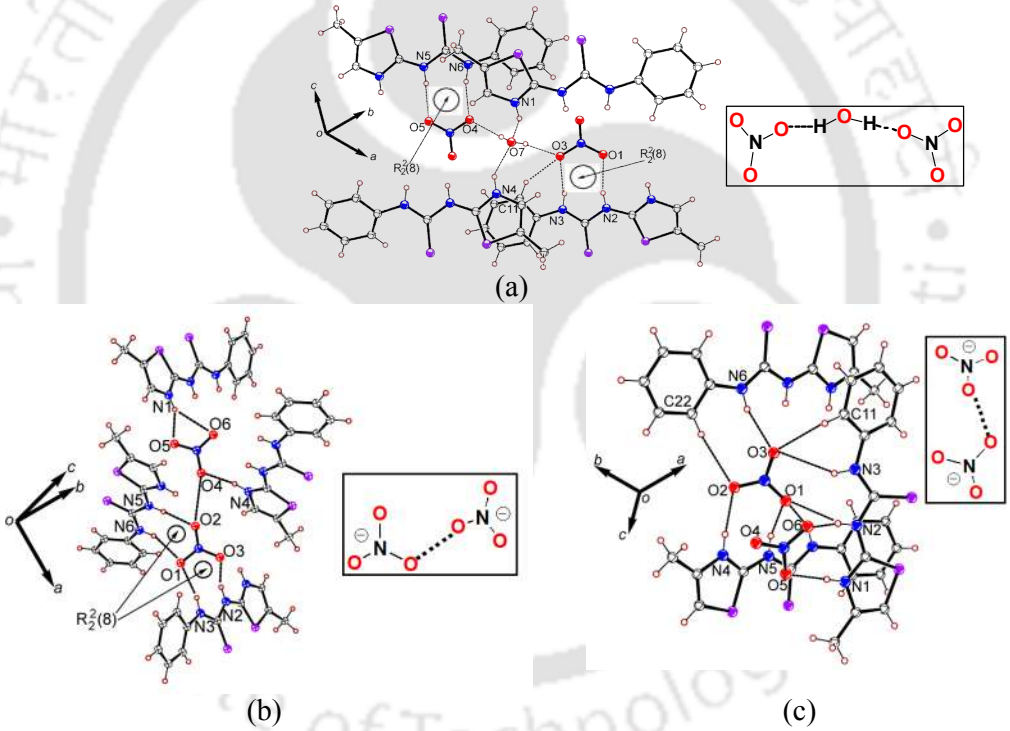

Figure 2.18: (a) Assembly of hydrated nitrate salt ***2.1c,*** *inset: water bridging nitrate anions. Hydrogen bonds in anhydrous nitrate salts (b)* ***2.1.1c****, and (c)* ***2.2c****, inset: nitrate**…**nitrate interactions.*

Unlike the hydrated form **2.1c**, in **2.1.1c** there is no water molecule bridging between the nitrate ions. Nitrate**…**nitrate interactions among the anions are observed in the solid state structure of **2.1.1c** (Figure 2.18b). Nitrate**…**nitrate interactions in urea derivatives in the solid state were reported earlier,[55] which had shorter

oxygen**…**oxygen distances than the distances observed by us. Nitrate**…**nitrate interactions in the solid state have a role in the packing of nitrate salts.[56] We also find a similar observation as shown in the packing diagram of anhydrous nitrate salt.

When **2.2** was acidified with nitric acid, we obtained only the anhydrous form (H**2.2**)NO_3 (**2.2c),** which crystallizes in monoclinic space group $P2_1/n$. The crystallographic asymmetric unit of the salt contains two protonated molecules of **2.2** and two planar NO_3^- anions. **2.2** is coordinated with nitrate ion through N-H**…**O, N^+-H**…**O^-, and C-H**…**O hydrogen bonds (Figure 2.18c). Like **2.1c** and **2.1.1c**, there are no cyclic synthons among the thiourea unit and the nitrate ions in **2.2c**. But as like **2.1.1c**, salt **2.2c** also has nitrate**…**nitrate interactions.

Table 2.5: Hydrogen bond parameters of **2.1c**, **2.1.1c** and **2.2c**

Compd No.	D-H**…**A [symmetry]	$d_{D\cdots H}$ Å	$d_{H\cdots A}$ Å	$d_{D\cdots A}$ Å	∠D-H···A (°)
2.1c	N(1)-H(1) ···O(7) [1+x,y,z]	0.86(3)	1.97(3)	2.760(4)	151(3)
	N(2)-H(2) ···O(1) [1-x,1-y,1-z]	0.82(3)	2.07(3)	2.857(4)	162(3)
	N(3)-H(3) ···O(3) [1-x,1-y,1-z]	0.85(3)	1.98(2)	2.818(3)	171(2)
	N(4)-H(4) ···O(7) [x,-1+y,z]	0.82(3)	2.12(3)	2.822(4)	143(3)
	N(5)-H(5) ···O(5)	0.85(3)	1.98(3)	2.808(3)	165(3)
	N(6)-H(6) ···O(4)	0.84(3)	2.02(3)	2.846(4)	170(3)
	O(7)-H(9P) ···O(4) [1-x,1-y,1-z]	0.81(4)	2.04(4)	2.830(4)	165(5)
	O(7)-H(10P) ···O(3)	0.74(3)	2.07(3)	2.798(4)	166(3)
	C(7)-H(7) ···S(2)	0.93(3)	2.68(3)	3.217(4)	118(2)
	C(14)-H(14) ···O(1) [-x,-y,1-z]	0.88(3)	2.56(3)	3.403(4)	162(3)
	C(14)-H(14) ···O(2) [-x,-y,1-z]	0.88	2.69	3.432	143
	C(18)-H(18) ···S(4)	0.96(3)	2.73(3)	3.257(4)	115(2)
	O(7)-H(9P) ···O(4)	0.80	2.04	2.830	165
	C(11)-H(11) ···O(3)	0.92	2.65	3.314	129
2.1.1c	N(1)-H(1) ···O(5) [x,-1+y,z]	0.86	1.86	2.660	154
	N(1)-H(1) ···O(6) [x,-1+y,z]	0.86	2.50	3.238	144
	N(2)-H(2) ···O(3)	0.86	1.95	2.756	155
	N(3)-H(3A) ···O(1)	0.86	2.10	2.947	167
	N(3)-H(3A) ···O(3)	0.86	2.55	3.231	137
	N(4)-H(4) ···O(4)	0.86	1.90	2.750	167
	N(5)-H(5) ···O(2)	0.86	2.05	2.879	161
	N(6)-H(6) ···O(1)	0.86	2.19	2.996	156
	N(6)-H(6) ···O(2)	0.86	2.47	3.213	145
2.2c	N(1)-H(1) ···O(5)	0.88(3)	1.85(3)	2.730(5)	179(4)
	N(2)-H(2) ···O(6)	0.86(2)	2.00(2)	2.833(5)	164(3)
	N(2)-H(2) ···O(1) [1/2-x,-1/2+y,1/2-z]	0.86(2)	2.58(3)	3.072(4)	117(2)
	N(3)-H(3A) ···O(1) [1/2-x,-1/2+y,1/2-z]	0.85(3)	2.37(3)	3.119(4)	147(3)
	N(3)-H(3A) ···O(3) [1/2-x,-1/2+y,1/2-z]	0.85(3)	2.57(3)	3.344(5)	152(2)
	N(4)-H(4) ···O(2) [1/2-x,-1/2+y,1/2-z]	0.89(4)	1.92(4)	2.801(5)	169(3)
	N(5)-H(5) ···O(1) [1/2-x,-1/2+y,1/2-z]	0.87(3)	1.90(3)	2.766(4)	169(3)
	N(6)-H(6) ···O(3) [1/2+x,1/2-y,1/2+z]	0.86(3)	2.14(3)	2.917(5)	150(3)
	C(7)-H(7) ···S(2)	0.98(4)	2.56(3)	3.203(5)	123(2)
	C(11)-H(11) ···O(3) [1/2-x,-1/2+y,1/2-z]	0.96(3)	2.51(2)	3.217(6)	130.6(19)
	C(14)-H(14) ···O(4) [1-x,-y,-z]	0.91(4)	2.41(4)	3.278(6)	160(3)
	C(18)-H(18) ···S(4)	1.02(3)	2.48(3)	3.226(6)	129(2)
	C(22)-H(22) ···O(2) [1/2+x,1/2-y,1/2+z]	0.94(4)	2.48(3)	3.493(6)	172(3)

2.2.4: Perchlorate assisted Assemblies of 2.1 and 2.2

The perchlorate salt (H**2.1**)$ClO_4 \cdot 2H_2O$ (**2.1d**) crystallizes in monoclinic space group $P2_1/a$. The asymmetric unit contains one protonated molecule of **2.1**, one perchlorate

anion, and two water molecules from crystallization. The two N-H bonds, N2-H and N3-H (Figure 2.19a), are connected to a water molecule through N2-H**…**O6 and N3-H**…**O6 hydrogen bonds. Two hydrogen-bonded water molecules are positioned linearly between two perchlorate anions. The O1, O2, O5, and O6 atoms are independently involved as hydrogen-bond acceptors. The perchlorate anion interacts with the water molecules, forming $R_3^5(14)$ and $R_3^4(12)$ synthons resulting in O-H**…**O hydrogen bonds (Figure 2.19c). Hydrogen bond parameters are listed in Table 2.6. Perchlorate anion with the aid of hydrogen bonds achieves water-assisted three-dimensional assembly. The xanthine perchlorate salt is a dihydrate,[57] in which the water molecules form hydrogen bonds with two donor sites and one acceptor site. In comparison to this, salt **2.1d** is also a dihydrate, but in this case water molecules participate in hydrogen bonds by providing two acceptor and two donor sites.

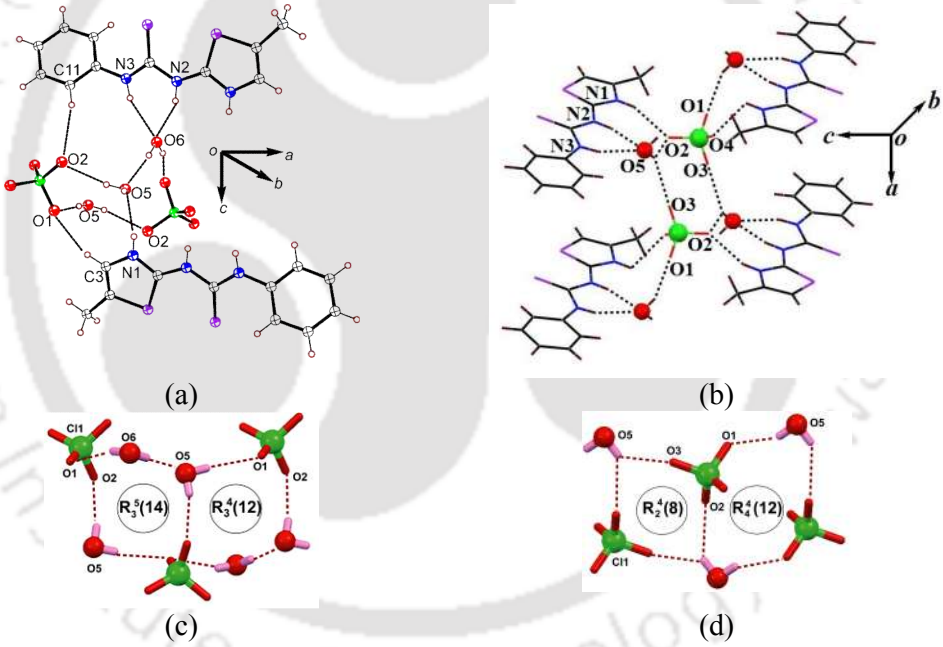

*Figure 2.19: Supramolecular assembly of (a) perchlorate salt **2.1d**, (b) perchlorate salt **2.2d**, (c) $R_3^5(14)$ and $R_3^4(12)$ hydrogen-bond synthons within the lattice of salt **2.1d**, (d) $R_2^4(8)$ and $R_4^4(12)$ hydrogen-bond synthons in salt **2.2d**.*

On the other hand, a monohydrate salt, (H**2.2**)$ClO_4 \cdot H_2O$ (**2.2d**), was obtained from the reaction of perchloric acid with compound **2.2**. The hydrogen-bond environment around perchlorate anion of hydrated salt **2.2d** is shown in Figure 2.19b. In the lattice of **2.2d**, the thiourea N-H and N^+-H of the 4-methylthiazole moiety act as hydrogen-

bond donors. The O2 and O5 atoms are involved in bifurcated hydrogen bonds. The monohydrate salt of **2.2** has water molecules participating in $R_2^4(8)$ and $R_4^4(12)$ synthons comprising O-H**…**O hydrogen bonds with the perchlorate ions (Figure 2.19d). Hydrogen bond parameters are listed in Table 2.6. This hexameric cyclic hydrogen-bonded assembly formed by perchlorate ions and water molecules looks like an open book. Similar open book like assemblies were earlier observed in water hexamers.[58]

Table 2.6: Hydrogen bond parameters of **2.1d** and **2.2d**

Compd No.	D-H···A [symmetry]	$d_{D-H(Å)}$	$d_{H\cdots A(Å)}$	$d_{D\cdots A(Å)}$	∠D-H···A (°)
2.1d	N(1)-H(1) ···O(5) [-x,1-y,-z]	0.86	2.02	2.85(3)	162
	N(2)-H(2) ··· ..O(6)	0.86	1.96	2.79(3)	160
	O(5)-H(5P) ···O(1) [1/2-x,-1/2+y,-z]	0.8(2)	2.2(3)	3.01(4)	178(1)
	O(5)-H(5Q) ···O(2)	0.8(3)	2.2(3)	2.94(4)	164(1)
	O(6)-H(6P) ···O(5)	0.8(3)	2.1(3)	2.87(4)	175(1)
	O(6)-H(6Q) ···O(1) [1/2-x,1/2+y,-z]	0.8(3)	2.3(3)	3.06(4)	165(1)
	N(3)-H(9A) ···O(6)	0.86	2.20	2.97(3)	150
	C(3)-H(3A) ···O(1) [-x,1-y,-z]	0.93	2.34	3.22(4)	159
	C(7)-H(7) ···S(2)	0.93	2.84	3.23(3)	106
	C(11)-H(11) ···O(2)	0.93	2.54	3.45(4)	165
2.2d	N(1)-H(1) ···O(2) [x,y,1+z]	0.86	2.11	2.870	146
	N(1)-H(1) ···O(4) [1-x,-y,1-z]	0.86	2.46	2.976	119'
	N(2)-H(2) ···O(5) [1-x,-y,1-z]	0.86	1.97	2.813	166
	N(3)-H(3) ···O(5) [1-x,-y,1-z]	0.86	2.23	3.037	157
	O(5)-H(5M) ···O(3) [1+x,y,z]	0.84	2.36	3.019	136
	O(5)-H(5M) ···O(2) [1-x,-y,-z]	0.84	2.58	3.173	129
	O(5)-H(5N) ···O(1)	0.84	2.07	2.853	154
	C(7)-H(7) ···S(2)	0.93	2.55	3.211	129

2.2.5: Sulphate/bisulphate assisted Assemblies of 2.1 and 2.2

The asymmetric unit of the sulfate salt $(H\mathbf{2.1})_2SO_4$ (**2.1e**), belongs to triclinic space group $P\bar{1}$ and contains two protonated molecules of **2.1** and one sulfate ion. Structural analysis of the salt **2.1e** shows that one sulfate ion interacts with four neighboring $(H\mathbf{2.1})^+$ ions as shown in Figure 2.20a. Among the four $(H\mathbf{2.1})^+$ ions, two are connected through $R_2^2(8)$ synthons through N-H**…**O hydrogen bonds between $(H\mathbf{2.1})^+$ and sulfate ions. The other two cations are connected through N^+-H**…**O^- bonds. The oxygen atom (O4) of the sulfate ion is involved in three N-H**…**O bonds. A similar structural pattern involving sulfate anion was observed in a urea derivative.[56] The O1 and O2 atoms of the cationic part act as hydrogen-bond acceptors in N-H**…**O and N^+-H**…**O^- hydrogen bonds ($d_{O1\cdots N5}$ = 2.66 Å; $d_{O2\cdots N3}$ = 2.93 Å; $d_{O2\cdots N6}$ = 2.90 Å) respectively. The hydrogen bond parameters are listed in Table 2.7.

Table 2.7: Hydrogen bond parameters of **2.1e**, **2.2e** and **2.1f**

Compd No.	D-H···A [symmetry]	$d_{D\cdots H}$ Å	$d_{H\cdots A}$ Å	$d_{D\cdots A}$ Å	∠D-H···A (°)
2.1e	N(1)-H(1) ···O(4)	0.82(6)	2.30(6)	2.946(6)	137(5)
	N(1)-H(1) ···O(1) [1-x,1-y,1-z]	0.82(6)	2.45(6)	3.001(6)	126(5)
	N(2)-H(2) ···O(2)	0.79(6)	2.59(6)	3.247(7)	142(6)
	N(2)-H(2) ···O(4)	0.79(6)	2.01(6)	2.732(6)	153(6)
	N(3)-H(3) ···O(2)	0.78(6)	2.18(6)	2.933(6)	161(5)
	N(4)-H(4) ···O(4)	0.90(6)	2.09(6)	2.807(6)	136(4)
	N(4)-H(4) ···O(1) [1-x,1-y,1-z]	0.90(6)	2.57(5)	3.165(5)	125(5)
	N(5)-H(5) ···O(1) [1-x,1-y,1-z]	0.78(5)	1.92(5)	2.665(6)	161(4)
	N(6)-H(6) ···O(2) [1-x,1-y,1-z]	0.80(5)	2.11(5)	2.898(6)	169(5)
2.2e	N(1)-H(1) ··· O(2)	0.81(5)	1.93(5)	2.734(5)	173(5)
	N(2)- H(2) ··· O(1)	0.88(5)	2.04(5)	2.846(5)	152(5)
	N(2)-H(2) ···O(2)	0.88(5)	2.58(5)	3.346(5)	146(4)
	N(3)- H(3) ··· O(1)	0.85(3)	2.15(3)	2.961(5)	161(4)
	O(4) - H(4) ···O(5)	0.86(5)	1.68(5)	2.526(6)	167(5)
	O(5)- H(5M) ··· O(3) [1+x,y,z]	0.85(4)	1.97(4)	2.766(7)	156(5)
	O(5)- H(5N) ··· O(2) [1-x,1-y,-z]	0.83(5)	2.15(5)	2.861(6)	143(5)
2.1f	N(1)-H(1) ···O(1) [x,1+y,z]	0.89(18)	1.76(19)	2.633(4)	166(2)
	O(2)-H(2A) ···O(1) [1/2-x,1/2+y,1/2-z]	0.87(4)	1.61(3)	2.475(4)	177(5)
	N(2)-H(2M) ···O(3) [1/2-x,1/2+y,1/2-z]	0.89(18)	1.86(19)	2.743(4)	165(2)
	N(2)-H(2M) ···O(3) [1/2-x,1/2+y,1/2-z]	0.87(2)	2.11(2)	2.911(4)	153(2)
	O(4)-H(4A) ···O(3) [-x,y,1/2-z]	0.82	1.80	2.598(3)	165
	C(7)-H(7) ···S(2)	0.93	2.55	3.205(4)	128

On the other hand, the reaction of **2.2** with sulfuric acid enabled us to isolate only the hydrated crystalline bisulfate salt, (H**2.2**)$HSO_4 \cdot H_2O$ (**2.2e**). Interactions of the bisulfate ion with **2.2** and water molecules in the lattice are shown in Figure 2.20b. Each bisulfate anion interacts with one **2.2** molecule and two water molecules through N-H**…**O and O^--H**…**O hydrogen bonds. The lattice water molecules bridge the bisulfate ions and form a $R_4^4(12)$ hydrogen-bonded synthon (Figure 2.20c). Atom O1 of a bisulfate ion is involved in two N-H**…**O bonds through N2-H and N3-H bonds of thiourea, whereas another atom O2 of bisulfate ion acts as a pivot for three hydrogen bonds with N1-H, N2-H, and O5-H bonds. The O3 atom of another bisulfate ion connects the O5-H bond of bridging water molecule. The O1 atom of bisulfate is hydrogen-bonded to N2-H and N3-H. The hydrogen bond parameters are listed in Table 2.7. It may be mentioned that bisulfate salts find application in various devices such as sensors and batteries.[59,60] A sulfate-$(water)_3$-sulfate assembly stabilized by urea-based receptor was reported earlier.[61] Bisulfate binding to crown ethers was also reported.[62] Besides these, one-dimensional bisulfate-water chainlike structure and two-dimensional sulfate-water anionic sheet in the solid state[63] were established earlier. But in our case, $[H\mathbf{2.2}]^+$ ions interact with water molecules in the lattice through O-H**…**O bonds from two sides, forming $R_4^4(12)$ synthon, which were not observed earlier in the bisulfate-water chains.

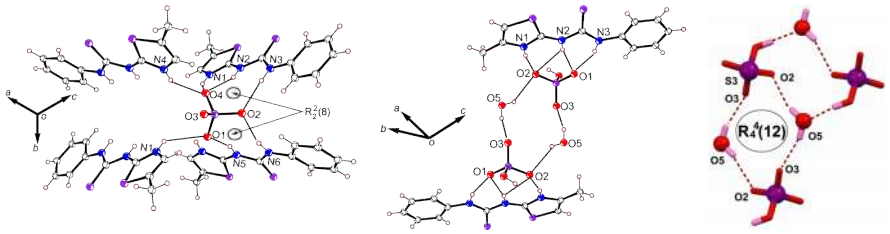

(a) (b) (c)

*Figure 2.20: (a) Crystal structure of salt **2.1e** showing environment of a sulfate ion, (b) weak interactions in the salt **2.2e**. (c) $R_4^4(12)$ hydrogen-bond synthon in bisulfate-(water)$_2$-bisulfate assembly formed within **2.2e**.*

2.2.6: Dihydrogenphosphate assisted Assemblies of 2.1 and 2.2

The reaction of orthophosphoric acid with **2.1** forms (H**2.1**)H_2PO_4 (**2.1f**); crystals of this salt belong to monoclinic space group *C2/c*. In the lattice of salt **2.1f**, both the N-H bonds of thiourea and the N-H bond of the protonated 5-methylthiazole act as hydrogen-bond donors as shown in Figure 2.21a. The protons of these bonds form strong hydrogen bonds with dihydrogen phosphate ions. The two N-H bonds of thiourea are connected to the O3 atom of dihydrogen phosphate ion, whereas the N-H bond of the protonated 5-methylthiazole is connected through a hydrogen bond to another oxygen atom of a dihydrogen phosphate ion. The anions form a cyclic interanionic assembly with $R_2^2(8)$ and $R_6^6(24)$ synthons as shown in Figure 2.21b. Atom O1 interacts with N1-H and O2-H to form two hydrogen bonds ($d_{D\cdots A}$ 2.63 and 2.47 Å and ∠D-H**…**A 166° and 177°, respectively). The hydrogen-bond acceptor atom O3 interacts with three N-H bonds, namely, N2-H and N3-H of thiourea and O4-H bonds of an anion, with D**…**A bond distances in the range 2.475-2.911 Å.

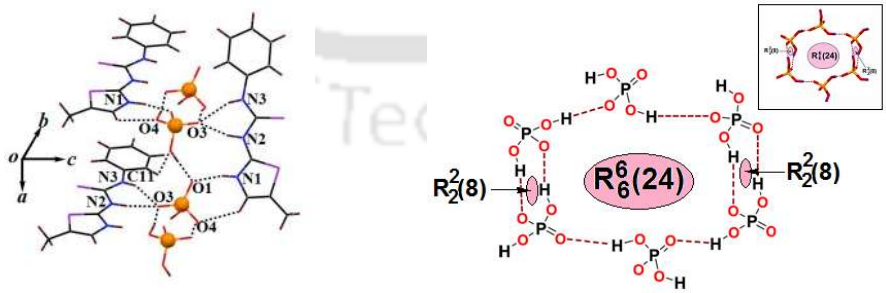

(a) (b)

*Figure 2.21: (a) Self-assembly of salt **2.1f**, (b) Hydrogen-bonded cyclic hexamer of the dihydrogen phosphate ions present in the lattice of **2.1f**, inset: hexamer is in stick model.*

Different types of dihydrogen phosphate assemblies are stabilized by using different organic hosts. For example, octameric[64] and dimeric[65] cyclic assemblies of dihydrogen phosphate anions as shown in Figure 2.22ab were reported earlier. Radu Custelcean et al. stabilized discrete $(H_2PO_4^-)_4$ and $(H_2PO_4^-)_6$ clusters as shown in Figure 2.22cd.[66] Custelcean et al. also provided a Cambridge Structural Database (CSD) survey of $(H_2PO_4^-)_n$ aggregates, established that these clusters display unique topologies and hydrogen-bonding connectivities.

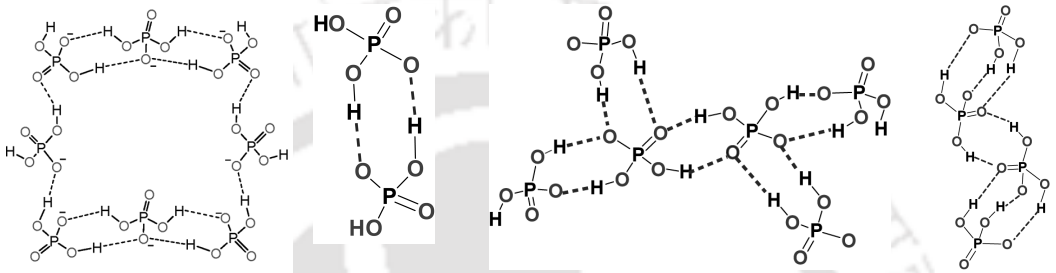

(a) (b) (c) (d)

Figure 2.22: (a) Octameric[22], (b) Dimeric[23], (c) Hexaeric[24], (d) Tetrameric[25] dihydrogen phosphate cluster.

In the present case, we have observed hydrogen-bonded cyclic hexameric assemblies of dihydrogen phosphate anions, which are held in the lattice by $(H\mathbf{2.1})^+$ ions. To the best of our knowledge, this is a new type of hexameric assembly of dihydrogen phosphate.

Table 2.8: Hydrogen bond parameters of **2.1e**, **2.2e** and **2.1f:**

Compd No.	D-H···A [symmetry]	$d_{D\cdots H}$ Å	$d_{H\cdots A}$ Å	$d_{D\cdots A}$ Å	∠D-H···A (°)
2.1e	N(1)-H(1) ···O(4)	0.82(6)	2.30(6)	2.946(6)	137(5)
	N(1)-H(1) ···O(1) [1-x,1-y,1-z]	0.82(6)	2.45(6)	3.001(6)	126(5)
	N(2)-H(2) ···O(2)	0.79(6)	2.59(6)	3.247(7)	142(6)
	N(2)-H(2) ···O(4)	0.79(6)	2.01(6)	2.732(6)	153(6)
	N(3)-H(3) ···O(2)	0.78(6)	2.18(6)	2.933(6)	161(5)
	N(4)-H(4) ···O(4)	0.90(6)	2.09(6)	2.807(6)	136(4)
	N(4)-H(4) ···O(1) [1-x,1-y,1-z]	0.90(6)	2.57(5)	3.165(5)	125(5)
	N(5)-H(5) ···O(1) [1-x,1-y,1-z]	0.78(5)	1.92(5)	2.665(6)	161(4)
	N(6)-H(6) ···O(2) [1-x,1-y,1-z]	0.80(5)	2.11(5)	2.898(6)	169(5)
2.2e	N(1)-H(1) ··· O(2)	0.81(5)	1.93(5)	2.734(5)	173(5)
	N(2)- H(2) ··· O(1)	0.88(5)	2.04(5)	2.846(5)	152(5)
	N(2)-H(2) ···O(2)	0.88(5)	2.58(5)	3.346(5)	146(4)
	N(3)- H(3) ··· O(1)	0.85(3)	2.15(3)	2.961(5)	161(4)
	O(4) - H(4) ···O(5)	0.86(5)	1.68(5)	2.526(6)	167(5)
	O(5)- H(5M) ··· O(3) [1+x,y,z]	0.85(4)	1.97(4)	2.766(7)	156(5)
	O(5)- H(5N) ··· O(2) [1-x,1-y,-z]	0.83(5)	2.15(5)	2.861(6)	143(5)
2.1f	N(1)-H(1) ···O(1) [x,1+y,z]	0.89(18)	1.76(19)	2.633(4)	166(2)
	O(2)-H(2A) ···O(1) [1/2-x,1/2+y,1/2-z]	0.87(4)	1.61(3)	2.475(4)	177(5)
	N(2)-H(2M) ···O(3) [1/2-x,1/2+y,1/2-z]	0.89(18)	1.86(19)	2.743(4)	165(2)
	N(2)-H(2M) ···O(3) [1/2-x,1/2+y,1/2-z]	0.87(2)	2.11(2)	2.911(4)	153(2)
	O(4)-H(4A) ···O(3) [-x,y,1/2-z]	0.82	1.80	2.598(3)	165
	C(7)-H(7) ···S(2)	0.93	2.55	3.205(4)	128

We could not obtain a crystalline salt from the reaction of orthophosphoric acid with **2.2**, but we did obtain a white precipitate from the reaction of phosphoric acid with **2.2**. Salt **2.1f**, which is derived from **2.1**, shows sharp P-O stretching at 988 and 1096 cm^{-1} from the dihydrogen phosphate anion,[67] and there is an overtone of O-H bending vibration at 2400 cm^{-1} due to the anion as shown in Figure 2.23a. In contrast to parent compound **2.1**, which has very broad and sharp N-H stretch at 3400 cm^{-1}, triphosphate salt **2.1f** has very broad less resolved absorptions spreading from 2500 to 3500 cm^{-1}. The white solid obtained from the reaction of **2.2** with phosphoric acid has broad and sharp N-H stretching at 3430 cm^{-1}, which is similar to the N-H stretching of parent **2.2** occurring at 3327 cm^{-1}. In addition to this, the IR spectrum is relatively simple and has a sharp P-O stretching frequency at 965 cm^{-1} as shown in Figure 2.23b, suggesting that the anhydrous phosphate salt was formed in this case. Low solubility of this salt in common solvents made it difficult to characterize further.

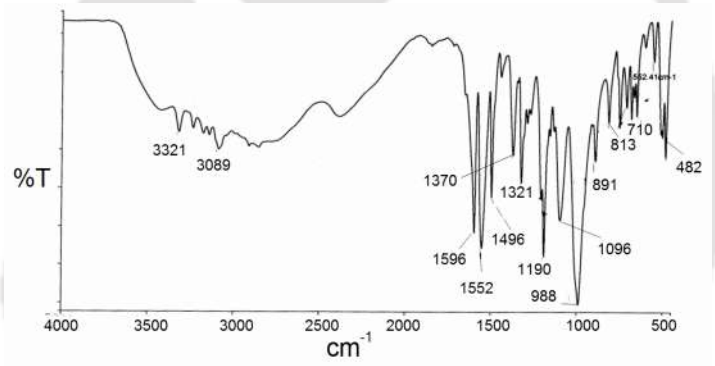

(a)

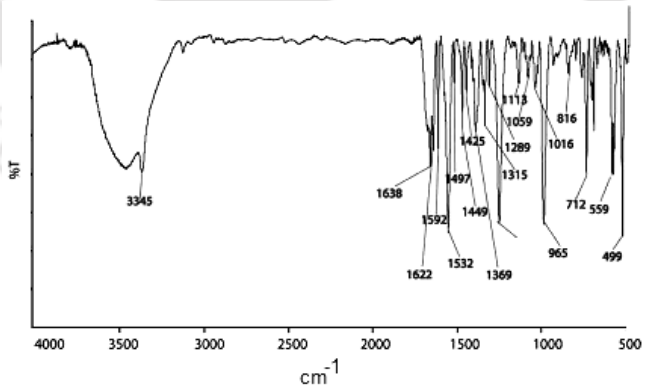

(b)

*Figure 2.23: IR-spectra (KBr) of (a) salt **2.1f**, (b) precipitate obtained from reaction **2.2** with phosphoric acid.*

2.4: Thermogravimetric study of hydrated Salts of 2.1 and 2.2

The number of water molecule present in the respective lattices of hydrated salts also confirmed by thermogravimetric analysis. Salt **2.2b** of composition $(H\mathbf{2.2})_2(Br)_2{\cdot}6H_2O$ loses 27.1% (calculated 28%) of its weight, corresponding to the loss of six water molecules (Figure 2.24), at temperature range 48-140 °C.

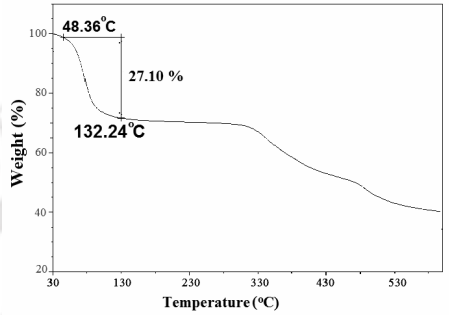

*Figure 2.24: Thermogram of **2.2b** (heating rate 5 °C/min).*

The thermogram of the hydrated salt **2.1c** having composition $(H\mathbf{2.1})_2(NO_3)_2{\cdot}H_2O$ showed that it loses a water molecule at 80.3 °C and the compound is unstable above 130 °C as shown in Figure 2.25a. Two water molecules of salt **2.1d** having composition $(H\mathbf{2.1})_2ClO_4{\cdot}2H_2O$ are lost at 120 °C (Figure 2.25b) which is a relatively higher temperature for evaporation of water molecules, showing that they are tightly held in the interstices.

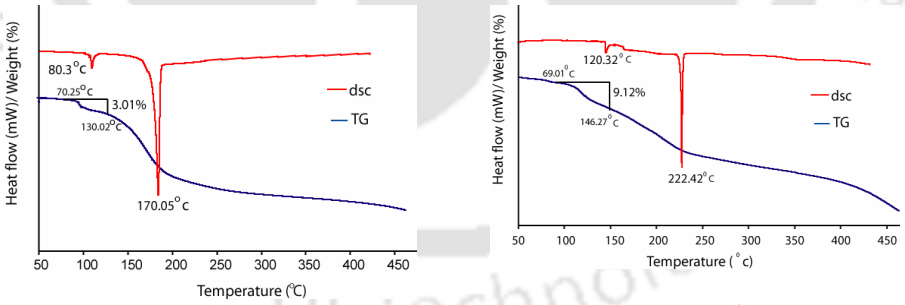

*Figure 2.25: Thermogram of (a) salt **2.1c** , (b) salt **2.1d** at heating rate of 5°C/min.*

The thermogram of monohydrated salt **2.2d** having composition $(H\mathbf{2.2})_2ClO_4{\cdot}H_2O$ differ from the dihydrate salt **2.1d** and it loses water molecules at 90 °C, which is much lower than the temperature required in the case of dihydrate salt **2.1d**. Salt **2.2e** having composition $(H\mathbf{2.2})_2HSO_4{\cdot}H_2O$ loses water molecules upon heating, which is reflected as two endothermic peaks at 55 and at 98 °C in differential scanning

calorimetry, and 4.8% weight loss was observed in the range 55-98 °C in thermogravimetry (Figure 2.26b).The corresponding theoretical loss for one molecule of water is 4.9%. Thus, the loss of water molecules occurs in two steps. In the hydrated bisulfate assembly, two water molecules bridges two bisulfate anions (Figure 2.20b). One of the bridging water molecules is lost at low temperature to modify the assembly, and the second loss occurs at relatively higher temperature from a reconstructed hydrated assembly formed by loss of one water molecule at a lower temperature. Thus, overall one water molecule per bisulfate anion is lost.

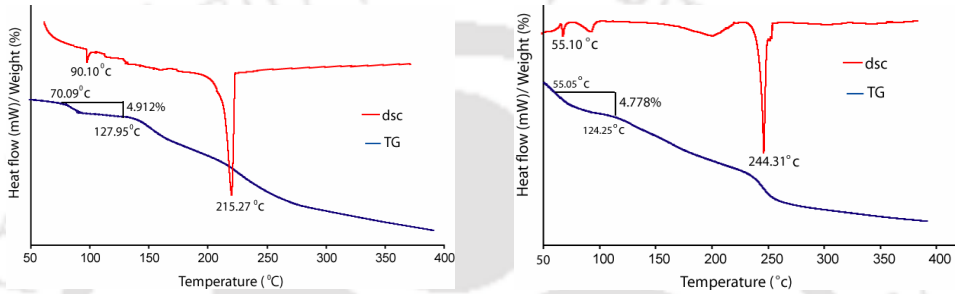

*Figure 2.26: Thermogram of (a) salt **2.2d**, (b) salt **2.2e** at heating rate of 5°C/min.*

Thus, comparison of the thermograms and structural patterns shows that thermal stabilities of hydrated anionic assemblies differ and the environment around the assemblies of hydrated anions as well as the types of anion-assisted assemblies decide the loss of water molecules from such assemblies of hydrated anions. Water loss may occur below or above the normal boiling point of water.

2.5: Conclusion

Generally, symmetric thiourea derivatives show *syn-syn* conformation;[68] however, *syn-anti* conformation is encountered in solvates under special circumstances.[69] The latter observation is a clear indication that solvent can enforce conformational changes through modification of self-assembly. From the results obtained by us, it is clear that the different orientations of the phenyl group of **2.1** could be achieved through change of solvent in the crystallization process. None of the polymorphs reported here is metastable, hence the interplay of weak interactions of solute and solvent guided the crystallization of the three polymorphs of **2.1** with different orientations of the phenyl ring. On the other hand, the intramolecular hydrogen bonds in **2.1** or **2.2** guided them to adopt a *syn-anti* arrangement in each case.

In the structure of each salt, the intramolecular hydrogen bond is absent; as a consequence they adopt the *syn-syn* conformation. Anhydrous chloride salts of **2.1** or **2.2** possess bifurcated hydrogen bonds, with the chloride ion as pivot connected to two N-H bonds of thiourea. We find that the chloride and bromide salts have large differences in compositions and self-assembly. The bromide salt of **2.1** is a one-dimensional polymeric chain, while **2.2** provided a platform for stabilization of a bromide-water cluster. The bromide ion in salt **2.1b** acts as a pivot of bifurcated hydrogen bonds with two N-H of thiourea to stabilize *syn-syn* geometry across the thiourea, whereas in the bromide salt **2.1b**, the oxygen of water molecule acts as pivot for bifurcated hydrogen bonds and the water molecules bridge bromide ions. The selective deprotonated salts of polyacids, such as the one formed from sulfuric acid and orthophosphoric acid by **2.1** and **2.2**, support the idea that the deprotonations are guided by stable crystalline product formation. For example, sulfuric acid is a strong acid: it selectively formed crystalline bisulfate salt with **2.2**, whereas with **2.1** it formed the corresponding sulfate salt. On the other hand, the dihydrogen phosphate salt was formed from orthophosphoric acid with **2.1**, but the corresponding salt of **2.2** could not be crystallized and is likely to be a phosphate salt. Partial deprotonation of orthophosphoric acid yielded an unconventional dihydrogen phosphate cluster held by $[H\mathbf{2.1}]^+$; similarly, partial deprotonation of sulfuric acid resulted in bisulfate-water assemblies stabilized by $[H\mathbf{2.2}]^+$. A structural comparison on the nitrate-assisted assemblies of hydrated and anhydrous salts of **2.1** showed that the hydrated nitrate salt adopts cooperative cyclic hydrogen bonded structure with a *syn-syn* conformation of the host cation. Absence of water molecules in the nitrate salt **2.1c** facilitated one nitrate to hold two host cations through cyclic hydrogen bonds, whereas there is another nitrate having hydrogen bonds with thiourea and nitrate anion. Thus, in the hydrated form of the nitrate salt, the water molecules competed and separated the two nitrate anions, which were found as pairs in the anhydrous form, possessing weak nitrate···nitrate interactions. This disruption made one of the nitrates bridge two host cations through bifurcated hydrogen bonds involving two oxygen atoms of nitrates with two independent acidic hydrogen atoms of two protonated methylthiazole units of two host cations as pivots. The other oxygen of the nitrate anion held another methylthiazole by N-H**…**O interaction. This causes the two nitro groups to be

symmetry-independent. From thermochemical studies, it has been established that dehydration temperatures of the hydrated assemblies of the salts are governed by the environment provided by the cations and hydrated anions and also by the type of anion-assisted assemblies.

Thus, in this Chapter polymorphs of similar energy with different orientations of the phenyl ring can be specifically crystallized from different solvents. The monomorphic nature of the positional isomer **2.2** arises from the tendency to form self-assembly of conformer locked through C-H**…**S hydrogen bonds. Formation of hydrated anion assembly and deprotonation of a polyacid to form crystalline salt is host-specific. Dehydration of the hydrated salts occurs above or below the normal boiling point of water, depending on the type of hydrated anion as well as anion-assisted assemblies. Novel clusters of hydrated bromide ions, cyclic assemblies of dihydrogen phosphate, and chainlike structure of assemblies of bisulfate-water are established by stabilizing them in cationic hosts.

2.6: Experimental Section

The detailed synthetic methodologies for synthesis of polymorphs and salts are described. Analytical data listed along with each compound. The instrumental details and the crystallographic parameters are provided in Appendix.

Synthesis of 1-(5-Methylthiazol-2-yl)-3-phenylthiourea (2.1): 5-Methylthiazol-2-ylamine (57 mg, 5 mmol) and phenyl isothiocyanate (67 mg, 5 mmol) were dissolved in dry dichloromethane (20 mL), and the solution was stirred for 6 h by placing the reaction vessel in an ice bath. The resulting solution was evaporated, and the precipitate was dried in vacuum. Yield 90%. ^{1}H NMR (400 MHz, $CDCl_3$) 7.58 (d, J = 10.0 Hz, 2H), 7.37 (t, J = 9.6 Hz, 2H), 7.25 (t, 1H), 6.96 (s, 1H), 6.71 (s, 2H), 2.26 (s, 3H). ESI MS [M + 1] 250.7944 (Calculated 250.0474). IR (cm^{-1}) 3440 (w), 3175 (m), 3022 (m), 2918 (m), 1627 (s), 1574 (s), 1536 (s), 1496 (s), 1370 (m), 1258 (s), 1180 (s), 1127 (s), 1023 (s), 724 (s). Polymorph **I** was crystallized from tetrahydrofuran, whereas Polymorph **II** and Polymorph **III** were crystallized from methanol and N,N-dimethylformamide, respectively.

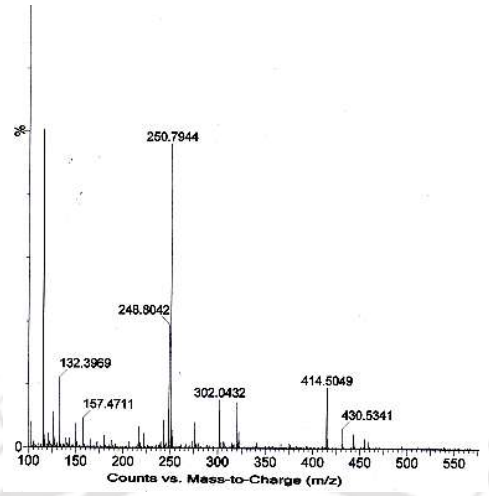

*Figure 2.27: ESI Mass spectra of **2.1***

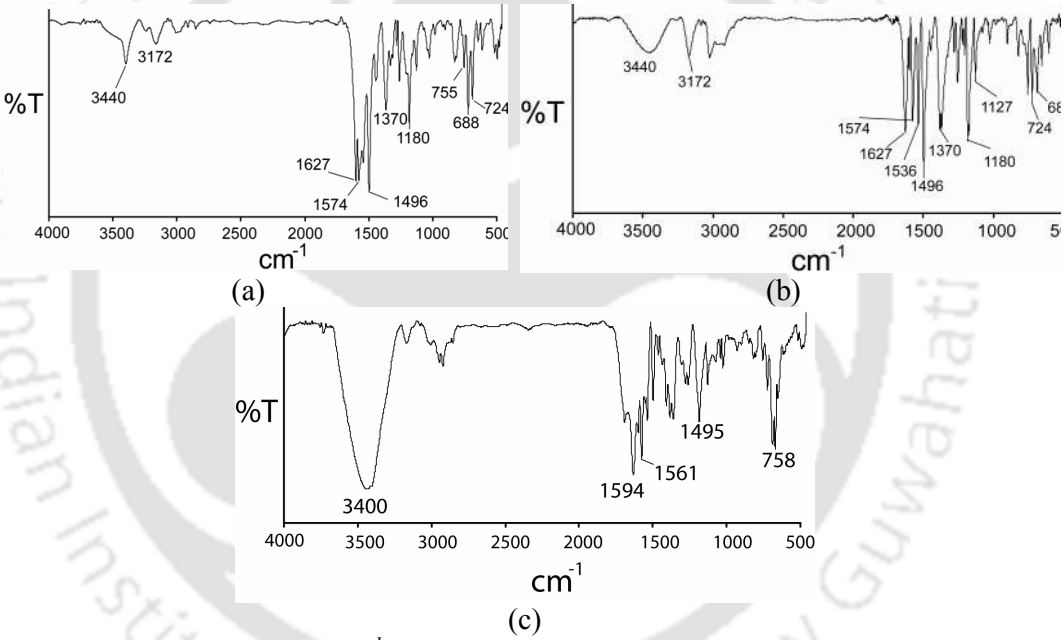

*Figure 2.28: FT-IR (KBr, cm^{-1}) spectra of (a) Polymorph **I**, (b) Polymorph **II** and (c) Polymorph **III.***

Synthesis of 1-(4-Methylthiazol-2-yl)-3-phenylthiourea (**2.2**): **2.2** was prepared by following a procedure similar to the synthesis of **2.1**, but 4-methylthiazol-2-ylamine was used in place of 5-methylthiazol-2-ylamine. Crystals of **2.2** were obtained from its methanol solution. Yield 92%. ^{1}H NMR (400 MHz, $CDCl_3$): 7.60 (d, J= 7.2 Hz, 2H), 7.37 (t, J = 7.6 Hz, 1H), 7.24 (t, J = 7.2 Hz, 2H), 6.37 (s, 1H), 2.29 (s, 3H). ESI MS [M + 1] 250.0490 (Calculated 250.0474). IR (cm^{-1}): 3433 (w), 3164 (m), 1594

(s), 1573 (s), 1531 (s), 1497 (s), 1372 (m), 1296 (s), 1260 (s), 1193 (s), 1132 (s), 731 (s), 686 (s), 648 (s), 486 (s).

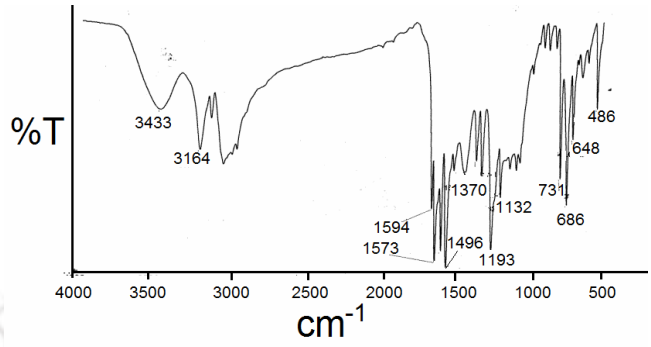

*Figure 2.29: FT-IR (KBr, cm^{-1}) spectra of compound **2.2**.*

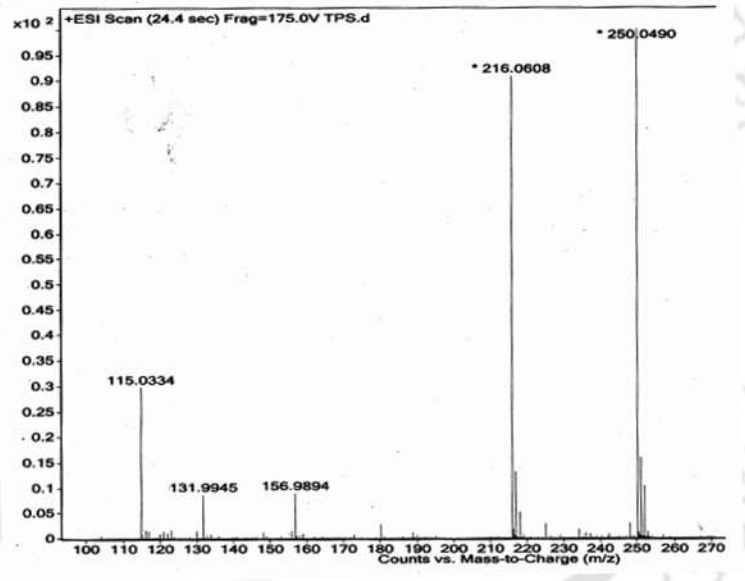

*Figure 2.30: ESI Mass spectra of **2.2***

Synthesis of Salt [H(2.1)]Cl (2.1a). Salt **2.1a** was obtained by adding a few drops of hydrochloric acid (37%, 0.4 mL) to a solution of **2.1** (25 mg, 0.1 mmol) in methanol (5 mL). After addition of acid, the solution was stirred at room temperature for 30 min and filtered. The filtrate, upon standing under ambient conditions, yielded colorless crystals of **2.1a** in 6-7 days. Yield 85%. ^{1}H NMR (DMSO-d_6, 400 MHz): 7.66 (m, 2H) 7.42 (d, J = 7.6 Hz, 2H), 7.32 (t, J = 7.6 Hz, 2H), 7.21 (s, 1H), 7.04 (t, J = 7.2 Hz, 2H), 2.32 (s, 3H). IR (cm^{-1}): 3052 (m), 1591 (s), 1560 (s), 1487 (s), 1409 (s), 1365 (m), 1317 (s), 1214 (s), 1183 (s), 819 (m), 757 (m), 688 (m).

Salt [H(2.1)]Br (2.1b): It was obtained by adding 0.4 mL of 37% hydrobromic acid to 5 mL of methanol solution of **2.1** (0.5 mmol). After the addition of acid, the solution was stirred at room temperature for 30 min and filtered. The filtrate was allowed to evaporate at room temperature; colorless crystals were obtained after a week. Yield: 82 %; ^{1}H-NMR ($CDCl_3$, 400 MHz): δ(ppm): 10.38 (s, 2H), 7.61 (d, J = 7.6 Hz, 2H), 7.37 (t, J = 7.6 Hz, 2H), 7.26 (d, J = 6.0 Hz 1H), 2.38 (s, 3H). IR (cm^{-1}): 3434 (w), 1595 (s), 1561 (s), 1525 (s), 1495 (s), 1405 (s), 1321 (s), 1195 (s), 1100 (s), 755 (s), 685 (m), 513 (m).

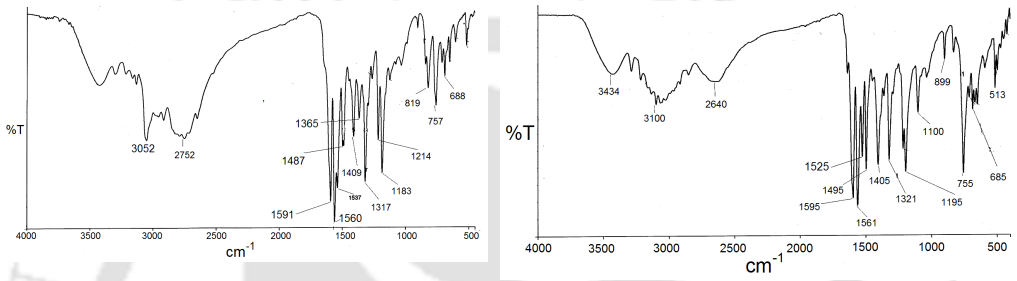

(a) (b)

*Figure 2.31: FT-IR (KBr, cm^{-1}) spectra of (a) salt **2.1a**, (b) salt **2.1b**.*

$[H(2.1)]_2(NO_3)_2.H_2O$ (2.1c) and $[H(2.1)NO_3]$ (2.1.1c): Equimolar amounts of **2.1** (124 mg, 0.5 mmol) and HNO_3 were dissolved in aqueous methanol (10 mL) as well as in methanol (10 mL) and was left for crystallization. Colorless crystals of **2.1c** and light yellow colored crystals of **2.1.1c** were formed after one week. Yield: 85%; ^{1}H NMR (DMSO-d_6, 400 MHz): 10.26 (s, 2H), 7.69 (d, J = 7.6 Hz, 2H), 7.26 (t, J = 7.6 Hz, 2H), 7.12 (s, 1H), 7.05 (t, 1H), 2.07 (s, 3H). IR (cm^{-1}): 3434 (w), 1766 (m), 1626 (m), 1384 (s), 1020 (m), 827 (m).

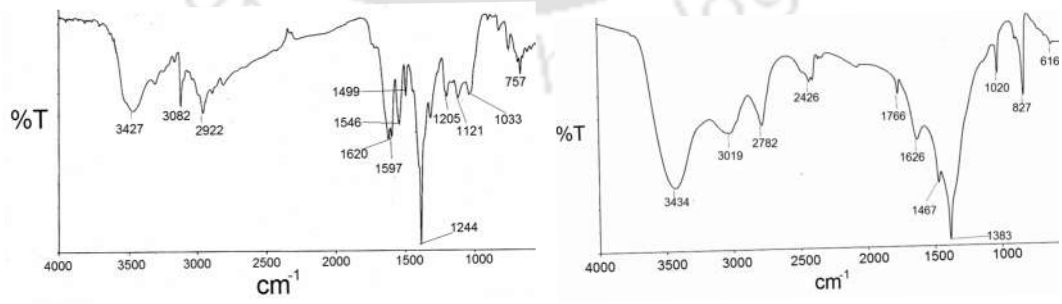

(a) (b)

*Figure 2.32: FT-IR (KBr, cm^{-1}) spectra of (a) salt **2.1c**, (b) salt **2.1.1c**.*

[H(2.1)]$ClO_4.2H_2O$ (2.1d): Equimolar amounts of **2.1** (124 mg, 0.5 mmol) and $HClO_4$ were dissolved in methanol (10 mL) and solution was left for crystallization. Colorless crystals were formed after one week. Yield, 93%; ^{1}H-NMR (DMSO-d_6, 400 MHz) 7.59 (d, J = 5.6 Hz, 2H), 7.47 (s, 1H), 7.41 (t, J = 7.2 Hz, 2H), 7.24 (t, J = 7.0 Hz, 2H), 7.12 (s,1H), 2.39 (s, 3H). IR (cm^{-1}): 3056 (m), 1591 (s), 1553 (s), 1496 (s), 1319 (s), 1216 (s), 1140 (m), 753 (s), 626 (s).

[H(2.1)]$_2SO_4$ (2.1e): **2.1** (249 mg, 1 mmol) and H_2SO_4 in 2:1 molar ratio were dissolved in methanol (15 mL) and kept for crystallization. Colorless crystals were formed after one week. Yield 96%. ^{1}H NMR (DMSO-d6, 400 MHz) 9.09 (s, 1H), 7.68 (d, J = 8.8 Hz, 2H), 7.28 (t, J = 7.6 Hz, 2H), 7.12 (s, 1H), 7.05 (t, J = 7.0 Hz 1H), 2.26 (s, 3H). IR (cm^{-1}): 2986 (m), 1607 (s), 1564 (s), 1531 (s), 1497 (s), 1322 (s), 1197 (s), 1038 (m), 761 (s), 605 (s).

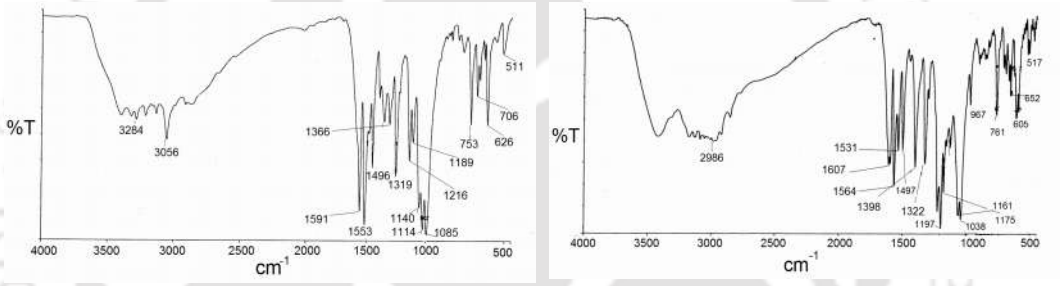

(a) (b)

*Figure 2.33: FT-IR (KBr, cm^{-1}) spectra of (a) salt **2.1d**, (b) salt **2.1e**.*

[H(2.1)]H_2PO_4 (2.1f): **2.1** (25 mg) was suspended in methanol (10 mL), and a few drops of orthophosphoric acid was added. After stirring for 30 mins, the clear solution was was formed, which on standing resulted block-shaped crystals after one week. Yield 82%; ^{1}H-NMR (DMSO-d_6, 400 MHz) 7.69 (d, J = 8.0 Hz, 2H), 7.46 (d, J = 7.2 Hz, 2H), 7.26 (t, J = 7.6 Hz, 2H), 7.06 (s, 1H), 7.02 (t, J = 8.0 Hz, 1H), 2.25 (s, 3H). IR (cm^{-1}): 3321 (m), 1596 (s), 1552 (s), 1496 (s), 1370 (s), 1321 (s), 1190 (s), 1096 (s), 988 (s), 891 (m), 813 (m), 710 (m), 651 (m), 501 (m).

[H(2.2)]Cl (2.2a): It was obtained by adding 0.4 mL of 37 % hydrochloric acid to methanol (5 mL) solution of **2.2** (25 mg). From the solution colorless crystals were obtained after a week. Yield: 88 %; ^{1}H-NMR (DMSO-d_6, 400 MHz) 9.70 (s, 2H), 7.46 (d, J = 4.4Hz, 2H), 7.30 (t, J = 7.2 Hz, 2H), 7.04 (t, J = 6.8 Hz, 1H), 6.80 (s, 1H),

2.35 (s, 3H). IR (cm^{-1}): 2663 (w), 1590 (s), 1559 (s), 1494 (s), 1417 (s), 1353 (s), 11.87 (s), 841 (m), 688 (m), 659 (m).

$[H(2.2)]_2(Br)_2.6H_2O$ (2.2b): It was obtained by adding 0.4 mL of 37 % hydrobromic acid to 5 mL of methanol solution of **2.2** (0.5 mmol). The solution was allowed to evaporate at room temperature, which yield colorless crystals in 6-7 days. Yield 92 %; ^{1}H-NMR (DMSO-d_6, 400 MHz) 9.20 (s, 2H), 7.47 (d, J = 7.6Hz, 2H), 7.33 (t, J = 7.2 Hz, 2H), 7.03 (t, J = 7.2 Hz, 1H), 6.70 (s, 1H), 2.32 (s, 3H). IR (cm^{-1}): 3381 (w), 3297 (m), 3067 (m), 1594 (s), 1561 (s), 1496 (s), 1420 (s), 1360 (s), 1323 (s), 1216 (s), 1190 (s), 757 (s), 719 (m), 686 (m), 654 (m).

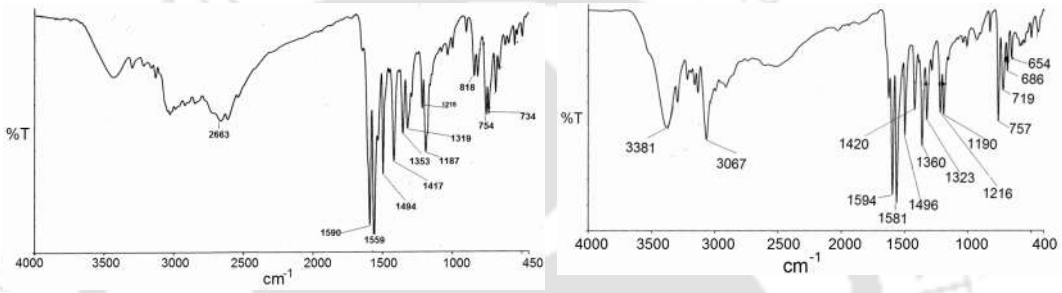

(a) (b)

*Figure 2.34: FT-IR (KBr, cm^{-1}) spectra of (a) salt **2.2a**, (b) salt **2.2b**.*

$[H(2.2)]NO_3$ (2.2c): A solution prepared from an equimolar amount of **2.2** (124 mg, 0.5 mmol) and conc. nitric acid. After one week, colorless crystals were obtained. Yield, 95 %. ^{1}H-NMR (DMSO-d_6, 400 MHz) 7.69 (d, J = 7.6 Hz, 2H), 7.27 (t, J = 4.8 Hz, 2H), 7.13 (s, 2H), 7.06 (t, J = 7.6 Hz, 1H), 6.50 (s, 1H), 2.21 (s, 3H). IR (cm^{-1}): 3432 (w), 1620 (m), 1546 (m), 1499 (m), 1205 (w), 1121 (w), 757 (m).

$[H(2.2)]ClO_4.H_2O$ (2.2d): Equimolar amounts of **2.2** (124 mg, 0.5 mmol) and perchloric acid (40 %) were dissolved in methanol (10 mL) and solution was left for crystallization. Colorless crystals were formed after three days. Yield, 96 %; ^{1}H NMR (DMSO-d_6, 400 MHz) 7.61 (d, J = 7.0 Hz, 2H), 7.44 (d, J = 8.0 Hz, 2H), 7.32 (t, J = 6.8 Hz, 2H), 7.23 (s, 1H), 7.06 (t, J = 7.0 Hz, 2H), 2.32 (s, 3H). IR (cm^{-1}): 3397 (w), 1594 (s), 1561 (s), 1496 (m), 1419 (m), 1360 (m), 1323 (s), 1144 (m), 1112 (m), 626 (s).

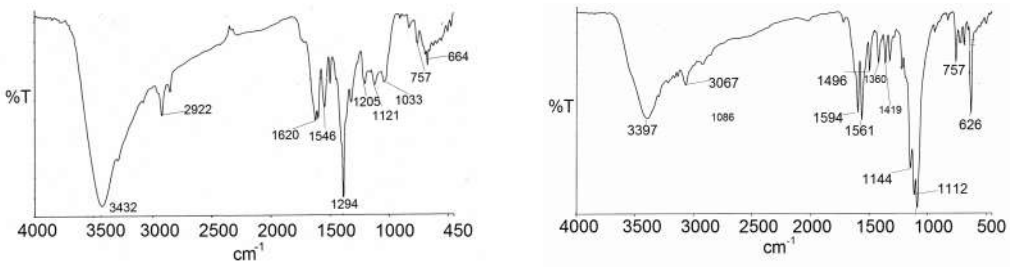

(a) (b)

*Figure 2.35: FT-IR (KBr, cm^{-1}) spectra of (a) salt **2.2c**, (b) salt **2.2d**.*

[H(2.2)]$HSO_4.H_2O$ (2.2e): It was obtained by adding 0.4 mL of 37 % of sulphuric acid to 5 mL methanolic solution of **2.2** (25 mg). Colorless crystals were formed within 6-7 days. Yield 73%; ^{1}H-NMR (DMSO-d_6, 400 MHz) 7.69 (d, J= 8.4 Hz, 2H), 7.28 (t, J = 3.6 Hz, 2H), 7.04 (t, J = 7.2 Hz, 1H), 6.53 (s, 1H), 2.21 (s, 3H). IR (cm^{-1}): 1327 (w), 3082 (m), 1624 (m), 1594 (s), 1559 (s), 1497 (s), 1358 (s), 1317 (s), 1234 (s), 1133 (s), 1046 (m), 762 (m), 692 (m).

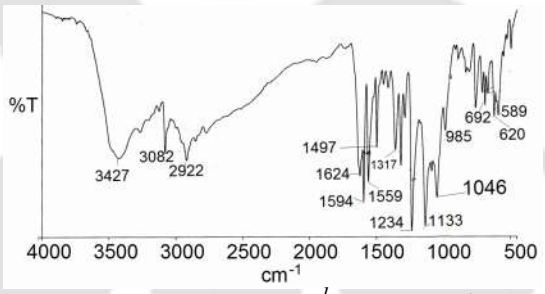

*Figure 2.36: FT-IR (KBr, cm^{-1}) spectra of salt **2.2e**.*

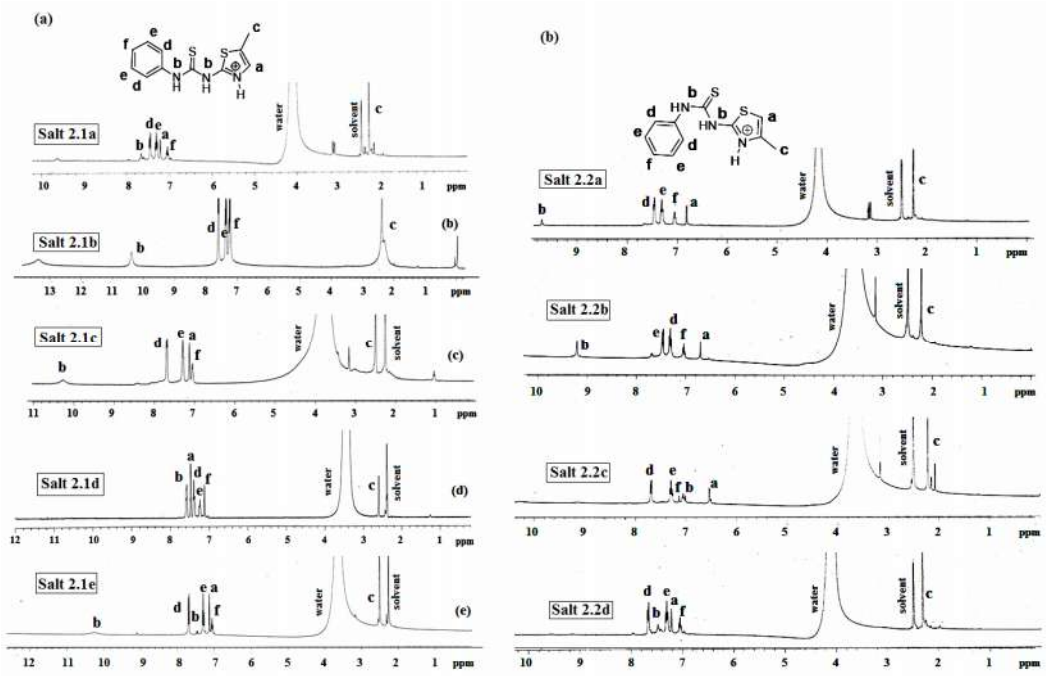

*Figure 2.37: ^{1}H-NMR (400 MHz, DMSO-d_6) of Salts of (a) compound **2.1**, (b) compound **2.2***

2.7: References

1. *Solid-State Characterization of Pharmaceuticals*; A. Zakrzewski, M. Zakrzewski, Eds. Assa International Inc.: Danbury, CT, USA, 2006.
2. *Polymorphism in the Pharmaecutical Industry*; R. Hilfiker, Ed. Wiley-VCH: Weinheim, Germany, 2006.
3. G. R. Desiraju, *Cryst. Growth Des.*, 2008, **8**, 3.
4. A. D. Bond, R. Boese, G. R. Desiraju, *Angew. Chem., Int. Ed.*, 2007, **46**, 615.
5. A. D. Bond, R. Boese, G. R. Desiraju, *Angew. Chem., Int. Ed.*, 2007, **46**, 618.
6. A. D. Bond, R. Boese, G. R. Desiraju, *Am. Pharm. Rev.*, 2007, May/June, 1.
7. J. Bernstein, Organic Solid State Chemistry, Elsevier, Amsterdam, 1978.
8. A. Nangia, *Acc. Chem. Res.*, 2008, **41**, 595.
9. D. J. W. Grant, Theory and origin of polymorphism, in: H. G. Brittain (Ed.), Polymorphism in Pharmaceutical Solids, Marcel Dekker Inc., New York, 1999, p. 1.
10. L. Yu, *Acc. Chem. Res*., 2010, **43**, 1257.
11. S. L. Price, *Chem. Soc. Rev.*, 2014, **43**, 2098.

12. J. Merchan, N. Yutronic, P. Jura, M. T. Garland, R. Baggio, *J. Inclusion Phenom. Macrocyclic Chem.*, 2006, **55**, 367.
13. E. Hough, D. G. Nicholson, *J. Chem. Soc., Dalton Trans.*,1978, 15.
14. M. G. B. Drew, A. Lund, D. G. Nicholson, *Supramol. Chem.*, 1997, **8**, 197.
15. D. Strugatsky, R. McNulty, K. Munson, C.-K. Chen, S. M. Soltis, G. Sachs, H. Luecke, *Nature*, 2013, **493**, 255.
16. A. R. L. Fraga, F. F. Ferreira, G. M. Lombardo, F. Punzo, *J.Mol. Struct.*, 2013, **1047**, 1.
17. C. I. Yeo, E. R. T. Tiekink, *Acta Crystallogr., Sect. E: Struct. Rep. Online*, 2011, **67E**, o2965.
18. T. Maris, M. J. Henson, S. J. Heyes, K. Prout, *Chem. Mater.*, 2001, **13**, 2483.
19. V. S. Bryantsev, B. P. Hay, *J. Phys. Chem. A*, 2006, **110**, 4678.
20. G. R. Desiraju, *Acc. Chem. Res*., 1996, **29**, 441.
21. G. R. Desiraju, *Acc. Chem. Res*., 1991, **24**, 290.
22. M. C. Etter, *Acc. Chem. Res.*, 1990, **23**, 120.
23. G. R. Desiraju, *Angew. Chem., Int. Ed.*, 1995, **34,** 2311.
24. U. D. Pete, C. M. Zade, J. D. Bhosle, S. G. Tupe, P. M. Chauhary, A. G. Dikundwar, R. S. Bendre, *Bioorg. Med. Chem. Lett.*, 2012, **22**, 5550.
25. T. Steiner, *Angew. Chem., Int. Ed*., 2002, **41**, 48.
26. P. Hobza, Z. Havlas, *Chem. Rev*., 2000, **100**, 4253.
27. E. J. Corey, T. W. Lee, *Chem. Commun.*, 2001, 1321.
28. A. Cosp, I. Larrosa, J. M. Anglada, J. M. Bofill, P. Romea, F. Urpi, *Org. Lett.*, 2003, **5**, 2809.
29. C. P. Brock, L. L Duncan, *Chem. Mater.*, 1994, **6**, 1307.
30. S. Kumar, K. Subramanian, R. Srinivasan, K. Rajagopalan, A. M. M. Schreurs, J. Kroon, T. Steiner, *J. Mol. Struct.*, 2000, **520**, 131.
31. S. Aitipamula, A. Nangia, *Chem. Eur. J.*, 2005, **11**, 6727.
32. K.M. Anderson, A. E. Goeta, K. S. B. Hancock, J. W. Steed, *Chem. Commun*., 2006, 2138.
33. J. B. Baruah, A. Karmakar, N. Barooah, *CrystEngComm*, 2008, **10**, 151.
34. K. Kawakami, *J. Pharm. Sci*., 2007, **6**, 982.

35. G. W. H. Hohne, W. Hemminger, H. -J. Flammersheim, *Differential Scanning Calorimetry, second rev. ed., Spinger-Verlag Publisher, Berlin, Heidelberg*, 2003.
36. P. Khakhlary, J. B. Baruah, *J. Mol. Struc*., 2014, **1078**, 188.
37. P. A. Gale, *Chem. Soc. Rev.*, 2010, **39**, 3746.
38. P.D. Beer, P.A. Gale, *Angew. Chem., Int. Ed.*, 2001, **40**, 486.
39. H. An, J. S. Bradshaw, R. M. Izatt, *Chem. Rev*., 1992, **92**, 543.
40. H. An, J. S. Bradshaw, R. M. Izatt, Z. Yan, *Chem. Rev*., 1994, **94**, 939.
41. P. Burkhard, C. H. Tai, J. N. Jansonius, P. F. Cook, *J. Mol. Biol*., 2000, **303**, 279.
42. B. T. Burlington, T. S. Widlanski, *J. Org. Chem*., 2001, **66**, 7561.
43. C. H. Tai, P. Burkhard, D. Gani, T. Jenn, C. Johnson, P. F. Cook, *Biochemistry*, 2001, **40**, 7446.
44. R. J. M. Courtemanche, T. Pinter, F. Hof, *Chem. Commun*., 2011, **47**, 12688.
45. B. L. Schottel, H. T. Chifotides, K. D. Dunbar, *Chem. Soc. Rev*., 2008, **37**, 68.
46. X.-P. Bao, L. Wang, L. Wu, Z. -Y. Li, *Supramol. Chem*., 2008, **20**, 467.
47. P. S. Lakshminarayanan, I. Ravikumar, E. Suresh, P. Ghosh, *Inorg. Chem*., 2007, **46**, 4769.
48. S. -I. Kondo, Y. Hiraoka, N. Kurumatani, Y. Yano, *Chem. Commun*., 2005, 1720.
49. J. W. Steed, *Chem. Soc. Rev*., 2010, **39**, 3686.
50. P. A. Gale, *Chem. Commun*., 2008, 4525.
51. R. M. Duke, E. B. Veale, F. M. Pfeffer, P. E. Kruger, T. Gunnaluagsson, *Chem. Soc.Rev*., 2010, **39**, 3936.
52. Z.-P. Deng, H.-L. Qi, L.-H. Huo, H. Zhao, S. Gao, *CrystEngComm*, 2011, **13**, 6632.
53. A. Bakhoda, H. R. Khavasi, N. Safari, *Cryst. Growth Des.*, 2011, **11**, 933.
54. M. A. Saeed, A. Pramanik, B. M. Wong, S. A. Haque, D. R. Powell, D. K. Chand, M. A. Hossain, *Chem. Commun.*, 2012, **48**, 8631.
55. S. Marivel, M. Arunachalam, P. Ghosh, *Cryst. Growth Des*., 2011, **11**, 1642.
56. Y. V. Nelyubina, K. A. Lyssenko, D. G. Golovanov, M. Y. Antipin, *CrystEngComm*, 2007, **9**, 991.

57. K. Biradha, S. Samai, A. C. Maity, S. Goswami, *Cryst. Growth Des*., 2010, **10**, 937.
58. C. Perez, M. T. Muckle, D. P. Zaleski, N. A. Seifert, B. Temelso, G. C. Shields, Z. Kisiel, B. H. Pate, *Science*, 2012, **336**, 897.
59. S. M. Haile, D. A. Boyens, C. R. I. Chisholm, R. B. Merie, *Nature*, 2001, **400**, 910.
60. C. R. I. Chisholm, S. M. Haile, *Solid State Ionics*, 2000, **229**, 136.
61. D. A. Jose, D. K. Kumar, B. Ganguly, A. Das, *Inorg. Chem.*, 2007, **46**, 5817.
62. D. Braga, M. Gandolfi, M. Lusi, M. Polito, K. Rubini, F. Grepioni, *Cryst. Growth Des.*, 2007, **7**, 919.
63. D. Sun, C. F. Yang, H. R. Xu, H. X. Zhao, Z. H. Wei, N. Zhang, L. J. Yu, R. B. Huang, L. S. Zhengab, *Chem. Commun.*, 2010, **46**, 8168.
64. M. A. Hossain, M. Isklan, A. Pramanik, M. A. Saeed, F. R. Fronczek, *Cryst. Growth Des.*, 2012, **12**, 567.
65. P. S. Lakshminarayanan, I. Ravikumar, E. Suresh, P. Ghosh, *Chem. Commun*., 2007, 5214.
66. A. Rajbanshi, S. Wan, R. Custelcean, *Cryst. Growth Des*., 2013, **13**, 2233.
67. U. Burget, G. Zundel, *Biophys. J.*, 1987, **52**, 1065.
68. G. A. Bowmaker, N. Chaichit, J. V. Hanna, C. Pakawatchai, B. W. Skelton, A. H. White, *Dalton Trans.*, 2009, 8308.
69. A. Okuniewski, J. Chjnacki, B. Becker, *Acta Crystallogr.*, *Sect. E: Struct. Rep. Online*, 2011, **67E**, o55.

Chapter 3

Conformational adjustment over hydrogen bonded synthons of thiourea/urea tethered thiazole

In preceding two Chapters the definition as well as some aspects of Polymorphism[1,2] is described. A new conformation in a molecule is generated as a result of a variation of torsion angle. While referring to conformation in crystal structures, it is important to differentiate between (a) Conformational adjustment and (b) Conformational change, as per IUPAC recommendations.[2,3] Conformational adjustment is observed in solid state as a result of change in molecular conformation in a flexible molecule to minimize lattice energy of the crystal. In such adjustment, a small conformational energy difference is utilized (adjustment energy, $\Delta E_{gas-crys}$) to improve the intermolecular interactions in the crystal. On the other hand, conformational change involves a change of gas-phase conformer. Conformations occupying distinct energy minima of a gas phase potential energy surface (gas-PES) as shown in Figure 3.1 are called conformer. In Figure 3.1, A_{cry} and B_{cry} are two conformations in solid state, while A_{gas} and B_{gas} are two conformers in gaseous phase. Transformation between B_{gas} to B_{cry}, A_{gas} to A_{cys} and vice-versa is conformational adjustment. But, transformation between A_{gas} to B_{gas} by crossing the energy barrier is called conformational change. Thus, all conformations are not conformers. If, in addition to a change in torsion angle, there is a well enough change in potential energy in the new conformation, then the new conformation is called as a conformer.

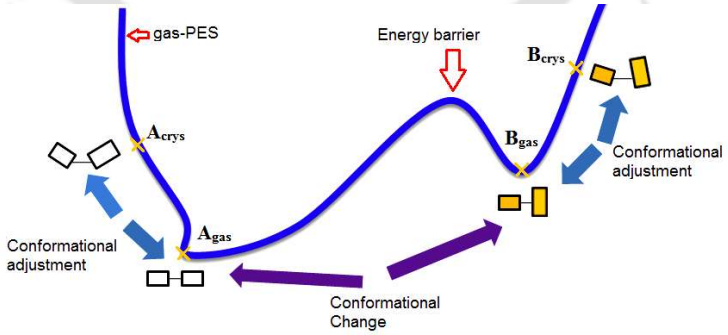

Figure 3.1: Schematic representation of gas-PES to explain the concepts of "conformational change" and "conformational adjustment".

When a gas phase conformer crosses the energy barrier to go from one energy minima to other energy minima of the gas-PES, then it is called conformational change. When two independent conformations are related by conformational adjustment, then are referred simply as polymorphs.[3] Apart from, single molecular polymorphism, polymorphism in multi-component systems has gained interest day by day. Multi-component crystal can also be termed as co-crystal. According to Dunitz, a co-crystal can be defined by, ''a crystal containing two or more components together''[4] Wohler[5] in 1844 has provided early example of cocrystals, which has now expanded fast to many domains of pharmaceuticals.[6-8] Predesigned non-covalent synthesis involving cocrystals is now fast moving towards understanding on multi component crystals.[9-15] Systematic uses of weak interactions,[16] complementary hydrogen bonds,[17-20] identification of synthons[21-23] which are descriptor of an assembly are some major factors, contributing to the faith of redesign non-covalent synthesis of multi-component crystals.[24-27] However, energy associated with each synthon is an important issue in dictating self-assemblies.[28] The idea on supramolecular synthons in non-covalent synthesis suggested by Desiraju[21] has been taken forward by Zaworotko and coworkers[22,23] to explain them in terms of homo-synthons and hetero-synthons for understanding of self-assemblies. Polymorphism of synthons has been identified[29,30] but similar issues in multi-component systems require attention. Conformational adjustments[3, 31-33]are widely observed in solvates and salts. Such adjustments may lead to conformational polymorphism.[34-36]Anion dependent conformational changes are generally observed in protonated hosts. There is also a need to study conformational changes on neutral host by an anion. Most of the conformational polymorphs or anion guided conformational changes are carried out in solution. Isolation of multi-component crystal possessing solvent as a component is of definite interest. Polymorphs arising due to rotation of C_{ipso}- N_{ipso} bonds over intramolecular hydrogen bonded synthons of thiazole derived thiourea are discussed in Chapter 2. Binary crystals of urea derivatives show conformational polymorphs.[37-41] Commonly observed synthons in urea can be reorganized by different intermolecular and intramolecular interactions.[42] Thiazole tethered thiourea derivatives stabilize hetero synthons between water and anions which is discussed in Chapter 2. Hence, there is a scope to form multi-component crystals by utilizing such hetero synthons and

conformational adjustments on host molecule possessing intramolecular hydrogen bond (Figure 3.2a) or intermolecular hydrogen bonds with anions or water

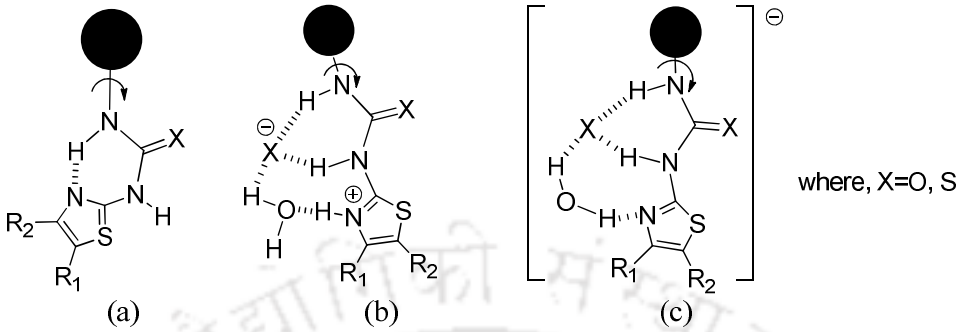

Figure 3.2: Models to show rotation of a top over (a) thiazole derived six-membered intramolecular hydrogen bonded synthon, (b) protonated thiazole locked by anion and water, (c) Neutral thiazole derived thiourea/ urea derivative holding an anion and water.

The latter two structures have bifurcated hydrogen bonded thiourea/urea;[43] one formed by X (anion) with two NH of protonated urea (Figure 3.2b) and other is a neutral host (Figure 3.2c). Use of long chain n-alkylammonium cation as counter ion may also affect conformation of a host coordinated to an anion. Solvent guided or anion guided conformational adjustments/changes are expected in these compounds as weak interactions of naphthalene ring contributes to supramolecular assembly in thiourea derivatives.[44]

A set of molecules shown in Chart 3.1 are chosen to understand generality of conformational adjustment in urea and thiourea derivative, which have options for intramolecular hydrogen bond.

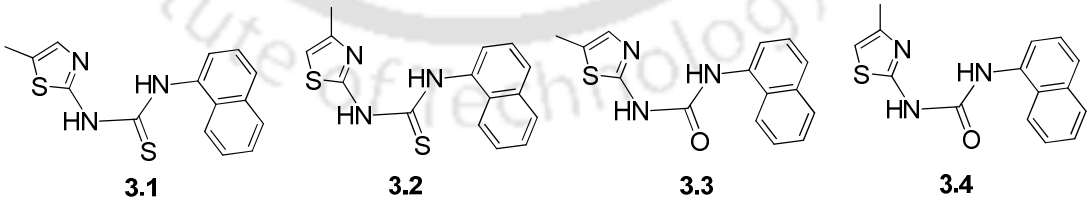

Chart 1: Different methylthiazole containing positional isomers of urea and thiourea derivatives.

3.1: Synthesis of 3.1, 3.2, 3.3 and 3.4

The compounds **3.1** and **3.2** were prepared by reaction of corresponding 4- or 5-methylaminothiazole with 1-naphthyl isothiocyanate. Likewise, compound **3.3** and **3.4** are synthesized by reacting 4- or 5-methylaminothiazole with 1-naphthyl isocyanate. These compounds were characterized by various spectroscopic techniques, such as IR spectroscopy, Mass spectrometry, ^{1}H-NMR.

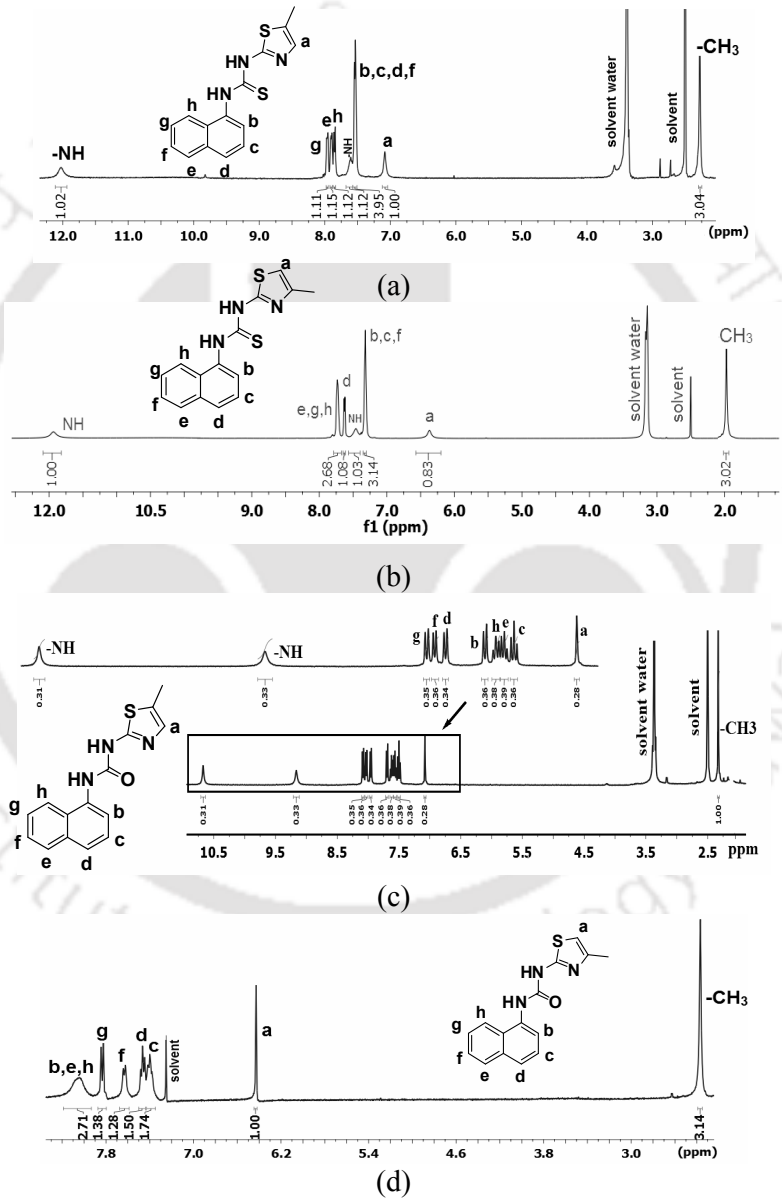

*Figure 3.3: ^{1}H-NMR (DMSO-d_6, 600 MHz) of (a) compound **3.1**, (b) compound **3.2**, (c) ^{1}H-NMR (DMSO-d_6, 400 MHz) of compound **3.3**, (d) ^{1}H-NMR ($CDCl_3$, 400 MHz) of compound **3.4.***

In the ^{1}H-NMR, the characteristic thiazolic protons (designated as-a) of **3.1** appears at 7.08 ppm (Figure 3.3a), whereas it appears at 6.60 ppm for **3.2** (Figure 3.3b). In case of compound **3.3**, the characteristic thiazolic protons (designated as-a) appear at 7.08 ppm (Figure 3.3c) and for compound **3.4** appear at 6.43 ppm (Figure 3.3d). Assignments of all other pecks are marked in their respective spectra.

3.2: Polymorphs of compound 3.1 and 3.2

We have attempted crystallization of **3.1** and **3.2** from various solvents. Depending on the solvent of crystallization crystals of two different polymorphs of these compounds in each case were obtained. In none of these cases concomitant crystallization of two polymorphs was observed. Polymorphs of compound **3.1** are designated as **3.1a** and **3.1b** while **3.2a** and **3.2b** for compound **3.2**. The crystallization results from various solvents are summarized in Table 3.1.

Table 3.1. Crystallization of Polymorphs of **3.1** and **3.2** from Different Solvents

Solvent	**3.1** (type of crystals)	**3.2** (type of crystals)
Acetone	-[a]	-[a]
Acetonitrile	-[a]	**3.2a**
Methanol	-[a]	**3.2a**
Ethanol	-[a]	**3.2a**
THF	-[a]	-[a]
DMF	**3.1a**	**3.2b**
DMSO	**3.1b**	**3.2b**
Diethylether	-[a]	**3.2a**
Ethyl acetate	-[a]	-[a]
Methanol: DMF (1:1)	**3.1a**	**3.2b**
Diethylether:DMSO (1:1)	**3.1a**	**3.2b**

[a]No suitable crystal with adequate edges.

Powder X-ray diffraction (PXRD) patterns from bulk samples of each polymorph were recorded independently and compared with PXRD data generated from CIF file of each polymorph. PXRD data as shown in Figure 3.4 shows phase purity of each polymorph.

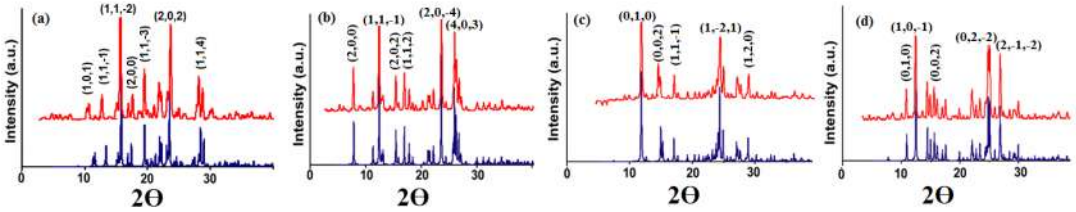

Figure 3.4: Powder XRD patterns of (a) ***3.1a;*** *(b)* ***3.1b;*** *(c)* ***3.2a;*** *(d)* ***3.2b****.(top/red one are experimental pattern and lower/blue one are generated from crystallographic information files)*

3.2.1: Supramolecular Assemblies of polymorphs of 3.1 and 3.2

Crystals of polymorph **3.1a** are of monoclinic $P2_1/n$ space group, whereas crystals of polymorph **3.1b** belong to monoclinic *C2/c* space group. Crystal packing shows that both polymorphs have intramolecular N-H**…**N hydrogen bonds between the N atom of the 5-methylthiazole unit with the thiourea N-H proton with average N**…**N distance 2.70 Å and N-H**…**N bond angle 140.5° (Table 3.2). This provides a *syn-anti* orientation across the thiourea units as shown in Figure 3.5a,b. The molecules of **3.1a** and **3.1b** took part in *non*-centrosymmetric dimer formation through $R_2^2(8)$ N-H**…**S hydrogen bonds, which is a common feature of thiourea derivatives.[45] Within the crystal packing of **3.1b,** molecules are arranged in an orderly manner along *b*-crystallographic axis, forming a channel like structure, where naphthyl groups are projected outward (Figure 3.5c).

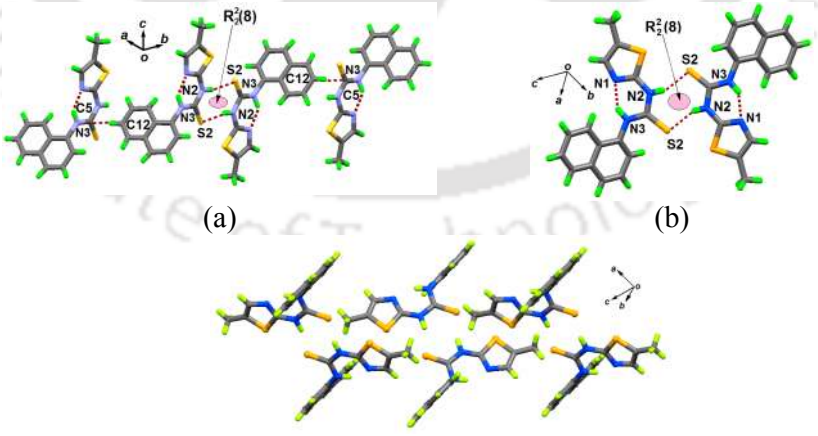

Figure 3.5: (a) Assembly of ***3.1a*** *having intramolecular N-H**…**N and intermolecular N-H**…**S bonds, (b) non-centrosymmetric dimer formed through N-H**…**S bonds in the packing of* ***3.1b****. (c) Packing patterns of* ***3.1b*** *along b-crystallographic axis.*

Both polymorphs **3.2a** and **3.2b** isolated from solution of **3.2** from different solvents (Table 3.1) belong to triclinic $P\bar{1}$ space group but with different cell parameters. Both the polymorphs contain one symmetry independent molecule in its asymmetric unit. Self-assemblies **3.2a** and **3.2b** are guided by intramolecular N-H**…**N hydrogen bonds with $d_{D\text{-}A}$ distances 3.336 Å and 3.259 Å respectively. **3.2a** and **3.2b** adopt *syn-anti* orientation across the thiourea moiety (Figure 3.6a,b) . The conventional *non*-centrosymmetric dimer formed through $R_2^2(8)$ N-H**…**S hydrogen bonds also present within the crystal lattice of **3.2a** and **3.2b**. Apart from these, packing pattern of **3.2a** is guided by weak N-H**…**π interaction which extends this *non*-centrosymmetric dimeric synthon to a one-dimensional chain like structure along *ac*-plane. (Figure 3.6c).

Individual molecules in these polymorphs have intramolecular hydrogen bond. In each case molecules form assembly with the help of homo dimeric $R_2^2(8)$ sub-assemblies. As discussed in Chapter 2, in phenyl-substituted derivatives, one positional isomer was found to be trimorphic and another as monomorphic. The monomorphic nature was explained on the basis of the locking of conformation through weak interactions. In the present cases such possibilities are absent and we obtained two polymorphs in each case. Each polymorph has intramolecular synthon comprising of N-H**…**N hydrogen bonds between the N atom of the methylthiazole with the thiourea N-H proton.

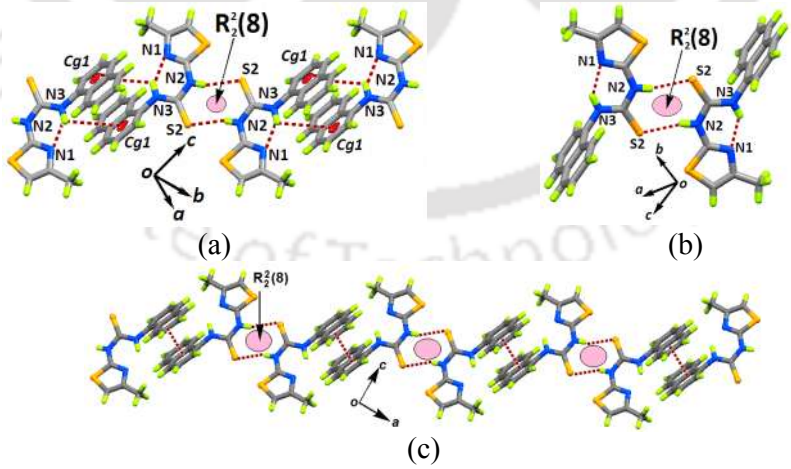

*Figure 3.6: (a) Assembly of **3.2a** having intramolecular N-H**…**N, intermolecular N-H**…**S and weak N-H**…**π ($d_{N\text{-}H\cdots Cg1}$= 3.977 Å) interactions, (b) non-centrosymmetric dimer formed through N-H**…**S bonds in lattice of **3.2b**, (c) 1-Dimensional chain like arrangement of **3.2a** along ac-plane.*

Due to intramolecular N-H**…**N hydrogen bond, all the polymorphs adopt *syn-anti* orientation across the thiourea unit (Figure 2.3b, Chapter 2). The differences in polymorphs arise from the orientations of naphthyl-groups over such synthons. In each case, hydrogen bonded homo-dimeric sub-assemblies are observed. These dimeric sub-assemblies are similar to the one found in ribbon structures (Figure 3.7b) of thiourea self-assemblies and are more stable than the chain structure[46,47] (Figure 3.7a). *Non*-centrosymmetric hydrogen bonded dimer formed through $R_2^2(8)$ N-H**…**S interactions, provides *trans*-disposition of naphthyl and thaizole groups. Such orientations occur to reduce the repulsion between the bulky units in the lattice. However, overall weak interactions in the respective self-assemblies are different.

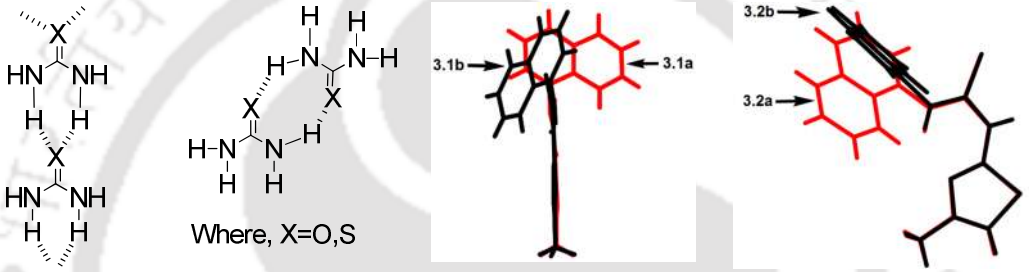

Figure 3.7: (a) Chain, (b) ribbon structure formed by thiourea derivatives. Overlay diagram showing orientations of the naphthyl group in (a) ***3.1a*** *and* ***3.1b****; (b)* ***3.2a*** *and* ***3.2b*** *(drawn by fixing the methylthiazole planes in one direction).*

Table 3.2: Hydrogen Bond Parameters of **3.1a**, **3.1b**, **3.2a**, **3.2b**

Compd No.	D-H**…**A [symmetry]	d_{D-H}(Å)	$d_{H\cdots A}$(Å)	$d_{D\cdots A}$(Å)	∠D-H···A(°)
3.1a	N(2)-H(2)···S(2) [-x,-y,-z]	0.91(3)	2.39(3)	3.271(3)	164(3)
	Intra N(3)-H(3A)···N(1)	0.92(3)	1.94(3)	2.707(4)	140(3)
	Intra C(14)-H(14)···N(3)	0.93	2.56	2.864(4)	100
3.1b	N(2)-H(2) …S(2) [-x,1-y,-z]	0.86	2.56	3.318(2)	147
	Intra N(3)-H(3A)···N(1)	0.86	2.00	2.694(3)	138
	Intra C(7)-H(7)···S(2)	0.93	2.78	3.198(2)	108
	Intra C(14)-H(14)···N(3)	0.93	2.54	2.853(3)	100
3.2a	N(2)-H(2)···S(2) [3-x,1-y,1-z]	0.86	2.50	3.336(18)	164
	Intra N(3)-H(3A)···N(1)	0.86	1.99	2.699(2)	140
	Intra C(14)-H(14)···N(3)	0.93	2.55	2.864(3)	100
3.2b	N(2)-H(2)···S(2) [2-x,1-y,1-z]	0.84(2)	2.45(2)	3.259(18)	162(2)
	Intra N(3)-H(3A)···N(1)	0.85(2)	2.05(2)	2.738(2)	138(2)
	Intra C(14)-H(14)···N(3)	0.93	2.58	2.885(3)	100

The orientations of the naphthyl-groups in all these polymorphs with respect to planes containing the methylthiazole units are different (Figure 3.7c-d). These differences occur due to the free rotation of the naphthyl-group connected to the thioamide bond competing with interplay of weak interactions of naphthyl group with surrounding.

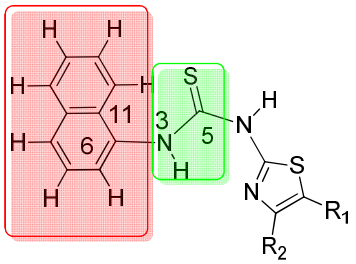

*Figure 3.8: Representation of the plane of the naphthyl ring with respect to thioamide plane in **3.1** and **3.2** (Numbers 3 corresponds to nitrogen atom of NH bond adjacent to naphathalene ring and 5 is carbon of thiourea part, whereas 6 and 11 in each case are carbons at α and β- position of naphthalene ring in respective sub-assembly).*

For explaining the orientations, two independent planes may be constructed with dihedral angle C11−C6−N3−C5 (**τ**) as illustrated in Figure 3.8. The torsional angle based on this dihedral plane for all the polymorph is listed in Table 3.3.

Table 3.3: Torsional angle of the polymorphs **3.1a**, **3.1b**, **3.2a** and **3.2b**.

	Polymorph **3.1a**	Polymorph **3.1a**	Polymorph **3.1a**	Polymorph **3.1a**
C11−C6−N3−C5 (**τ**)	101.79°	135.32°	-125.59°	87.82°.

3.2.2: DFT and Differential scanning calorimetry Study

Gas phase energies from B3LYP/6-31++g(d,p)-level calculations showed that polymorphs **3.1a** and **3.1b** have almost identical energy. The energy difference between **3.2a** and **3.2b** also negligible. The energies calculated are listed in Table 3.4.

Table 3.4: Energy calculated at B3LYP/6-31++G(d,p) level

Polymorph	Energy (in HF)	Energy (in kcal/mol)	Difference (in kcal/mol)
3.1a	-1540.1338736	-966448.80333737	0.00006903
3.1b	-1540.13387371	-966448.8034064	
3.2a	-1522.0354983	-955091.89894688	0.00006275
3.2b	-1522.0354984	-955091.89900963	

Conformational polymorphs of amide derivatives shows phase transitions.[48] But, we did not observe phase transition other than melting in any polymorph. Differential scanning calorimetry of the two polymorphs of **3.1** also of the two polymorphs of **3.2** showed conventional melting points. Polymorph **3.1a** and **3.1b,** shows endothermic pecks at 195.47°C and 193.01°C respectively (Figure 3.9a,b), corresponding to melting. While in DSC curve of polymorph **3.2a** and **3.2b** endothermic pecks appear

at 195.47 ^{o}C and 193.01^{o}C respectively, due to melting of the compound as shown in Figure 3.9c,d.

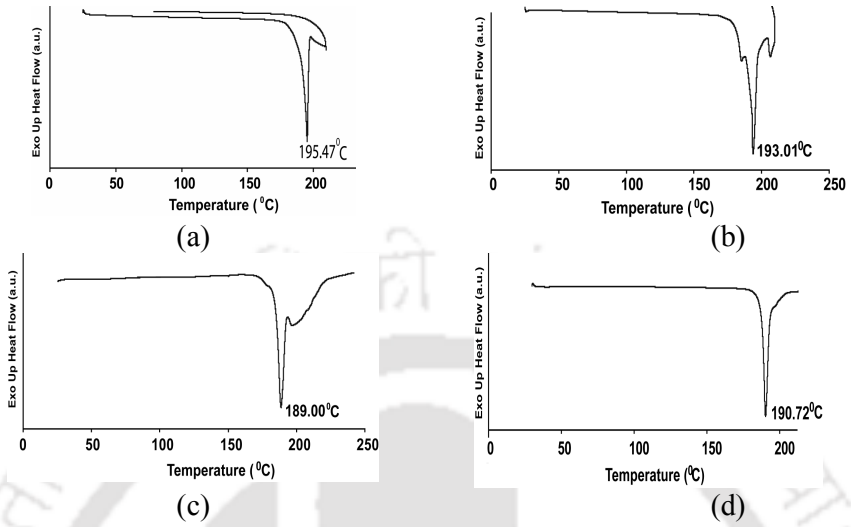

Figure 3.9: DSC plots obtained from heating at a rate of 5° C/min. of the polymorph (a) ***3.1a****; (b)* ***3.1b****; (c)* ***3.2a*** *and (d)* ***3.2b.***

3.3: Supramolecular Assemblies of 3.3 and 3.4

Crystallization of **3.3** and **3.4** from various solvents did not yield polymorphs of any of these compounds. Compound **3.3** crystallizes in triclinic $P\bar{1}$ space group, while **3.4** crystallizes in monoclinic $P2_1/c$ space group. The packing patterns of the compounds **3.3** and **3.4** showed that one -NH of urea is involved in intramolecular N-H**…**N hydrogen bonds with N-atom of the methylthiazole unit (Table 3.5). Due to such hydrogen bonded interactions, conformational locking takes place to provide *syn-anti* orientation across a uncommon conformer found in urea derivatives.[44] Generally, *syn*-conformation is common in urea derivatives to form chain type structures by using tape-motifs.[49] The *non*-centrosymmetric dimer are build up by N-H**…**O bonds adopting $R_2^2(8)$ graph set notation as shown in Figure 3.10a. These isosteric synthons may be for predesigned non-covalent synthesis. The assembly of oxygen atom of urea compound **3.3** acts as trifurcated hydrogen bond acceptor.[44] In which the principal bond is N-H**…**O bond and other two hydrogen bonds are weak C-H**…**O bonds. The C-H**…**O bond with a hydrogen atoms of the -CH_3 groups help to form $R_4^4(16)$ synthon whereas one of the -CH of naphthyl group participates in the formation of robust $R_4^4(35)$ synthon (Figure 3.10c).

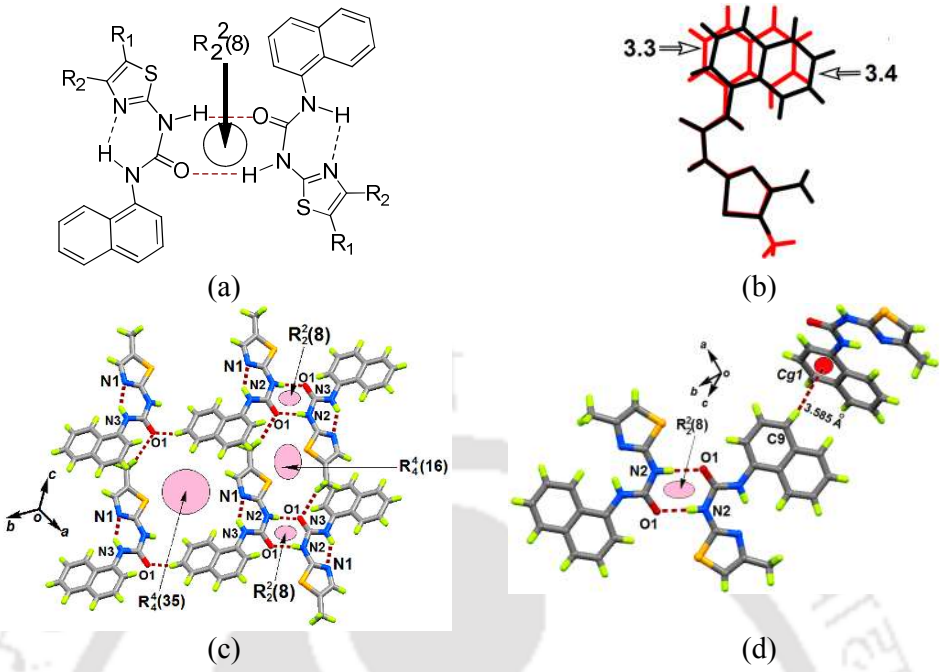

*Figure 3.10: (a) Dimeric sub-assemblies present in **3.3** and **3.4**, (b) overlaid diagram of **3.3** and **3.4** by fixing the thiazole rings in one plane. Hydrogen-bonded assembly within the crystal lattice of (c) **3.3** and (d) **3.4**.*

On the other hand, the self assembly of **3.4** has dimeric synthon formed through $R_2^2(8)$ N-H**…**O bonds, which are held to another such unit through C-H**…**π interaction as shown in Figure 3.10d. Since these represent intramolecular hydrogen bonded synthon having naphthalene as top, we looked at the orientation of naphthalene in these molecules. We find that the two molecules **3.3** and **3.4** have different orientations of naphthalene groups across the urea plane, the C11−C6−N3−C5 dihedral angles are 126.0° and 171.14° respectively.

Despite of having similar conformation of **3.3** or **3.4** as that of **3.1** or **3.2,** we obtain only one form of crystals in each case. Strength of N-H**…**S and N-H**…**O bonds are comparable[49] thus such bonds with solvents would not have made a difference in thiourea derivatives with respect to a structurally similar urea derivative. Due to such a reason, similar dimeric intermolecular synthons as that of thiourea derivatives are formed in the case of urea derivatives also. But in the latter case, these synthons are formed through N-H**…**O bonds. The size of sulphur atom is larger than oxygen to provide more room for flexibility of atom at its proximity. Thus, monomorphic behavior of urea is likely to arise from the C=O and C=S to participating in other

weak hydrogen bond interaction schemes. Theoretical comparison as well as experimental data of literature support that the packing pattern may slightly differ in analogous thiourea from urea.[46,47]

Table 3.5: Hydrogen Bond Parameters of **3.3, 3.4** and **3.5**

Compd No.	D-H…A [symmetry]	d_{D-H}(Å)	$d_{H\cdots A}$(Å)	$d_{D\cdots A}$(Å)	∠D-H···A(°)
3.3	N(2)-H(2)···N(4) [-x,-y,-z]	0.86	2.00	2.861(8)	175
	N(5)-H(5)···N(1) [-x,-y,-z]	0.86	2.02	2.876(8)	174
3.4	N(2)-H(2)···O(1) [1-x,1-y,-z]	0.78(3)	2.010(3)	2.783(4)	172.5(19)
	Intra N(3)-H(3A)···N(1)	0.87(19)	2.04(19)	2.747(3)	137.6(16)
	Intra C(14)-H(14)···N(3)	0.93	2.54	2.853(4)	100
3.5	N(1)-H(1)···O(2) [1/2-x,1/2+y,z]	0.86	1.89	2.742(4)	174
	N(2)-H(2)···Cl(1) [1/2-x,1/2+y,z]	0.88(2)	2.28(2)	3.141(2)	166(2)
	O(2)-H(2P)···Cl(1) [1/2-x,1/2+y,z]	0.83(5)	2.33(5)	3.132(4)	162(4)
	O(2)-H(2Q)···Cl(1)	0.94(5)	2.21(5)	3.134(3)	166(4)
	N(3)-H(3A)···Cl(1) [1/2-x,1/2+y,z]	0.90(2)	2.58(2)	3.409(2)	152.6(18)
	C(3)-H(3)···Cl(1) [-x,1-y,-z]	0.93	2.62	3.547(3)	171
	Intra C(7)-H(7)···O(1)	0.93	2.31	2.859(3)	117
	Intra C(14)-H(14)···N(3)	0.93	2.58	2.880(4)	100

3.4: Reaction of compound 3.1 with acids

We had attempted preparation of salts of the compound **3.1** to search for a possibility of hydrogen bonded synthon shown in Figure 3.2b. But, compound **3.1** underwent cyclization reaction in presence of different acid such as HCl, HBr, HNO_3, $HClO_4$, and H_3PO_4. In each case the compound **3.5** (Equation 3.1) was formed.

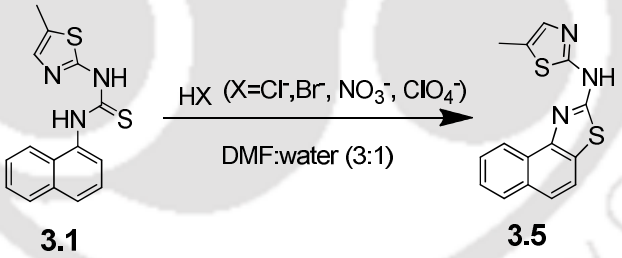

*Equation 3.1: Acid catalysed cyclization of compound **3.1**.*

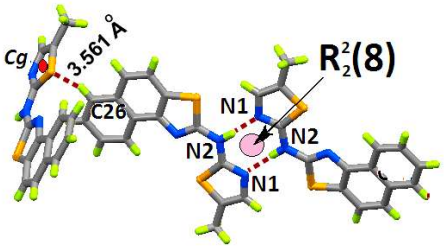

*Figure 3.11: Dimeric assembly held by C-H…π interactions in **3.5**.*

Such a cyclized product of naphthalene derivative under acidic condition is not surprising as there are many reactions relating to formation of heterocyclic ring over α and β- carbon of naphthalene rings.[27] From structural point of view, the compound **3.5** has similarity to the parent compound to adopt dimeric assemblies (Figure 3.11). The dimeric assemblies have $R_2^2(8)$ synthons between the aminothiazole parts of two neighboring molecules by N-H**…**N bonds. The intermolecular hydrogen bonded dimeric assemblies are held to each other through C-H**…**π interactions involving the methyl group of the methylthiazole ring.

3.5: Anion Guided Assemblies of compound 3.3

Compound **3.3** and **3.4** were treated with several inorganic acids such as hydrochloric, hydrobromic, nitric, perchloric and sulphuric acid, in order to obtain synthons as shown in Figure 3.2b. We successfully isolated two crystalline salts of urea derivatives **3.3** hydrochloric or perchloric acid as shown in Equation 3.2. Chloride salt **3.3a** and perchlorate salt **3.3b** were obtained as hydrate.

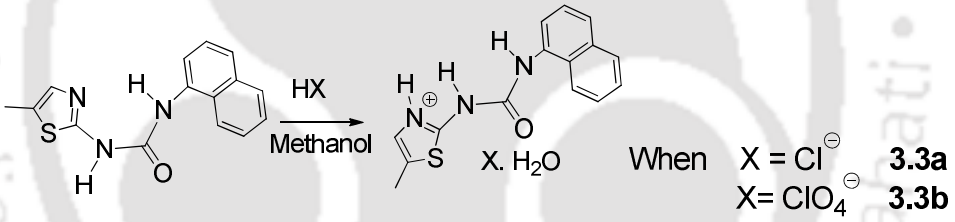

*Equation 3.2: Crystalline salts of urea derivative **3.3**.*

3.5.1: Chloride Assisted Assemblies of compound 3.3

The chloride salt **3.3a** has one protonated molecule of **3.3**, a chloride atom and a water molecule from crystallization in its asymmetric unit. Two N-H protons from urea forms bifurcated hydrogen bonds with chloride ions (Figure 3.12a). The water molecules form hydrogen bonds with chloride ions forming a 1-dimensional zig-zag chain as shown in Figure 3.12b. The N^+-H proton of 5-methylthiazole unit form hydrogen bond with water molecule. Each water molecule act as bifurcated hydrogen bond donors and is also connected to the N^+-H as hydrogen bond acceptor. This provides cyclic synthon with $R_3^3(8)$ notation. Self-assembling of the aquated anion occurs through O2-H**…**Cl1 hydrogen bonds. Interaction of -CH proton of 5-methylthiazole with chloride ion formed robust cyclic synthon with graph set notation

$R_6^6(14)$. Overall packing pattern shows that the chloride ions are involved in trifurcated hydrogen bond acceptor. Due to protonation of the thiazole nitrogen, the intramolecular N-H**…**N hydrogen bond present in the parent compound is lost and new synthon as shown in Figure 3.12a is formed. Cations in the chloride salt adopt *syn-syn* conformation across the urea moeity. This suggests clearly the change of orientations of the parent urea scaffold which had a *syn-anti* orientation due locked geometry.

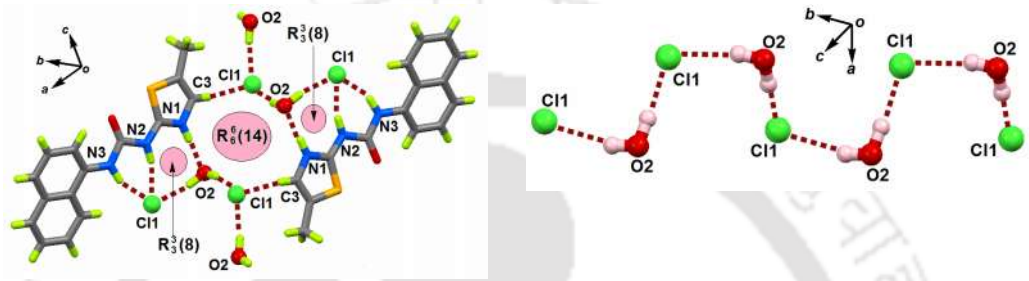

Figure 3.12: (a) Various weak interactions in salt ***3.3a,*** *(b) aquated chloride ions in the crystal lattice of* ***3.3a****.*

Table 3.6: Hydrogen Bond Parameters of **3.3a** and **3.3b**

Compd No.	D-H**…**A [symmetry]	d_{D-H}(Å)	$d_{H\cdots A}$(Å)	$d_{D\cdots A}$(Å)	∠D-H···A(°)
3.3a	N(1)-H(1)···O(4) [1-x,3/2+y,-z]	0.86	2.09	2.921(8)	163
	N(2)-H(2)···O(6) [x,1+y,z]	0.89(6)	1.99(5)	2.796(9)	150(5)
	N(3)-H(3A)···O(6) [x,1+y,z]	0.86	2.21	2.988(8)	151
	O(6)-H(6P)···O(2)	0.93(9)	2.26(11)	2.945(10)	130(7)
	O(6)-H(6Q)···O(5) [1-x,-1/2+y,-z]	0.93(7)	2.15(8)	3.035(10)	161(7)
	C(1)-H(1A)···O(3) [-1+x,2+y,z]	0.96	2.52	3.425(11)	156
	Intra C(7)-H(7)···O(1)	0.93	2.23	2.860(10)	124
	Intra C(14)-H(14)···N(3)	0.93	2.56	2.871(11)	100
3.3b	N(2)-H(2)···Cl(1) [1-x,1/2+y,1/2-z]	0.80(4)	2.37(4)	3.133(4)	161(3)
	N(3)-H(3A)···Cl(1) [1-x,1/2+y,1/2-z]	0.81(3)	2.47(3)	3.235(4)	159(3)
	Intra C(7)-H(7)···O(1)	0.93	2.47	2.896(5)	108
	Intra C(14)-H(14)···N(3)	0.93	2.61	2.912(5)	100
	C(20)-H(20A)···Cl(1) [1+x,y,z]	0.97	2.76	3.726(4)	171

3.5.2: Perchlorate Assisted Assemblies of compound 3.3

The perchlorate salt **3.3b** crystallizes in monoclinic $P2_1$ space group, having a protonated host, a perchlorate anion and a water molecule from crystallization. Two -NH protons of urea forms bifurcated hydrogen bonds with oxygen atom of the water molecule of crystallization. The N^+-H proton of 5-methylthiazole unit form hydrogen bonds with oxygen atom of the perchlorate anion. Here, each water molecule acts as a bifurcated hydrogen bond acceptor. Conformation of the cation is *syn-syn* across the

urea moiety. The perchlorate ion forms various types of hydrogen bonded assemblies with the water molecule of crystallization as shown in Figure 3.13b.

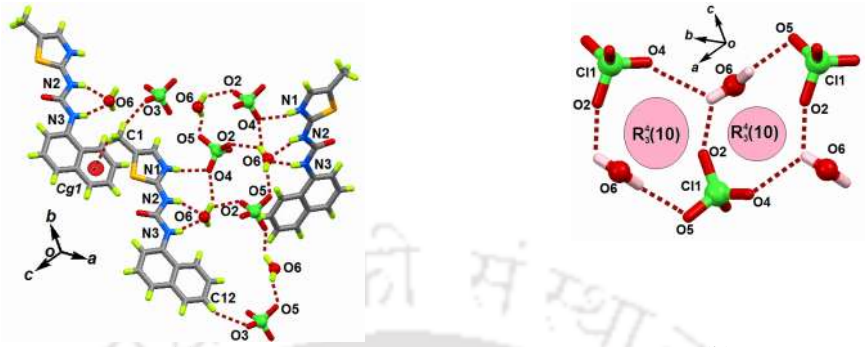

*Figure 3.13: The self-assembly of salt **3.3b**, (d) Aquated perchlorate ions within the crystal lattice of **3.3b.***

The marked differences in structures of the two salts are the bifurcated hydrogen bonds. Perchlorate anion did not participate in bifurcated hydrogen bonds despite of having a negative charge on the oxygen atom but chloride ion are part of bifurcated hydrogen bond with -NH of urea. Two compounds have different bifurcated synthons, hence not suitable to make direct comparison on conformational adjustments across two independent synthon formed by aid of anions. But, orientations of the protonated hosts are distinctly different.

3.6: Cocrystals of 3.3 with tetrabutylammoniumchloride

Three different cocrystals of **3.3** with tetrabuylammoinum chloride (TBACl) were crystallized concomitantly. One type of crystals was identified as simple 1:1 cocrystal with TBACl **3.3c** and other two were polymorphs of hydrated cocystals designated as **3.3d** and **3.3e** (Equation 3.3).

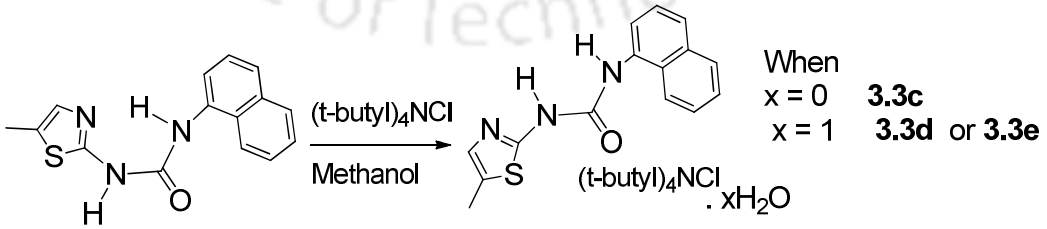

*Equation 3.3: Cocrystllization of **3.3** with tetrabutylammonium chloride.*

Crystal morphologies of the cocrystals are different as shown in Figure 3.14. Therefore the crystals were handpicked from the mixture of three types of crystals

(a) (b) (c)

Figure 3.14: Photograph of co crystals (a) ***3.3c,*** *(b)* ***3.3d*** *and (c)* ***3.3e****.*

3.6.1: Supramolecular Assemblies of 3.3c, 3.3d and 3.3e

Anhydrous cocrystal **3.3c** has bifurcated hydrogen bond with chloride ion. The N-H**…**Cl bonds have H**…**Cl distances 2.39(4) Å and 2.40(4) Å respectively with $d_{D...A}$ as 3.184(4) Å and 3.222(4) Å (Table 3.7). These are hydrogen bonds with moderate strength. Terabutylammonium cations are held by C-H**…**O and C-H**…**Cl hydrogen bonds in the self-assembly of **3.3c** as illustrated in Figure 3.15a. Due to coordination of urea to the anion, two rings across the urea moiety are organized *syn* to each other. This leaves scope to have conformational adjustments on naphthyl as well as thiazole ring. Conventionally aminothiazole adopts *syn* orientation by projecting the thiazole nitrogen and -NH in the same direction.[29] Participation of chloride ions in bifurcated bonds prohibits formation of tape motifs (Figure 3.7a).

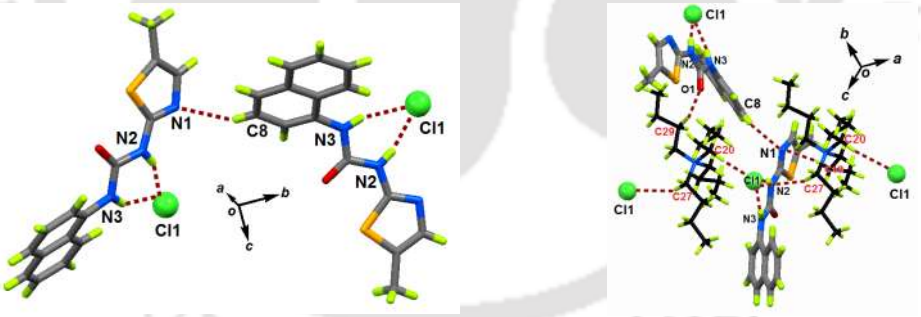

(a) (b)

Figure 3.15: (a) Hydrogen bond interaction between chloride ion and protonated host in the lattice of co-crystal ***3.3c****, (b) hydrogen bonded assembly of cocrystal* ***3.3c****.*

Hydrated cocrystals **3.3d** and **3.3e** crystallized in triclinic $P\bar{1}$, and monoclinic $P2_1/c$ space group respectively. The former has about half the unit cell volume as that of the latter. Principal synthons involved in these cocrystals are similar. Both the hydrated cocrystals **3.3d** and **3.3e** have bifurcated hydrogen bond between two NH and a chloride ion. This is similar to the anhydrous form **3.3c**.

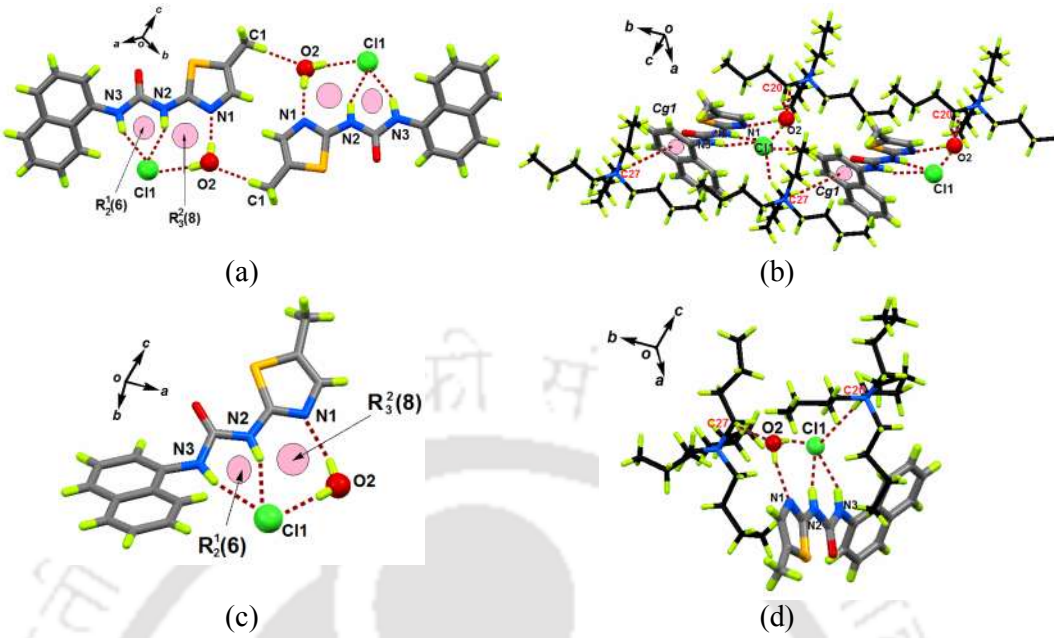

Figure 3.16 **:** *(a) Hydrogen bond interactions among chloride ion, cationic host and water molecule from crystallization within the crystal lattice of* ***3.3d****, (b) Supramolecular assembly of co-crystal* ***3.3d****, (c) Hydrogen bond environment of aquated* Cl^- *ions of* ***3.3e,*** *(d) Supramolecular assembly of co-crystal* ***3.3e.***

In the case of anhydrous forms **3.3d** and **3.3e** nitrogen atom of the thiazole ring is involved in C-H**…**N hydrogen bond. But in the hydrated form these are associated with hydrogen bond with water molecules through N-H**…**O bonds. The chloride ions are also hydrogen bonded with water molecules. Both the polymorph have water molecule serving as bridge to connect chloride ion with nitrogen atom of thiazole. This makes cyclic hydrogen bonded synthon with $R_3^2(8)$ graph set notation. Hence, packing of the two polymorphs are guided by $R_3^2(8)$ and $R_2^1(6)$ synthons. The lattice water molecule besides acting as hydrogen bond donors to chloride ions, it also involves in C-H**…**O bonds with the C-H of methyl group. It does so by acting as hydrogen bond acceptor. The hydrogen bond parameters of the isosteric synthons are comparable (Table 3.7). Hence, the major differences in structures of the two polymorphs arise from the orientations of the naphthalene groups. The C5-N3-C6-C11 dihedral angles in the synthon polymorphs are -151.62 and -144.68 respectively.

Table 3.7: Hydrogen Bond Parameters of **3.3a** and **3.3b**

Compd No.	D-H…A [symmetry]	d_{D-H}(Å)	$d_{H\cdots A}$(Å)	$d_{D\cdots A}$(Å)	∠D-H···A(°)
3.3c	N(2)-H(2)···Cl(1)	0.84(4)	2.39(4)	3.184(4)	159(4)
	O(2)-H(2P)···Cl(1)	0.92(3)	2.32(4)	3.229(4)	168(4)
	O(2)-H(2Q)···N(1)	0.93(6)	2.06(6)	2.982(6)	173(5)
	N(3)-H(3A)···Cl(1)	0.86(4)	2.40(4)	3.222(4)	160(3)
	C(1)-H(1A)···O(2)	0.96	2.56	3.484(6)	162
	Intra C(7)-H(7)···O(1) [1-x,-y,-z]	0.93	2.40	2.901(6)	114
	Intra C(14)-H(14)···N(3)	0.93	2.56	2.874(6)	100
	C(20)-H(20B)···O(2) [1+x,1+y,z]	0.97	2.59	3.433(6)	146
3.3d	O(1)-H(1P)···N(1)	0.93(10)	2.01(11)	2.916(8)	163(10)
	N(2)-H(2)···Cl(1)	0.86	2.40	3.228(5)	161
	O(1)-H(2Q)···Cl(1)	0.93(4)	2.31(5)	3.231(7)	170(4)
	N(3)-H(3A)···Cl(1)	0.86	2.45	3.267(5)	158
	Intra C(7)-H(7)···O(2)	0.93	2.52	2.963(7)	110
	Intra C(14)-H(14)···N(3)	0.93	2.56	2.865(8)	100
	C(27)-H(27A)···O(1) [1-x,-1/2+y,1/2-z]	0.97	2.55	3.425(8)	150
3.3e	N(2)-H(2)···O(1) [2-x,-y,1-z]	0.89(3)	1.94(3)	2.826(3)	173(2)
	Intra N(3)-H(3A)···N(1)	0.91(2)	1.92(2)	2.704(3)	144(2)
	Intra C(7)-H(7)···O(1)	0.95(2)	2.22(2)	2.877(3)	125.5(19)

Such concomitant polymorphs are not usual but though there are examples on crystallization of two or more polymorphs concomitantly whose energy differences are very small.[50,51] Similar synthons were observed in the polymorphs of binary urea crystal.[37-41] Beside packing patterns, there is also difference in N-H**…**O hydrogen bonds bond parameters of the tapes. Thus, the hydrogen bond parameters of the two bifurcated hydrogen bonds in the polymorphs were analyzed. The Cl**…**H distance of N(2)-H(2)**…**Cl bond is 2.39(4) Å in **3.3d** and 2.40(4) Å in **3.3e** whereas Cl**…**H distance of N(3)-H(3))**…**Cl bond it was 2.40 Å and 2.45 Å respectively. The N(2)-H(2)**…**Cl angles are 159(4)° and 161°; N(3)-H(3)**…**Cl angles were 160(3)° and 158° respectively. Hence the bifurcated hydrogen bonded synthons are comparable.

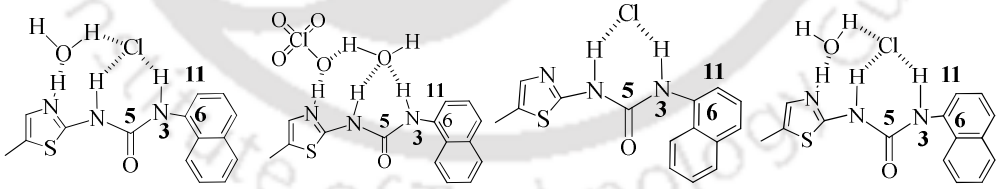

*Figure 3.17: Different types hydrogen bonded sub-assemblies found in salts **3.3a**, **3.3b** and cocrystals **3.3c-3.3e** (Numbers 3 and 5 in each figure corresponds to nitrogen atom of NH bond adjacent to naphathalene ring, 6 and 11 in each case are carbons of at α and β- position of naphthalene ring respective sub-assembly).*

From the above results, it is clear that the principal hydrogen bonded synthons in the self-assemblies of the urea salts **3.3a-3.3b** and cocrystals **3.3c-3.3d** have synthons A-

D shown in Figure 3.17. The perchlorate salt and chloride salt have sharp differences in the bifurcated hydrogen bond synthons of urea. In case chloride salt the chloride is the hydrogen bond acceptor (Figure 3.17A) and in the perchlorate salt oxygen atoms of the perchlorate do not participate in bifurcated hydrogen bond. But it does so by the forming bifurcated bond between urea and water molecule (Figure 3.17B). Furthermore, there are examples of multi-component systems where reversible hydration and dehyhydration retain crystalline nature and those structures have conformational adjustments.[52] None the less, both **3.3c** and **3.3d** have similar synthons but different conformational adjustments over cyclic sub-assemblies through different orientations of naphthyl group. The torsion angles of C5-N3-C6-C11 in **3.3c** and **3.3d** are 156.00 ° and 174.50° respectively. Thus, the independent but identical synthons has different conformational adjustments. The self assembly of anhydrous cocrystal is guided by bifurcated hydrogen bonds of NH and chloride ion to form sub-assembly C (Figure 3.17C). But in the hydrated cocrystals have bifurcated hydrogen bonded synthon between chloride and NH of urea. In such synthon water molecule lock the assembly by anchoring thiazole through O-H**…**N and O-H**…**Cl bonds. The sub-assembly formed in hydrated form is marked as D Figure 3.17. The orientation of naphthyl group of anhydrous cocrystal **3.3c** has large difference from the orientations of similar naphthyl groups in two polymorphs of hydrated cocrystals (**3.3d** and **3.3e**) (Figure 3.18a). In the hydrated cocrystals water molecule participates in hydrogen bonds to lock the rotation of thiazole ring, whereas naphthyl groups can adjust its conformation. Accordingly different torsion C5-N3-C6-C11 angles in these cocrystals are observed, which are 139.04°, -151.62 °and -144.68° respectively. The sub-assemblies found in **3.3d** and **3.3e** have very close similarities in bond parameters. These sub-assemblies are stabilized by electrostatistically guided hydrogen bonds, being robust makes room for adjustment of the naphthyl groups by rotation of C_{ipso}-N_{ipso} bond to adopt different conformational adjustments.

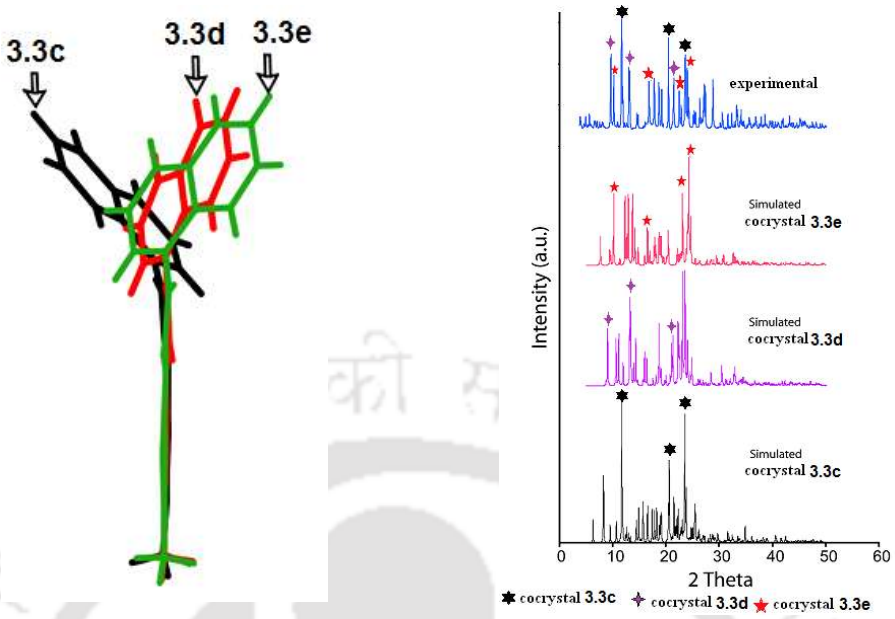

(a) (b)

*Figure 3.18: (a) Overlay diagram showing orientations of the naphthyl group in neutral hosts of cocrystals **3.3c**, **3.3d** and **3.3e** (drawn by fixing the 5-methylthiazole plane in one direction).(b) Experimental PXRD pattern of the crystals **3.3c-3.3e** and individual PXRD of cocrystals generated from respective crystallographic information file.*

Although polymorphs of binary urea cocrystals with organic compounds have been explored.[37-41] There is an ample scopes to look forward polymorphism in multicomponent crystals. The cocrystals of urea with tetrabutylammonium chloride provided us the basis to explore neutral urea interacting with chloride ion in different supramolecular environments. The concomitant formation of cocrystals was established experimentally by PXRD of the mixture of polymorphs and individual PXRD patterns generated from the crystallographic information files. The powder PXRD pattern shown at the top in Figure 3.18b has all the principal diffractions of the polymorphs. The identifiable characteristic peaks are marked in the figures with different symbols to show their presence in the mixture.

3.7: Conclusion

A general approach on polymorphism by rotation over intramolecular hydrogen bonded synthon of thiourea derivatives has been established. Compound **3.1** and **3.2** shows dimorphic behavior due to the free rotation of naphthyl group over intramolecular hydrogen bonded six-membered synthon. Isosteric homodimeric hydrogen bonded N-H**…**S synthons guided the assembly of each polymorph of thiourea derivative **3.1** or **3.2**. Corresponding urea derivative **3.3** and **3.4,** adopt *syn-anti* conformation across the urea moiety due to the presence of intramolecular hydrogen bond. Isosteric *non*-centrosymmetric hydrogen bonded synthon but guided by N-H**…**O bond present within the crystal lattice of compound **3.3** or **3.4.** Despite of having similar conformation, **3.3** and **3.4** did not show polymorphism. Anion guided the *anti*-conformation of the parent form to *syn*-form in the cationic host of the salts. Neutral multi-component crystals of urea derivative **3.3** with tetrabutylammonium chloride were isolated. In multi-component crystals the conformational adjustment over hetero synthons took place due to local environment change and through interplay of weak supramolecular interactions.

3.8: Experimental section

Synthesis of 1-(5-Methyl-thiazol-2-yl)-3-naphthalen-1-yl-thiourea (3.1): 5-Methylthiazol-2-yl-amine (23 mg, 2 mmol) and 1-Naphthyl isothiocyanate (37 mg, 2 mmol) were dissolved in diethylether (20 mL), and the solution was stirred for 6 hrs. The resulting solution was evaporated, and the precipitate was dried in vacuum. Yield: 90%.^{1}H NMR (400 MHz, DMSO-d_6): δ 12.03 (s, 1H), 7.96 (m, 1H), 7.90 (m,1H), 7.86 (d, 8.0 Hz, 1H), 7.60 (s, 1H), 7.53 (m, 4H), 7.08 (s, 1H), 2.28 (s, 3H). ESI MS: calcd mass for (M+1) $C_{15}H_{13}N_3S_2$, 300.0631; found, 300.0600 [M+ 1]. IR (cm^{-1}): 3460 (w), 3250 (m), 1620 (m), 1550 (s), 1550 (s), 1500 (s), 1360 (s), 1190 (s), 824 (m), 774 (s), 708 (s), 651(s), 523 (s). Polymorph **3.1a** was crystallized from dimethylformamide, whereas polymorph **3.1b** was crystallized from dimethyl sulfoxide.

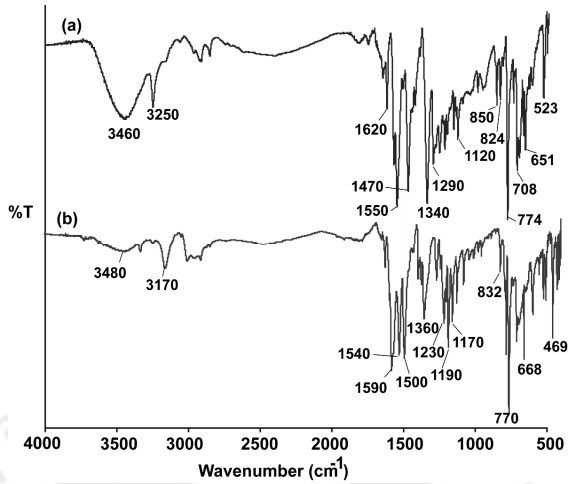

Figure 3.19: FT-IR spectra (KBr, cm^{-1}) of polymorph (a) ***3.1a,*** *(b)* ***3.1b.***

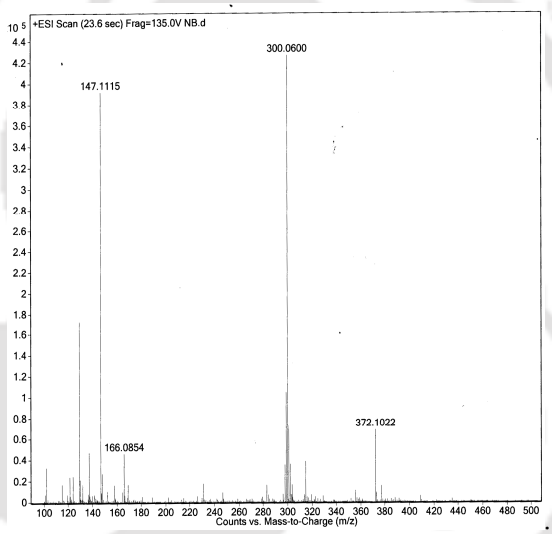

Figure 3.20: ESI mass spectra of ***3.1***

Synthesis of 1-(4-Methyl-thiazol-2-yl)-3-naphthalen-1-yl-thiourea (3.2): Compound **3.2** was prepared by following a procedure similar to the synthesis of **3.1**, but 4-methylthiazol-2-ylamine was used in place of 5-methylthiazol-2-ylamine. Yield 92%. ^{1}H NMR (600 MHz, DMSO-d_6): δ 12.16 (s, 1H), 7.96 (m, 3 H), 7.86 (d, 1H), 7.69 (s, 1H), 7.54 (m, 3H), 6.60 (s, 1H), 2.20 (s, 3H). ESI MS: calcd mass for (M+1) $C_{15}H_{13}N_3S_2$, 300.0631; found, 300.0639 [M+ 1]. IR (cm^{-1}): 3470 (w), 1570 (s), 1530 (s), 1510 (s), 1380 (m), 1210 (s), 857 (m), 768 (s), 695 (s), 513 (m). Polymorph **3.2a** was crystallized from diethylether, whereas polymorph **3.2b** was crystallized from dimethylformamide.

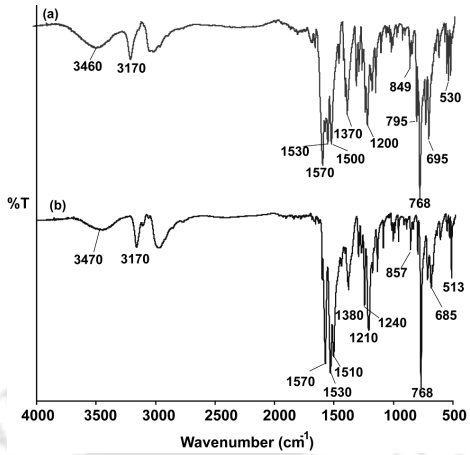

Figure 3.21: FT-IR spectra (KBr, cm^{-1}) of (a) ***3.2a,*** *(b)* ***3.2b.***

Synthesis of 1-(5-methyl-thiazol-2-yl)-3-naphthalen-1-yl-urea (3.3): 5-Methylthiazol-2-yl-amine (23 mg, 2 mmol) and 1-Naphthyl isocyanate (35 mg, 2mmol) were dissolved in dry dichloromethane (20 mL), and the solution was stirred for 6 hrs. The resulting solution was evaporated, and the precipitate was dried in vacuum. Yield: 95%. ^{1}H NMR (400 MHz, DMSO-d_6): δ 10.67 (s, 1H), 9.16 (s, 1H), 8.08 (d, 8.0 Hz, 1H), 8.03 (d, 8.0 Hz, 1H), 7.96 (d, 8.0 Hz, 1H), 7.69 (d, 8.0 Hz, 1H), 7.62 (t, 8.0 Hz, 1H), 7.65 (d, 12.0 Hz, 1H), 7.50 (t, 8.0 Hz, 1H), 7.08 (s, 1H), 2.08 (s, 3H). ESI MS: calcd mass for (M+1) $C_{15}H_{11}N_3OS$, 284.0859; found, 284.0922 [M+ 1]. IR (cm^{-1}): 3430 (w), 2930 (w), 1720 (m), 1680 (s), 1610 (m), 1550 (s), 1510 (m), 1260 (s), 763 (s), 523 (s).

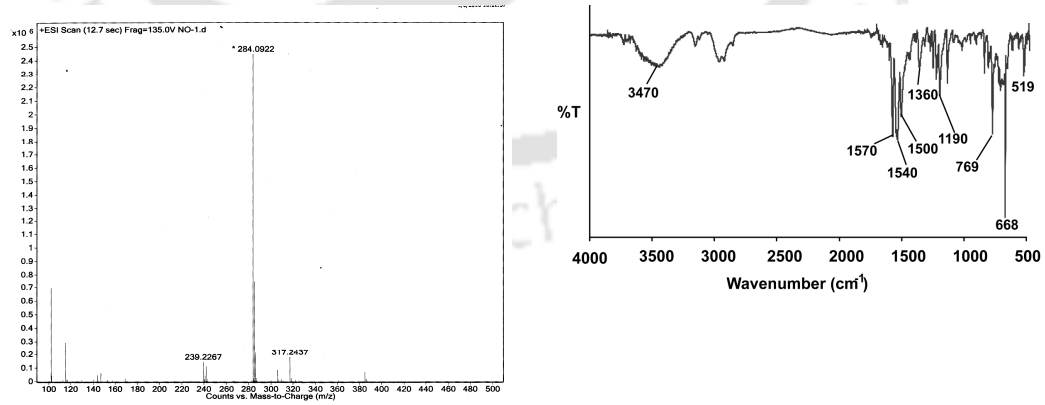

(a) (b)

Figure 3.22: (a) ESI mass spectra of compound ***3.3****, (b) FT-IR spectra (KBr, cm^{-1}) of* ***3.3****.*

1-(4-Methyl-thiazol-2-yl)-3-naphthalen-1-yl-urea (3.4): Compound **3.4** was prepared by the procedure similar to the synthesis of **3.3**, but 4-methylthiazol-2-ylamine was used in place of 5-methylthiazol-2-ylamine. Yield 90%. ESI MS: calcd mass for (M+1) $C_{15}H_{11}N_3OS$, 284.0859; found, 284.0900 [M+ 1]**.** ^{1}H NMR (400 MHz, $CDCl_3$): δ 8.03 (bs, 3H),7.84 (d, 8.0 Hz,1H), 7.64 (d, 8.0 Hz,1H), 7.46 (t, 12 Hz, 1H), 7.40 (t, 12 Hz, 1H), 6.43 (s, 1H), 2.37 (s, 3H). IR (cm^{-1}): 3460 (w), 2980 (m), 1690 (s), 1640 (s), 1590 (s), 1510 (s), 1410 (s), 1320 (s), 1250 (s), 1140 (s), 1020 (m), 796 (s), 770 (s), 741 (s), 668 (s), 558 (m).1020 (m), 796 (s), 770 (s), 741 (s), 668 (s), 558 (m).

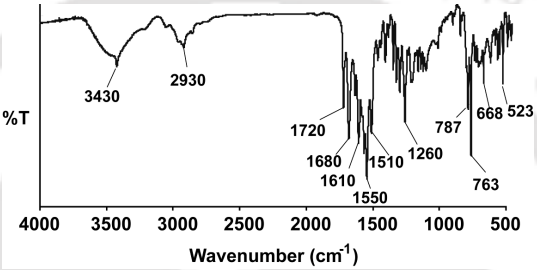

*Figure 3.23: FT-IR spectra (KBr, cm^{-1}) of **3.4**.*

Synthesis of (5-Methyl-thiazol-2-yl)-naphtho[1,2-d]thiazol-2-yl-amine (3.5): Compound **3.5** was obtained by adding few drops of inorganic acids such as hydrochloric acid, hydrobromic acid (37%, 0.4 mL) to a solution of **3.1** (29 mg, 0.1 mmol) in dimethylformamide:methanol (3:1) medium. After addition of acid, the solution was stirred at room temperature for 30 min and filtered. The filtrate, upon standing under ambient conditions, yielded pink colored crystals of **3.5** within 15 days. Yield 85%. ESI MS: calcd mass for (M+1) $C_{15}H_{11}N_3S_2$, 298.0474; found, 298.0466 [M+ 1]. IR (cm^{-1}): 3470 (w), 1570 (s), 1540 (s), 1500 (s), 1360 (m), 1190 (m), 769 (s), 668 (s).

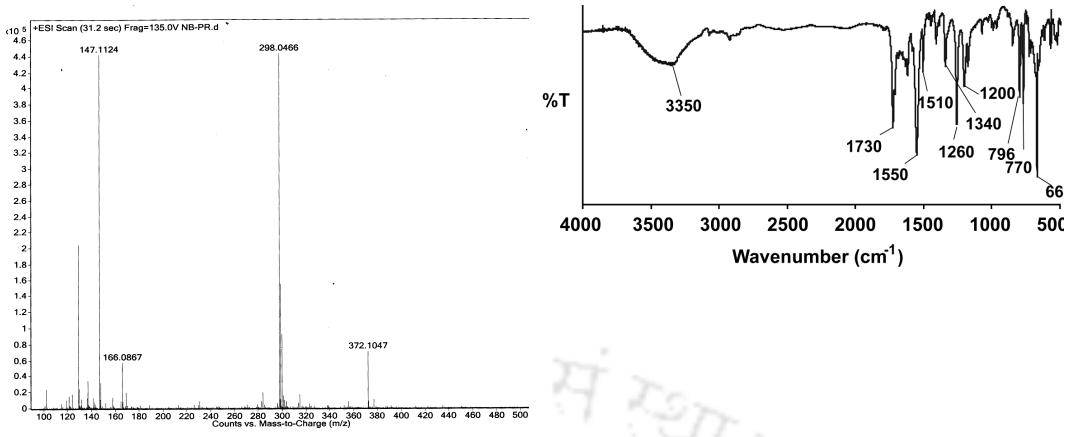

(a) (b)

*Figure 3.24: (a) ESI mass spectra of compound **3.5,** (b) FT-IR spectra (KBr, cm^{-1}) of **3.5**.*

Salt [(3.3)H$^+$Cl$^-$].H2O (**3.3a**) : Salt **3.3a** was obtained by adding a few drops of hydrochloric acid (37%, 0.4 mL) to a solution of compound **3.3** (28 mg, 0.1 mmol) in methanol (5 mL). After addition of acid, the solution was stirred at room temperature for 30 min and filtered. The filtrate, upon standing under ambient conditions, yielded colorless crystals of 3.3a obtained in 6-7 days. Yield 85%.^{1}H NMR (400 MHz, DMSO-d$_6$): δ 9.66 (m, 1H), 8.20 (t, 8.0 Hz, 1H), 7.98 (d, 8.0 Hz, 1H), 7.95 (d, 8.0 Hz, 1H), 7.68 (d, 8.0 Hz, 1H), 7.55 (m, 2H), 7.47 (t, 8.0 Hz, 1H), 7.14 (m,1H), 2.31 (s, 3H). IR (cm^{-1}): 3350 (w), 1730 (s), 1550 (s), 1510 (m), 1340 (m), 1260 (s), 1200 (m), 796 (m), 668 (s).

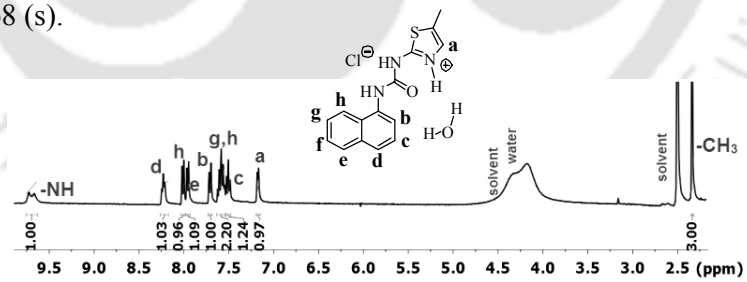

Figure 3.25: ^{1}H-NMR (DMSO-d$_6$, 400 MHz) of salt 3.3a.

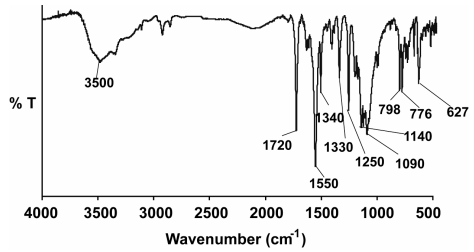

*Figure 3.26: FT-IR spectra (KBr, cm^{-1}) of **3.3a.***

Synthesis of Salt [(3.3)$H^+ClO_4^-$].H_2O (3.3b): Compound **3.3** (141 mg, 0.5 mmol) and perchloric acid (60%, 0.5 mL) were dissolved in methanol (10 mL), and the solution was left for crystallization. Colorless crystals were formed after 3 days. Yield 96%. ^{1}H NMR (400 MHz, DMSO-d_6): δ 9.21 (s, 1H), 8.05 (d, 8.0 Hz, 1H), 7.98 (d, 8.0 Hz, 1H), 7.94 (d, 8.0 Hz, 1H), 7.68 (d, 8.0 Hz, 1H), 7.62-7.52 (m, 2H), 7.48 (t, 8.0 Hz, 1H). 7.12 (s, 1H), 2.31 (s, 3H). IR (cm^{-1}): 3500 (w), 1720 (s), 1550 (s), 1330 (m), 1250 (s), 1090 (m), 798 (m), 627 (s).

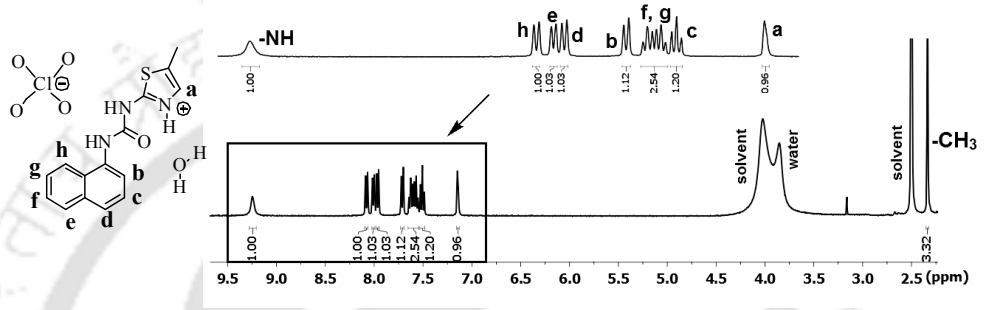

*Figure 3.27: ^{1}H-NMR (DMSO-d_6, 400 MHz) of salt **3.3b.***

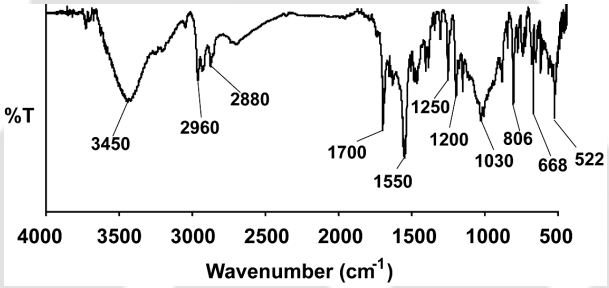

*Figure 3.28: FT-IR spectra (KBr, cm^{-1}) of **3.3a.***

Synthesis of cocrystals [(3.3)TBACl] (3.3c), [(3.3)TBACl].H_2O (3.3d or 3.3e) : Concomitant crystallization of **3.3c**, **3.3d** and **3.3e** was obtained by slow evaporation of a 15 mL methanol solution of **3.3** in the presence of excess TBACl. The crystals thus obtained were isolated by filtration and dried at room temperature. Isolated yield: 72% (considering formation of **3.3c**, **3.3d** and **3.3e** in one pot). ^{1}H NMR (400 MHz, DMSO-d_6): δ 8.05 (d, 8.0 Hz, 1H), 7.90 (m, 2H), 7.72 (d, 8.0 Hz, 1H) , 7.59-7.47 (m, 3H), 7.04 (s, 1H), 4.61 (s, 2H), 3.25-3.21 (m, 8H), 2.38 (s, 3H), 1.70-1.62 (m, 8H), 1.41 (h, 8.0 Hz, 8H), 1.02 (t, 12H). IR (cm^{-1}): 3450 (w), 2970 (m), 1700 (s), 1650 (w), 1550 (s), 1250 (s), 1030 (s), 806 (s), 668 (s).

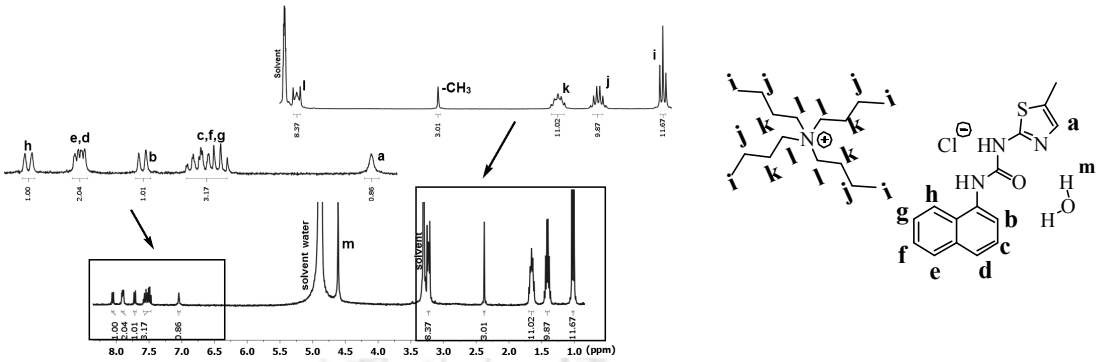

*Figure 3.29: ^{1}H-NMR (DMSO-d_6, 400 MHz) of compound **3.3c**.*

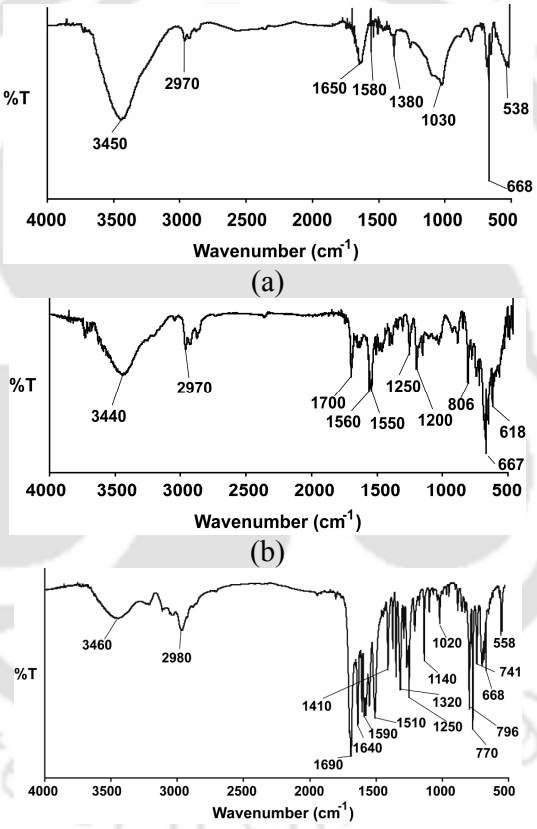

*Figure 3.30: FT-IR spectra (KBr, cm^{-1}) of (a) **3.3c**, (b) **3.3d**, (c) **3.3e***

3.9: References

1. J.-P. Brog, C.-L. Chanez, A. Crochet, K. M. Fromm. *RSC Adv*., 2013, **3**, 16905.
2. A. Nangia, *Acc. Chem. Res*., 2008, **41**, 595.
3. A. J. Cruz-Cabeza, J. Bernstein, *Chem. Rev*., 2014, **114**, 2170.
4. J. D. Dunitz, *CrystEngComm*, 2003, **5**, 506.
5. F. Wohler, *Annalen*, 1844, **51,** 145.
6. O. Almarsson, M. J. Zaworotko, *Chem. Commun*., 2004, 1889.
7. J. Wouters, L.Quere, *Pharmaceutical Salts & Co-crystals*. Cambridge: RSC Publishing, 2012.
8. G. P. Stahly, *Cryst. Growth Des.*, 2009, **9,** 4212.
9. N. A. Mir, R. Dubey, G. R. Desiraju, *IUCrJ*, 2016, **3,** 96.
10. R. Dubey, G. R. Desiraju, *IUCrJ*, 2015, **2,** 402.
11. G. Bolla, A. Nangia, *Chem. Commun.*, 2015*,* **51,** 15578.
12. C. B. Aakeroy, J. Desper, J. Urbina, *Chem. Commun.*, 2005, 2820.
13. C. Seaton, N. Blagden, T. Munshi, I. Scowen, *Chem. Eur. J.*, 2013, **19,** 10663.
14. S. Tothadi, P. Sanphui, G. R. Desiraju, *Cryst. Growth Des.*, 2014, **14,** 5293.
15. R. Dubey, N. A. Mir, G. R. Desiraju, *IUCrJ* 2016, **3**, 102.
16. M. C. Etter, *Acc. Chem. Res.*, 1990, **23,** 120.
17. M. L. Peterson, E. A. Collier, M. B. Hickey, H. Guzman, O. Almarsson, *in Organic Crystal Engineering: Frontiers in Crystal Engineering, ed.* E. R. T. Tiekink, J. J. Vittal and M. J. Zaworotko, Wiley, 2010, 67.
18. C. B. Aakeroy, N. R. Champness, C. Janiak, *CrystEngComm*, 2010, **12,** 22.
19. J. F. Remenar, S. L. Morissette, M. L. Peterson, B. Moulton, J. M. MacPhee, H. R. Guzman, O. Almarsson, *J. Am. Chem. Soc.*, 2003, **125,** 8456.

20. O. S. Bushuyev, T. Fiscic, C. J. Barrett, *Cryst. Growth Des.*, 2016, **16,** 541.
21. G. R. Desiraju, *Angew. Chem., Int. Ed.*, 1995, **34,** 2311.
22. R. D. B. Walsh, M. W. Bradner, S. Fleischman, L. A. Morales, B. Moulton, N. Rodriguez-Hornedo, M. J. Zaworotko, *Chem. Commun.*, 2003, **2,** 186.
23. J. A. Bis, M. J. Zaworotko, *Cryst. Growth Des.*, 2005, **5**, 1169.
24. A. D. Bond, *CrystEngComm*, 2007, **9,** 833.
25. A. Mukherjee, S. Tothadi, G. R. Desiraju, *Acc. Chem. Res.*, 2014, **47,** 2514.
26. C. B. Aakeroy, A. M. Beatty, B. A. Helfrich, *Angew. Chem., Int. Ed.* 2001, **40,** 3240.
27. L. R. MacGillivray, J. L. Reid, J. A. Ripmeester, *J. Am. Chem. Soc.*, 2000, **122***,* 7817.
28. J. D. Dunitz, A. Gavezzotti, *Cryst. Growth Des.*, 2012, **12***,* 5873.
29. A. Mukherjee, G. R. Desiraju, *Chem. Commun.*, 2011, **47**, 4090.
30. N. J. Babu, S. Cherukuvada, R. Thakuria, A. Nangia, *Cryst. Growth Des.*, 2010, **10,** 1979.
31. D. Pogoda, J. Janczak, V. Videnova-adrabinska, *Acta Crystallogr.*, 2016, **72B,** 263.
32. W. Auwarter, A. Weber-Bargioni, A. Riemann, A. Schiffrin, O. Groning, R. Fasel, J. V. Barth, *J. Chem. Phys.*, 2006, **124***,* 194708.
33. F. Hof, C. Nuckolls, S. L. Craig, T. Martin, J. Rebek, Jr., *J. Am. Chem.Soc.*, 2000, **122,** 10991.
34. J. Bernstein, A. T. Hagler, *J. Am. Chem. Soc.*, 1978, **100,** 673.
35. W. C. McCrone, *Polymorphism, in physics and chemistry of the organic solid state,* ed. Fox, D.; Labes M. M.; Weissberger, A.; Wiley-Interscience, New York, 1965, **2**, 725.
36. G. R. Desiraju, *Cryst.Growth Des.*, 2008, **8,** 3.
37. S. Tothadi, *CrystEngComm*, 2014, **16,** 7587.
38. S. Aitipamula, P. S. Chow, R. B. H.Tan, *CrystEngComm*, 2014, **16,** 3451.

39. S. Aitipamula, P. S. Chow, R. B. H. Tan, *CrystEngComm*, 2010, **12,** 3691.
40. S. Aitipamula, P. S. Chow, R. B. H. Tan, *Cryst.Growth Des.*, 2010, **10,** 2229.
41. S. Aitipamula, A. B. H. Wong, P. S. Chow, R. B. H. Tan, *CrystEngComm*, 2013, **15,** 5877.
42. P. Byrne, D. R. Turner, O. L. Gareth, N. Clarke, J. W. Steed, *Cryst. Growth Des.*, 2008, **8,** 3335.
43. R. Taylor, O. Kennard, W. Versichel, *J. Am. Chem. Soc.*, 1984, **106,** 244.
44. J. T. Lenthall, J. A. Foster, K. M. Anderson, M. R. Probert, J. A. K. Howard, J. W. Steed, *CrystEngComm*, 2011, **13,** 3202.
45. A. Masunov, J. J. Dannenberg, *J. Phys. Chem. B*, 2000, 104, 806.
46. A. Masunov, J. J. Dannenberg, *J. Phys. Chem. A*, 1999, **103,** 178.
47. J. J. Kane, R. -F. Liao, F. W. Fowler, J.W. Lauher, *J. Am. Chem. Soc.*, 1995, **117,** 12003.
48. A. L. Grzesiak, M. Lang, K. Kim, A. J. Matzger, *J. Pharm. Sci.*, 2003, **92,** 2260.
49. C. L. Andersen, C. S. Jensen, K. Mackeprang, L. Du, S. Jorgensen, H. G. Kjaergaard, *J. Phys. Chem. A*, 2014, **118,** 11074.
50. D. E. Lynch, L. J. Nicholls, G. Smith, K. A. Byriel, C. H. L. Kennard, *Acta Crystallogr.*,1999, **55B,** 758.
51. A. Carletta, C. Meinguet, J. Wouters, A. Tilborg, *Cryst. Growth Des.*, 2015, **15,** 2461.
52. J. Bernstein, R. J. Davey, J. O. Henck, *Angew. Chem., Int. Ed.*, 1999, **38,** 3440.

Chapter 4

Imine-tautomers of aminothiazole derivatives: intriguing aspects of chemical reactivities

Signal transduction in organic molecules are generated through structural or chemical changes by interactions with analytes.[1-7] Various sensors are devised based on the nature of energy used to cause signal transductions.[1-7] Many compounds sensitive to local environment have been found to be useful as sensors.[8,9] Among small molecules, thiazoles can be used to detect various metal ions and anions. Some of the examples were discussed in chapter 1 of the thesis. For instances 2-(4-phenyl-thiazol-2-yl)-phenol (**1.46**) is used to detect Ga^{3+} and HSO_4^{1-} ions.[10] It shows 'ON' and 'OFF' fluorescence responses towards Ga^{3+} ions. On the other hand, **1.46**-Ga^{3+} complex shows selectivity toward HSO_4^-. Fluorescence changes occur due to inhibition of excited state intramolecular proton transfer (ESIPT) as illustrated in Figure 4.1. Chemosensor **1.46** is already mentioned as F^- sensor in Chapter 1.

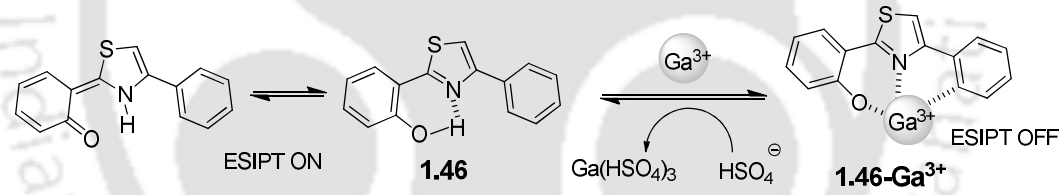

*Figure 4.1: Keto-enol form of **1.46** contributing to fluorescence emission.*

The functional unit anchored to thiazole may cause specific signal transduction by binding to a substrate. Such principles are already in practice. For example visual detection of nitro-aromatics is possible due to selective binding with 10-methylphenothiazine (Figure 4.2a).[11]

(a) (b)

Figure 4.2: (a) 1:1 co-crystal of 10-methylphenothiazine and 1,3-dinitrobenzene, (b) chemical structure of 1,4-bis(5-phenyl-2-oxazolyl)benzene.

The crystal structure showed alternating π stacking of the electron-rich 10-methylphenothiazine and the electron-poor 1,3-dinitrobenzene. Dichloromethane solvate of 1,4-bis(5-phenyl-2-oxazolyl)benzene shows tunable blue and red luminescence.[12] (Figure 4.2b). Nature has also gifted thiazolic molecule like luciferin (**1.16**, Chapter 1) which shows bioluminescence. Luciferin **1.16** has a hydroxybenzothiazole connected to carboxythiazole through C-C bond. The phosphorescence behavior of Luciferin **1.16** is due to a decarboxylative oxidation process. This indicates that appropriately chosen thiazole derivatives may be useful as optical materials.

Aminothiazole can be functionalized with thiourea. There are documented applications of thiourea derivatives in organo-catalysis[13] and in molecular recognition.[14] Thiourea also act as analytical reagents in various detection purposes.[15] Besides these, thiourea derivatives have structural interest as they adopt several conformers across the thiourea unit[16] as discussed in Chapter 2. On the other hand, N,N'-dialkylthiourea are known to adopt *trans-trans*, *trans-cis* and *cis-cis* orientations.[17] The energy differences between and *trans-trans* are in the range of 0.1-1.4 kcal/mol whereas the difference between *cis-trans* and *cis-cis* is about 3.9-9.6 kcal/mol.[18] In general, positional isomers have significantly contributed to the understanding of the structure-property relationships of molecules and related materials in solid state.[19] On the other hand, stereoisomer of pharmaceutical compounds are well known to show different biological activities.[20,21] In spite of these facts there is a need to understand aggregation behavior of set of isomers to develop new molecule-based functional materials.[22-25] Hence, to make a clear understanding on role of solvent upon solid state structure and in molecular/ion recognition, we have chosen positional isomers of thiourea based aminothiazole derivative (**4.1** and **4.2**).

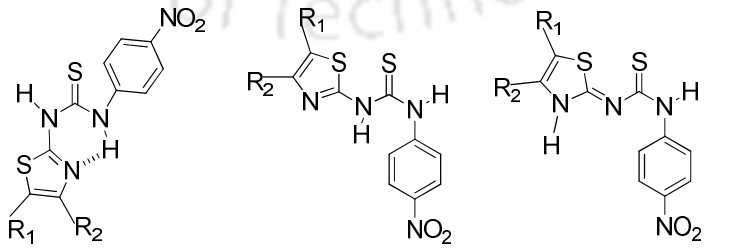

*Figure 4.3: (a-b) Conformers of amine form and (c) imine form of **4.1** or **4.2**.*

The positional isomers of thiazole derivatives such as 1-(5-methylthiazol-2-yl)-3-(4-nitrophenyl)-thiourea (**4.1**) and 1-(4-methylthiazol-2-yl)-3-(4-nitrophenyl)-thiourea (**4.2**) may show amine-imine tautomerism (Figure 4.3). Thus, several solvent and ion guided processes were taken up to make distinction of such forms at all present in solution.

4.1: Synthesis of nitro substituted thiourea tethered thiazole 4.1 and 4.2

The compounds **4.1** and **4.2** were prepared by reaction of corresponding 4- or 5-methylaminothiazole with 4-nitrophenyl isothiocyanate. These compounds were characterized by various spectroscopic techniques, such as IR spectroscopy, mass spectrometry and ^{1}H-NMR.

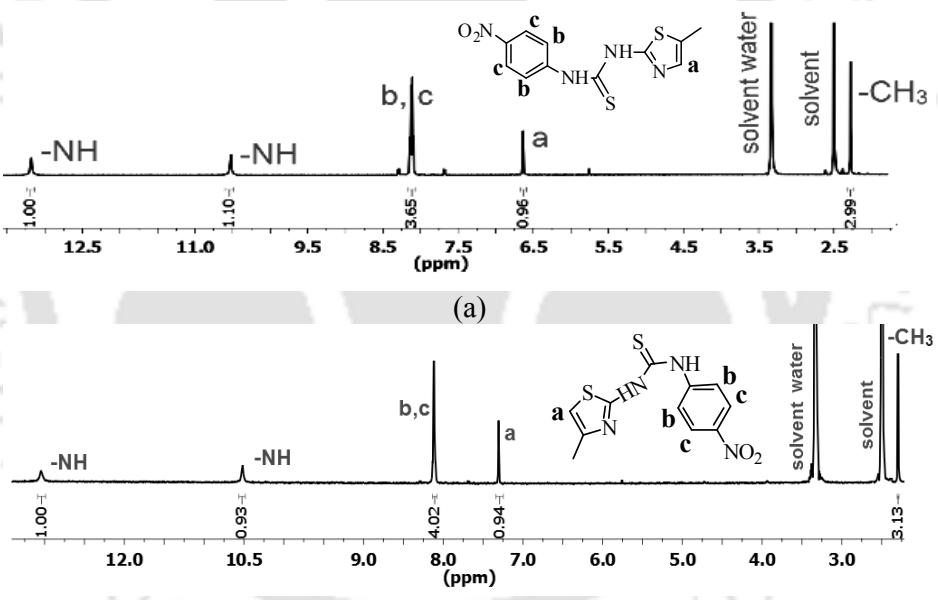

*Figure 4.4: ^{1}H-NMR (600 MHz, DMSO-d_6) spectra of (a) **4.1** and (b) **4.2***

In the ^{1}H-NMR, the characteristic thiazolic protons of **4.1** appears at 6.65 ppm (Figure 4.4a), whereas it appears at 7.30 ppm for **4.2** (Figure 4.4b). The mass spectrum of **4.1** shows a peak at 295.0341 (Calculated 295.0325), corresponding to [M+1] peak (Figure 4.22b). Compound **2.2** shows peck at 295.0299 (Calculated 295.0325), corresponding to [M+1] (Figure 4.23b).

4.1.1: Supramolecular assemblies of 4.1 and 4.2

Crystals of both these compounds (**4.1** and **4.2**) were obtained from slow evaporation of solution in dimethylformamide solution. Crystal structures of **4.1** and **4.2** have shown that both these isomers adopt imine form in solid state (Figure 4.5a,b). This is reflected in the C4-N1 and C4=N2 bond distances in the respective structures as listed in Table 4.1.

Table 4.1: Selected C4-N1 and C4=N2 bond parameter of compound **4.1** and **4.2**.

	Observed Bond distance		Conventional Bond distance	
Compound	C4-N1	C4=N2	C-N	C=N
4.1	1.351Å	1.338	1.47Å	1.27-1.29Å
4.2	1.351Å	1.334		

These bond lengths are close to conventional C=N bond distances. But the C4-N1 bond distances are far away from regular C-N bond length (Table 4.1). In Chapter 2, we have shown that N-thizole-N'-phenylthiourea derivative (**2.1** and **2.2**) posses amine form of thiourea. The only structural difference of compounds **4.1** and **4.2** arises from the earlier set of compounds **2.1** and **2.2** is the presence of 4-nitro group. Thus, it is clear that the nitro group present on **4.1** and **4.2** helped the imine form to be present in solid state by virtue of its electron withdrawing nature.

Compound **4.1** crystallizes in triclinic $P\bar{1}$ space group having three symmetry independent molecules in its asymmetric unit, whereas, asymmetric unit of compound **4.2** has one molecule and it crystallizes in monoclinic *C2/c* space group. Self assembly of **4.1** has two independent dimeric synthons. One is a conventional $R_2^2(8)$ N-H**…**S type and another is $R_2^2(24)$ formed by N-H**…**O hydrogen bonds. Both synthons guide the packing pattern of **4.1** to adopt chain-like arrangements of molecules. Assembling among the three symmetry-independent molecules of **4.1** takes place to form two independent arrays of interacting molecules as shown in Figure 4.5c. Carbon atoms of each symmetry independent molecule assigned with different colors for simplification (Figure 4.5c). Robust synthons are thus formed in accordance with Etters rule, (mentioned in Chapter 1) by maximum utilization of the hydrogen bond formation sites and according to priority of the bond strengths.[35,36] Due to such an effect there are two N-H**…**S bond distances seen in the self-assembly of **4.1**, which are 3.596(4)Å and 3.576(4)Å and respective N-H**…**S bond angles are 167.0° and 166.0° (Table 4.2). For comparison, N-methyl-N'-tertbutylthiourea

adopting *cis-trans* conformation, has ∠N-H**…**S 169.2° for *cis* part, whereas *trans* part has ∠N-H**…**S as 146.5°. It has N-H**…**S bond distances 3.521Å and 3.512Å respectively. The two ∠N-H**…**S angles of **4.1** are 154(3)° and N-H**…**S distance as 3.496(3)Å.[18]

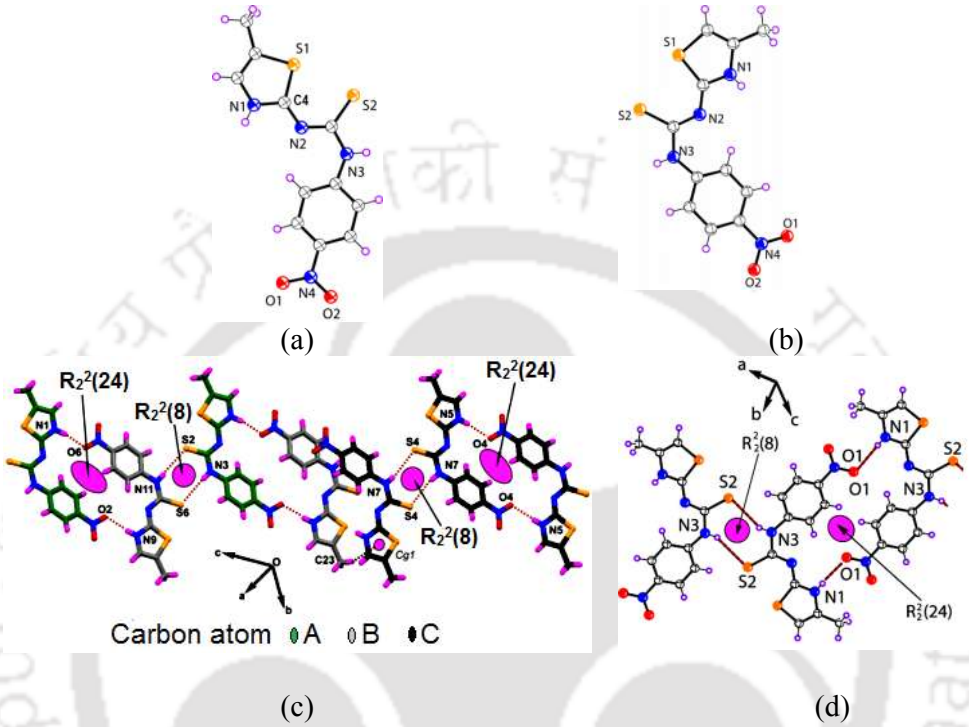

Figure 4.5: Structure of (ORTEP drawn with 50% thermal ellipsoids) (a) ***4.1*** *(b)* ***4.2****. Different dimeric hydrogen bonded synthons in the assemblies of (c)* ***4.1****. (d)* ***4.2***

Assembly of **4.2** has an array by similar kind of hydrogen-bonded sub-assemblies (Figure 4.5d). Imine forms do not have provision to form hydrogen bonds analogous to conventional N,N'-dialkylthiourea. Thiourea derivatives form dimer, linear or cyclic chain through intermolecular hydrogen bonds.[18] Hence, solid state assemblies of imine tautomer **4.1** or **4.2** has close structural resemblances to substituted thiocarbamide.

4.2: Reactivity of compounds 4.1 and 4.2 towards solvents

It has been suggested in the literature that assemblies formed in solution and the solid state may have some correlation.[28] The synthons in the solid state may also be reflections of the self-assemblies that were originally present in solution.[29] Acetylimino-thiozoles showed solvent dependent amine-imine tautomerism.[30]

Various concomitant polymorphs formed in mixture of solvents suggested that the individual component of solvent guide the formation conformational polymorphs.[31] Furthermore solvent plays a crucial role in catalytic reactions of thiourea derivatives.[32,33] The carbonyl functional group can form hydrogen bond with thiourea through N-H**…**O hydrogen bonds; such moderate hydrogen bond interactions are shown to be about 7 kcal/mol at room temperature.[34] Thus, reactivities with solvents and crystallization of the positional isomers **4.1** and **4.2** from different solvents were studied. Compound **4.1** and **4.2** should be able to form solvates with carbonyl containing or related solvents. With such an anticipation we prepared of solvates of **4.1** and **4.2** with dimethylformamide (DMF) or dimethylacetamide (DMA) having C=O as acceptor of hydrogen bond. On the other hand, dimethylsulfoxide (DMSO) has S=O as the acceptor to form hydrogen bond with a thiourea derivative. We find that the isomers **4.1** and **4.2** showed distinguishable reactivities in different solvents (Scheme 4.1). For example, the compound **4.1** form solvates with dimethylacetamide and dimethylsulphoxide, namely [(**4.1**).DMSO] (**4.1a**) and [(**4.1**).DMA] (**4.1b** and **4.1.1b**). Whereas, crystallization of **4.2** from these solvents, resulted hydrolyzed products namely hydrated 1-(4-methylthiazol-2-yl)-3-(4-nitrophenyl)-urea (**4.2b)**. Thus, compound **4.2** was relatively easy to hydrolyze by traces of moistures present in these solvents. Thiazole derivatives form salts on reaction with mineral acids but we find that reaction of hydrobromic acid with **4.2** in DMSO solvent gave a brominated compound **4.2a** (Scheme 4.1).

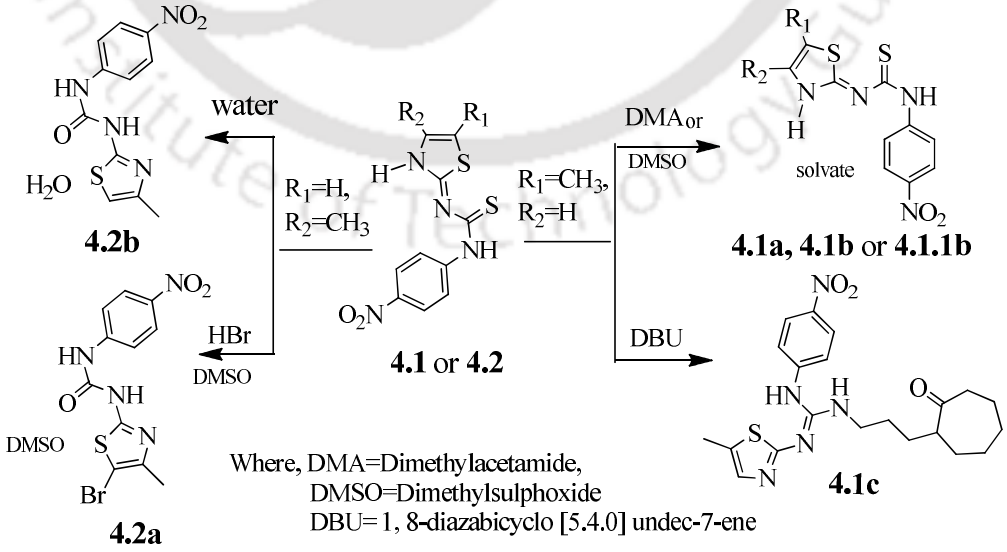

*Scheme 4.1: Reactivity of compound **4.1** and **4.2** towards different solvents.*

4.2.1: Reaction of 4.1 with DBU

The compound **4.1** reacted with 1,8-diazabicyclo [5.4.0] undec-7-ene (DBU) to give ring opened product (**4.1c**). This ring opening reaction of DBU occurs without help of a reagent. A plausible reaction mechanism is given in Scheme 4.2. The water present in solvent dimethylformamide interacts at the imine C-atom of DBU, thereby activating the imine N-atom. The activated N- atom attracts on the C-atom of thiocarbonyl moiety of compound **4.1**. Intermediate **4.1´** thus formed. Subsequently, the intermediate **4.1´** undergoes rearrangement and released dihydrogen sulphide (H_2S) gas, giving the ring opened product **4.1c**.

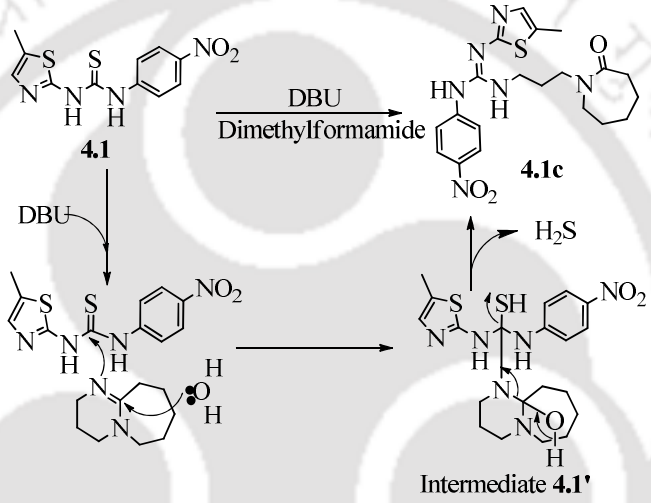

*Scheme 4.2: A plausible mechanism on formation of **4.1c**.*

This observation is significant from the point that it cautions on the limitation of using DBU as a solvent while performing a reaction with a thiourea derivative. This result is also important as there is scope to discover ring opening reactions of DBU. Literature suggests ring opening of DBU do occur with benzoxazinones as shown in Figure 4.6, but as exceptional case. [45]

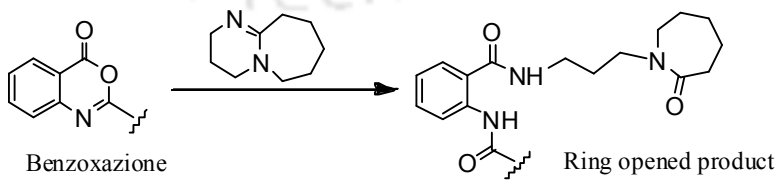

Figure 4.6: Ring opening reaction of DBU.

4.2.2: Supramolecular assemblies of DMSO and DMA solvate of 4.1

Structural elucidation of **4.1a** (DMSO solvate of **4.1)** has revealed that two DMSO molecules act as intervening connecting molecules between two host molecules through weak interactions. This results in the formation of cyclic sub-assemblies between two DMSO and two **4.1** molecules as illustrated in Figure 4.7a. Formation of such sub-assemblies may be alternatively described as incorporation of bridging dimethylsulphoxide molecules through N-H**…**O and C-H**…**O hydrogen bonds between the host molecules. Thus, the original $R_2^2(24)$ dimeric sub-assembly observed in the packing pattern of the unsolvated **4.1** were disrupted. The self-assembly of solvate **4.1a** has an R_2^2 (8) N-H**…**S type synthon as found in the parent compound. A view from the *b*-crystallographic axis has revealed that the DMSO molecules are intercalated between the layers of host molecules, forming a zig-zag chain-like arrangement (Figure 4.7b). Upon crystallization of **4.1** from the DMA solvent, two different types of crystalline solvate of **4.1** were obtained; these solvates are designated as **4.1b** and **4.1.1b**. Both the forms have identical composition, but different crystal morphology as depicted in Figure. 4.8a. Principal difference between the two crystalline forms is that one form has crystallographically disordered solvent molecules, but the other one holds solvent molecules without crystallographic disorder. Polymorphic molecules having crystallographic disorder as found in the present case may be described as a metastable state.[36,37] Generally metastable forms have higher solubility.[38]

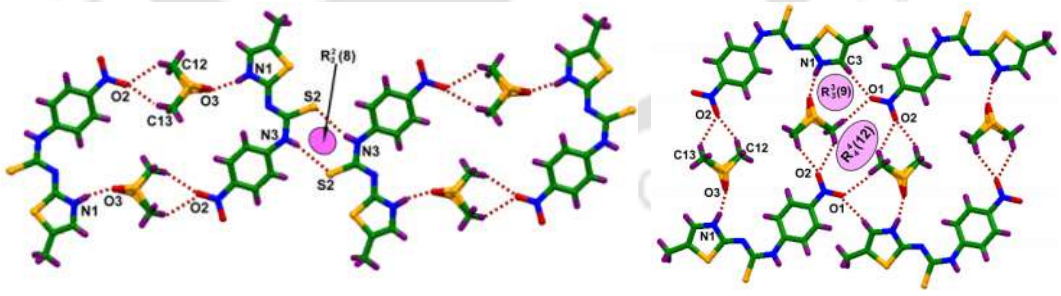

(a) (b)

*Figure 4.7: (a) Various hydrogen bonded assemblies in the crystal lattice of **4.1a**, (b) Zig-zag arrangement of DMSO molecules intercalated between the layers of host molecules of **4.1a**.*

Generally molecular conformations and crystal lattice energy differs by energy of the order of <5 kcal mol^{-1}, and compensation of these two types of energies may

contribute to the stabilization of strained conformers.[39] Structure elucidation shows both the DMA solvates (**4.1b** and **4.1.1b**) have distinguishable unit cell volume (Appendix Table) and different packing patterns. The metastable form **4.1.1b** has a higher density with smaller crystal volume over the more stable form **4.1b** (Table 4.2). This is due to energy associated with disordered state of the solvent molecules is compensated by the crystal lattice energy to have a more tightly packed structure. We obtained a very small quantity of crystals of the metastable form **4.1.1b**; hence the powder XRD pattern of the mixture of the two forms was taken. Upon heating the mixture of the two forms under mild conditions at 50 °C for about 10 minutes the metastable form **4.1.1b** transforms to the stable form **4.1b**, which was confirmed by comparing the samples before heating and after heating as illustrated in Figure. 4.8b.

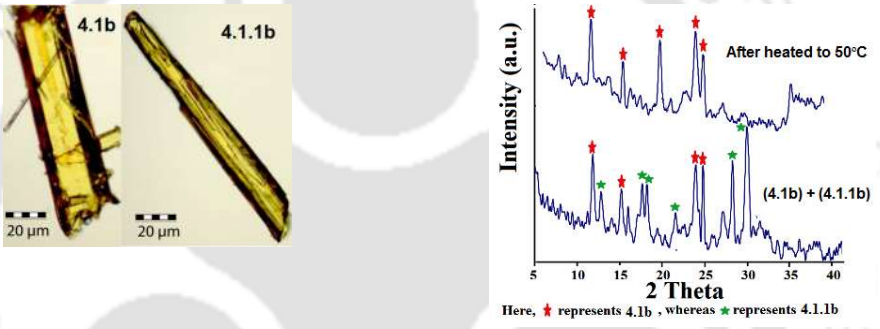

(a) (b)

*Figure 4.8: (a) Crystal morphologies of **4.1b** and **4.1.1b**, (b) Overlapping of powder XRD of (**4.1b**+**4.1.1b**) sample with after heating mixed crystal of **4.1b** and **4.1.1b** at 50 ºC for 10 mins.*

Structural elucidation shows that solvate **4.1b** has $R_2^2(8)$ and R_2^2 (24) type dimeric sub-assembly of host molecules formed through N-H**…**S and N-H**…**O hydrogen bonds as shown in Figure 4.9a. Dimethylacetamide molecules are present as pairs of hydrogen bonded molecules within the $R_2^2(24)$ dimeric sub-assembly by N-H**…**O bonds. The structure of solvate **4.1b** carries the signature of the parent compound and retains the $R_2^2(24)$ and $R_2^2(8)$ sub-assemblies found in the parent compound. On the other hand, metastable form **4.1.1b** has robust $R_2^2(24)$ sub-assemblies found in the parent **4.1** are disrupted by interactions with the DMA molecules. But, $R_2^2(8)$ synthon formed between two host molecules through N-H**…**S bonds is retained. The metastable form **4.1.1b** has only one cyclic type of hydrogen bonded sub-assemblies, that is $R_2^2(8)$, guided by N-H**…**S bonds. In this case the dimethylformamide

molecules are present as a discrete unit (Figure 4.9b) but in a disordered manner by sharing of the carbon atoms as well as the nitrogen atoms at two equivalent positions.

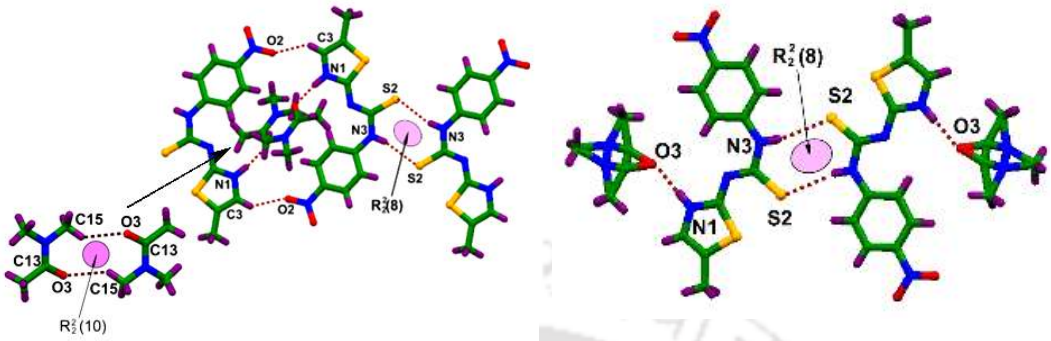

(a) (b)

*Figure 4.9: (a) Hydrogen bonded cyclic sub assemblies in the self-assemblies of the solvate (a) **4.1b** and (b) **4.1.1b**.*

4.2.3: Conformational adjustment among the solvates of 4.1

Important aspects of the solvates of **4.1** are the conformational adjustments of the host projecting the nitrobenzene ring in different orientations across the plane of the C=S bond. For comparing the orientations of the thiazole ring, an overlaid diagram of **4.1** with hosts of each solvate is drawn by fixing the nitrophenyl unit in one plane (Figure. 4.10). The metastable form **4.1.1b** has a larger difference in the torsion angle than the stable form **4.1b** with respect to the parent form **4.1** as shown in Figure 4.10. It may be suggested that the metastable form on standing reorganizes to the stable form. Thus, the metastable solvate is an intermediate stage formed by conformational adjustments.[40] It is seen that the solvents play an important role in shifting the orientation of the thiazole moiety in each solvate.

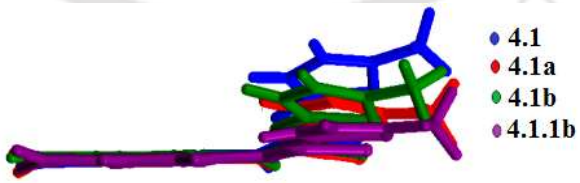

*Figure 4.10: Overlaid structural diagram of **4.1** and different solvates drawn by fixing the nitrophenyl group in one plane.*

There is current interest in the mechanistic aspect of polymorphs guided by solvents. Earlier, it was shown that polymorphic structures can be due to desolvation of assemblies formed by a substrate interacting with a solvent.[41] In the case of

metastable solvate **4.1.1b**, the presence of a crystallographically disordered solvent molecule is an additional support to the role played by solvent to guide the formation of a polymorph.

Table 4.2: Hydrogen bonds parameters of **4.1**, **4.2**, **4.1a**, **4.1b**, **4.1.1b**, **4.1c**, **4.3**, **4.2a** and **4.2b**.

Compd No.	D-H…A [symmetry]	$d_{D-H(Å)}$	$d_{H\cdots A(Å)}$	$d_{D\cdots A(Å)}$	∠D-H···A (°)
4.1	N(1)-H(1) ···O(4)	0.86	2.05	2.880(4)	163
	N(3)-H(4A) ···S(4) [x,y,1+z]	0.86	2.74	3.567(4)	161
	N(5)-H(5A) ···O(1)	0.95(4)	1.94(4)	2.876(5)	168(4)
	N(7)-H(7A) ···S(2) [x,y,-1+z]	0.86	2.75	3.596(4)	167
	N(9)-H(9A) ···O(6) [-x,1-y,1-z]	0.82(4)	2.09(4)	2.898(5)	169(4)
	N(11) -H(11A) ···S(6) [-x,1-y,-z]	0.86	2.74	3.576(4)	166
	C(7)-H(7) ···S(4) [x,y,1+z]	0.93	2.84	3.646(4)	146
	C(11)-H(11) ···N(2)	0.93	2.27	2.849(6)	120
	C(18)-H(18) ···N(6)	0.93	2.37	2.892(5)	115
	C(29)-H(29) ···N(10)	0.93	2.32	2.861(5)	117
4.2	N(1)-H(1) ···O(1) [-x,1-y,-z]	0.72(3)	2.23(3)	2.946(3)	175(3)
	N(3)-H(3A) ···S(2) [1/2-x,-1/2-y,-z]	0.80(3)	2.76(3)	3.496(3)	154(3)
	C(11)-H(11) ···N(2)	0.93	2.34	2.874(4)	116
4.1a	N(1)-H(1) ···O(3)	0.86(2)	1.87(2)	2.711(3)	165(2)
	N(3)-H(3A) ···S(2) [-x,-y,1-z]	0.79(2)	2.76(2)	3.5255(19)	163.7(19)
	C(8)-H(8) ···O(3) [1-x,1-y,1-z]	0.93	2.50	3.211(4)	133
	C(11)-H(11) ···N(2)	0.93	2.34	2.901(2)	118
	C(12)-H(12A) ···O(2) [1-x,2-y,1-z]	1.04(4)	2.54(4)	3.318(4)	131(3)
	C(13)-H(13A) ···O(1) [-1+x,y,-1+z]	0.98(4)	2.58(4)	3.564(4)	176(4)
	C(13)-H(13B) ···O(2) [1-x,2-y,1-z]	0.97(4)	2.58(4)	3.280(3)	130(3)
4.1b	N(1)-H(1) ···O(3)	0.91(3)	1.87(3)	2.764(3)	171(3)
	N(3)-H(3A) ···S(2)	0.86	2.67	3.4918(19)	159
	C(3)-H(3) ···O(2)	0.93	2.57	3.275(4)	133
	C(7)-H(7) ···S(2)	0.93	2.81	3.660(3)	152
	C(11)-H(11) ···N(2)	0.93	2.28	2.851(3)	119
	C(13)-H(13A) ···O(3)	0.96	2.34	2.695(3)	101
4.1.1b	N(3) -H(1) ···S(2) [1-x,-y,1-z]	0.769(19)	2.820(19)	3.5541(17)	160.5(17)
	N(1)-H(2) ···O(3)	0.88(2)	1.86(2)	2.739(3)	175.6(19)
	C(7)-H(7) ···S(2)	0.93	2.83	3.659(2)	149
	C(8)-H(8) ···O(2)	0.93	2.56	3.305(3)	137
	C(11)-H(11) ···N(2)	0.93	2.32	2.893(2)	120
	C(14)-H(14A)···O(3)	0.87(4)	2.30(3)	2.586(4)	100(3)
4.1c	N(3)-H(3A) ···O(1)	0.94(3)	2.14(3)	2.982(4)	150(3)
	N(5)-H(5) ···N(1)	0.95(3)	1.91(3)	2.655(4)	134(2)
	C(8)-H(8) ···O(3)	0.93	2.51	3.365(4)	152
	C(11)- H(11) ···N(2)	0.93	2.28	2.873(4)	121
	C(12)- H(12A) ···O(1)	0.97	2.47	3.100(3)	123
4.3	N(3) -H(3A) ···O(2A)	0.86	2.09	2.931(7)	165
	C(7) -H(7) ···O(2A)	0.93	2.59	3.358(8)	140
	C(11) -H(11) ···N(2)	0.93	2.25	2.847(6)	121
	C(12) -H(12A) ···O(2A)	0.96	2.46	2.794(11)	100
4.2a	N(2) -H(2) ···O(4) [-1+x,y,z]	0.86	2.23	3.010(3)	150
	N(3) -H(3) ···O(4) [-1+x,y,z]	0.86	1.96	2.800(3)	165
	C(1) -H(1C) ···Br(1)	0.96	2.89	3.390(3)	114
	C(7) -H(7) ···O(1)	0.93	2.24	2.850(2)	123
	C(12) -H(12B)···N(1) [-x,1-y,-z]	0.96	2.59	3.470(4)	152
	C(13) -H(13C) ···O(1) [1-x,1-y,-z]	0.96	2.51	3.300(3)	139

4.2.4: Comparison of hydrolytic stability between 4.1 and 4.2

The solvates of **4.1** could be isolated through crystallization from dry solvents. But the solvated product of **4.2** could not be obtained. Since crystallization from DMSO and DMA are slow, prolonged standing of **4.2** for crystallization in dry solvents caused hydrolysis of **4.2** by picking up traces of moisture from the air. These observations pointed out that the solvent interacts with the host molecules **4.1** or **4.2** to provide an intermediate stage for hydrolysis. The difference in reactivity is due to the position of the two methyl groups present in these compounds. In such reactions the approach of a water molecule would be easier when the methyl group of thiazole is away from the hydrolysis site. In the assembly shown in Figure 4.5a, **4.1** have the methyl group in close proximity to the thioketone, which is a steric factor to act as a barrier to an approaching water molecule. A similar assembly of **4.2** has the methyl group away from such a position; hence the approach of a water molecule is easier. These results substantiated that the difference in hydrolytic stability of **4.1** and **4.2** stems from the position of the hydrophobic methyl group on the aromatic thiazole ring.

4.3: Interactions of metal ions with 4.1 and 4.2: spectroscopic studies

Small heterocyclic organic molecules are useful for selective detection of ions.[42-46] Advantage of using thiazole positional isomers was observed in distinctions of iron ions and copper ions.[47] On the other hand, toxic mercury ions can be selectively detected by hydrolysis of thiourea derivatives. Earlier, Lee et al., synthesized a rhodamine-6G phenylthiourea derivative (**L1**),[48] which is a novel dual chemosensors for the selective and sensitive naked-eye recognition of Hg^{2+} and F^- ions. Hg^{2+}-promoted spirolactam ring opening of the rhodamine moiety induced urea formation through the diphenylcarbodiimide intermediate from the thiourea moiety.

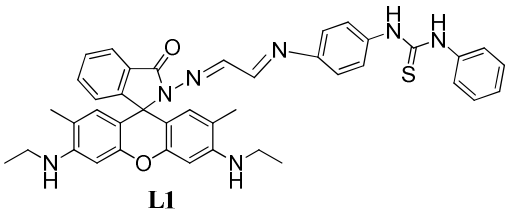

L1

Figure 4.11: A thiourea based sensor for Hg^{2+}

With these points in mind, interactions of **4.1** and **4.2** with different metal ions have been studied. Due to 4-nitrophenyl chromophore present in the **4.1** and **4.2**, they have broad UV absorbance maximum at 400 nm and 390 nm (Figure 4.12a, 4.12c) respectively. Interactions of **4.1** and **4.2** were checked with chloride salts of various metal ions. Only interactions of Hg^{2+} ions with **4.1** and **4.2** resulted characteristic colorimetric change.

4.3.1: Absorbance study of 4.1 and 4.2 with Hg^{2+}

The compound **4.1** and **4.2** has absorbance at 400 nm and 390 nm respectively (Figure 4.12a, 4.12c). To obtain a quantitative appraisal of the interaction between **4.1** or **4.2** with Hg^{2+}, titration experiments were carried out (Figure 4.12b, 4.12d) with the aid of visible spectroscopic changes.

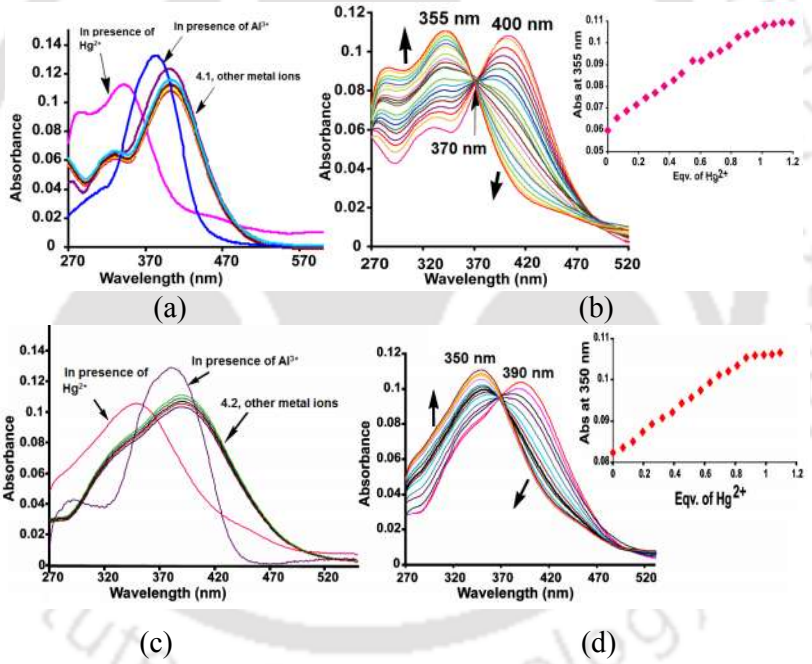

*Figure 4.12: UV-Visible spectra of (a) **4.1** (5 µM) in the presence of 10 equivalents of various metal ions in dimethylformamide solution. (b) **4.1** (5 µM, 4.0 mL) with incremental addition of the Hg^{2+} in dimethylformamide solution. inset: change in absorbance at 355 nm with the equivalents of Hg^{2+} added into the solution. (c) **4.2** (7.5 µM) in the presence of 10 equivalents of various metal ions in dimethylformamide solution. (d) **4.2** (7.5 µM, 4.0 mL) with incremental addition of the Hg^{2+} in dimethylformamide solution. inset: change in absorbance at 350 nm with the equivalents of Hg^{2+} added into the solution.*

Incremental addition of Hg^{2+} to **4.1** rendered a systematic growth of the absorbance maxima at 355 nm with a simultaneous decrease of the peak at 400 nm. An isosbestic point was generated at 370 nm. Similarly, for **4.2**, growth of absorption maxima at 350 nm occurs with a decrease in the absorbance at 390 nm. This change also passes through an isosbestic point at 368 nm. The new absorption peaks corresponds to the hydrolysed products namely 1-(5-methylthiazol-2-yl)-3-(4-nitrophenyl)-urea (**4.1^{p}**) and 1-(4-methylthiazol-2-yl)-3-(4-nitrophenyl)-urea (**4.2^{p}**) respectively. On the basis of isosbestic point, it is clear that the reaction passes through single intermediate. Thus, the changes are attributed to hydrolysis by Hg^{2+} ions. Addition of one equivalent of Hg^{2+} showed the saturation of intensity of the absorbance peak at 355 nm (inset of Figure. 4.12b).

The Job's plots confirmed that **4.1** or **4.2** forms 1: 1 complex with Hg^{2+} (Figure 4.13a, 4.13b). The binding constants for [(**4.1**)–Hg^{2+}] or [(**4.2**)–Hg^{2+}] complexes calculated by using Benesi-Hildebrand equation are 3.33×10^5 M^{-1} and 2.5×10^5 M^{-1} for **4.1** and **4.2** respectively (Figure 4.14a, 4.14b).

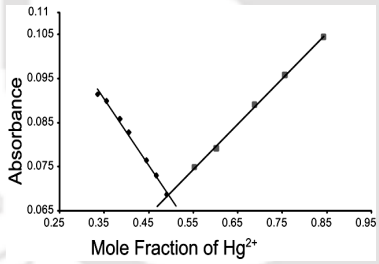

(a)

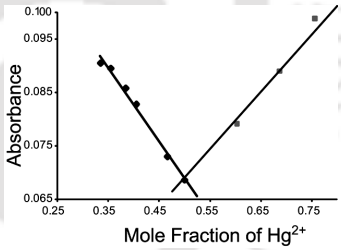

(b)

*Figure 4.13: Job plot for the determination of the stoichiometry of (a) **4.1** and Hg^{2+} in the complex (absorbance at 355nm). (b) **L^{2}** and Hg^{2+} in the complex (absorbance at 350 nm).*

The binding constants are high enough to endorse strong binding affinity of **4.1** or **4.2** toward Hg^{2+} ions in solution. Hence, the compounds **4.1** or **4.2** are independently capable to detect Hg^{2+} ions. The detection limit was calculated according to the IUPAC method[49] were 3.97 ppb and 7.6 ppb for **4.1** or **4.2** respectively (Figure 4.14c, 4.14d). The Environmental Protection Agency (EPA) standard for the maximum allowable level of inorganic Hg^{2+} ions in drinking water is 2.0 ppb.[50] For soil such limit is 0.89 ppm.[51] Mercury ions being toxic[52-56] have been tested with various

sensing molecules that requires pre-treatment and involves complicated synthetic procedures.[57-62] Though **4.1** has detection limit slightly higher to the limit set by US EPA of Hg^{2+} in drinking water, detection limit of both the compounds are below the EPA value for Hg^{2+} in soil. On addition of Al^{3+} ions also brought a slight spectral change in the UV-Visible spectra of **4.1** and **4.2** (Figure 4.12a,c). But, these changes were insignificant and different as compared to colorimetric change induced by Hg^{2+}. In this case the shift is attributed to a complex formation without hydrolysis.

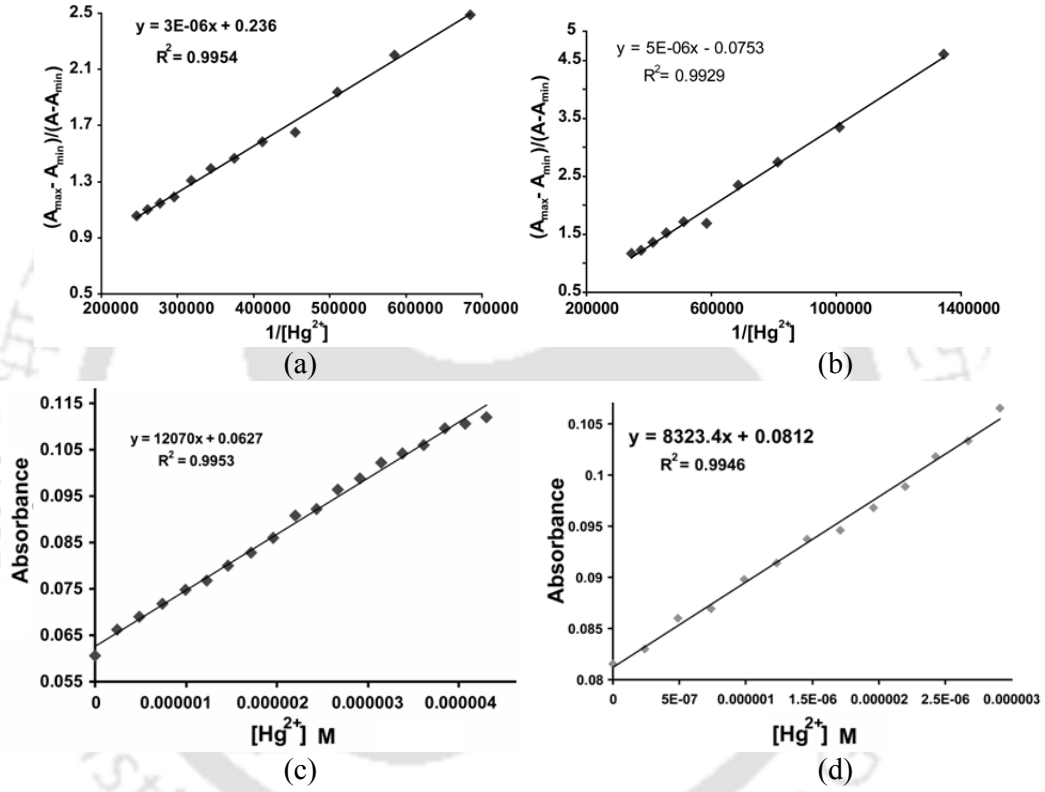

Figure 4.14: Benesi–Hildebrand plot of (a) ***4.1*** *for titration with Hg^{2+}, (b)* ***4.2*** *for titration with Hg^{2+}. Absorbance versus concentration plot for measuring the detection limit (c) (3σ/k, σ= 0.0000753) of Hg^{2+} by* ***4.1****, (d) (3σ/k, σ= 0.000101222) of Hg^{2+} by* ***4.2****.*

UV-titration of **4.1** and **4.2** performed in DMF: water (9: 1 v/v) (Figure 4.15a, 4.15b). The detection limit were found to be 3.06 ppb and 4.99 ppb for **4.1** or **4.2** respectively with Hg^{2+} in DMF: water (9:1 v/v) medium, this shows that the presence of water in DMF solution do not deter the detection process, making it advantageous to work in less non-aqueous conditions.

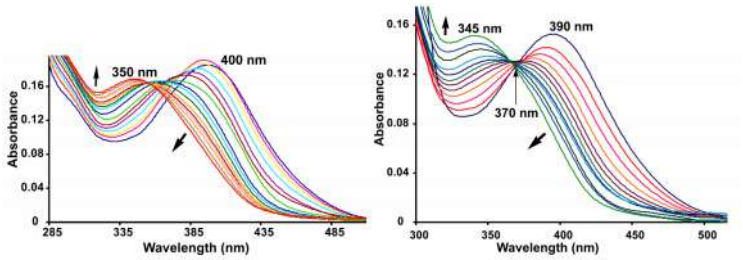

(a) (b)

Figure 4.15: UV-Visible titration spectra of (a) ***4.1*** *(6.0 μM) in the presence of different concentrations of* Hg^{2+} *(0.31, 0.62, 0.93, 1.2, 1.5, 1.86, 2.16, 2.47, 2.78, 3.08, 3.39, 3.69, 3.99, 4.29, and 4.6μM respectively) (b)* ***4.2*** *(7.5 μM) in presence of different concentrations of* Hg^{2+} *(0.31, 0.62, 0.93, 1.2, 1.5, 1.86, 2.16, 2.47, 2.78, 3.08 and 3.39 μM respectively) at room temperature in DMF/water (9 : 1, v/v) medium.*

4.3.2: ^{1}H-NMR study of 4.1 and 4.2 with Hg^{2+}

^{1}H-NMR spectra of **4.1** and **4.2** were recorded in absence of Hg^{2+} and at different Hg^{2+} concentrations (Figure 4.16a, 4.16b). ^{1}H-NMR spectra of **4.1** in DMSO-d_6 showed signals from two -NH protons of thiourea designated as H^1 and H^2 at 13.2 ppm and 10.5 ppm in Figure 4.16a. The aromatic protons of nitrophenyl group (b,c) appear as mutiplet centering at 8.11 ppm. By adding different equivalents of Hg^{2+} to the solution of **4.1** showed the thiourea protons (H^1 and H^2) were gradually shifted to lower chemical shift values (downfield). The chemical shifts of the closely spaced nitrophenyl protons (b, c) gradually separated from each other as the amounts of Hg^{2+} ions in the solution was increased. At one point of addition, only one -NH proton was observed and other NH nearly disappeared (marked as blue star in Figure 4.16a). This was attributed to the formation of intermediate [**(4.1)**-Hg^{2+}] species as shown in Scheme 4.2. Further addition of Hg^{2+}, two new signals for -NH protons reappear at δ 10.72 and 9.69, also the δ value of thiazole proton was shifted from 6.62 to 7.01.These observations indicate the formation of respective urea derivative namely 1-(5-methylthiazol-2-yl)-3-(4-nitrophenyl)-urea ($4.1^{\mathbf{P}}$), hence the final spectra in the titration mixture resembles with the ^{1}H-NMR of $\mathbf{4.1^P}$, which is shown separately in the spectra given at the top of the Figure 4.16a.

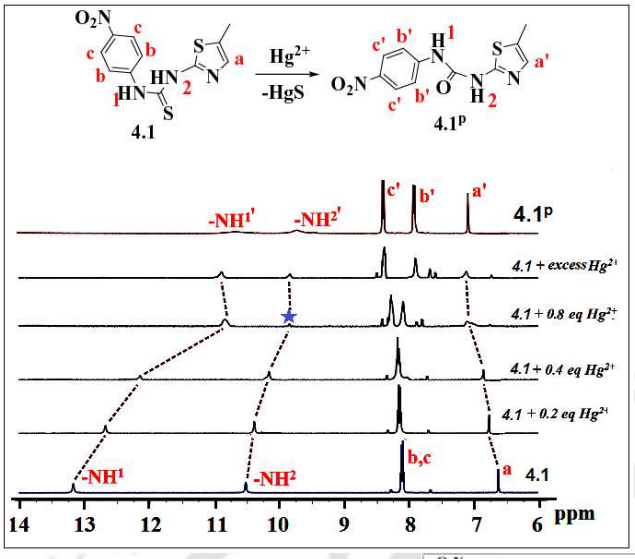

(a)

*Figure 4.16: (a) ^{1}H-NMR (DMSO-d_6, 600MHz) spectra of **4.1** showing the 6-14 ppm region during titration with Hg^{2+} (0.2, 0.4, 0.8 eq and excess Hg^{2+}).*

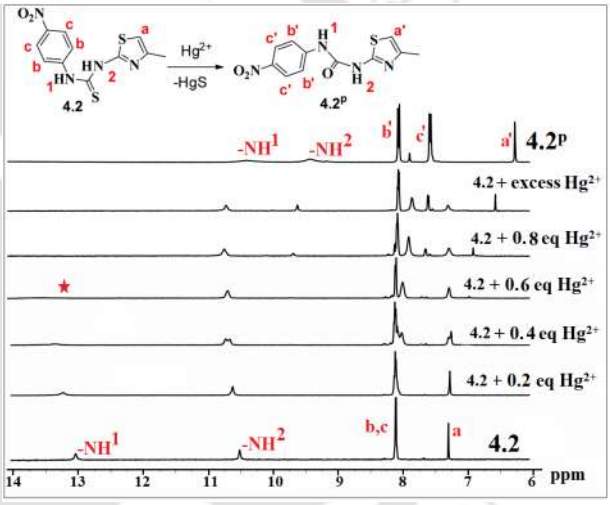

(b)

*Figure 4.16: (b) ^{1}H-NMR (DMSO-d_6, 600MHz) spectra of **4.2** showing the 6-14 ppm region during titration with Hg^{2+} (0.2, 0.4, 0.6, 0.8 eq and excess Hg^{2+}).*

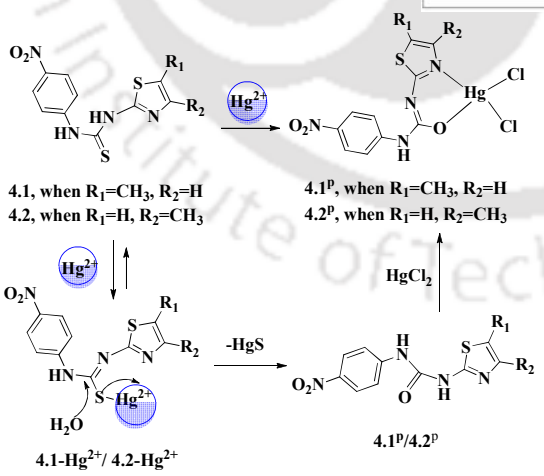

*Scheme 4.2: Hydrolysis of **4.1** and **4.2** and complexation with Hg^{2+}.*

Similar titration of Hg^{2+} with the compound **4.2** is also performed (Figure 4.16b). In this case, initially shifting of the thiourea protons (H^1 and H^2) to downfield is not observed on addition of Hg^{2+}. But, as the amounts of Hg^{2+} ions in the solution was increased, the chemical shifts of the closely spaced nitrophenyl protons (b, c) gradually separated from each other. At one point of addition of Hg^{2+} one of the thiourea protons disappeared (marked as red star in Figure 4.16b). This also attributes to the formation of intermediate [**4.2**-Hg^{2+}] as shown in Scheme 4.2. Further addition of Hg^{2+}, shifted the newly appeared -NH to downfield. Final spectra resemble with the hydrolyzed urea derivative namely, 1-(4-methylthiazol-2-yl)-3-(4-nitrophenyl)-urea (**4.2^{P}**), as shown on the top of Figure 4.16b.

4.3.3: Mass Spectrometry study of 4.1 and 4.2 with Hg^{2+}

The ^{1}HNMR experiments and UV spectroscopy experiments complement each other to explain the hydrolysis. But due to dissimilarity in time scale, sampling amounts there is differences in the quantitative explanations; hence to confirm further the reaction products of **4.1** and **4.2** with Hg^{2+} were investigated by ESI mass.

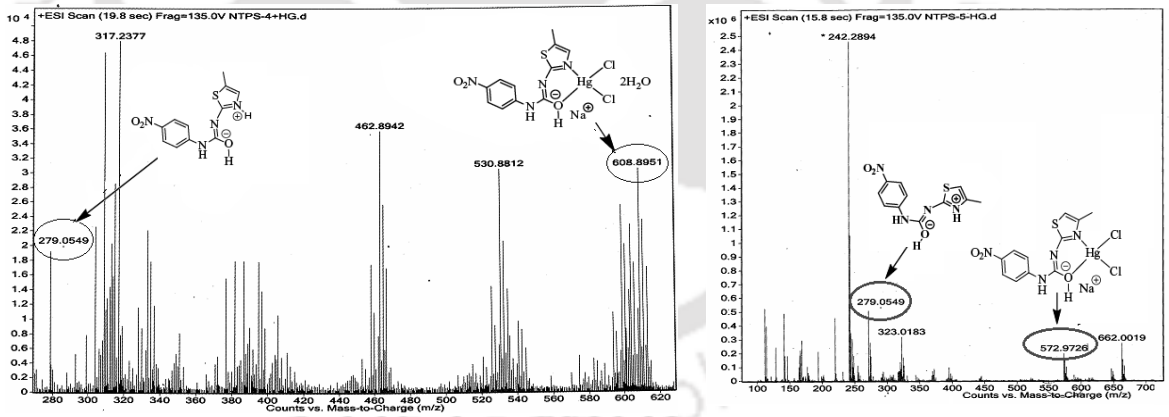

(a) (b)

*Figure 4.17: ESI-mass spectra of (a) **4.1**, (b) **4.2** with $HgCl_2$ showing 1:1 complex formation of respective urea derivative of **4.1** and **4.2** with Hg^{2+}*

ESI mass spectra gave evidence on the formation of urea derivative after addition of Hg^{2+} to **4.1** and **4.2**. Upon the addition of Hg^{2+} ions a peak at m/z = 279.05 [**(4.1)+H**]$^+$ or [**(4.2)+H**]$^+$ for $C_{11}H_{11}N_4O_3S$ appeared in the mass spectra (Figure 4.17a,b). In each case, the respective urea derivatives (**4.1^{p}**, **4.2^{p}**) formed through Hg^{2+} assisted

reactions, gets coordinated to Hg^{2+} which is evident in the mass peak observed at 608.89 for $C_{11}H_{14}Cl_2HgN_4O_5S$ corresponding to [**(4.1)** + Na^++ $2H_2O$ +$2Cl^-$], and at 572.97 for $C_{11}H_{10}Cl_2HgN_4O_3S$ corresponding to [**(4.2)** + Na^+ + $2Cl^-$]

4.3.4: Zinc complex of 4.1

On interaction of **4.1** with zinc chloride no UV-spectral change was observed as shown in Figure 4.18a. A neutral tetra coordinated zinc complex having composition [Zn{(**4.1**)$^{1-}$}$_2$].DMF (**4.3**) was isolated from a stoichiometric reaction. In this complex two deprotonated **4.1** (designated as **4.1**$^{1-}$) coordinate through nitrogen and sulphur atoms to a Zn^{2+} ion as shown in Figure 4.18b. The complex has a distorted square planar geometry having the nitrogen atoms opposite side of each other and the sulphur atoms also opposite sides.

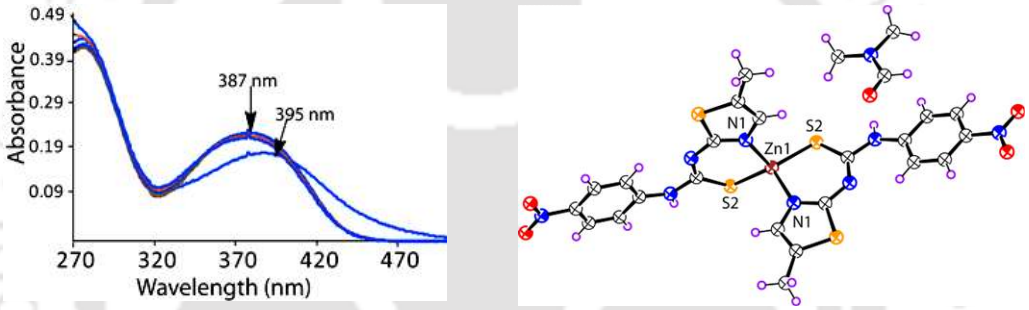

(a) (b)

*Figure 4.18: (a) Absorption spectra of **4.1**(1 μM) with the addition of Zn^{2+} (1×10^{-2} M) followed by Hg^{2+} (1×10^{-2} M), (b) Structure of the complex [Zn{(**4.1**)$^{1-}$}$_2$].DMF **(4.3)** (ORTEP drawn with 50% thermal ellipsoids).*

The metal ligand bond distances of the complex **4.3** have Zn1-N1, 2.004 Å and Zn1-S2, 2.272 Å are comparable to conventional Zn-N 2.017 Å bonds distances [33] found in four coordinated zinc amionthiazole complex. Formation of complex **4.3** with deprotonated **4.1**, does not shift the position of absorbance of the parent compound **4.1.** Hence, this complexation is not suitable for its detection through UV-visible spectroscopy.

4.4: Interaction of anions with 4.1 and 4.2: UV-Vis spectroscopic studies

Anions are significant to guide supramolecular assemblies of organic salts.[63-65] Thiazole derivatives belong to a family of cytotoxic compounds in which anions may play important role in performance of such activity.[66] On the other hand, basicity associated with ions like fluoride or acetate ions deprotonate different thiourea compounds.[67-69] Hence we examined the ability and selectivity of the compounds **4.1** and **4.2** to detect anions. The binding selectivity of **4.1** and **4.2** was checked with various anions such as, F^-, Br^-, Cl^-, I^-, SO_4^{2-}, HSO_4^-, PF_6^-, NO_3^-, HPO_4^-, $H_2PO_4^-$, OAc^-, ClO_4^- etc by taking the respective tetrabutylammonium salts. Only tetrabutylammonium fluoride (TBAF) able to induce a significant colorimetric response in DMF as well as DMSO solvent. It may be mentioned that tetrabutylammonium hydroxide on interaction with **4.1** and **4.2** generated absorption peak at 410 nm. This is in contrast to the absorbance peak observed at 417 nm by interactions with fluoride ions. Other salts hardly influenced the UV-spectral pattern of **4.1** and **4.2.**

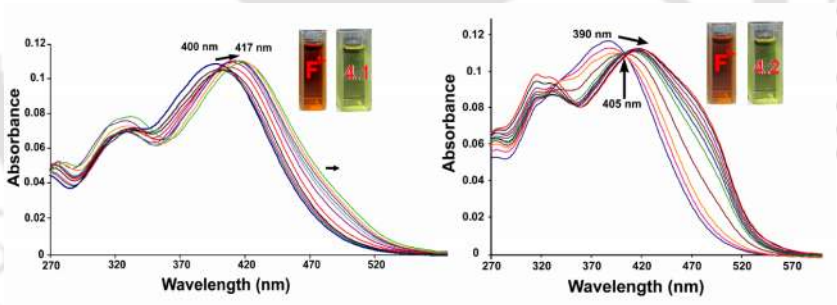

*Figure 4.19: Absorption spectra of (a) **4.1** (5 μM) (b) **4.2** (7.5 μM) with F^- in DMF.*

Interaction of F^- with **4.1** and **4.2** resulted in the emergence of a new absorbance maximum at 417 nm, with subsequent disappearance of the original peak at around 395 nm. These changes caused visual color change from yellow to orange red (Figure 4.19a, 4.19b: inset). UV-visible titration experiments revealed the systematic increase in the absorbance at 417 nm with concurrent decrease of the absorbance at around 395 nm with the gradual addition of tetrabutylammonium fluoride to **4.1** and **4.2** (Figure. 4.19a, 4.19b). From these experiments selective colorimetric response towards the

fluoride ions is attributed to the formation of strong hydrogen bonds with the positional isomers, which are designated as [(**4.1**)-F^-] or [(**4.2**)-F^-] complexes.

4.4.1: ^{1}H-NMR study of 4.1 and 4.2 with F^{1-}

The ^{1}H-NMR spectra of **4.1** in DMSO-d_6 displayed the signals for the two -NH protons of thiourea at 13.18 ppm and 10.52 ppm. Upon addition of fluoride ions, the signals of the -NH protons gradually weakened and broadened due to strong hydrogen bond between -NH and fluoride ions. The chemical shifts of the aromatic ring protons were not affected. Excess amount of fluoride led to the deprotonation, and thus formed a peak at 9.47 ppm which is assigned to HF_2^- formed in situ (Figure 4.20a). Hence, fluoride sensing is a combined effect of hydrogen bond formation followed by deprotonation of the compound **4.1**.

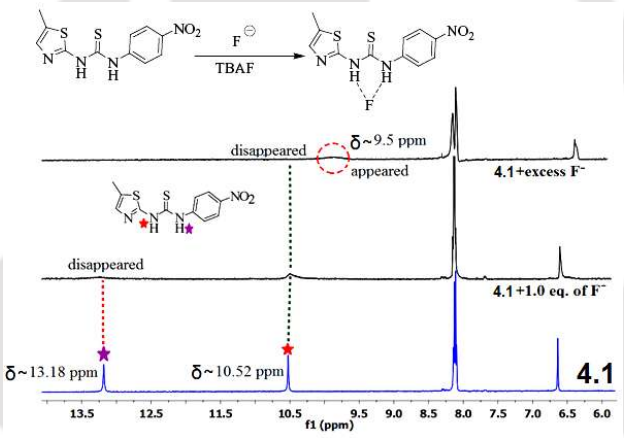

(a)

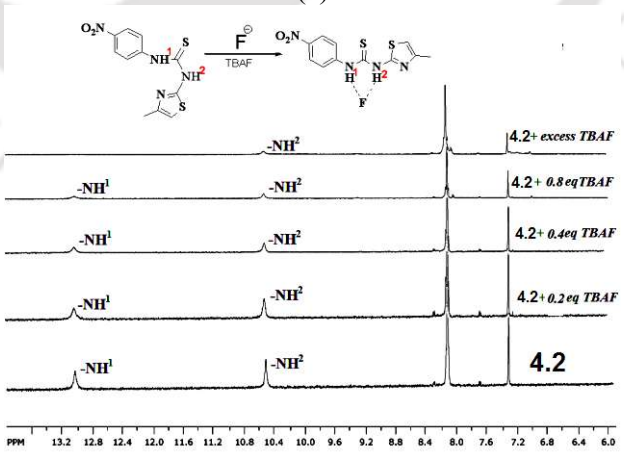

(b)

*Figure 4.20: ^{1}H-NMR (DMSO-d_6, 600MHz) spectra in the region of 6-14 ppm of (a) **4.1**, (b) **4.2** during titration with Hg^{2+}.*

Similar titration was carried out with **4.2** (Figure 4.20b**)** and a similar trend was established in this case also. In the case of **4.2** excess addition of fluoride did not cause deprotonation. This observation clearly indicated the relative reactivity differences between the two positional isomers.

4.4.2: Competitive interactions of Hg^{2+} and F^- ions towards 4.1 and 4.2

Control experiments were carried out to ascertain a possible interference of Hg^{2+} ions in the detection of fluoride ions. Addition of a solution Hg^{2+} ion to a solution of **4.1** gradually shifted the absorption maximum from 400 nm to 355 nm, no appreciable change in absorption spectra of this solution by adding solution of fluoride ions was observed. But, reversing the sequence of addition, namely fluoride ions added first and then Hg^{2+} ions, causes gradual blue shift of the absorption peck at 417 nm due to [(**4.1**)-F^-] complex and ultimately shifted the peak to 355 nm as shown in Figure 4.21a. The compound **4.2** had shown a similar behavior towards Hg^{2+} and fluoride ions as that of **4.1** (Figure 4.21b). These observations show the hydrolysis of thiourea derivatives (**4.1** or **4.2**) to urea derivatives (**4.1^p** or **4.2^p**) is not affected by the presence of fluoride ions. Respective urea derivative formed by catalytic hydrolysis did not significantly change the visible spectra on interaction with fluoride ions. Similar effects were seen in DMSO as a solvent.

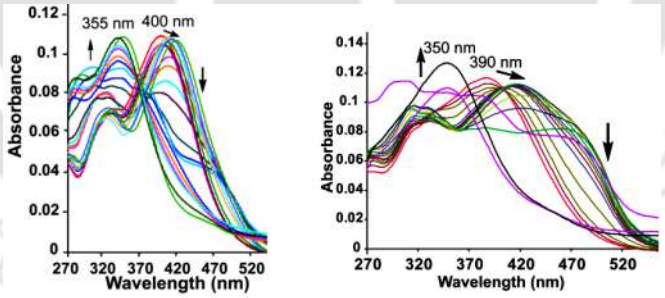

(a) (b)

*Figure 4.21: Absorption spectra of (a) **4.1** (1 μM**)** with the addition of F^- (1×10^{-4} M) (as TBAF) followed by Hg^{2+}(1×10^{-4} M), (b) **4.2** (1 μM**)** with the addition of F^- (1×10^{-2} M) (as TBAF) followed by Hg^{2+}(1×10^{-3} M).*

4.4.3: Interaction of Bromide (Br^-) with 4.2

Between the two positional isomers, **4.2** reacted with hydrobromic acid and it yielded a very selective bromo derivative **4.2a** as illustrated in Scheme 4.3. Though this reaction was slow and yet this was an interesting reaction as it was specific to

compound **4.2**. The compound **4.2** underwent hydrolysis and reacted with hydrobromic acid to form the brominated product **4.2a**.

The hydrobromic acid in DMSO has been identified as a brominating agent in a recent article.[70] However, the selectivity among the **4.1** and **4.2** to undergo the bromination reaction was an important result pointing out that the directing affect of the nitrogen to the electrophile to attack at a γ-position with respect to the nitrogen atom, and such site was occupied by a methyl group in the compound **4.1**. On the other hand, the compounds **4.1** and **4.2** were in imine forms hence the reactivity of these two compounds were also different from the similar thiazole derivative 1-(5-methylthiazol-2-yl)-3-(phenyl)-thiourea that do not have the nitro group. As discussed in Chapter 2, in the latter case salt formation with hydrobromic acid was observed. In earlier study a thiazole based naphthoquinone compound was suggested as bromide sensor,[71] on the other hand imidazole derivatives[72] were shown to be useful in detection of bromide ions.

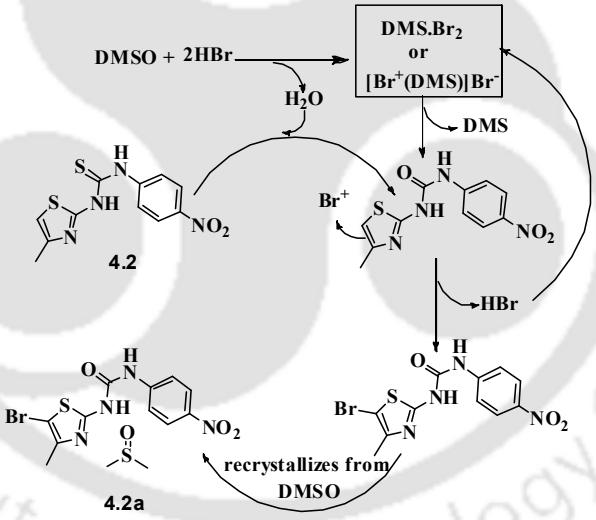

*Scheme 4.3: Proposed mechanistic path on the formation of **4.2a**.*

4.5: Conclusions

We addressed here, the need of a robust and holistic approach for on intrinsic reactivities from the substituent effect on the positional isomers based on thiazole tethered thiourea. The two 1-(5-methylthiazol-2-yl)-3-(4-nitrophenyl)-thiourea (**4.1**) and 1-(4-methylthiazol-2-yl)-3-(4-nitrophenyl)-thiourea (**4.2**) which exist in imine forms provided a basis for divulging information on how sensitive their reactivity

towards various solvents and ions that may inevitably affect the crystal engineering aspects. Conformational adjustments of polymorphic solvates with respect to unsolvated host molecules have revealed the multiple ways of adjusting conformation by same solvent on a particular host. Such results added value to the conventional proposals on solvent guided conformational changes often used to generate polymorphs through crystallization. Self-assemblies of the positional isomers by simple alteration of position on a ring can be a factor to show different numbers of molecules in asymmetric unit. This enforced differences in overall packing patterns of two isomers. The position of the methyl-substituent contributed different hydrolytic stability of the two positional isomers. Chemodosimetric signal transductions during hydrolysis by mercuric ions are reflected in UV-visible absorptions of **4.1** and **4.2**. The fluoride ions can be detected from selective changes in visible spectra. On the other hand, a highly selective bromination reaction was observed in which 1-(4-methylthiazol-2-yl)-3-(4-nitrophenyl)-thiourea (**4.2**) enables one to differentiate the two positional isomers through their chemical reactivities. All these results have shown that utmost attentions on chemical reactivity of different positional isomers and as well as substituent effect in homologous series are essential prior to making a designed generalized non-covalent synthesis.

4.6: Experimental Section

The detailed synthetic methodologies for synthesis of the solvates, adduct and metal complex are described. Analytical data are provided with each compound. The instrumental details and crystallographic parameters are provided in Appendix.

Synthesis of 1-(5-methylthiazol-2-yl)-3-(4-nitrophenyl)-thiourea (4.1): 5-Methylthiazol-2- ylamine (0.057 g, 5 mmol) and 4-nitrophenyl isothiocyanate (0.090 g, 5 mmol) were dissolved in dry dichloromethane (20 mL) and the reaction mixture was placed in an ice bath. The solution was stirred for 6 hs. The resulting solution was evaporated, and the precipitate was dried in vacuum. The precipitate was recrystallised by dissolving in mixture of DMF and dichlormethane (1:1 ratio) which yielded yellow crystals. Yield, 90 %. ^{1}H-NMR (600 MHz, DMSO-d_6): 13.18 (s, 1H), 10.53 (s, 1H), 8.13 (d, 9.0 Hz, 2H), 8.11 (d, 9.72 Hz, 2H), 6.65 (s, 1H), 2.28 (s, 3H). ESI MS: calcd mass for M+1 $C_{11}H_{10}N_4O_2S_2$, 295.0245; found, 295.0341 [M+ 1]. IR

(cm^{-1}): 3189 (w), 1593 (s), 1530 (s), 1497(m), 1437 (s), 1367 (s), 1327 (m), 1297 (s), 1168 (s), 1111 (s), 901 (m), 842 (m), 663 (m), 451(m).

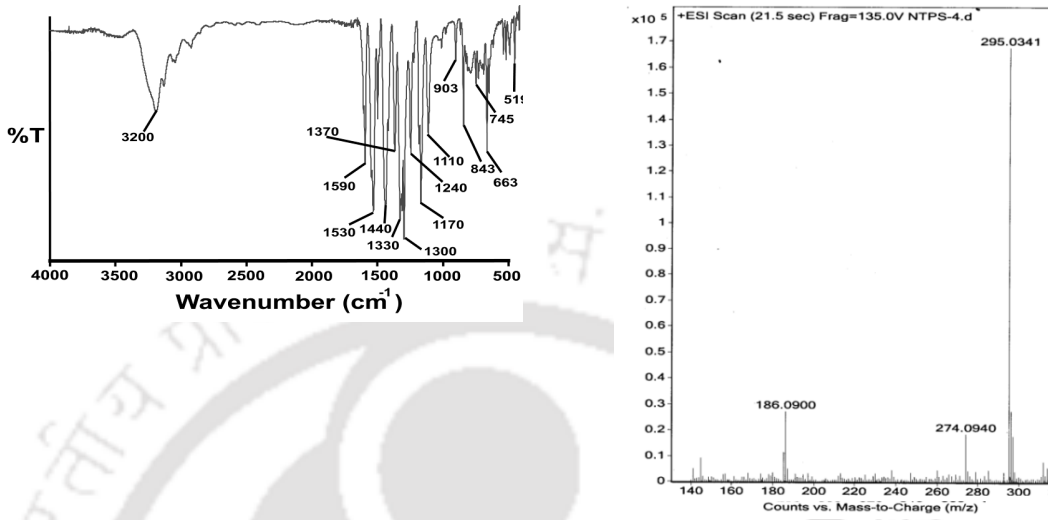

(a) (b)

*Figure 4.22: (a) FT-IR spectra (KBr, cm^{-1}) of **4.1,** (b) ESI mass spectra of **4.1***

Synthesis of 1-(4-methylthiazol-2-yl)-3-(4-nitrophenyl)-thiourea (**4.2**): A similar procedure to the synthesis of **4.1** was followed to prepare **4.2**, but 4-methylthiazol-2-yl-amine was used in place of 5-methylthiazol-2-yl-amine. Crystals of **4.2** were obtained by recrystallization from a solution in methanol. Yield, 92 %. ^{1}H-NMR (600 MHz, DMSO-d_6): 13.05 (s, 1H), 10.52 (s, 1H), 8.12 (s, 4H), 7.30 (s, 1H), 2.07 (s, 3H). ESI MS calcd mass for M+1, $C_{11}H_{10}N_4O_2S_2$, 295.0245; found, 295.0299 [M+ 1]. IR (KBr, cm^{-1}): 3193 (w), 1593 (s), 1529 (s), 1497 (m), 1435 (s), 1366 (s), 1327 (s), 1297 (m), 1244 (m), 1168 (s), 1111 (s), 902 (m), 842 (m), 662 (m), 537 (m). While recrystallization of **4.2** from mixed solvent comprising of dimethylformamide: water (3:1) led to crystallization of 1-(4-methylthiazol-2-yl)-3-(4-nitrophenyl)urea.H_2O namely, **4.2b** was crystallized after 15 days. Yield, 88 %. IR (KBr, cm^{-1}): 3431 (w), 3076 (w), 1690 (s), 1620 (s), 1581 (s), 1513 (s), 1331 (s), 1254 (s), 1206 (s), 1110 (s), 970 (m), 841 (m), 750 (m), 556 (m). ^{1}H-NMR (400 MHz, DMSO-d_6): 8.20 (d, 7.6 Hz, 2H), 7.68 (d, 8.0 Hz, 2H), 6.55 (s, 1H), 2.49 (s, water proton), 2.30 (s, 3H).

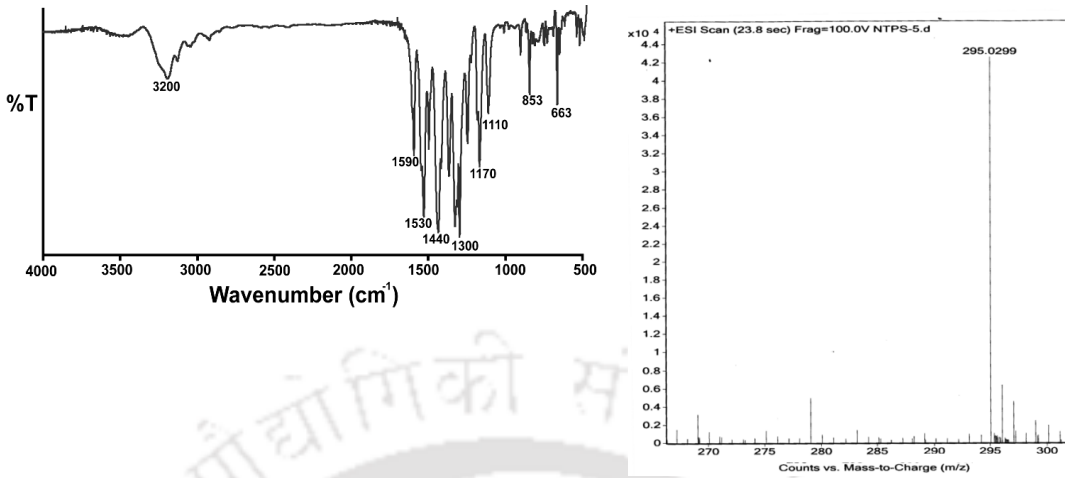

(a) (b)

*Figure 4.23: (a) FT-IR spectra (KBr, cm^{-1}) of **4.2,** (b) ESI mass spectra of **4.2***

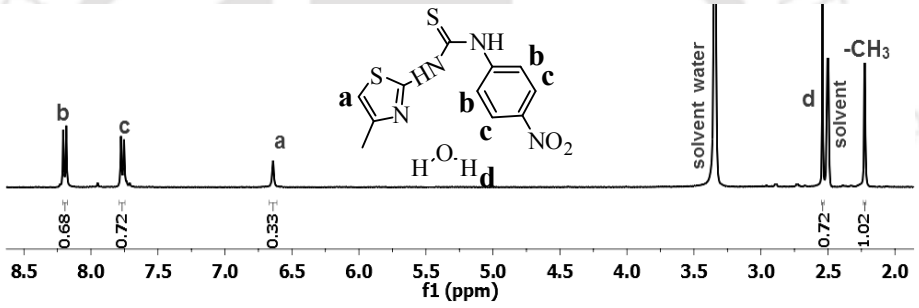

*Figure 4.24: ^{1}H-NMR spectra (400MHz, DMSO-d_6) of **4.2b**.*

Synthesis of solvate 4.1a: The compound **4.1** (0.340 g, 1.5 mmol) was dissolved in DMSO (10 mL). The solution was kept undisturbed at room temperature for crystallization. Yellow crystals of **4.1a** were obtained after 4 days. Yield, 94 %. IR (KBr, cm^{-1}): 3447 (w), 3241 (m), 1606 (m), 1594 (m), 1550 (s), 1500 (s), 1454 (s), 1375 (s), 1330 (s), 1166 (s), 1014 (s), 844 (m), 749 (m), 668 (m), 637 (m), 503 (m). ^{1}H-NMR (400 MHz, DMSO-d_6): 13.24 (s), 10.75 (s), 8.32 (s, 4H), 7.52 (s), 2.75 (s, DMSO protons), 2.70 (s, 3H).

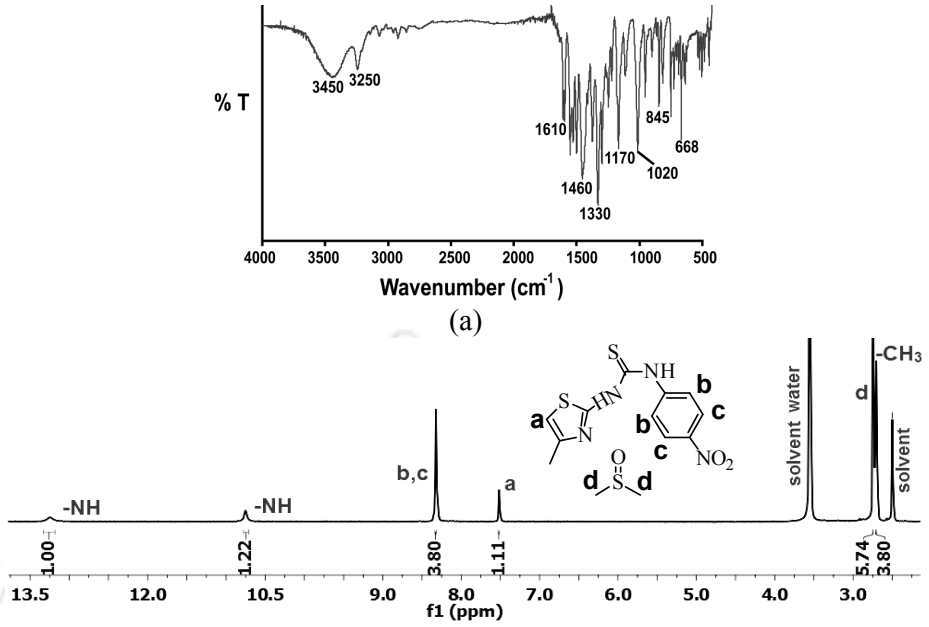

*Figure 4.25: (a) FT-IR spectra (KBr, cm^{-1}) of **4.1a**, (b) ^{1}H-NMR spectrum (400 MHz, DMSO-d$_6$) of DMSO solvate **4.1a**.*

Synthesis of solvate 4.1b and 4.1.1b:

A solution of the compound **4.1** (0.340 g, 1.5 mmol) in DMA (5 mL) yielded a mixture of block shaped yellow crystals of **4.1b** along with few needle shaped yellow crystals of **4.1.1b** after one week. Yield, 82 % **(2a**) and 6 % (**2.1a**). Spectroscopic features of **2a**: IR (KBr, cm^{-1}): 3481 (w), 3228 (m), 1605 (s), 1593 (m), 1544 (s), 1445 (s), 1326 (s), 1297 (s), 1165 (s), 1115 (m), 1021 (m), 815 (m), 720 (m) 668 (s), 599 (m), 518 (m). ^{1}H-NMR (400 MHz, DMSO-d$_6$): 13.06 (s, 1H), 10.55 (s, 1H), 8.12 (s, 4H), 7.32 (s, 1H), 2.94 (s, 3H), 2.78 (s, 3H), 2.29 (s, 3H), 1.96 (s, 3H). The amount of **4.1.1.b** was too low and less stable; thus Single Crystal-XRD was used as the tool to find out the structure.

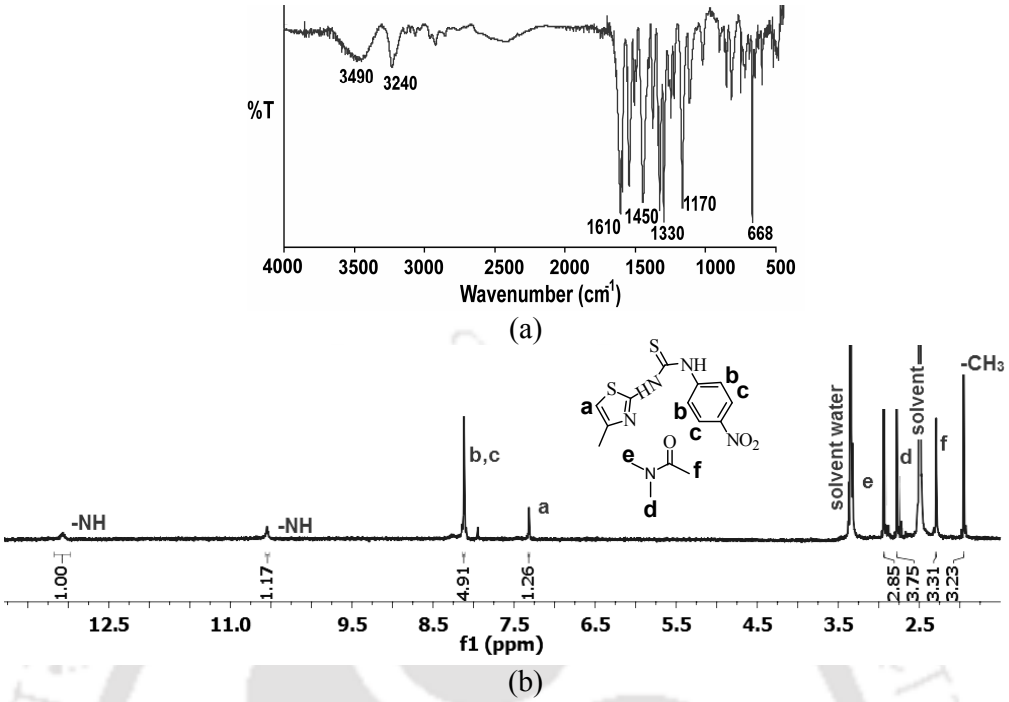

*Figure 4.26: (a) FT-IR spectra (KBr, cm^{-1}) of **4.1b,** (b) ^{1}H-NMR spectrum (400 MHz, DMSO-d$_6$) of DMSO solvate **4.1b**.*

Synthesis of 4.1c: A solution of **4.1** (0.294 g, 1mmol) with 1,8-diazabicyclo [5.4.0] undec-7-ene (0.15 mL) in DMF (0.5 mL) on standing yielded yellow crystals of **4.1c** after 10 days. Yield, 82 %. ESI MS: calcd for M+1 of 431.1787 for $C_{20}H_{26}N_6O_3S$; found mass 431.1799 [M+ 1]. IR (KBr, cm^{-1}): 3421 (w), 2932 (m), 1647 (s), 1595 (m), 1505 (m), 1325 (s), 1254 (w), 1111 (s), 1017 (s), 852 (s), 751 (m), 618 (m). ^{1}H-NMR (400 MHz, DMSO-d$_6$): 8.20 (d, 8.8 Hz, 2H), 7.59 (s, 2H), 6.89 (s, 1H), 3.46 (s, 2H), 3.43 (t, 6Hz, 2H), 3.34 (t, 7.6Hz, 2H), 2.52 (m, 2H), 1.76 (m, 8H).

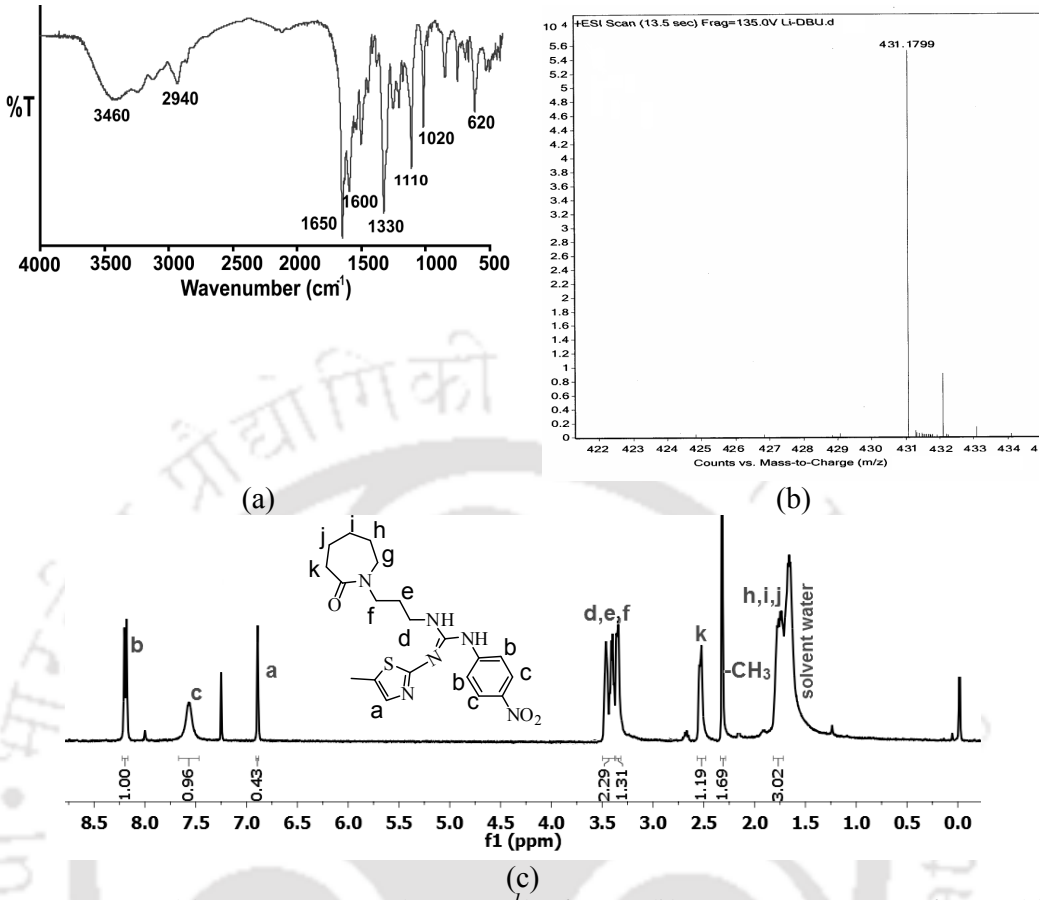

*Figure 4.27: (a) FT-IR spectra (KBr, cm^{-1}) of **4.1c**, (b) ESI mass spectra of **4.1c**, (c) ^{1}H-NMR spectra (400 MHz, $CDCl_3$) of **4.1c**.*

Synthesis of 4.2a: The compound **4.2** (0.294 g, 1mmol) was dissolved in minimum volume of DMSO and hydrobromic acid was added (37 %, 0.4 mL). The solution turned red. The red solution on slow evaporation yiellded red crystals of **4.2a** after 15 days. The crystals were filtered and air dried. Yield, 82 %. ESI MS calcd for M+1 for $C_{11}H_9BrN_4O_3S$, 356.9579; found mass, 356.9642 (M+1), 358.9621 (M+3). IR (KBr, cm^{-1}): 3447 (w), 2924 (m), 1747 (m), 1647 (w), 1261 (s), 1020 (s), 801 (s), 668 (s). ^{1}H-NMR (400 MHz, DMSO-d_6) : 9.41 (s, 1H) 8.17 (d, 9.2 Hz ,2H), 7.71 (d, 5.6 Hz ,2H), 2.62 (s, CH_3 of DMSO) 2.30 (s, 3H).

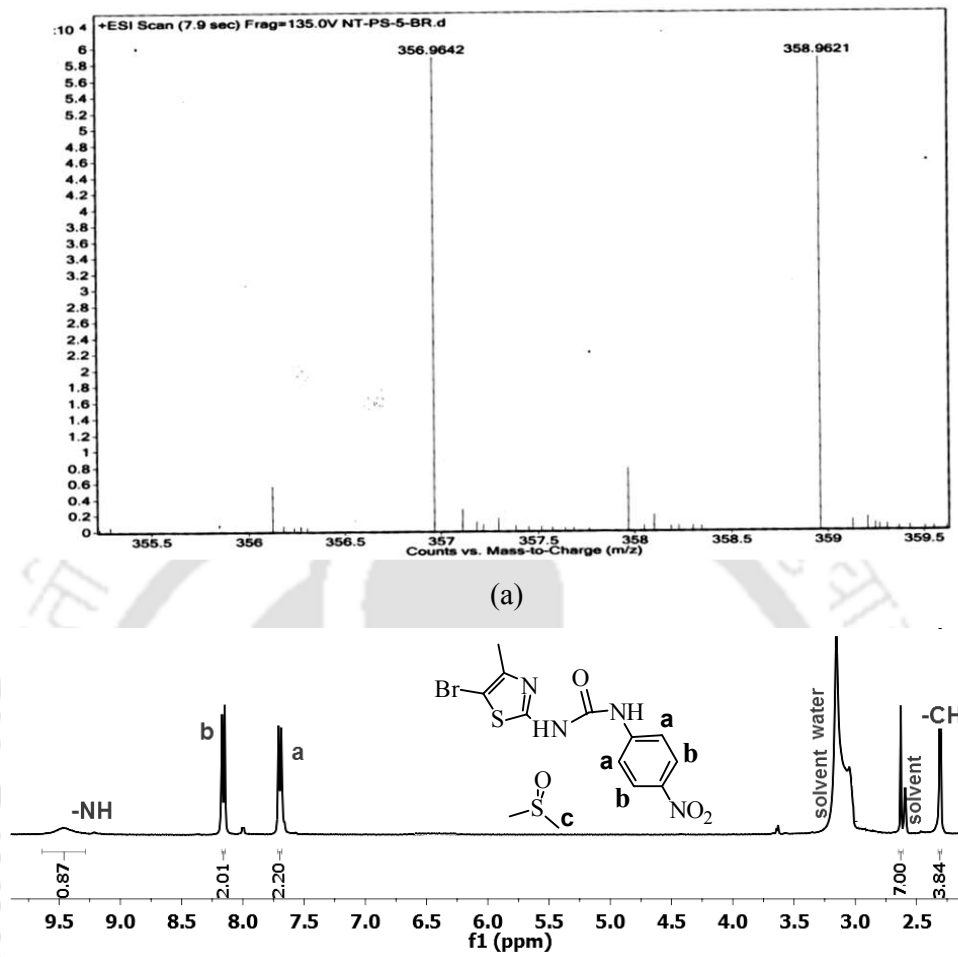

*Figure 4.28: (a) ESI mass spectra of **4.2a**, (b) ^{1}H-NMR spectra (400MHz, DMSO-d_6) of **4.2a**.*

Synthesis of [Zn{(4.1)$^{1-}$}$_2$].DMF (4.3): To a well-stirred solution of **4.1** (0.147 g, 0.5 mmol) in DMF solid anhydrous zinc chloride (0.068 g, 0.5 mmol) was added. The resulting solution was stirred for about 4 hrs. The reaction mixture was then filtered, and the filtrate was kept undisturbed for crystallization. After 3-4 days, yellow crystals of **4.3** appeared. Yield 82 %. ESI mass calcd for M+1 for $C_{22}H_{18}N_8O_4S_4Zn$: 650.9625, found mass 650.7755 (M+1). IR (KBr, cm^{-1}): 3438 (w), 2924 (m), 2845 (m), 1622 (m), 1382 (s), 1327 (w), 1260 (m), 1113 (m), 1018 (m), 668 (m). ^{1}H-NMR (400 MHz, DMSO-d_6): 10.40 (s, 1H), 8.17 (d, 6.36 Hz, 2H), 7.94 (d, 8.52 Hz, 2H), 7.08 (s, 1H), 2.31 (s, 3H).

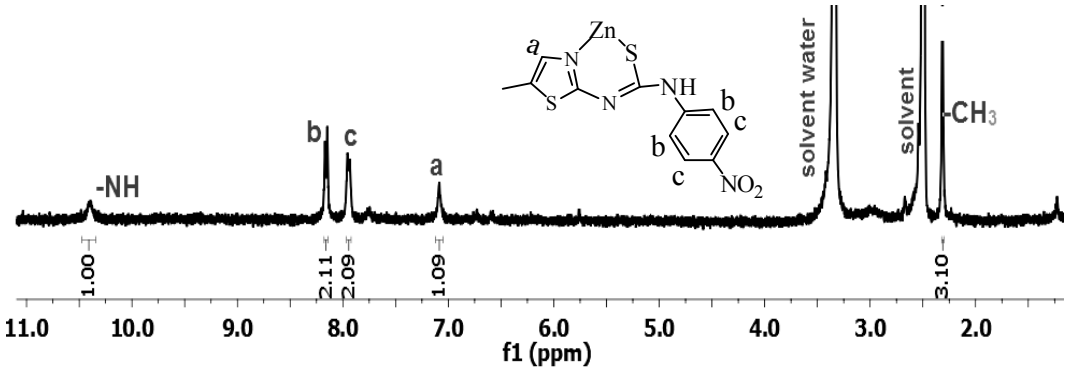

(a)

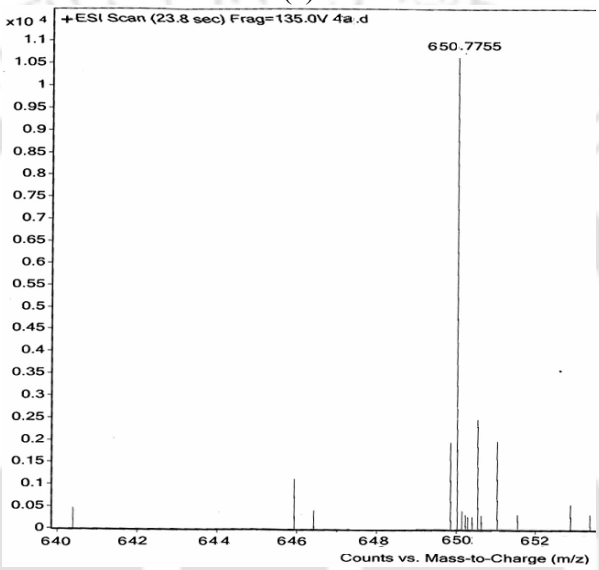

(b)

*Figure 4.29: (a) ^{1}H-NMR spectra (400 MHz, DMSO-d_6) of complex **4.3**, (b) ESI mass spectrum of **4.3**.*

4.7: References

1. B. Valeur, I. Leray, *Coord. Chem. Rev.*, 2000, **205**, 3.
2. V. Balzani, *Molecular Devices and Machines: A Journey into the Nanoworld*; Wiley-VCH: Weinheim, Germany, 2003.
3. A. P. deSilva, H. Q. N. Gunaratne, T. Gunnlaugsson, A. J. M. Huxley, C. P. McCoy, J. T. Rademacher, T. E. Rice, *Chem. Rev.*, 1997, **97**, 1515.
4. A. Bianchi, K. Bowman-James, E. GraciaEspana, Eds.; *Supramolecular Chemistry of anions*; Wiley-VCH: Weinheim, Germany, 1997.
5. R. Martinez-Manez, F. Sancenon, *Chem. Rev.*, 2003, **103**, 4419.

6. C. Sukasai, T. Tuntulani, *Chem. Soc. Rev.*, 2003, **32**, 192.
7. P. D. Beer, P. A. Gale, *Coord. Chem. Rev.*, 2001, **213**, 79.
8. A. Marini, A. Munoz-Losa, A. Biancardi, B. Mennucci, *J. Phys. Chem. B*, 2010, **114**, 17128.
9. E. Buncel, S. Rajagopal, *Acc. Chem. Res.*, 1990, **23**, 226.
10. B.-Y. Kim, H.-S. Kim, A. Helal, *Sensors and Actuators B*, 2015, **206**, 430.
11. S. Keith McNeil, Steven P. Kelley, C. Beg, H. Cook, R. D. Rogers, D. E. Nikles, *ACS Appl. Mater. Interfaces*, 2013, **5**, 7647.
12. D. Yan, G. Fan, Y. Guan, Q. Meng, C. Li, J. Wang, *Phys.Chem. Chem. Phys.*, 2013, **15**, 19845.
13. A. G. Doyle, E. N. Jacobsen, *Chem. Rev*., 2007, **107**, 5713.
14. E. K. Feuster, T. E. Glass, *J. Am. Chem. Soc*., 2003, **125,** 16174.
15. V. B. Bregovic, N. Basaric, K. Mlinaric-Majerski, *Coord. Chem. Rev*., 2015, **295**, 80.
16. C. I. Yeo, E. R. T. Tiekink, *Acta Crystallogr*., 2011, **67E**, o2965.
17. P. K. Gosavi, U. Agarwala, C. N. R. Rao, *J. Am. Chem. Soc*., 1967, **89**, 235.
18. R. Castelcean, M.G. Gorbunova, P.V. Bonnesen, *Chem Eur. J*., 2005, **11**, 1459.
19. G. Fan, D. Yan, *Scientific Reports*, 2014, **4**, 4933.
20. J. Wermuth, S. L. Goodman, A. Jonczyk, H. Kessler, *J. Am. Chem. Soc*., 1997, **119**, 1328.
21. S. Park, C. Anderson, R. Loeber, M. Seetharaman, R. Jones, N. Tretyakova, *J. Am. Chem. Soc.*, 2005, **127**, 14355.
22. L. Yu, *Acc. Chem. Res.*, 2010, **43**, 1257.
23. J. D. Wuest, *Nat. Chem*., 2012, **4**, 74.
24. J. W. Chen, B. Xu, X. Y. Ouyang, B. Z. Tang, Y. Cao, *J. Phys. Chem. A*, 2004, **108**, 7522.
25. S. Kobatake, S. Takami, H. Muto, T. Ishikawa, M. Irie, *Nature*, 2007, **446**, 778.
26. M. C. Etter, *Acc. Chem. Res.*, 1990, **23,** 120.
27. M. C. Etter, J. C. McDonald, J. Bernstein, *Acta Crystallogr.*, 1990, **B46**, 256.

28. H. D. Clarke, M. B. Hickey, B. Moulton, J. A. Perman, M. L. Peterson, L.Wojtas, O. Almarsson, M. J. Zaworotko, *Cryst. Growth Des*., 2012, **12**, 4194.
29. N. A. Mir, R. Dubey, G. R. Desiraju, *IUCrJ*, 2016, **3**, 96.
30. T. N. Birkinshaw, S. A. Harkin, P. T. Kaye, G. D. Meakins, *J. Chem. Soc., Perkin Trans.*, *1*, 1982, 939.
31. P. Khakhlary, J. B. Baruah, *J. Mol. Struct.*, 2014, **1078**, 188.
32. A. Wittkopp, P. R. Schreiner, *Chem. Eur. J.*, 2003, **9**, 407.
33. T. Okino, Y. Hoashi, T. Furukawa, X. Xu, Y. Takemoto, *J. Am. Chem. Soc.*, 2005, **127**, 119.
34. P. R. Schreiner, A. Wittkopp, *Org. Lett.*, 2002, **4**, 217.
35. S. B. Bhavkar, A. Roy, R. L. Gawade, V. G. Puranik, G. J. Sanjayan, *Syn. Commun.*, 2014, **44**, 2955.
36. J. Bernstein, G. M. J. Schmidt, *J. Chem. Soc., Perkin Trans. 2*, 1972, 951.
37. M. V. Patwadkar, R. J. Gonnade , R. Vaidhyanathan, *CrystEngComm*, 2014, **16**, 15 8638.
38. M. H. Cohen, G. A. Williams, R. Sridhara, G. Chen, W. D. McGuinn Jr., D. Morse, S. Abraham, A. Rahman, C. Liang, R. Lostritto, A. Baird, R. Pazdur, *Clin. Cancer Res.*, 2004, **10**, 1212.
39. A. Nangia, *Acc. Chem. Res.*, 2008, **41**, 595.
40. A. J. Cruz-Cabeza, J. Bersntein, *Chem. Rev.*, 2014, **114,** 2170.
41. V. Ischenko, U. Englert, M. Janson, *Chem. Eur. J.*, 2005, **11**, 1375.
42. J. R. Askim, M. Mahmoudia, K. S. Suslick, *Chem. Soc. Rev.*, 2013, **42**, 8649.
43. A. P. de Silva, H. Q. N. Gunaratne, T. Gunnlaugsson, A. J. M. Huxley, C. P. McCoy, J. T. Rademacher, T. E. Rice, *Chem. Rev.*, 1997, **97,** 1515.
44. B. Valeur, I. Leray, *Coord. Chem. Rev.*, 2000, **205,** 3.
45. J. S. Kim, D. T. Quang, *Chem. Rev.*, 2007, **107,** 3780.
46. L. Prodi, F. Bolletta, M. Montalti, N. Zaccheroni, *Coord. Chem. Rev.*, 2000, **205,** 59.
47. N. Phukan, A. Goswami, J. B. Baruah, *Inorg. Chim. Acta*, 2015, **435**, 239.
48. J. -Y. Lee, B. A. Rao, J.-Y. Hwang, Y.-A. Son, *Sensors and Actuators B*, 2015, **220**, 1070.

49. IUPAC Compendium of Analytical Nomenclature, Definitive Rules, 1997, web edition, ed. J. Lnczédy, T. Lengyel and A. M. Ure, IUPAC, 2002.
50. Mercury Update: Impact on Fish Advisories. EPA Fact Sheet EPA- 823-F-01-011; EPA, Office of Water: Washington, DC, 2001.
51. http://www.epa.state.il.us/land/ccdd/new-max-allowable-concentrations-table.pdf
52. T. W. Clarkson, L. Magos, *Crit. Rev. Toxicol.*, 2006, **36**, 609.
53. A. M. Pena, M. I. Rodriguez-Caceres, D. B. Gil, M. C. Mahedero, M. C. Hurtado-Sanchez, R. Babiano, *Am. J. Anal. Chem.*, 2011, **2,** 605.
54. N. Y. Ho, L. Yang, J. Legradi, O. Armant, M. Takamiya, S. Rastegar, U. Strahle, *Environ. Sci. Technol.*, 2013, **47,** 3316.
55. I. Onyido, A. R. Norris, E. Buncel, *Chem. Rev*., 2004, **104**, 5911.
56. T. Tsuda, T. Yorifuji, M. Harada, *Environ. Health Perspect.*, 2011, **119**, A284.
57. A. Balamurugan, H. Lee, *Sensors and Actuators*, 2015, **B216**, 80.
58. S. -L. Kao, S. -P. Wu, *Sensors and Actuators*, 2015, **B212**, 382.
59. G. V. Ramesh, T. P. Radhakrishnan, *ACS Appl. Mater. Interfaces*, 2011, **3**, 988.
60. C. Dıez-Gil, R. Martınez, I. Ratera, T. Hirsh, A. Espinosa, A. Tarraga, P. Molina, O. S. Wolfbeisd, J. Veciana, *Chem. Commun.*, 2011, **47**, 1842.
61. G. Chen, Z. Guo, G. Zeng, L. Tang, *Analyst*, 2015, **140**, 5400.
62. Supramolecular Chemistry of Anions; A. Bianchi, K. Bowman-James, E. Garcia-Espan, Eds.; Wiley-VCH, New York, 1997.
63. Themed issue: P. A. Gale, T. Gunnalaugsson, Supramolecular Chemistry of Anionic Species. *Chem. Soc. Rev.*, 2010, **10**, 3595.
64. M. Arunachalam, S. Chakraborty, S. Marivel, P. Ghosh, *Cryst. Growth Des.*, 2012, **12**, 2097.
65. H. -H. Wang, L. Xue, C. -L. Yu, Y. -Y. Qian, H. Jiang, *Dyes and Pigments*, 2011, **91**, 350.
66. S. Stolte, J. Arning, U. Bottin-Weber, M. Matzke, F. Stock, K. Thiele, M. Uerdingen, U. Welz-Biermann, B. Jastorff, J. Ranke, *Green Chem.*, 2006, **8**, 621.

67. V. Kumar, M. P. Kaushik, A. K. Srivarstava, A. Pratap, V. Thiruvenkatam, T. N. GuruRow, *Anal. Chim. Acta*, 2010, **663**, 77.
68. R. M. Duke, T. Gunnlaugsson, *Tetrahedron Lett.*, 2007, **48** 8043.
69. E. J. Jun, K. M. K. Swamy, H. Bang, S. J. Kim, J. Yoon, *Tetrahedron Lett.*, 2006, **47**, 3103.
70. S. Song, X. Sun, X. Li, Y. Yuan, N. Jiao, *Org. Lett.*, 2015, **17**, 2886.
71. B. R. Jali, J. B. Baruah, *ChemPlusChem*, 2013, **78**, 589.
72. A. Caballero, N. G. White, P. D. Beer, *Angew. Chem. Int. Ed.*, 2011, **50**, 1845.

भारतीय प्रौद्योगिकी संस्थान गुवाहाटी
Indian Institute of Technology Guwahati

Chapter 5 (Part A)

Polymorphs of thiazole-derived imines tethered Hydroxyaromatics

Different orientations of functional groups of imine,[1-3] amide,[4,5] urea,[6,7] and thiourea[8] derivatives in solid state generates polymorphs. Energy required for carbon-carbon or carbon-heteroatom single bond rotations are comparable to weak supramolecular interactions.[9-11] Hence, subtle stimuli can change a conformation facilitating formation of a particular polymorph. Imines can show *syn* and *anti* conformation. For example, N-benzylideneaniline (Figure 5.1a) which is the simplest phenyl substituted imine derivative having nonplanar structure;[12] whereas corresponding C=C analogue stilbene[13] and N=N analogue *trans*-azobenzene[14] are planar. Due to such nonplanar arrangement, various conformations are possible in imine derivatives; for example, N-(p-methylbenzylidene)-p-methylaniline (Figure 5.1b) showed three polymorphs having planar or nonplanar geometry,[15-17] where differences in structures arises from the orientation of the phenyl rings. In this particular example, it was observed that the nonplanar conformation was more stable by 6.57 kJ/mol over the planar conformation.

(a) (b)

Figure 5.1: (a) N-benzylideneaniline, (b) N-(p-methylbenzylidene)-p-methylaniline.

Similarly, p-chloro-N-(p-chlorobenzylidene)aniline (Figure 5.2a) shows conformational polymorphs,[18,19] in which planar form has higher stability by 4.39 kJ/mol.[20,21] Structural studies carried out on a series of fluoro substituted positional isomers of N-benzylideneanilines (Figure 5.2b) have clearly indicated that the packing patterns of the isomers are largely influenced by fluorine atom as substituent.[22]

(a) (b)

Figure 5.2: (a) p-Chloro-N-(p-chlorobenzylidene)aniline, (b) N-benzylideneanilines

Thus, there is a necessity to look for conformationally flexible unit on supramolecular synthon to form conformational polymorphs guided by solvents. For such a purpose, we have chosen imines derived from *ortho*-hydroxyaromatic carbonyl compounds. Earlier, Kaitner et al. isolated three polymorphic forms of the imine 1-{3-[(2-hydroxy-3-methoxy-benzylidene)- amino]-phenyl}-ethanone (Figure 5.3). Two out of the three, were synthesized by mechanochemical syntheses, under solvent-free conditions.

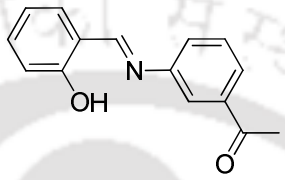

Figure 5.3: Imine 1-{3-[(2-hydroxy-3-methoxy-benzylidene)-amino]-phenyl}-ethanone

Imines derived from *ortho*-hydroxyaromatic carbonyl compounds can be considered as perspective candidate as they form six-membered cyclic intramolecular hydrogen bonds.[23-28] Such hydrogen bonded cyclic structures constructed above a phenyl ring may be compared with naphthyl rings as illustrated in Figure 5.4.

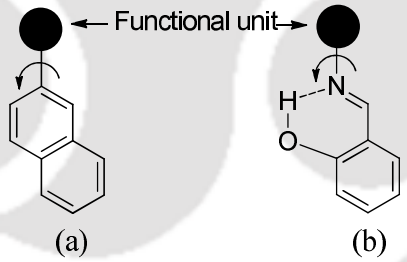

Figure 5.4: Schematic figures showing rotation of a top unit over (a) naphthalene, (b) intramolecularly hydrogen-bonded six-membered ring.

In these examples barrier of single bond rotation of a substituent attached on a C-atom of naphthyl group or N-atom of hydrogen bonded cyclic structures should differ due to uneven electronic distribution. Careful choice of intramolecularly hydrogen bonded six-member rings may favor specific conformation. A similar effect is important in formation of polymorphs.[29–35] Imines belongs to a class of compound called Schiff bases,[36,37] they have potential to study for polymorphs due to different orientations, as shown in Figure 5.4. Crystallization of various polymorphs[5,38] are guided by solvents. Solvent-guided crystallization of applied pharmaceuticals[39-47] has found great

importance in the area of crystal engineering. Crystallization conditions play role to obtain stable polymorphs,[48−56] and different methodologies are adopted for crystallization of polymorphs.[57-63] For imines, it was suggested that presence of disorder in crystalline environment contributes to the lattice energy to stabilize a high-energy conformation, which leaves scope to study solvent-guided polymorphs in imines.[64] Thiazole has N- and S-atoms in a five-member planar ring separated by an intervening carbon; thus, the orientation of such a planar unit across an unsymmetrical planar unit, like (a) and (b) in Scheme 5.1, would lead to polymorphs. Functional groups play a crucial role in controlling the orientation of a phenyl ring across C=N, as in substituted N-benzylideneanilines show different orientation.[65] In an anticipation to obtain polymorphs over intramolecularly hydrogen-bonded cyclic unit, polymorphism in 2-[(E)-(5-methylthiazol-2-ylimino)methyl]phenol (**5.1**) and 1-(E)-[(5-methylthiazol-2-ylimino)methyl]naphthalen-2-ol (**5.2**) were studied. 5-Methyl-substituted thiazole was chosen because the methyl group would contribute a steric factor to stabilize or destabilize the particular conformation(s) generated through C−N rotation.

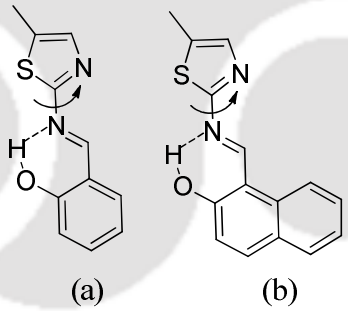

*Scheme 5.1: Thiazole tethered hydroxyaromatic imines **5.1** and **5.2**.*

5.1: Synthesis of thiazole derived imines 5.1 and 5.2

Compounds **5.1** and **5.2** were prepared by reaction of corresponding salicylaldehyde or 2-hydroxy-1-naphthaldehyde with 5-Methylthiazol-2-yl-amine. These compounds were characterized by various spectroscopic techniques, such as IR spectroscopy, mass spectrometry and ^{1}H-NMR. The characteristic imine proton (designated as- c) appear at 8.97 and 9.91 ppm for **5.1** and **5.2** respectively as shown in Figure 5.5a,b. In FT-IR spectrum **5.1** shows C=N stretching frequency at 1608 cm^{-1} and 1630 cm^{-1}, while **5.2** shows at 1621 cm^{-1}. Compound **5.1** shows ESI-HRMS at 219.1045

(calc.219.0594) which corresponds to M+1 peak. Mass peak appear at 269.0711(calc.269.0750) corresponding to M+1 peak.

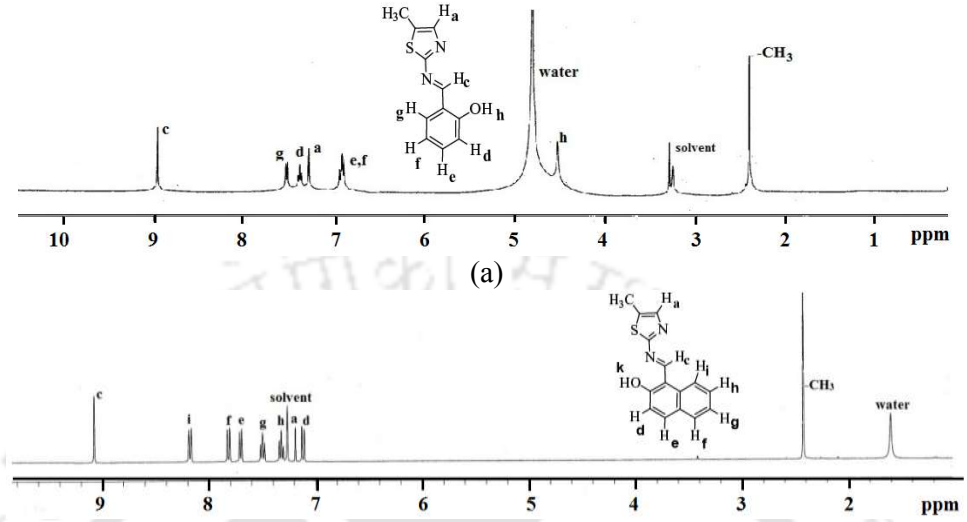

*Figure 5.5: (a) ^{1}H-NMR (CD_3OD, 400 MHz) of compound **5.1**, (b) ^{1}H-NMR ($CDCl_3$, 400 MHz) of compound **5.2**.*

5.2: Polymorphs of 5.1 and 5.2

Crystallization of compound **5.1** or **5.2**, from different solvents resulted either needle-type or block-type crystals as shown in Figure 5.6a,b. Crystals were identified to be polymorphs of the respective compounds **5.1** or **5.2**. In none of these cases, crystals of both morphologies formed together. Accordingly, polymorphs of **5.1** are designated as **5.1a** and **5.1b.** Whereas, **5.2a** and **5.2b** for compound **5.2**. The crystallization results from various solvents are summarized in Table 5.1.

(a) (b)

*Figure 5.6: Photograph of crystals of polymorphs (a) **5.1a** and **5.1b, (b) 5.2a** and **5.2b.***

Polymorph **5.1a** was the result when compound **5.1** was crystallized from solvents such as tetrahydrofuran, dimethylformamide, ethanol, acetonitrile, dimethyl sulfoxide, dichloromethane and ethyl acetate, whereas crystallization of **5.1** from methanol gave

polymorph **5.1b**. The crystal morphologies of **5.1a** and **5.1b** are easily distinguishable, as shown in Figure 5.6a.

Table 5.1: Crystallization of polymorphs of **5.1** or **5.2** from different solvents

Solvent	**5.1**(type of crystals)	**5.2** (type of crystals)
Acetone	No suitable crystal	**5.2b** (block)
Acetonitrile	**5.1a** (needle)	**5.2b** (block)
Methanol	**5.1b** (needle)	**5.2a** (needle)
Ethanol	**5.1a** (needle)	**5.2b** (block)
THF	**5.1a** (needle)	No suitable crystal
DMF	**5.1a** (needle)	**5.2b** (block)
Dichloromethane	**5.1a** (needle)	No suitable crystal
Acetonitrile:Methanol (1:1)	**5.1b** (block)	**5.2b** (block)
Methanol : Ethanol (1:1)	**5.1b** (block)	**5.2a** (needle)
Methanol : THF (1:1)	**5.1b** (block)	**5.2b** (block)
Acetonitrile : THF (1:1)	**5.1a** (needle)	**5.2b** (block type)

Two polymorphs **5.2a** and **5.2b** from compound 5.**2** were isolated by crystallization at ambient conditions from solution in methanol or acetonitrile respectively. However, when needle shape crystals of **5.2a** were dissolved in acetonitrile solvent, on crystallization block type crystals of polymorph **5**.**2b** were formed. Whereas dissolution of block type of crystals of **5.2b** in methanol are recrystallizes as block type only. Needle shape crystals of **5.2a** when dissolved in 1:1 mixed solvent of methanol: acetonitrile and recrystallised it also yielded crystals of **5.2b** only. Thus it is much easier to obtain the crystals of polymorph **5.2b** than that of **5.2a**. Powder X-ray diffraction (PXRD) patterns from bulk samples of each polymorph were recorded independently and compared with PXRD data generated from the CIF files for each polymorph as shown in Figure 5.7abcd. PXRD pattern show phase purity of each polymorph. In none of the cases did the use of wet solvent lead to solvated or hydrated crystals of the parent compounds.

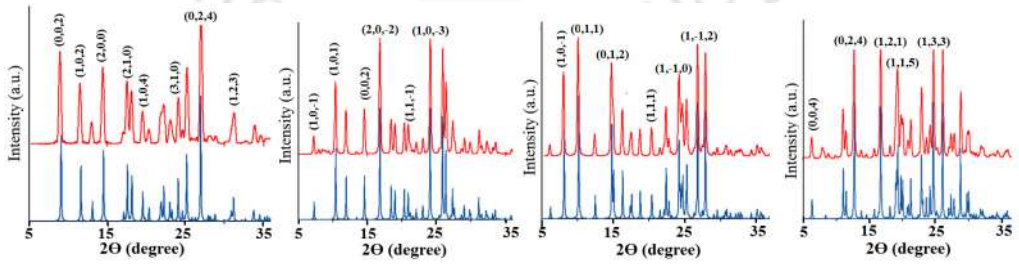

Figure 5.7: PXRD patterns of polymorph (a) ***5.1a****, (b)* ***5.1b****, (c)* ***5.2a*** *and (d)* ***5.2b*** *(in each case top/red = experimental, bottom/blue = simulated).*

5.3: Supramolecular Assembly of polymorphs of 5.1

Polymorph **5.1a** crystallizes in orthorhombic *Pbca* space group, having one molecule in its asymmetric unit. Polymorph **5.1b,** also have one molecule in its asymmetric unit, belong to monoclinic space group $P2_1/n$. The structure of polymorph 5.1b was reported earlier;[66] hence, we determined the structure again for comparison. Both polymorphs have intramolecular hydrogen bonds between the hydroxy group and the N-atom of the imine as shown in Figure 5.8a,b. Differences in the orientation of the thiazole ring with respect to the hydroxyphenyl unit are shown in Figure 5.8c. In polymorph **5.1a** thiazole nitrogen is *cis* to hydroxy group of phenyl moiety, but in polymorph **5**.**1b,** it is *trans*, as shown in the overlaid diagrams (Figure 5.8c) of molecules of two polymorphs. Polymorph **5.1a** self assembles through weak C-H**…**O hydrogen bonds as depicted in Figure 5.8a. Whereas polymorph **5**.**1b** self assembles through C-H**…**π interactions. Hydrogen bond parameters are listed in the Table 5.2.

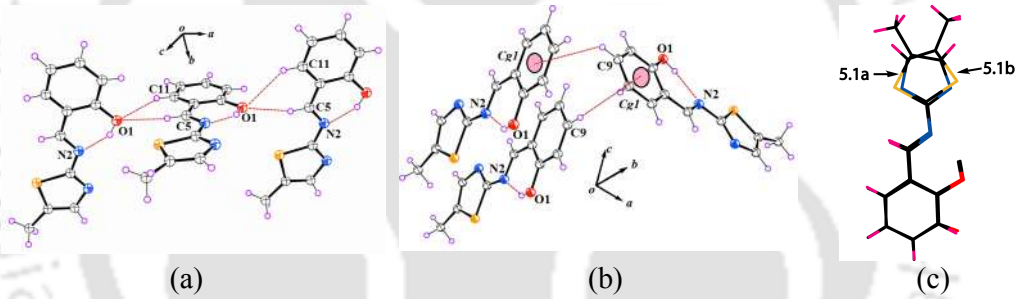

(a) (b) (c)

*Figure 5.8: (a) Hydrogen bonds in polymorph **5.1a**, (b) C-H**…**π interactions in **5.1b** ($d_{C9-H\cdots\pi}$=3.531 Å, where π is the centroid of the phenyl ring), (c) Overlaid diagram of molecules of polymorphs **5.1a** and **5.1b** drawn by keeping hydroxyphenyl unit fixed.*

Table 5.2: Hydrogen-bond parameters of polymorphs **5.1a, 5.1b**, **5.2a** and **5.2b**.

Compd	D-H···A	d_{D-H}(Å)	$d_{H\cdots A}$(Å)	$d_{D\cdots A}$(Å)	∠D-H···A (°)
5.1a	O(1)-H ··· N(2)	0.90(3)	1.82(3)	2.611(2)	145(2)
	C(5)-H··· S(1)	0.94(2)	2.570(2)	3.027(3)	110.3(1)
	C(5)-H··· O(1) [1/2+x,y,1/2-z]	0.94(2)	2.476(2)	3.365(3)	157.7(2)
5.1b	O(1)-H···N(2)	0.82(2)	1.90(2)	2.620(2)	146(2)
	C(5)-H···N(1)	0.93(3)	2.48(3)	2.816(2)	101(3)
5.2a	O(1)-H··· N(2)	0.93(3)	1.71(3)	2.557(2)	151(3)
	C(1)-H··· O(1)	0.96(3)	2.72	3.620	156.5(4)
5.2b	O(1)-H··· N(2)	0.90(3)	1.74(3)	2.566(3)	152(4)
	O(2)-H··· N(4)	0.96(4)	1.71(4)	2.566(4)	148(3)
	C(5)-H···N(1)	0.98(3)	2.38(3)	2.791(4)	105(2)
	C(20)-H··· N(3)	0.99(3)	2.41(3)	2.798(4)	102.5(2)

5.4: Supramolecular Assembly of polymorphs of 5.2

Crystals of polymorph **5.2a** belong to triclinic $P\bar{1}$ space group and crystals of **5.2b** belonging to orthorhombic $P2_12_12_1$ space group. Crystal morphologies of two polymorphs are shown in Figure 5.6b respectively. Once again, these polymorphs also slightly differ in their respective orientations of thiazole ring with respect to naphthalene ring as shown in Figure 5.9c. Polymorph **5.2a** exists as dimeric assemblies in its crystal lattice through very weak C-H**…**O bonds (Figure 5.9a). Structure shows presence of intramolecular O-H**…**N hydrogen bond (Table 5.2). Asymmetric unit of polymorph **5.2b** contains two symmetry independent molecules in its asymmetric unit (Z′= 2). Both symmetry independent molecules (designated as X and Y) are connected to each other through C-H**…**N hydrogen bonds via a C-H of naphthyl ring interacting with nitrogen atom of thiazole unit of a neighboring molecule of **5.2b** as shown in Figure 5.9b. Naphthyl rings are parallel in the lattice with centroid to centroid distance 3.932 Å, suggests π-π interactions among the naphthyl rings. These suggest that packing pattern of **5.2a** is guided by C-H**…**O bonds while **5.2b** is guided by π- π stacking interactions.

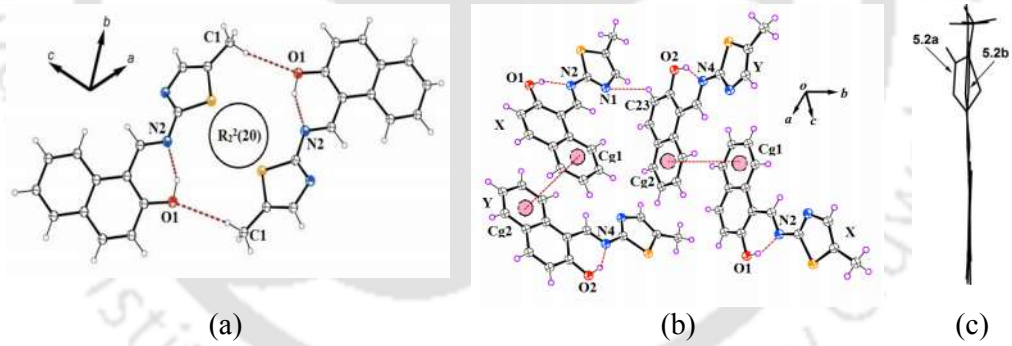

(a) (b) (c)

*Figure 5.9: (a) Hydrogen bonds in polymorph **5.2a**, (b) π-π Stacking interactions in lattice of **5.2b** with $d_{Cg1\cdots Cg2}$= 3.932 Å, (c) Overlay diagram of molecules from polymorphs **5.2a** and **5.2b** shown by fixing hydroxynaphthyl unit in one plane.*

Gas phase DFT calculation at B3LYP/6-31++G(d, p) energy level showed that energy difference between polymorph **5.1a** and **5.1b** to be 8.74 KJ/mol. On the other hand, similar calculation showed negligible difference between the energy of polymorphs **5.2a** and **5.2b**. Different torsion angles related to orientation of thiazole ring with respect to hydroxyphenyl groups of each polymorph are listed in Table 5.3. Polymorph **5.1a** and **5.1b** has wide difference in torsion angle. But, difference in

torsion angle for polymorph **5.2a** and **5.2b** is comparatively less. Torsion angle differences observed in each form confirm independent orientations in each polymorph.

Table 5.3: Torsion angles in polymorphs of **5.1** and **5.2**

Compound	Torsion angle	Polymorph **5.1a**	Polymorph **5.1b**
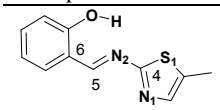	N1-C4-N2-C5	178.68	-3.02
	S1-C4-N2-C5	-3.77	179.14
	C4-N2-C5-C6	178.53	177.89
	Torsion angle	Polymorph **5.2a**	Polymorph **5.2b**
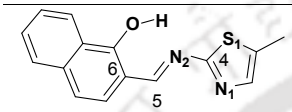	N1-C4-N2-C5	23.62	9.27 (-3.46)#
	S1-C4-N2-C5	-158.11	-170.77 (178.23)#
	C4-N2-C5-C6	175.89	-179.54 (179.28)#

Torsion angle from symmetry independent molecule is shown in parenthesis

5.5: Differential scanning calorimetry study

Differential scanning calorimetry (DSC) is used to study the thermal interconversion between the polymorphs of **5.1** or **5.2**. Since present molecules have different orientations having near-planar structures of individual molecules, thermal effect may organize such molecules to show interesting thermal properties.[13] Thus, DSC of the samples as well as polarized hot stage optical micrographic study along with powder XRD patterns were recorded.

5.5.1: Differential scanning calorimetry study of polymorphs of 5.1

DSC of polymorph **5.1a** showed an endothermic peak at 117.83 ºC due to melting and Subsequent cooling shows a exothermic peak at 75.34 ºC, due to recrystallization as shown in Figure 5.10a. Similar DSC plot to that of the first heating-cooling cycle was observed when the samples of polymorphs used for the first cycle were heated for the second time. Endothermic peak corresponding to melting appeared at temperature 106.77 ºC on second heating cycle for polymorph **5.1a** and exothermic peak appear at 77.41ºC, due to recrystallization as shown in Figure 5.10b. The recrystallization, upon cooling is further verified through polarized hot stage optical micrographic study as shown in Figure 5.11.

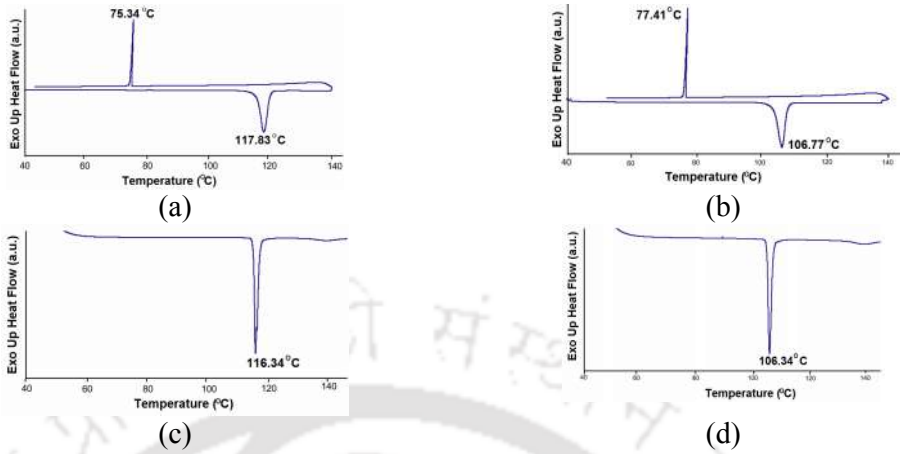

*Figure 5.10: DSC plots from (a) first heating and cooling cycle of polymorph **5.1a** and (b) second heating and cooling cycle of polymorph **5.1a,** (c) first heating of polymorph **5.1b**, (d) second heating of polymorph **5.1b.***

50°C | 117°C(1st melting) | 75°C (1st cooling) recrystallization | 106°C (2nd melting) | 77°C (2nd cooling) (recrystallization)

*Figure 5.11: Hot-stage microscopic images of polymorph **5.1a** from temperature range 50-120 ° C.*

The recrystallized form is identical as parent polymorph **5.1a,** which is confirmed by PXRD pattern as shown in Figure 5.12. PXRD of polymorph **5.1a**, after heated to 117 ºC was overlaid with the PXRD pattern of the parent polymorph **5.1a.** We found that both patterns tally to each other as shown in Figure 5.12. Thus, it is confirmed that melted sample of polymorph **5.1a**, upon cooling recrystallizes to its parent form.

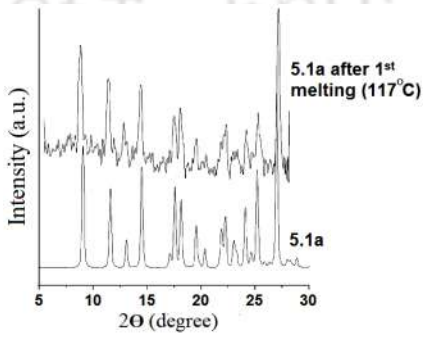

*Figure 5.12: PXRD pattern of polymorph **5.1a***

Polymorph **5.1b,** showed an endothermic peak due to melting, at 116.34 ºC in DSC. No exothermic peak appeared upon cooling. When samples of polymorphs used for the first cycle were heated for the second time, and an endothermic peak at 106.34 ºC appeared, corresponding to melting.

5.5.2: Differential scanning calorimetry study of polymorphs of 5.2

DSC of polymorphs **5.2a** and **5.2b** have revealed several interesting features. Polymorph **5.2a**, during first heating has an exothermic process at 129 ºC; which corresponds to transformation of polymorph **5.2a** to polymorph **5.2b**. A small depression followed by exothermic peak is attributed to melting of residual amount of polymorph **5.2a**. Polymorph **5.2b** thus formed melts, corresponding to the endothermic peak at 142 ºC. On cooling, melted **5.2b** crystallizes to form polymorph **5.2a** at 89 ºC, which is reflected in an unsymmetrical exothermic peak as shown in Figure 5.13a. For the second heating cycle of polymorph **5.2a** showed, two endothermic peaks; one corresponding to melting of **5.2a** at 125 ºC followed another endothermic peak from the residual amount of original polymorph **5.2b**, which melts at 140 ºC slightly lower than first cycle as it is a residual amount as shown in Figure 5.13b.

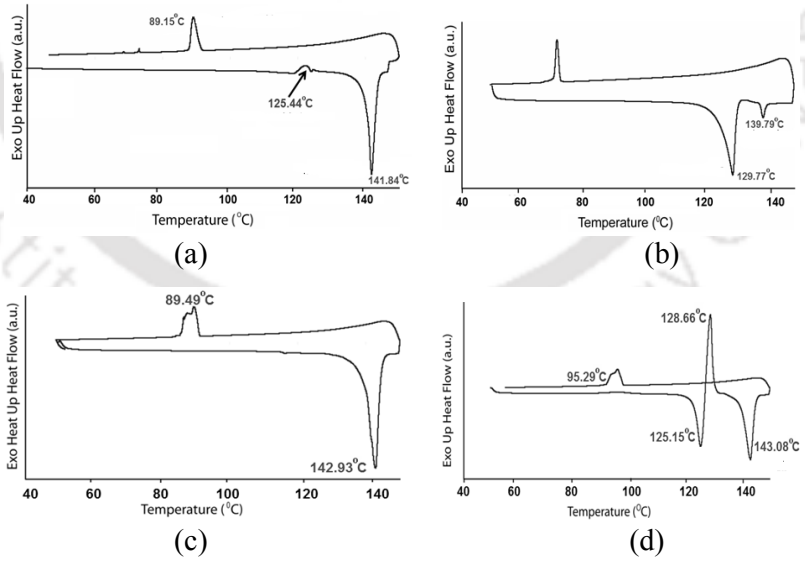

*Figure 5.13: DSC plots from (a) first heating and cooling in cycle of polymorph **5.2a**; (b) second cycle of heating and cooling for polymorph **5.2a**,(c) first heating and cooling in cycle of polymorph **5.2b**, (d) second cycle of heating and cooling for polymorph **5.2b** (heating rate 5 °C/min).*

Polymorph **5.2b** showed a melting at 142 ºC, but while cooling it showed two very closely spaced exothermic peaks at 89 ºC and 88 ºC as shown in Figure 5.13c. These two peaks are attributed to crystallization of polymorph in two independent forms, namely polymorph **5.2a** and polymorph **5.2b**. DSC of the second heating cycle, and later appears as an endothermic process at 125 °C for melting of polymorph **5.2a**, followed by an exothermic process at 129 °C for conversion of polymorph **5.2a** to polymorph **5.2b**, as shown in Figure 5.13d. A similar melting point was observed in the second heating cycle of DSC of **5.2a**. In the second heating cycle of polymorph **5.2b**, polymorph **5.2a** that formed during crystallization from the melt converts to the parent polymorph **5.2b**. Finally, the parent polymorph **5.2b** melts at 142 °C.

The thermal events occurring in polymorph **5.2a** and polymorph **5.2b** are represented schematically in Scheme 5.2 and Scheme 5.3 respectively.

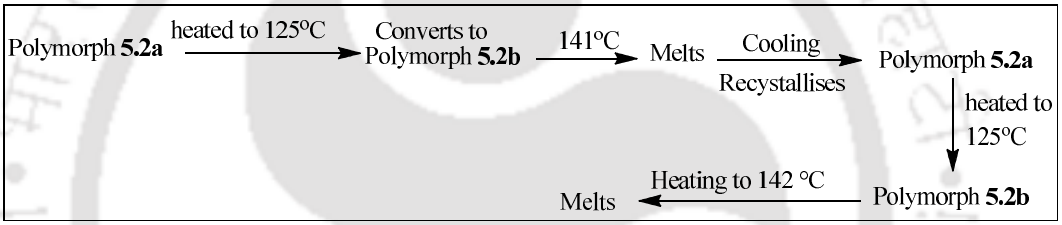

*Scheme 5.2: Thermal events of Polymorph **5.2a**.*

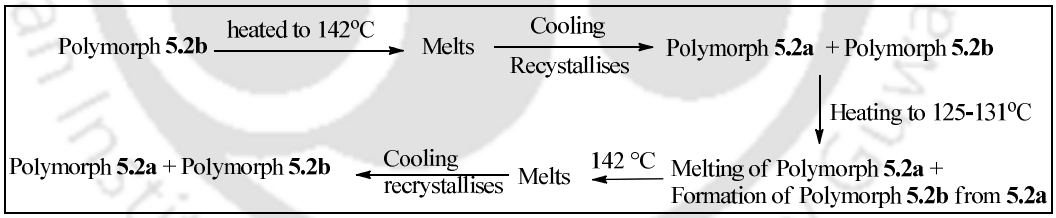

*Scheme 5.3: Thermal events of Polymorph **5.2b***

Hot-stage images were directly taken on a polarized hot-stage microscope, with crystals of polymorph **5.2a** and **5.2b** during the different heating cycles are shown in Figure 5.14, and they support the entire processes shown in Schemes 5.2 and 5.3.

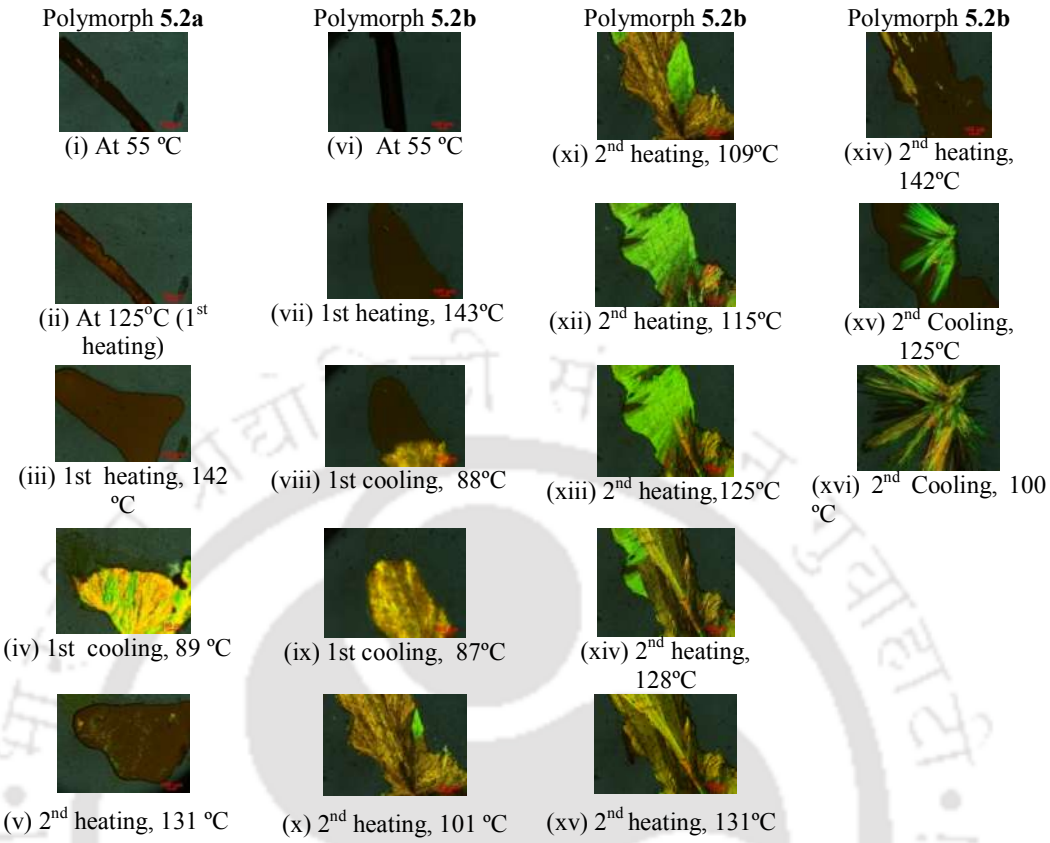

*Figure 5.14: Hot-stage microscopic images of **5.2a** and **5.2b** from temperature range 50-150 ºC.*

In the first cycle of polymorph **5.2a** [Figure 5.14(ii)−(iv)], polymorph **5.2b**, formed from polymorph **5.2a** through a transformation at 125 °C, melts at 142°C, and then crystallization of melted polymorph **5.2b** returns polymorph **5.2a**, which on heating again melts at 131 °C [Figure 5.14(v)]. On the other hand, polymorph **5.2b**, on heating in the first cycle, melts at 143 °C [Figure 5.14(vii)], and on cooling it crystallizes in two forms, polymorphs **5.2a** and **5.2b** [Figure 5.14(viii)-(ix)]. On heating, **5.2a** starts melting from 101 °C, and while melting [Figure 5.14(x)-(xiii)] it simultaneously converts to polymorph **5.2b** during 125-131 °C [Figure 5.14(xii)-(xv)]. Finally, polymorph **5.2b** melts at 142 °C [Figure 5.14(xiv)]. When this melt cools, it recrystallizes as both polymorphs **5.2a** and **5.2b** [Figure 5.14(xv) and (xvi)]. Further, the whole thermal events in polymorph **5.2a** and **5.2b** is verified through PXRD pattern as shown in Figure 5.15a, b

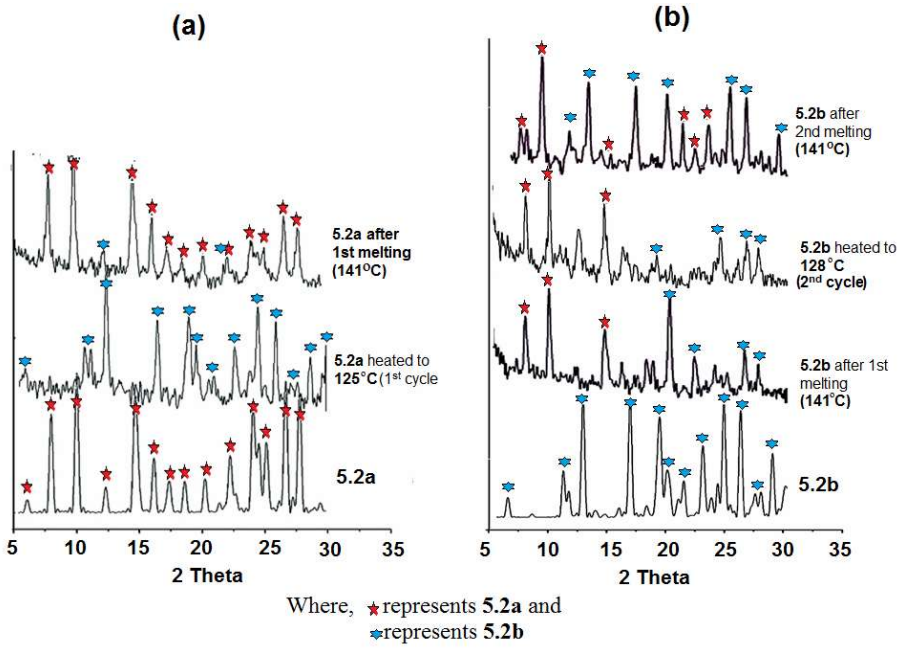

*Figure 5.15: PXRD pattern at various temperatures of (a) polymorph **5.2a**, (b) polymorph **5.2b**.*

We have recorded the PXRD of sample of polymorph **5.2a** after heated to 125º C. The PXRD pattern of the heated **5.2a** sample tally with the PXRD pattern of **5.2b** as shown in Figure **5.15a**. Again reheating of the latter sample to 141º C, resulted in melting of converted polymorph **5.2b**, from polymorph **5.2a**. The melted sample after cooling of polymorph **5.2b** has almost similar PXRD pattern with polymorph **5.2a**, with negligible resemblance with PXRD pattern of polymorph **5.2b.** This is corresponds to the unsymmetrical exothermic peak in first heating cycle of polymorph **5.2a** (Figure 5.13a). Polymorph **5.2b** upon heating to 141º C undergoes melting. The PXRD pattern upon cooling of the melted sample of **5.2b** has resemblance with both polymorph **5.2a** and **5.2b** to some extent as shown in Figure 5.15b. This is attributed to the two very closely spaced exothermic peaks as shown in Figure 5.13c. This observation signifies that on cooling polymorph **5.2b** recrystallizes to both **5.2a** and **5.2b**. Upon reheating of the sample containing both **5.2a** and **5.2b,** polymorph **5.2a** undergoes melting at 125ºC, simultaneously converted to polymorph **5.2b**, ultimately melted at 142º C. Final PXRD pattern of the melted sample after cooling show resemblance with both forms **5.2a** and **5.2b,** corresponds to the closely spaced exothermic peaks (Figure 5.15b).

5.6: Conclusion

It has been established that polymorphs arise due to different orientations of the thiazole ring via C-N bond rotation over the intramolecularly hydrogen bonded six-membered ring. Polymorphs of **5.1** are not interconvertible. The polymorphs of compound **5.2** are interconvertible. Polymorph **5.2a** is converted to a metastable polymorph **5.2b**, which on crystallization from melt reforms both polymorphs. This opens new avenues to carry out studies on similar systems for reversible transformations, showing switching properties.

5.7: Experimental section

2-[(5-Methylthiazol-2-ylimino)-methyl]-phenol (5.1): 5-Methylthiazol-2-yl-amine (57 mg, 5 mmol) and salicylaldehyde (61 mg, 5 mmol) were dissolved in dry methanol (20 mL) and the solution was refluxed for 6 hrs. The resulting solution was evaporated, and the precipitate was dried in vacuum. Yield, 90 %. ^{1}H-NMR (400MHz, $CDCl_3$): 8.97 (s, 1H), 7.55 (d, 8.0 Hz, 1H), 7.42 (t, 7.2 Hz, 1H), 7.29 (s, 1H), 6.92 (m, 2H). 2.42 (s, 3H) ESI mass: [M + 1]: 219.1045; Calcd mass for $C_{11}H_{10}N_2OS$, 218.0514. IR (cm^{-1}): 2919 (m), 1608 (s), 1566 (s), 1529 (s), 1494 (s), 1430 (m), 1365 (m), 1280 (s), 1189 (s), 1153 (s), 1136 (s), 1034 (m), 982 (m), 902 (s), 786 (s), 624 (m), 531 (s). Polymorph **5.1a** was crystallized from tetrahydrofuran, whereas polymorph **5.1b** was crystallized from methanol

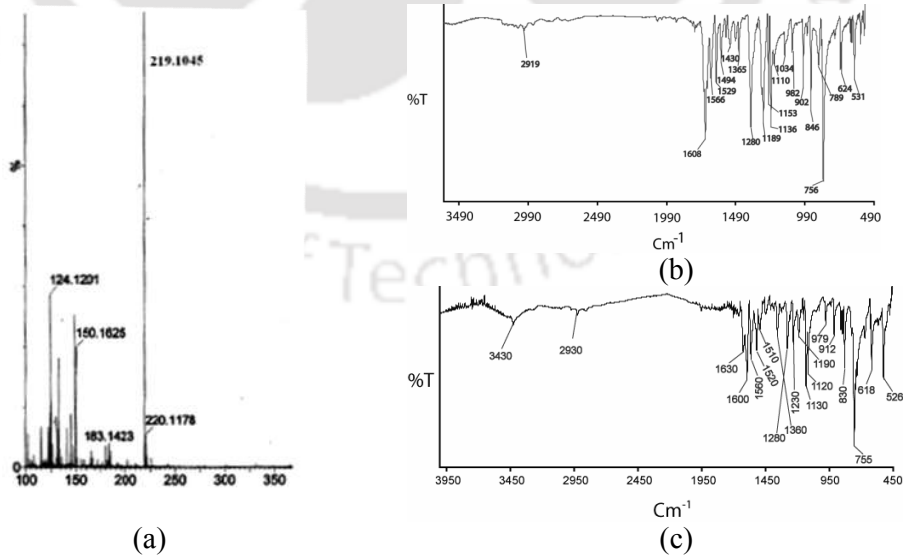

*Figure 5.16: (a) ESI mass spectra of **5.1**. IR-spectra (KBr) of polymorph (b) **5.1a**, (c) **5.1b**.*

1-[(5-Methylthiazol-2-ylimino)-methyl]-naphthalen-2-ol (5.2): 5-Methylthiazol-2-yl-amine (57 mg, 5 mmol) and 2-hydroxy-1-naphthaldehyde (86 mg, 5 mmol) were dissolved in dry methanol (20 mL) and the solution was refluxed for 6 hrs. The resulting solution was evaporated, and the precipitate was dried in vacuum. Yield, 95 %. ^{1}H-NMR (400 MHz, $CDCl_3$): 9.91 (s, 1H), 8.19 (d, 8.4 Hz, 1H), 7.82 (d, 8.8 Hz, 1H), 7.71 (d, 8.4 Hz, 1H), 7.49 (t, 7.2 Hz, 1H), 7.34 (t, 7.2 Hz, 1H), 7.19 (s, 1H), 7.10 (d,1.2 Hz,1H), 2.42 (s, 3H). ESI mass: [M + 1]: 269.0711. Calcd. mass for $C_{15}H_{12}N_2OS$: 268.0670. IR (cm^{-1}): 3439 (wb), 1621(s), 1599 (s), 1556 (s), 1524 (m), 1390 (m), 1320 (s), 1224 (m), 1187 (m), 1133 (s), 1081 (m), 1032 (w), 852 (m), 745 (s), 627 (m), 539 (w), 507 (s). Polymorph **5.2a** was crystallized from methanol solution of **5.2**, whereas polymorph **5.2b** was crystallized from acetonitrile solution of **5.2**.

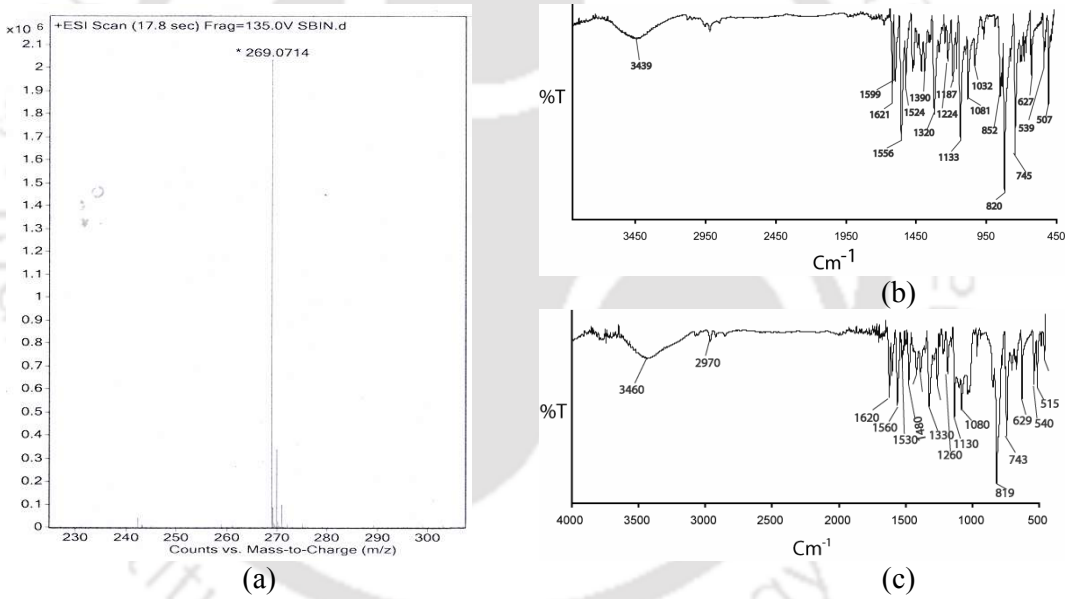

*Figure 5.17: (a) ESI mass spectra of **5.2**. IR-spectra (KBr) of polymorph (b) **5.2a**, (c) **5.2b**.*

5.8: References

1. F. Arod, P. Pattison, K. J. Schenk, G. Chapuis, *Cryst. Growth Des*., 2007, **7**, 1679.
2. M. Rubcic, N. Galic, I. Halasz, T. Jednacak, N. Judas, J. Plavec, P. Sket, P. Novak, *Cryst. Growth Des.*, 2014, **14**, 2900.
3. D. Cincic, I. Brekalo, B. Kaitner, *Cryst. Growth Des.*, 2012, **12**, 44.
4. W. I. F. David, K. Shankland, C. R. Pulham, N. Blagden, R. J. Davey, M. Song, *Angew. Chem., Int. Ed.*, 2005, **44**, 7032.
5. P. Khakhlary, J. B Baruah, *J. Mol. Struct.*, 2013, **1078**, 188.
6. M. C. Etter, Z. Urbanczyk-Lipkowska, M. Zia-Ebrahimi, T. W. Panunto, *J. Am. Chem. Soc.*, 1990, **112**, 8415.
7. W. F. DeSouza, N. Kambe, Z. J. Jin, N. Kanehisa, Y. Kai, N. Sonoda, *J. Org. Chem.*, 1995, **60**, 7058.
8. C. I. Yeo, E. R. T. Tiekink, *Acta Crystallogr.*, *Sect. E* 2011, **67**, o2965.
9. T. Steiner, *Angew. Chem., Int. Ed*., 2002, **41**, 48.
10. A. Nangia, *In Organic crystal engineering: Frontiers in crystal engineering*; R. T. Edward, J. J. Vittal, M. Zaworotko, Eds.; John Wiley & Sons, Ltd.: Chichester, UK, 2010; p 151.
11. G. R. Desiraju, T. Steiner, The weak hydrogen bond. *In Structural Chemistry and Biology*; Oxford University Press: New York, 2001.
12. H. B. Burgi, J. D. Dunitz, C. Zust, *Acta Crystallogr., Sect. B*, 1968, **24**, 463.
13. H. B. Burgi, J. D. Dunitz, *Helv. Chim. Acta*, 1970, **53**, 1747.
14. J. M. Robertson, I. Woodward, *Proc. R. Soc*. A, 1937, **162**, 568.
15. J. Bernstein, I. Bar, A. Christensen, *Acta Crystallogr.*, *Sect. B*, 1976, **32**, 1609.
16. I. Bar, J. Bernstein, *Acta Crystallogr.*, *Sect. B*, 1978, **33**, 1738.
17. I. Bar, J. Bernstein, *Acta Crystallogr.*, *Sect. B*, 1982, **38**, 121.
18. J. Bernstein, G. M. J. Schmidt, *J. Chem. Soc., Perkin Trans. 2*, 1972, 951.
19. J. Bernstein, I. Izak, *J. Chem. Soc., Perkin Trans. 2*, 1976, 429.
20. A. T. Hagler, J. Bernstein, *J. Am. Chem. Soc.*, 1978, **100**, 673.

21. A. T. Hagler, J. Bernstein, *J. Am. Chem. Soc.*, 1978, **100**, 6349.
22. G. Kaur, P. Panini, D. Chopra, A. RoyChoudhury, *Cryst. Growth Des.*, 2012, **12**, 5096.
23. O. Dominguez, B. Rodriguez-Molina, M. Rodriguez, A. Ariza, N. Farfan, R. Santillan, *New J. Chem.*, 2011, **35**, 156.
24. K. Ogawa, Y. Kasahara, Y. Ohtani, J. Harada, *J. Am. Chem. Soc.*, 1998, **120**, 7107.
25. T. Fujiwara, J. Harada, K. Ogawa, *J. Phys. Chem. A*, 2009, **113**, 1822.
26. M. Rodriguez, R. Santillan, Y. Lopez, N. Farfan, V. Barba, K. Nakatani, E. V. Garcia-Baez, I. I. Padilla-Martinez, *Supramol. Chem.*, 2007, **19**, 641.
27. S. D. Chatziefthimiou, Y. G. Lazarou, E. Hadjoudis, T. Dziembowska, I. M. Mavridis, *J. Phys. Chem. B*, 2006, **110**, 23701.
28. M. A. Al-Douh, H. Osman, S. A. Hami, *Univ. Aden J. Nat. Appl.Sc.*, 2010, **14**, 325.
29. J. Bernstein, *Polymorphism in molecular crystals*; Oxford University Press: Oxford, 2002.
30. G. R. Desiraju, *Cryst. Growth Des.*, 2004, **4**, 1089.
31. A. Nangia, *Cryst. Growth Des.*, 2006, **6**, 2.
32. V. S. Kumar, A. Addlagatta, A. Nangia, W. T. Robinson, C. K. Broder, R. Mondal, I. R. Evans, J. A. K. Howard, F. H. Allen, *Angew. Chem., Int. Ed.*, 2002, **41**, 3848.
33. J. Bernstein, *Cryst. Growth Des*., 2011, **11**, 632.
34. K. R. Seddon, *Cryst. Growth Des*., 2004, **4**, 1087.
35. A. J. Cruz-Cabeza, J. Bernstein, *Chem. Rev.*, 2014, **114**, 2170.
36. T. T. Tidwell, *Angew. Chem., Int. Ed*., 2007, **46**, 2.
37. P. A. Vigato, S. Tamburini, *Coord. Chem. Rev.*, 2004, **248**, 1717.
38. N. Phukan, J. B. Baruah, *Cryst. Growth Des*., 2014, **14**, 2640.
39. K. Kawakami, Y. Asami, I. Takenoshita, *J. Pharm. Sci.*, 2010, **99**, 76.
40. T. Mukuta, A. Y. Lee, T. Kawakami, A. S. Myerson, *Cryst. Growth Des*., 2005, **5**, 1429.
41. S. Datta, D. J. W. Grant, *Cryst. Growth Des.*, 2005, **5**, 1351.

42. S. H. Thorat, M. V. Patwadkar, R. J. Gonnade, R. Vaidhyanathan, *CrystEngComm*, 2014, **16**, 8638.
43. F. Wang, J. A. Wachter, F. J. Antosz, K. A. Berglud, *Org. Process Res. Dev.*, 2000, **4**, 391.
44. J. Cornel, P. Kidambi, M. Mazzotti, *Ind. Eng. Chem. Res*., 2010, **49**, 5854.
45. B. O'Sullivan, B. Glennon, *Org. Process Res. Dev*., 2005, **9**, 884.
46. J. Chen, B. Sarma, J. M. B. Evans, A. S. Myerson, *Cryst. Growth. Des.*, 2011, **11**, 887.
47. D. Jing, Y. Wang, Z. Chen, L. Zhou, J. Wang, *Chem. Sci. Eng*., 2011, **5**, 442.
48. C.-H. Gu, V. Jr. Young, D. J. W. Grant, *J. Pharma Sci*., 2001, **90**, 1878.
49. M. Kobari, N. Kubota, I. Hirasawa, *CrystEngComm*, 2014, **16**, 6049.
50. T. Arishima, K. Sato, *J. Am. Oil Chem. Soc*., 1989, **66**, 1614.
51. R. J. Davey, N. Blagden, S. Righini, H. Alison, E. S. Ferrari, *J. Phys. Chem. B*, 2002, **106**, 1954.
52. R. Davey, N. Blagden, M. Quayle, *Cryst. Growth Des.*, 2001, **1**, 59.
53. N. Blagden, R. J. Davey, H. F. Lieberman, L. Williams, R. Payne, R. Roberts, R. Rowe, R. Docherty, *J. Chem. Soc., Faraday Trans.*, 1998, **94**, 1919.
54. N. Blagden, R. Davey, G. Dent, M. Song, W. David, C. Pulham, K. Shankland, *Cryst. Growth Des.*, 2005, **5**, 2218.
55. R. A. Chiarella, A. L. Gillon, R. C. Burton, R. J. Davey, G. Sadiq, A. Auffret, M. Cioffi, C. A. Hunter, *Faraday Discuss.*, 2007, **136**,179.
56. R. Kobayashi, Y. Fujimaki, T. Ukita, Y. Hiyama, *Org. Process Res. Dev*., 2006, **10**, 1219.
57. Y. Diao, K. E. Whaley, M. E. Helgeson, M. A. Woldeyes, P. S. Doyle, A. S. Myerson, T. A. Hatton, B. L. Trout, *J. Am. Chem.Soc.*, 2012, **134**, 673.
58. M. Lang, A. L. Grzesiak, A. J. Matzger, *J. Am. Chem. Soc*., 2002,**124**, 14834.

59. S. J. Bonafede, M. D. Ward, *J. Am. Chem. Soc*., 1995, **117**, 7853.

60. J. Zaccaro, J. Matic, A. S. Myerson, B. A. Garetz, *Cryst. Growth Des.*, 2001, **1**, 5.

61. A. V. Trask, W. D. S. Motherwell, W. Jones, *Chem. Commun*., 2004, 890.

62. P. W. Carter, M. D. Ward, *J. Am. Chem. Soc.*, 1994, **116**, 769.

63. J.-M. Ha, J. H. Wolf, M. A. Hillmyer, M. D. Ward, *J. Am.Chem. Soc.*, 2004, **126**, 3382.

64. J. Bernstein, I. Bar, *J. Phys. Chem*., 1982, **86**, 3223.

65. J. Harada, M. Harakawa, K. Ogawa, *Acta Crystallogr., Sect. B*, 2004, **60**, 589.

66. C.-N. Zhang, M.-H. Yang, Y.-F. Zheng, *Acta Crystallogr., Sect. E*, 2007, **63**, o2040.

भारतीय प्रौद्योगिकी संस्थान गुवाहाटी
Indian Institute of Technology Guwahati

Chapter 5 (Part B)

Detection of Al^{3+} and Zn^{2+} ions by 2-(5-methylthiazol-2-yliminomethyl) phenol

Schiff basses are routinely used in analytical chemistry for detection of metal ions.[1-9] The stability of Schiff base towards hydrolysis in the presence of different metal ions is an important issue of analytical chemistry, [10] which can decide the stability of modified surface such as multiwall carbon nano-tube.[11-14] However, hydrolyzed or decomposed products from a Schiff base may also interact with metal ions. Hydrolytic cleavage of the C=N bond is well documented in the literature[15-18] and has been successfully used in the detection of metal ions.[19-21] For example, Nb^{5+} is selectively detected by hydrolytic cleavage of Schiff base (E)-ethyl 3-((pyren-1-ylimino)methyl)benzoate (Figure 5.18).

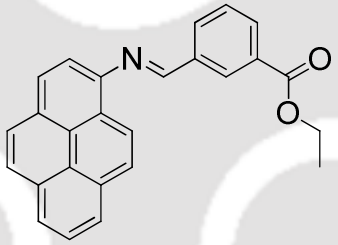

Figure 5.18: Schiff base (E)-ethyl 3-((pyren-1-ylimino)methyl)benzoate

Viewing this, we used Schiff base 2-(5-methylthiazol-2-yliminomethyl) phenol (**5.1)** for selective detection of Al^{3+} ions. Aluminium is a toxic element, [12–15] so selective detection of such element would be necessary.

5.9: Interaction of 5.1 with Al^{3+}

5.9.1: Fluorescence study

The synthesis and characterization of **5.1** is given in part A of this Chapter. Schiff base **5.1** (Scheme 5.1a) shows dual fluorescence emission peaks at 425 nm and 525nm; when excited at 365 nm. It is likely that the presence of intra or inter-molecular hydrogen bond (a and b in Figure 5.19) of **5.1** leads to dual fluorescence emission in methanol.[28] On interaction with Al^{3+}, Schiff base **5.1**, shows a new emission peak at 446 nm as shown in Figure 5.19.

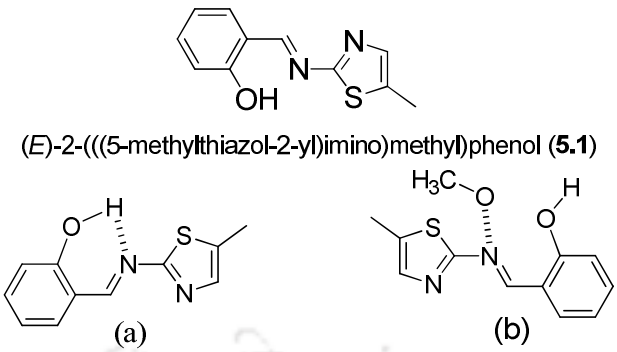

*Figure 5.19: (a) Intra and (b) inter-molecular hydrogen bond of Schiff base **5.1** in methanol.*

Schiff base **5.1** undergoes fast catalytic hydrolysis by Al^{3+} ions to form 2-hydroxybenzaldehyde and 2-amino-5-methylthiazole under neutral condition. Al^{3+} can hydrolyze **5.1** in the presence or absence of other metal ions. The hydrolytic cleavage of **5.1** can be monitored by fluorescence spectroscopy as shown in Figure 5.20a. The new emission peak at 446nm grows due to formation of 2-hydroxybenzaldehyde that interacts with Al^{3+} ions. Since, interaction of 2-hydroxybenzaldehyde with aluminium chloride results in emission at 446 nm, when excited at 365 nm as shown in Figure 5.20b.The intensity of the new emission peak at 446 nm enhances untill the hydrolysis of Schiff base **5.1** is completed. 1 µL of 10^{-2} M Al^{3+} ion solution can hydrolyze completely 2000 µL of 10^{-5} M solution of **5.1** in methanol**.**

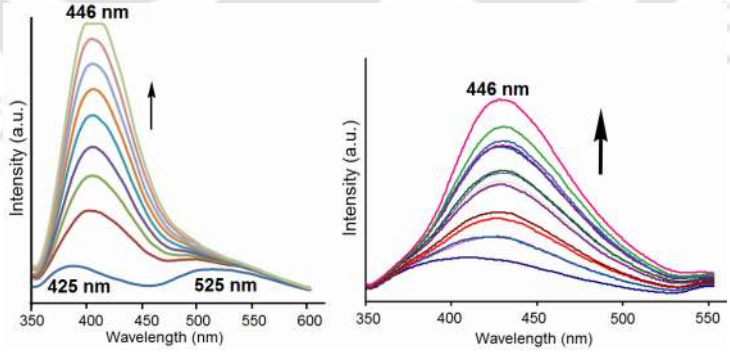

(a) (b)

*Figure 5.20: Increase in fluorescence intensity at 446nm (λ_{ex}=365nm) monitored at two minutes intervals of a solution of (a) **5.1** (10^{-5} M, 2mL) after addition of Al^{3+} (10^{-2}M, 1 µL) in methanol, (b) 2-hydroxybenzaldehyde (10^{-5} M, 2mL) on addition of Al^{3+} (10^{-2} M, 1 µL in each aliquots) in methanol.*

To check the effect of the thiazole part in such emission controlled experiments were performed. Al^{3+} ions along with 2-amino-5-methylthiazole (1:1 molar ratio) have emission at 386 nm, and on addition of 2-hydroxybenzaldehyde leads to emission at 446 nm at the cost of the former emission as shown in Figure 5.21. This shows that the other product formed from hydrolysis of Schiff base **5.1** does not interfere in the kinetic or binding of Al^{3+} ions.

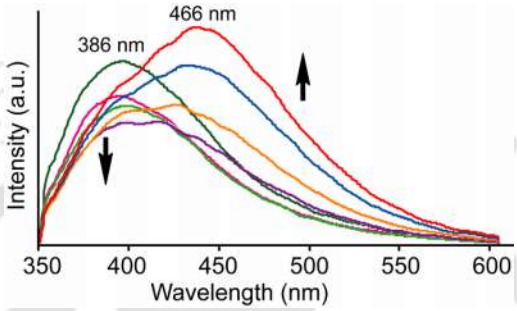

Figure 5.21: Changes in fluorescence of a solution of 2-amino-5-methylthiazole (10^{-5} M, 2 mL) with Al^{3+} (10^{-2} M, 1 μL in each aliquot) followed by addition of 2-hydroxybenzaldehyde (10^{-5} M, 1 μL in each aliquot) (The characteristic peak at 446 nm grows).

5.8.2: ^{1}H-NMR study

The reaction of **5.1** with Al^{3+} was monitored by ^{1}H-NMR by adding different proportions of Al^{3+} ions to solution of **5.1** as shown in Figure 5.22.

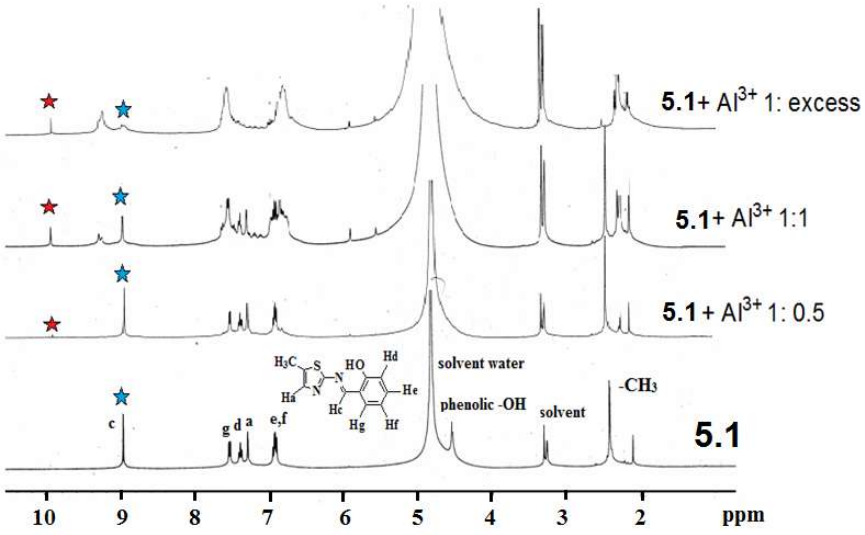

*Figure 5.22: ^{1}H-NMR spectra (400 MHz, CD_3OD) of 2-(5-methylthiazol-2-yliminomethyl)phenol (**5.1**) with different amounts of Al^{3+} ions.*

The characteristic imine proton (designated as c, marked as ★) appeared at ~8.98 ppm. By gradual addition of Al^{3+} (in form of $AlCl_3$), the imine peak slowly start disappearing. The aldehyde proton (-CHO, marked as ★) of 2- hydroxybenzaldehyde slowly start appearing at ~10.00 ppas shown in Figure 5.22. The aromatic region peaks gradually gets broadened.

5.10: Interaction of 5.1 with Zn^{2+}: Fluorescence study

Addition of Zn^{2+} ions to a solution of Schiff base **5.1** leads to a strong emission peak at 490 nm as shown in Figure 5.23a. This peak is attributed to 1:1 complex formation of Zn^{2+} with Schiff base **5.1**. The characteristic emission at 490 nm shown by Zn^{2+} with **5.1**, was not interfered by the other metal ions such as $Ni^{2+,}$ Cu^{2+}, Hg^{2+}, In^{3+}, Na^{+}, Li^{+} etc. However, Al^{3+} ion is an exception to this, upon addition of catalytic amount of Al^{3+} ions under neutral condition to a solution containing equimolar amount of **5.1** and Zn^{2+} ions, the fluorescence emission at 490 nm decreases and a new emission peak at 446 nm develops as shown in Figure 5.23b.The new emission peak at 446nm grows due to formation of 2-hydroxybenzaldehyde that interacts with Al^{3+} ions as well as Zn^{2+} ions. The intensity of the new emission peak at 446 nm enhances until the hydrolysis of the Schiff base **5.1** is completed.

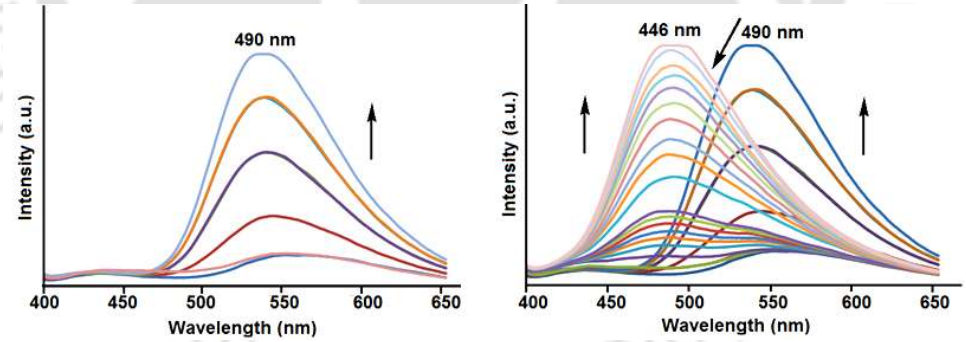

(a) (b)

Figure 5.23: Increase in fluorescence intensity of (a) ***5.1*** *(10^{-5} M, 2mL) on addition of Zn^{2+} (10^{-2}M, 1 μL aliquots) in methanol; (b) upon addition of Al^{3+} (10^{-2} M, 1 μL) to the Zn^{2+} containing solution (a).*

The distinct emissions from interaction with Zn^{2+} may be attributed to the species shown in Figure 5.24. Deprotonated binuclear Zn-complex (Figure 5.24) would take the emission to higher wavelength, due to extensive conjugation.

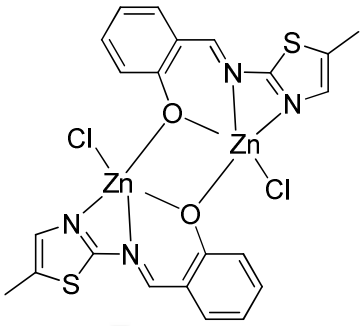

*Figure 5.24: Plausible 1:1 complexes of Zn^{2+} with **5.1** in solution*

The relative binding of Al^{3+} ion with 2- hydroxybenzaldehyde is 16 times higher than Zn^{2+} ion (Figure 5.25a and 5.25b). Thus, the relative binding constant of **5.1** with Zn^{2+} ion is 26.5 times higher than the binding constant of Zn^{2+} ion with 2-hydroxybenzaldehyde (Figure 5.25b and 5.25c). In other words, Al^{3+} catalyses the hydrolysis of the [Zn^{2+}-**5.1**] complex due to the higher affinity of Al^{3+} ions to bind to the 2-hydroxybenzaldehyde.

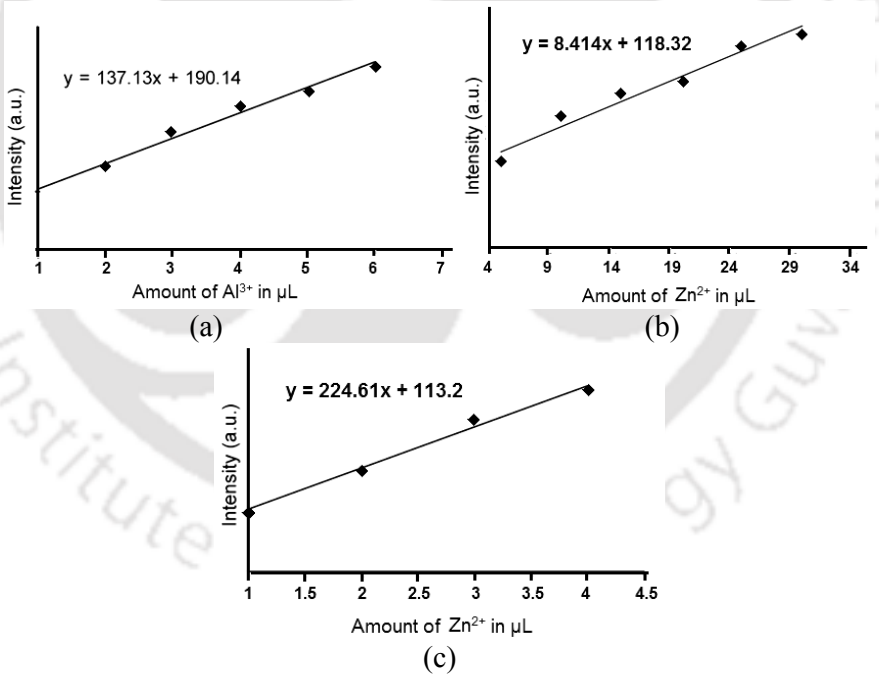

*Figure 5.25: Change of fluorescence intensity of a solution of 2-hydroxybenzaldehyde at 446 nm (2 mL, 10^{-5}M) on addition of (a) Al^{3+} (10^{-2}M, 1 µL in each aliquot) in methanol, (b) Zn^{2+} (10^{-2} M, 5 µL in each aliquot). (c) Change of fluorescence emission at 490 nm of a solution of the Schiff base **5.1** (2 mL, 10^{-5}M) after addition of Zn^{2+} (10^{-2}M, 1 µL in each aliquot) in methanol.*

The relative rate of hydrolysis of Schiff base **5.1** by Al^{3+} ions in the presence of Zn^{2+} ions is reduced by 1.5 times (from the relative change in fluorescence intensity with time, Figure 5.26) than in absence of Zn^{2+}.

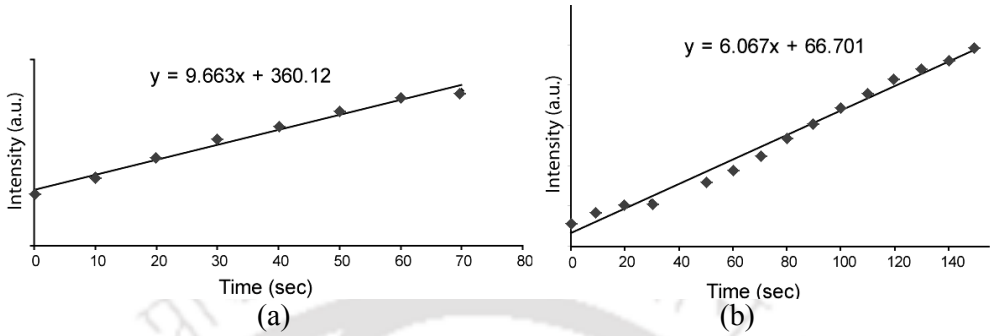

Figure 5.26: Change of fluorescence intensity of a solution of Schiff base ***5.1*** *(10^{-5}M, 2 mL) at 446 nm (10^{-5}M, 2 mL) on addition of (a) Al^{3+} (10^{-2} M, 1 µL) with respect to time. (b) Zn^{2+} (10^{-2}M, 4 µL in each aliquot) four times followed by addition of Al^{3+} (10^{-2}M, 1 µL)*

Analogously, the relative increments in emission intensities with time are obtained from independent titrations/kinetics, these suggest the rates of catalytic hydrolysis of **5.1** by Al^{3+} ions marginally reduce by the presence of ions such as Ni^{2+}, Co^{2+}, Hg^{2+}, Sn^{2+}, Na^{+}, Li^{+} and In^{3+} as shown in Figure 5.27.

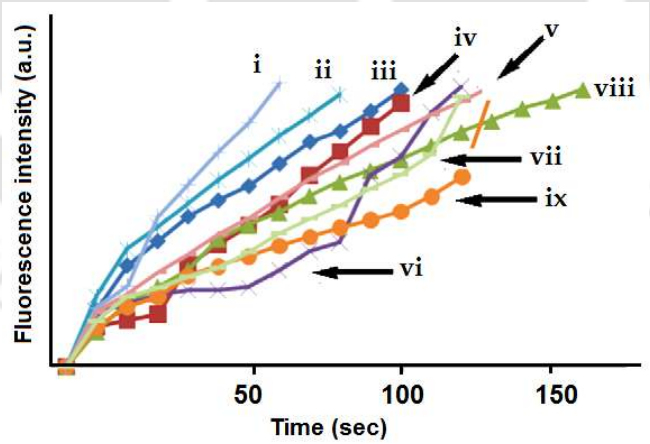

Figure 5.27: Change of fluorescence intensity of a solution of Schiff base ***5.1*** *(10^{-5} M, 2 mL) at 446 nm (λ_{ex} =365 nm) in methanol with (i) Co^{2+}, (ii) Ni^{2+}, (iii) Li^{+}, (iv) Na^{+}, (v) Hg^{2+}, (vi) Cu^{2+}, (vii) In^{3+}, (viii) Mn^{2+}, (ix) Ca^{2+} ions (in each case 10^{-2} M, 10 µL) on addition of Al^{3+} ions (10^{-2}M, 1 µL).*

5.11: Conclusion

Here, we have showed the importance of Schiff base **5.1,** as useful substrate to detect toxic Al^{3+} ions in the presence of various metal ions. Further, Schiff base **5.1** can be applied to detect Zn^{2+} ions in the absence of Al^{3+} ions.

5.12: References

1. J.M. Cano-pavon, M.L. Trujillo, A.G. de Torres, *Anal. Chim. Act*a, 1980, **117**, 319.
2. C. Jiang, B. Tang, R. Wang, J. Yen, *Talanta*, 1997, **44**, 197.
3. D. Karak, S. Lohar, A. Sahana, S. Guha, A. Banerjee, D. Das, *Anal.Methods*, 2012, **4** 1906.
4. M.P. Manuel-Vez, M. Garcia-Vargas, *Talanta*, 1994, **41**,1553.
5. M.S.J. Briggs, J.S. Fossey, C.J. Richards, B. Scott, J. Whately, *Tetrahedron Lett.*, 2002, **43**, 5169.
6. L.Wang, W. Qin, X. Tang, W. Dou, W. Liu, Q. Teng, X. Yao, *Org. Biomol. Chem.*, 2010, **8**, 3751.
7. C. Gou, S.-H. Qin, H.-Q. Wu, Y.Wang, J. Luo, X.-Y. Liu, *Inorg. Chem. Commun.*, 2011, **14**, 1622.
8. X.-H. Jiang, B.-D. Wang, Z.-Y. Yang, Y.-C. Liu, T.-R. Li, Z.-C. Liu, *Inorg. Chem. Commun.*, 2011, **14**, 1224.
9. D. Maity, T. Govindaraju, *Eur. J. Inorg. Chem.*, 2011 5479.
10. S. Samanta, B. Nath, J.B. Baruah, *Inorg. Chem. Commun*., 2012, **22**, 98.
11. M. Salavati-Niasari, M. Bazarganipour, *Appl. Surf. Sci.*, 2009, **255**, 7610.
12. M. Salavati-Niasari, M. Bazarganipour, *J. Mol. Catal. A Chem.*, 2007, **278**, 173.
13. M. Salavati-Niasari, M. Bazarganipour, *Inorg. Chem. Commun.*, 2006, **9**, 332.
14. M. Salavati-Niasari, M. Bazarganipour, *Appl. Surf. Sci.*, 2008, **255**, 2963.
15. R. H. Kayser, R. M. Pollack, *J. Am. Chem. Soc.*, 1977, **99**, 3379.
16. T. Okuyama, H. Shibuya and T. Fueno, *J. Am. Chem. Soc.,* 1982, **104**, 730.
17. R. M. Pollack, R. H. Kayser, J. R. Damewood, *J. Am. Chem. Soc*., 1977, **99**, 8232.

18. T. Okuyama, H. Nagamatsu, M. Kitano and T. Fueno, *J. Org. Chem*., 1986, **51**, 1516.
19. P. N. Basa and A. G. Sykes, *J. Org. Chem.,* 2012, **77**, 8428.
20. M. H. Lee, T. V. Giap, S. H. Kim, Y. H. Lee, C. Kang and J. S. Kim, *Chem. Commun*., 2010, **46**, 1407.
21. H. S. Jung, J. H. Han, Z. H. Kim, C. Kang, J. S. Kim, *Org. Lett.,* 2011, **13**, 5056.
22. J.D. Birchall, *Aluminum in Chemistry Biology and Medicine*, Wiley, New York, 1992.
23. N. Singla, D.K. Dhawan, *J. Neurosci. Res*., 2012, **90**, 698.
24. M.H. VanBenthem, G.D. Gillispie, *J. Phys.Chem*., 1984, **88,** 2954.

Chapter 6 (Part A)

Anion guided conformational adjustments by protonation leading to conformation reversal

Challenges in small molecule self-assemblies are to understand the reasons of selectively in adopting a particular conformation in crystal lattice. Molecular conformation is subtle but important properties of organic solids.[1] Material properties are controlled by conformations,[2] for which self assemblies of small molecules requires understanding. Ordered structures require the knowledge of inherent driving forces that arises from hydrogen bond,[3,4] van der Waals force,[5] dipole-dipole interaction[6] etc.

Conformers of thiazole-2-carboxylic acid (TCA)[7] were studied by Fausto et al. using the matrix-isolation method, combined with photoinduced conformational transformations as shown in Figure 6.1. Majority of TCA molecules, adopted *trans*-form, due to the intramolecular O-H**…**N hydrogen bond.

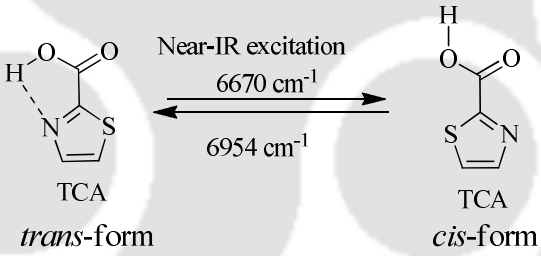

Figure 6.1: Conformational transformations in thiazole-2-carboxylic Acid (TCA).

Such results suggest that conformational adjustments by factors like anions and solvents need a systematic understanding. Self assemblies of derivative of amino thiazole **6.1** are chosen for study, in anticipation of observing conformation adjustments under different conditions. Moreover, aminothiazole unit is an important component of many medicinal compounds,[8-11] hence their supramolecular aspects draw general attention. In this Chapter, a situation is visualized, where orientation of a thiazole ring occur in absence of intramolecular hydrogen bond, but would be guided by intermolecular hydrogen bonds. To fulfill such purpose, amine derivative (**6.1**) (Figure 6.2) of the imine 2-(E)-(5-methylthiazol-2-ylimino)methyl)phenol (**5.1**)

[Chapter 5 (Part A)] was synthesized. Compound **6.1** would have several options to form self-assemblies illustrated as (a-f) of Figure 6.2.

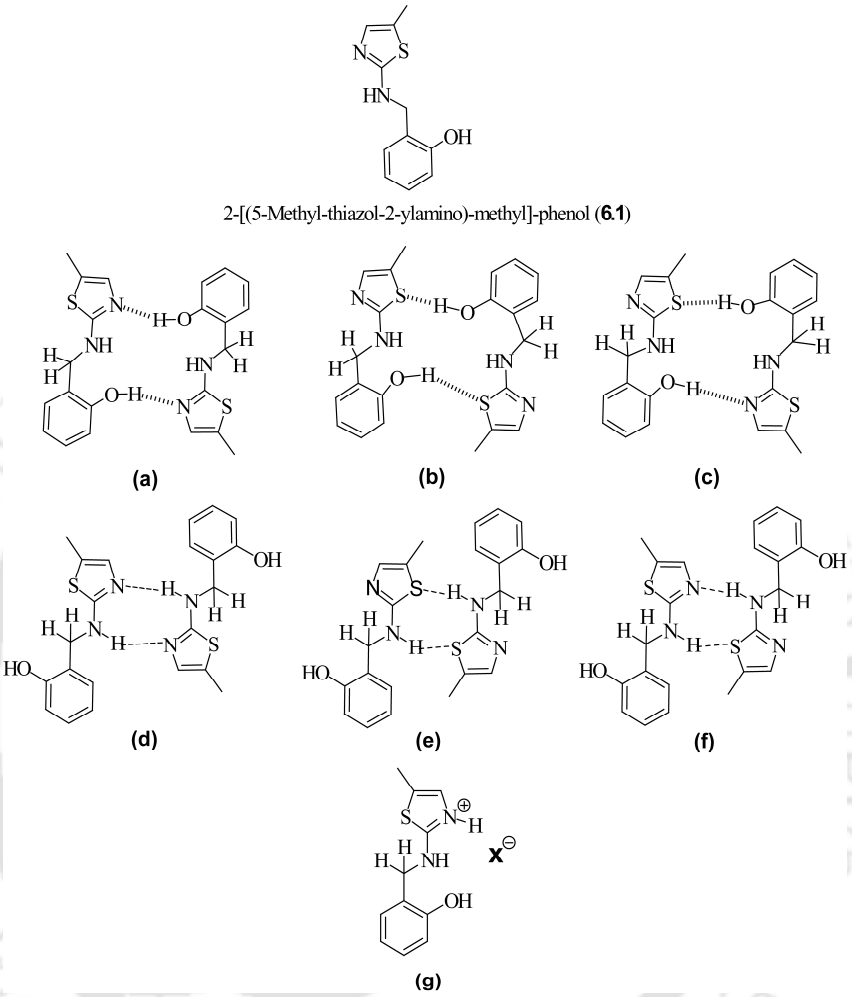

*Figure 6.2: (a-f) are some dimeric assemblies of compound **6.1**; (g) representative salt structure of compound **6.1**.*

Syn or *anti* conformations A and B of thiazole derivatives illustrated in Figure 6.3, would generate polymorphs. Further, to these Protonation of **6.1** (Figure 6.2g), would result in salts where conformational adjustment as per anion may be possible.[12-17] *Syn* or *anti* conformations of protonated thiazole derivative C and D as shown in Figure 6.3. With these logics in mind we have synthesized various salt structures of **6.1**, and investigated their assemblies.

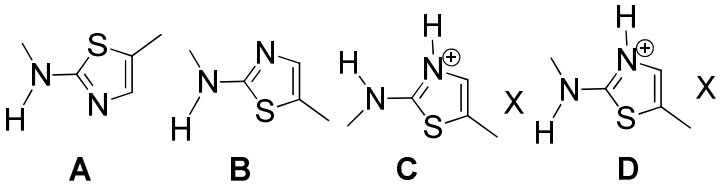

Figure 6.3: Syn and anti conformation of aminothiazole (A and B) and aminothiazolium salt (C and D).

6.1: Synthesis of aminothiazole derivative 6.1

The compound **6.1** was prepared by reducing (C=N) of the imine 2-(E)-[(5-methylthiazol-2-ylimino)methyl]phenol (**5.1**). The compound was characterized by various spectroscopic techniques, such as IR spectroscopy, ^{1}H-NMR and mass spectrometry.

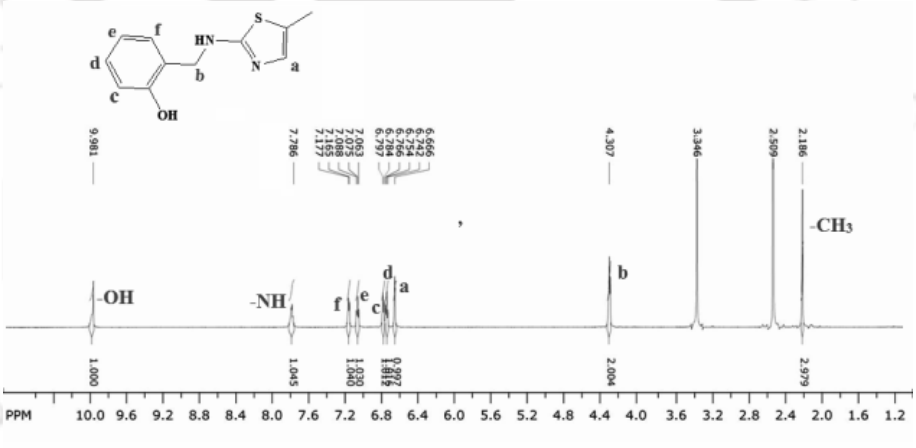

*Figure 6.4: ^{1}H-NMR spectra (600 MHz, DMSO-d_6) of compound **6.1**.*

^{1}H-NMR spectra the methylene protons (designated as -b) appear at 4.3 ppm (Figure 6.4). The mass spectrum of **6.1** shows a peak at 221.1015 (Calculated 221.0749), corresponding to [M+1] peak.

6.1.1: Supramolecular assembly of 6.1

Compound **6.1** crystallizes in monoclinic $P2_1/c$ space group, having one molecule of **6.1** in its asymmetric unit. Structural elucidation showed that **6.1** possess an overall twisted geometry in which the aminothiazole ring has NH and the sulphur atom of the ring *syn* to each other (Figure 6.5a). This conformer is not generally observed in amino thiazole derivatives due to lesser stability of N-H**…**S bond.[18] Stabilization of the uncommon conformer can be explained by considering self-assembly of the

compound as illustrated in Figure 6.5b. N-H**…**O, O-H**…**N and C-H**…**π interactions guided the assembly of compound **6.1**. The assemblies has dimers of **6.1** arranged in head to tail manner (considering the thiazole containing end as head and phenol as tail) held together by O-H**…**N bonds.[19] On the other hand, intermolecular N2-H2N**…**O1 hydrogen bonds involving phenolic oxygen contribute to the assembly. Phenolic oxygen atom plays dual role, it acts as hydrogen bond donor as well as hydrogen bond acceptor (Table 6.1). Again, aliphatic hydrogen C1-H1A is engaged in C-H**…**π interactions (C1A**…***Cg1* = 3.549 Å) and thereby extending the three-dimensional structure of **6.1** (Figure 6.5b).

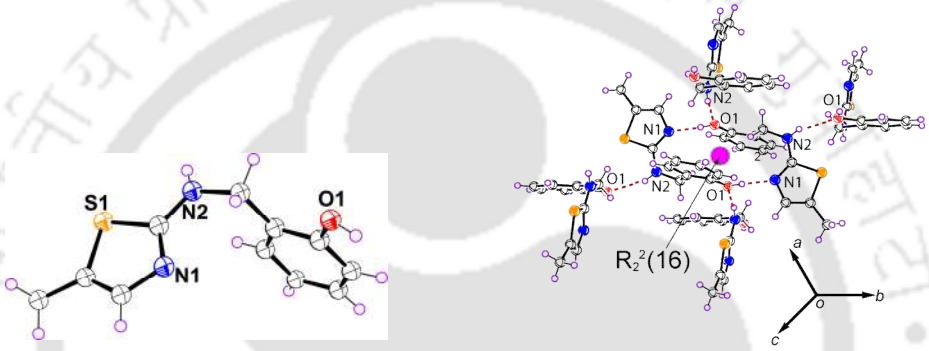

(a) (b)

*Figure 6.5: (a) Structure of the compound **6.1** (with 50% thermal ellipsoids) and (b) hydrogen bonded self-assembly of **6.1**.*

6.2: Anion guided assemblies of 6.1

Generally self-assembly of a salt is different from the parent compound. As the thiazole ring is prone towards protonation, we have synthesized chloride (**6.1a**), bromide (**6.1b**) and nitrate (**6.1c**) (Scheme 6.1) salt of **6.1**, in anticipation of phenol group controlling the packing pattern. Partly motivation of such an investigation to choose a phenol substituted aminothiazole derivative also retraces to their role as potential antiretroviral compounds.[20]

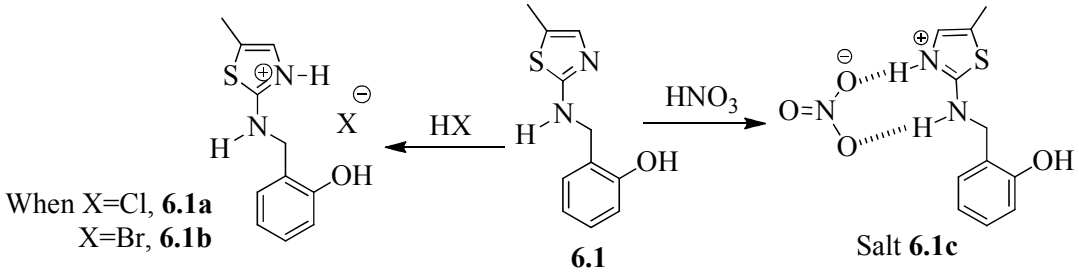

*Scheme 6.1: Synthesis of Salts of compound **6.1**.*

Chloride salts **6.1a** crystallizes in monoclinic space group $P2_1/c$. Asymmetric unit of **6.1a** contains a cationic host molecule with a chloride ion. The N-H, N^+-H and OH group of the cationic host **6.1** are involved in hydrogen bond with the chloride as shown in Figure 6.6b. C-H**…**π interactions in lattice of salt **6.1a** remains as that in the parent compound **6.1.** Thus, there is C-H···π interaction having donor acceptor distance 3.223 Å accompanied by weak C-H**…**O hydrogen bonds (C1**…**O1 = 3.584(1) Å, ∠C1-H1C**…**O1 = 164.22) in the lattice of **6.1a** connects two cations in head to tail manners as shown in Figure 6.6b. The cationic host of salt **6.1a** has similar orientation of the thiazole ring across C-NH bond to that parent compound; but to accommodate the respective anion in packing pattern definite conformational adjustment in each case has taken place. Each chloride ion is engaged with three cations through three strong hydrogen bonds. The assembly formation is explained on the basis of the Etter's rules[21] and the coordination ability of the halide ions. According to Etter's rules the hydrogen bonds with higher strength are formed first. Halide ions generally prefer to form hydrogen bonds to maintain a T-shaped geometrical environment,[22] which is affected by the high priority O-H**…**O and N-H**…**O bonds in these salts. There are two N-H**…**Cl with donor acceptor distances 3.150 Å and one O-H**…**Cl interaction with $d_{D...A}$ 3.098 Å. These provide the adequate environment so that the NH and S atoms are in *syn* orientation as shown in the Figure 6.6a.

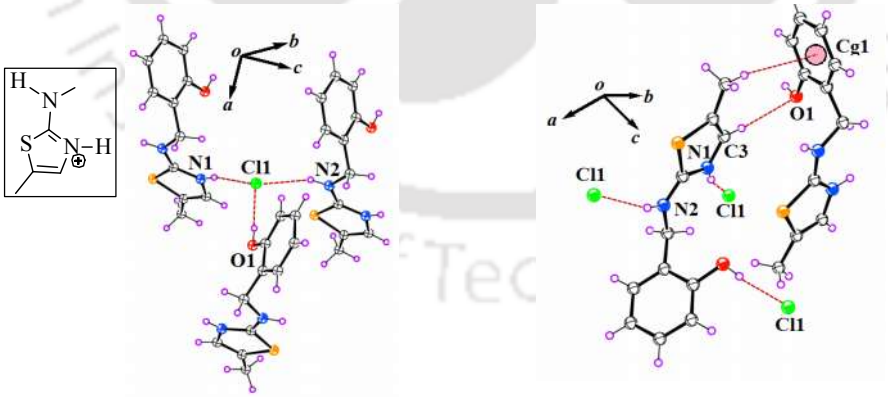

(a) (b)

Figure 6.6: (a) T-shaped hydrogen bond environment around a chloride ion in ***6.1a****, inset: anti-conformation of the thiazolic end, (iv) C-H**…**π interactions in solid state structure of* ***6.1a****.*

The bromide salt of **6.1b** is in a 1: 1 ratio of cation and anion; it crystallizes in the monoclinic space group $P2_1/c$ and the asymmetric unit contains one cationic host molecule and one bromide ion. The cations and anions are mainly held together by electrostatic interactions and hydrogen bonding. Chloride or bromide ion hydrogen bonds with three cations (two with -NH and one -OH group). The protonated host molecules arranged in head to tail manner as shown in Figure 6.7b through C-H**…**π interactions with the C1A**…**Cg1 distance 3.290 Å. Assembly of **6.1b** also follows Etter's rules.[21] The cationic host of salt **6.1b** also posses similar orientation of the thiazole ring across C-NH bond to that parent compound; that is NH and S atoms are in *syn* orientation (*anti*-conformation) as shown in the Figure 6.7b.

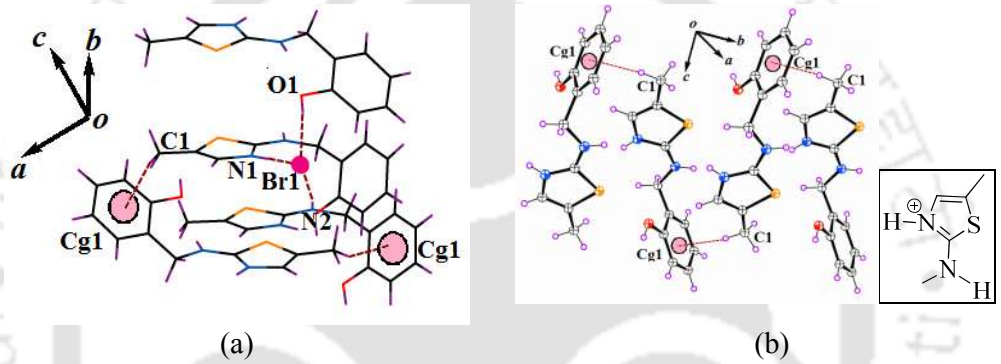

(a) (b)

Figure 6.7: (a) Various noncovalent interactions between cationic host and spherical bromide anion in salt ***6.1b****, (b) Showing C-H···π interactions arranging the cations in head to tail manner in the lattice of* ***6.1b****.*

Table 6.1: Hydrogen parameters for compound **6.1** and salts **6.1a-6.1c**

Compd.	Hydrogen bonds	d_{D-H}(Å)	$d_{H\cdots A}$(Å)	$d_{D\cdots A}$(Å)	∠D-H···A (°)
6.1	O(1)-H···N(1) [-x,1-y,-z]	0.84(2)	1.90(2)	2.740(2)	179(3)
	N(2)-H··· O(1) [-x,-1/2+y,1/2-z]	0.81(2)	2.21(2)	2.974(2)	156.3(19)
	C(11)-H···N(2)	0.93(19)	2.55(19)	2.907(3)	102.9(13)
6.1a	N(1)-H···Cl(1)	0.87(2)	2.27(2)	3.1188(17)	164.2(19)
	O(1)-H···Cl(1) [x, 3/2-y,-1/2+z]	0.82(2)	2.28(2)	3.0975(15)	176(3)
	N(2)-H···Cl(1) [x,-1+y,z]	0.86(3)	2.37(3)	3.1831(15)	159(5)
	C(5)-H···N(1)	0.97(4)	2.60(2)	2.950(3)	102(4)
6.1b	N(1)-H···Br(1)	0.86(2)	2.43(2)	3.256(10)	159.94(2)
	O(1)-H···Br(1)	0.82(4)	2.43(3)	3.241(8)	171.38(3)
	N(2)-H···Br(1)	0.86(2)	2.49(2)	3.307(11)	159.41(2)
6.1c	N(1)-H···O(3) [-x,-y,1-z]	0.84(2)	1.97(2)	2.796(4)	173(4)
	O(1) -H···O(2) [1/2+x,1/2-y,-1/2+z]	0.89(5)	2.40(4)	3.045(4)	130(4)
	O(1) -H···O(4) [1/2+x,1/2-y,-1/2+z]	0.89(5)	2.06(5)	2.942(4)	174(4)
	N(2)-H···O(2) [-x,-y,1-z]	0.84(18)	2.10(19)	2.908(4)	162(4)
	C(3)-H···O(3) [-1+x,y,z]	1.01(4)	2.38(3)	3.275(5)	148(3)
	C(3)-H···O(4) [-1+x,y,z]	1.01(4)	2.46(4)	3.421(5)	158(2)
	C(8)-H ···O(4) [1/2+x,1/2-y,-1/2+z]	0.97(4)	2.45(3)	3.215(5)	135(3)
	C(11)-H···N(2)	0.99(4)	2.57(3)	2.910(6)	100(2)
	C(11)-H···O(2) [-x,-y,1-z]	0.99(4)	2.37(4)	3.337(6)	166(3)

The nitrate salt **6.1c** is a 1:1 electrolyte and crystallizes in a monoclinic space group $P2_1/n$. The crystallographic asymmetric unit of **6.1c** contains one host cation and a nitrate anion. Nitrate ion being planar, three oxygen atoms of each nitrate is associated with three neighbor cations of **6.1** as illustrated in Figure 6.7b. The N^+-H and N-H bonds and phenolic O-H of cationic part act as hydrogen bond donor to nitrate anion (Figure 6.8a). Nitrate ions form dimeric assembly or get sandwiched between cationic hosts,[23,24] Nitrates also forms lamellar structure with cation such as in guanidinum nitrate.[25] In the present salt the cyclic hydrogen bonded $R^2_2(8)$ type sub-assemblies formed between the cation and anion disturb dimer formation. The phenolic -OH group of cation participates in hydrogen bond formation on the other face of the nitrate ion, hence the nitrate ions remain segregated in the self-assembly within the hydrogen bond environment created by the cations. Accordingly, nitrate ions contribute to form layers comprising of cations and anions. While forming such a layer the cations adopt a planar structure which is reflected in the N1-C4-N2-C5 dihedral angle shown in Table 6.2. Importantly, the nitrate salt has the opposite conformer of the thiazole across the C-NH bond as that of the one found in the parent compound. The crystal packing of **6.1c** shows nitrate ions arranges as dimeric unit along the *b*-crystallographic axis is shown in Figure 6.8b.

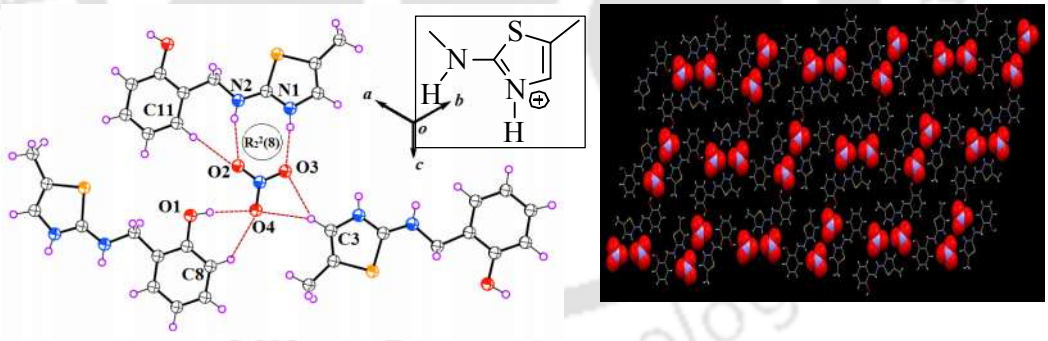

(a) (b)

*Figure 6.8: (a) Coordination mode of NO_3^- anion in the salt **6.1c**,inset: syn conformation of the thiazole end, (b) One dimensional sheet like structure of nitrate ion with cationic host along b-crystallographic axis.*

Different anion distorts the conformation of compound **6.1** to different extent by forming salt. The change in conformation in the cationic part of the salt is reflected in their respective torsion angles as shown in Table 6.2. The cation of chloride (**6.1a**) and bromide salt (**6.1b)** has less difference in torsion angle than the nitrate salt (**6.1c**),

with respect to the parent compound **6.1**. An overlaid diagram is drawn by placing respective cations of salts with parent **6.1** as shown in Figure **6.9**. The conformational adjustment taken place in various cation of the salt guided by anions, corresponding to parent **6.1** is illustrated in Figure 6.9.

Table 6.2: The dihedral angles in the compound **6.1** and the salts

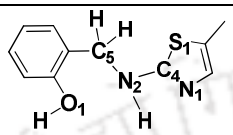	τ_1=N1-C4-N2-C5 (°)	τ_2=S1-C4-N2-C5 (°)
6.1	-0.09	178.44
6.1a	1.72	177.39
6.1b	-1.17	178.60
6.1c	175.44	-4.70

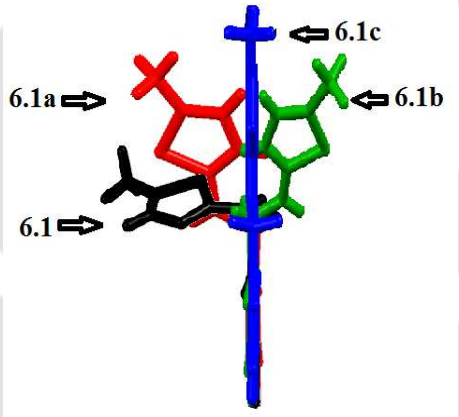

*Figure 6.9: Overlaid diagram of **6.1** with cationic hosts of **6.1a**, **6.1b** and **6.1c** drawn by fixing hydroxyphenyl unit in one plane.*

6.3: Conclusion

Compound **6.1** posses the uncommon form of conformation in solid state under ambient condition due formation of dimeric sub-assemblies. Conformational adjustments in the various salts take place, due to the directional properties of hydrogen bonds involving phenolic OH group to form respective favorable packing pattern. Cations in chloride and bromide salt adopt *anti*- conformation. But, nitrate salt has *syn*- conformation. In a nutshell, conformation reversal by forming salt is shown. Large number of systems that can be imagined which provides basis for understanding conformational adjustments.

6.4: Experimental Section

Synthesis of 2-[(5-Methylthiazol-2-ylamino)-methyl]-phenol (**6.1**): 2-(E)-[(5-methylthiazol-2-ylimino)methyl] phenol (**5.1**) (1.09 g. 5 mmol) was dissolved in dry methanol (30 ml) was placed over an ice bath. To this solution sodium borohydride (37 mg, 10 mmol) was added in small quantities, stirred for 2 hrs. Resulting solution was evaporated, and precipitate was extracted with ethyl acetate and product was purified by column chromatography. Yield, 90 %. Melting point 132 °C. ^{1}H-NMR (600 MHz, DMSO-d_6): 9.98 (s, 1H), 7.79 (s, 1H), 7.16 (d, 7.2 Hz, 1H), 7.07 (t, 7.8 Hz, 1H), 6.79 (d, 7.8 Hz, 1H), 6.75 (d, 7.2 Hz, 1H), 6.66 (s, 1H), 4.30 (s, 2H), 2.18 (s, 3H). ^{13}C-NMR (DMSOd_6, 150 MHz): δ 168.0, 155.2, 134.8, 129.1, 128.1, 125.5, 119.4, 118.9, 115.7, 42.8, 11.6. HRMS: Calcd. for $C_{11}H_{13}N_2OS$ [M + 1], 221.0749; found 221.1015. IR (KBr, cm^{-1}): 3369 (s), 3052 (w), 1596 (m), 1574 (s), 1497 (m), 1399 (s), 1354 (s), 1291 (s), 1243 (s), 1142 (s), 1102 (s), 1041 (w), 895 (s), 753 (s).

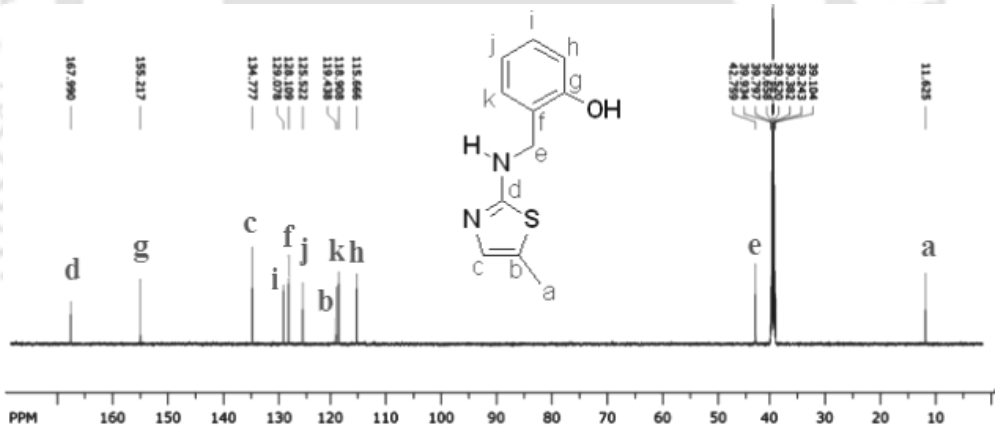

*Figure 6.10: ^{13}C-NMR spectra (150 MHz, DMSO-d_6) of compound **6.1**.*

The chloride (**6.1a**) bromide (**6.1b**) and nitrate (**6.1c**) salts were obtained by reacting compound **6.1** (25 mg) with corresponding acid (in case of hydrochloric or hydrobromic acid 37 % in water, 0.4 ml; or conc.nitric acid, 0.5 ml) in methanol (5 ml) at room temperature. Filtrate from such reaction mixtures after 6-7 days yielded colorless crystals. Chloride salt (**6.1a)**: Yield, 85 %. 1H-NMR (DMSO-d_6, 600 MHz): 7.22 (d, 3.6Hz, 1H), 7.15 (t, 4.2 Hz, 1H), 7.08 (s, 1H), 6.86 (d, 2.4Hz, 1H), 6.79 (t, 6.6Hz, 1H), 4.43 (s, 2H), 2.22 (s, 3H). HRMS Calcd. for C11H13N2OS [M^+], 221.0749; found, 221.0762. IR (KBr, cm^{-1}): 3480 (w), 3180 (w), 1590 (m), 1580 (s),

1530 (s), 1500 (s), 1380 (m), 1300 (m), 1260 (m), 1200 (s), 1130 (m), 1000 (m), 734 (s), 687 (s), 668 (s).

Bromide salt (**6.1b):** Isolated yield, 82 %. 1H-NMR (DMSO-d6, 600 MHz): 7.18 (d, 7.8 Hz, 1H),7.17 (d, 1.2 H z 1H), 7.15 (s, 1H), 6.88 (d, 7.8 Hz, 1H), 6.81 (d, 7.22 Hz, 1H), 4.45 (s, 2H), 2.25 (s, 3H). ^{13}C-NMR (DMSO-d_6, 100 MHz): δ 167.6, 155.7, 129.6, 129.6, 122.7, 121.3, 120.1, 119.1, 115.3, 44.8, 11.8. HRMS Calcd. for C11H13N2OS [M^+], 221.0749; found, 221.0744. IR (KBr, cm^{-1}): 3453 (w), 3172 (m), 2922 (m), 2809 (w), 1608 (s), 1503 (m), 1461 (s), 1441 (s), 1351 (m), 1320 (m), 1262 (s), 1231 (s), 1182 (m), 1025 (s), 877 (m), 755 (s), 560 (m).

Nitrate salt **(6.1c):** Isolated yield: 85 %; 1H-NMR (DMSO-d_6, 600 MHz): 9.99 (s, 1H), 8.61 (s, 1H), 7.25 (d, 7.2 Hz, 1H), 7.17 (t, 7.8 Hz, 1H), 7.11 (s, 1H), 6.90 (d, 7.8 Hz, 1H), 6.79 (t, 7.2 Hz, 1H), 4.48 (s, 2H), 2.23 (s, 3H). ^{13}C-NMR (DMSO-d_6, 150 MHz): δ 167.6, 155.6, 129.5, 121.7, 119.9, 119.0, 115.3, 44.7, 34.2, 30.7, 11.8. HRMS Calcd. for C11H13N2OS [M^+], 221.0749; found, 221.0746. IR (KBr, cm^{-1}): 3381 (w), 1617 (s), 1503 (m), 1453 (w), 1345 (w), 1263 (m), 1144 (m), 1109 (m), 1087 (m), 758 (s), 626 (s).

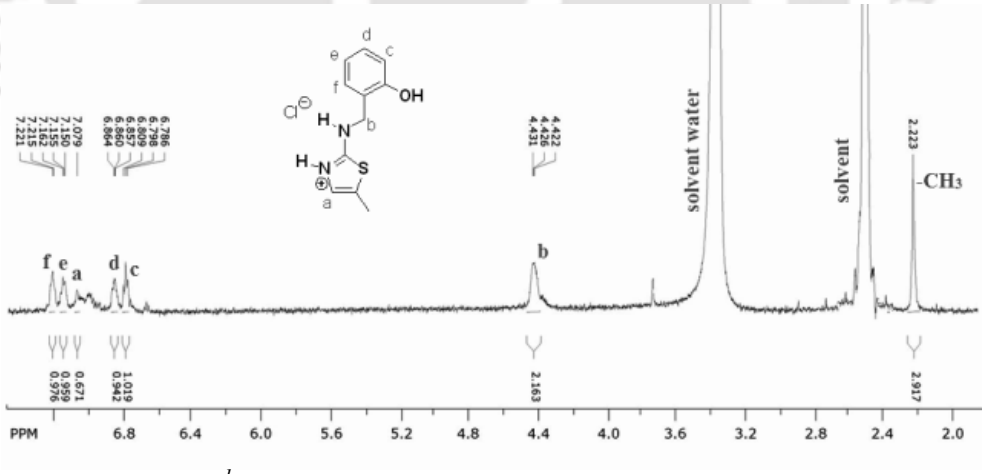

*Figure 6.11: ^{1}H-NMR spectra (600 MHz, DMSO-d_6) of compound **6.1a**.*

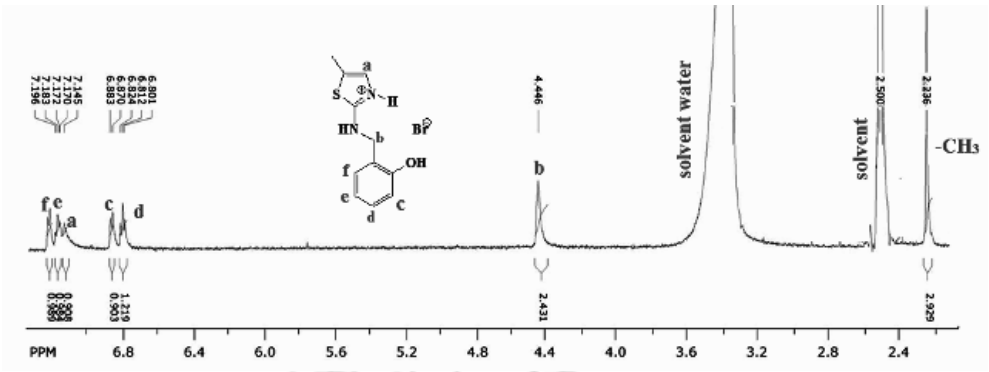

*Figure 6.12: ^{1}H-NMR spectra (600 MHz, DMSO-d_6) of compound **6.1b**.*

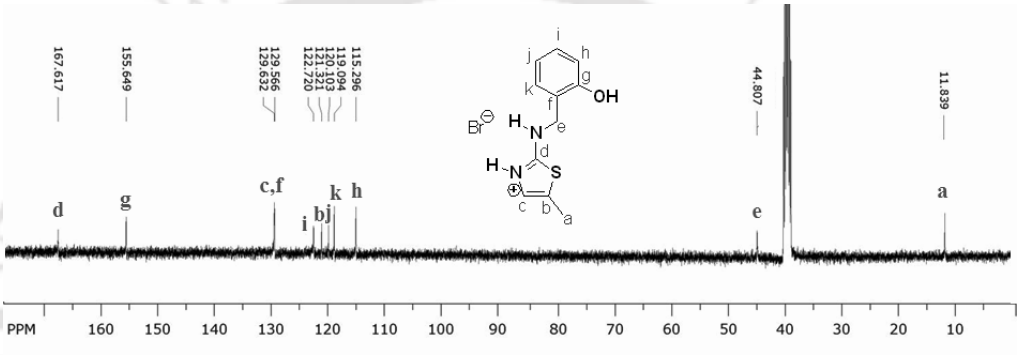

*Figure 6.13: ^{13}C-NMR spectra (100 MHz, DMSO-d_6) of compound **6.1b**.*

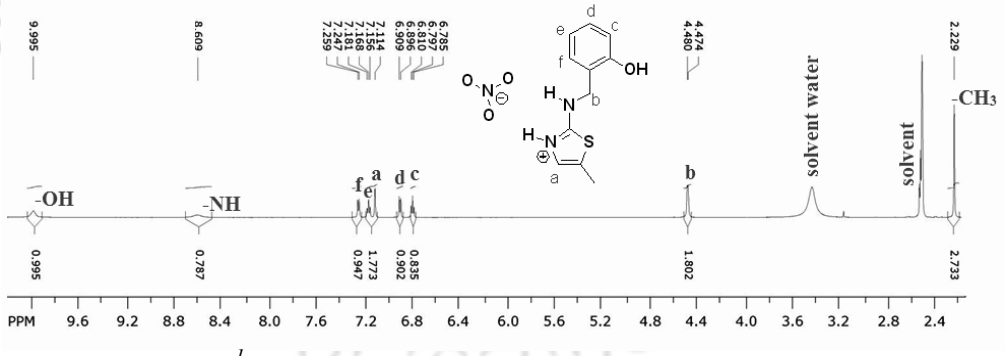

*Figure 6.14: ^{1}H-NMR spectra (600 MHz, DMSO-d_6) of compound **6.1c**.*

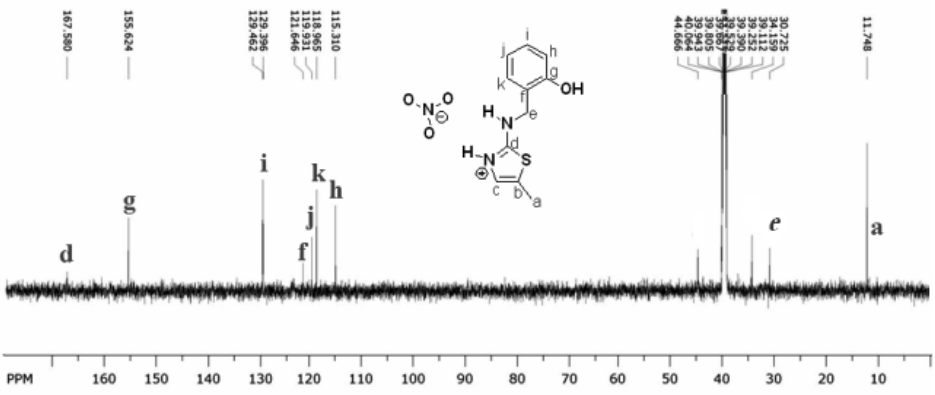

*Figure 6.15: ^{13}C-NMR spectra (150 MHz, DMSO-d_6) of compound **6.1c**.*

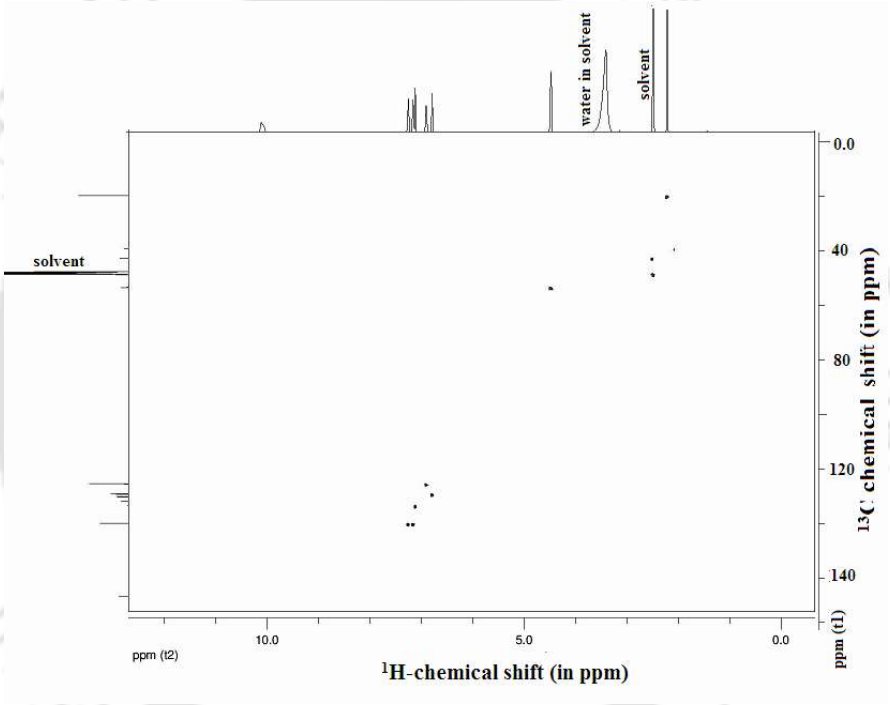

*Figure 6.16: ^{1}H-^{13}C HETCOR NMR spectra (150 MHz, DMSO-d_6) of the compound **6.1c**.*

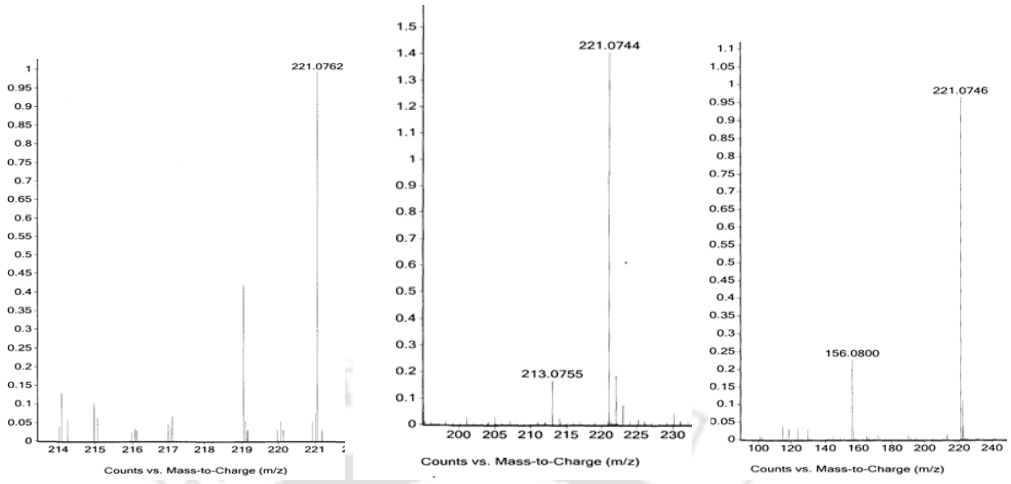

(a) (b) (c)

Figure 6.17: HRMS of the compounds (a) ***6.1a****, (b)* ***6.1b****, and (c)* ***6.1c*** *(all dissolved in methanol).*

6.5: References

1. Corradini, P.X-ray Studies of Conformation: Observation of Different Geometries of the Same Molecule. *Chem. Ind. (Milan)*, 1973, **55**, 122.
2. G. M. Whitesides, J. P. Mathias, C. T. Seto, *Science,* 1991, **254**, 1312.
3. J. A. Theobald, N. S. Oxtoby, M. A. Phillips, N. R. Champness and P. H. Beton, *Nature*, 2003, **424**, 1029.
4. M. Stohr, M. Wahl, C. H. Galka, T. Riehm, T. A. Jung, L. H. Gade, *Angew. Chem., Int. Ed*., 2005, **44**, 7394.
5. J. P. Rabe, S. Buchholz, *Science*, 1991, **253**, 424.
6. T. Yokoyama, S. Yokoyama, T. Kamikado, Y. Okuno and S. Mashiko, *Nature*, 2001, **413**, 619.
7. A. Halasa, I. Reva, L. Lapinski, M. J. Nowak, R. Fausto, *J. Phys. Chem. A*, 2016, **120**, 2078.
8. G. S. Paulekuhn, J. B. Dressman, C. Saal, *J. Med. Chem.*, 2007, **50**, 6665.
9. M. E. Webb, A. Marquet, R. R. Mendel, F. Rebeille, A. G. Smith, *Nat. Prod. Rep*., 2007, **24**, 988.
10. Y. Suzuki, M. Ojika, Y. Sakagami, R. Fudou, S. Yamanaka, *Tetrahedron*, 1998, **54**, 11399.

11. A. Kleemann, J. Engel, B. Kutscher, D. Reichert, Pharmaceutical Substances: Syntheses, patents, applications. 4th Eds. Georg Thieme Verlag, Stuttgart, 2000.
12. A. J. Cruz-Cabeza, J. Bersntein, *Chem. Rev.*, 2014, **114**, 2170.
13. M. C. T. Fyfe, P. T. Glink, S. M. J. F. Stoddart, A. J. P. White, D. J. Williams, *Angew. Chem. Int. Ed*., 1997, **36**, 2068.
14. P. D. Beer, P. A.Gale, *Angew. Chem., Int. Ed*., 2001, **40**, 486.
15. Z. P. Zhang, R. Schreiner, *Chem. Soc. Rev*., 2009, **38**, 1187.
16. Z. Y. Zhang, Z. P. Deng, L. H. Huo, H. Zhao, S. Gao, *CrystEngComm*, 2013, **15**, 5261.
17. X. -H. Ding, S. Wang, Y. -H. Li, W. Huang, *Inorg. Chem. Front.*, 2015, **2**, 263.
18. H. S. Biswal, S. Wategaonkar, *J. Phys. Chem. A*, 2009, **113**, 12763.
19. G. R. Desiraju, *Angew. Chem., Int. Ed.*, 1995, **34**, 2311.
20. M. Mori, A. Nucci, M. C. D. Lang, N. Humbert, C. Boudier, F. Debaene, S. Sanglier-Cianferani, M. Catala, P. Schult-Dietrich, U. Dietrich, C. Tisne, Y. Mely, M. Botta, *ACS Chem. Biol*. 2014, **9**, 1950.
21. M. C. Etter, *Acc. Chem. Res.*, 1990, **23**, 120.
22. C. Tamuly, R. J. Sarma, A. S. Batsanov, A. E. Goeta, J. B. Baruah, *Acta Crystallogr*., 2005, **C61**, o324 and references therein.
23. Y. V. Nelyubina, K. A. Lyssenko, D. G. Golovanov, M. Y. Antipin, *CrystEngComm*, 2007, **9**, 991.
24. S. Marivel, M. Arunachalam, P. Ghosh, *Cryst. Growth Des.* 2011, **11**, 1642.
25. K. Bouchouit, N. Benali-Cherif, L. Benguedouar, L. Bendheif, H. Merazig, *Acta Crystallogr.*, 2002, **58E**, o1397.

Chapter 6 (Part B)

Solvent and anion facilitated conformational adjustments in benzylamine substituted thiazolamine

Conformation adjustment[1-5] by anions in amino thiazole derivative 6.1 was shown part A of this Chapter. Conformation adjustment may lead to conformational polymorphism.[1,6] There is a large interest on conformational polymorphs with molecules such as vitamin D_3. Vitamin D_3 is a steroid hormone and a typical example of chemically and physically unstable drug. The α and β conformer of vitamin D_3 is shown in Figure 6.18.[7] The β-form has more stability than α-form.

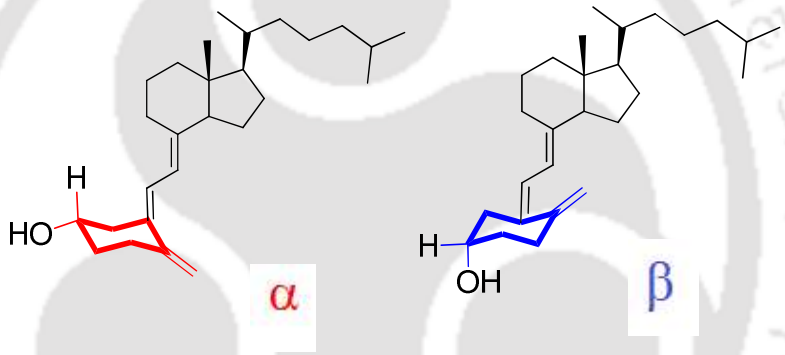

Figure 6.18: Chemical structure of two conformational conformers of vitamin D_3

We have been probing *syn* or *anti* forms A and B illustrated in Figure 6.3 (Part A) of thiazole derivatives **6.1**.[8] These derivatives are prone towards Protonation, hence the cationic forms also can have similar conformers (C and D in Figure 6.3) and one may utilize the hydrogen bonding ability of aminothiazole to stabilize any of such forms by hydrogen bonds. However, the *syn* and *anti* forms of a salt will differ in numbers of participating hydrogen bonds than the parent aminothiazole. Apart from conventional *syn* or *anti* form of a mono-substituted aminothiazole derivative, another model is visualized, where two $–CH_2-$ and two –NH groups can orient the methyl-thiazole rings across a rigid phenylene unit. To fulfill this purpose, we have synthesized N,N'-(1,4-phenylene-bis(methylene))-*bis*(5-methylthiazol-2-amine) (**6.2**). Here, we choose to study more complex situations of conformational adjustments than studied in Part A of this chapter.

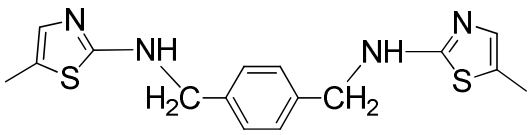

N,N'-(1,4-phenylene-bis(methylene))-bis(5-methylthiazol-2-amine)

6.2

Several structures illustrated in Figure 6.19 can be the basis for conformational adjustments. Conformational adjustments[1] can take place in any of these forms by rotations of C-N bonds connecting amine group to thiazole ring as well as amine to the methylene group to provide an overall spatial orientation.

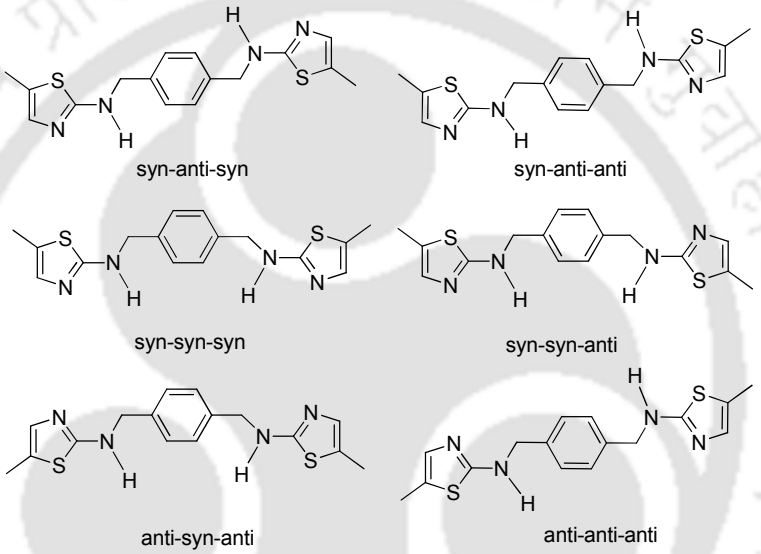

Figure 6.19: Several skeletons of N,N'-(1,4-phenylene-bis(methylene))-bis(5-methylthiazol-2-amine) ***6.2*** *for conformational adjustments.*

On the other hand, anions with different shape and hydrogen bond ability would influence conformation of the cationic part of a salt. Structural study on such salts would enable one to judge the hierarchical effect of hydrogen bond guided by electrostatic interactions[9] over the other non-covalent interactions of the parent compound.[10]

6.6: Synthesis of *bis*-aminothiazole derivative 6.2

The compound N,N'-(1,4-phenylene-*bis*(methylene))-*bis*(5-methylthiazol-2-amine) (**6.2**) was prepared by reacting 5-methylthiazol-2-yl-amine with terephthalaldehyde followed by reduction with sodium borohydride. The compound **6.2** was

characterized by various spectroscopic techniques, such as IR spectroscopy, ^{1}H-NMR and mass spectrometry.

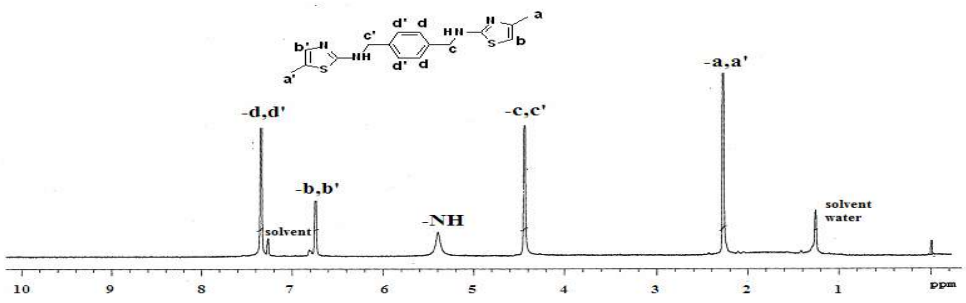

*Figure 6.21: ^{1}H-NMR ($CDCl_3$) spectrum of **6.2**.*

Both the sides across the phenylene unit are equvilent. So, the characteristics four benzylic protons (designated as-c,c′) appear at 4.43 ppm all together as shown in Figure 6.21. The mass spectrum of **6.1** shows a peak at 331.1072 (Calculated 331.1053), corresponding to [M+1] peak.

6.7: Polymorphs of compound 6.2

We have attempted crystallization of compound **6.2**, from series of solvent at ambient temperature. After crystallization from different solvents two forms were isolated, which are abbreviated as **6.2a** and **6.2b**. The crystallization results are summarized in Table 6.3.

Table 6.3: Crystallization of polymorphs of **6.2** from different solvents.

Solvents	6.2a	6.2b
MeCN	6.2a (needle)	--
MeOH	6.2a (needle)	--
DMF	6.2a (needle)	--
DMF:$CHCl_3$ (1:1)	6.2a (needle)	6.2b (block)
$CHCl_3$	--	6.2b (block)

The results from the Table 6.3 clearly suggests the specificity in obtaining crystals of the polymorphs **6.2a** or **6.2b** as one component from different solutions except in the case of solution in mixed solvent where we observed concomitant crystallization of both the forms. We evaluated their phase purity of the crystals in each case by analyzing the experimentally observed powder X-ray diffraction patterns of the bulk of the crystals. Comparison of the indexed powder XRD-patterns generated from the

CIF files have shown satisfactory resemblance to show that only crystals of a particular type of polymorphs were formed depending on the solvent of crystallization as shown in Figure 6.22.

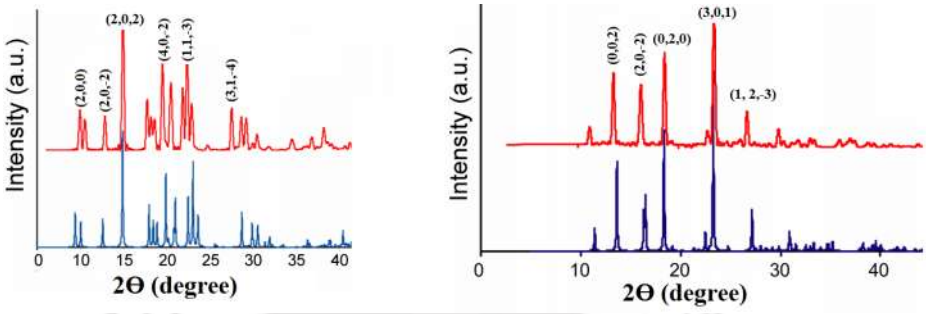

(a) (b)

Figure 6.22: PXRD patterns of (a) ***6.2a,*** *(b)* ***6.2b*** *(red = experimental, blue = generated from CIF).*

6.7.1: Supramolecular assembly of polymorphs of 6.2

From crystallographic point of view, common features of **6.2a** and **6.2b** is that both belongs to monoclinic space group *C2/c*, but have difference in cell parameters. The polymorph **6.2a** has lower crystal density lower than **6.2b**. The assembly of both the polymorphs are guided by $R_2^2(8)$ synthon with N-H**…**N type hydrogen bonds as shown in the Figure 6.23a and Figure 6.23b. However, polymorph **6.2b** has weak C-H**…**π interactions as depicted in Figure 6.23c. Overlaid diagram of the two structures (Figure 6.23d) drawn by fixing the phenylene planes of two polymorphs on top of each other showed their non-superimposablity and different projection of aminothiazole unit. Hence, there are two types of geometrical arrangements of the compound **6.1**, one resembling ***S***-geometry and another ***l***-geometry leading to polymorphs. Such orientations arise from the adjustments on rotations through two C-N bonds, one is C4-N2 bond and other is the C5-N2 bond as shown in Figure 2.23e. Among them, the C4-N2 bond is responsible to provide orientation of the thiazole ring, whereas the C5-N2 bond provided the overall orientations of the aminothiazole units across the phenylene units. The rotations of the two C-N bond contribute to the conformational adjustments of the molecule **6.2**. Conformational adjustment leads to difference in orientations of the molecules within their respective crystal lattices. This difference reflected in their packing patterns. ***S***-shaped molecules of polymorph **6.2a** arranged in a chain-like structure in an orderly manner along the *ab*-crystallographic

plane whereas ***l-***shaped molecules of polymorph **6.2b** do not have the phenylene rings lying in the plane, but apparently perpendicular with the thiazole rings (Figure 6.24ab).

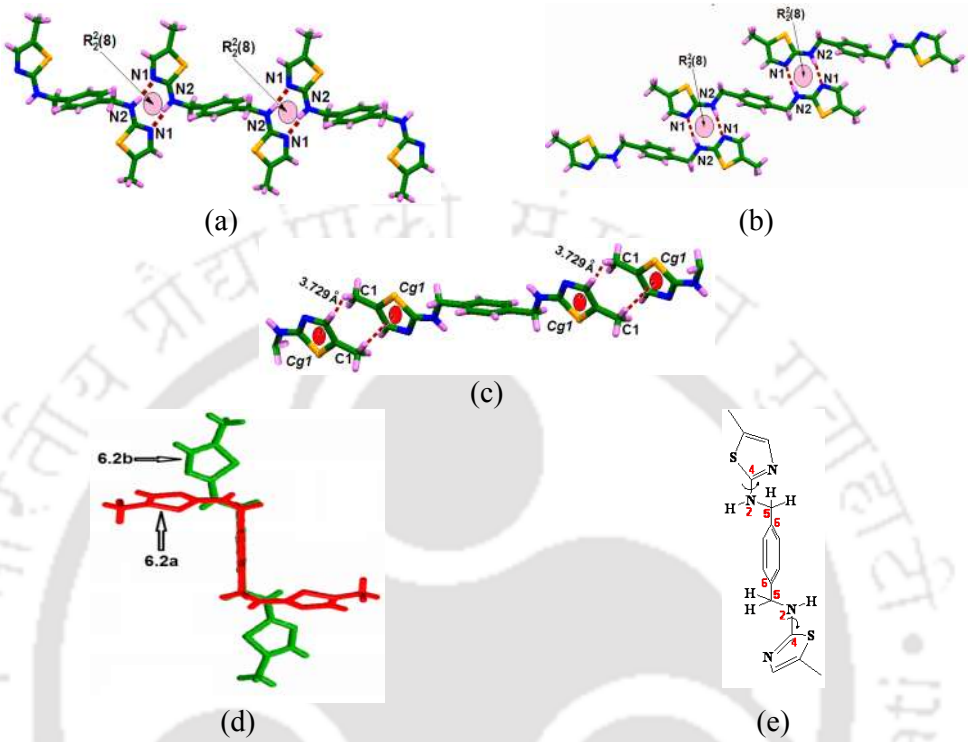

Figure 6.23: Assembly of (a) ***6.2a*** *and (b)* ***6.2b*** *showing intermolecular N-H···N interactions. (c) C-H…π ($d_{C1\text{-}H\ldots Cg1}$= 3.729 Å) within the packing pattern of* ***6.2b****. (d) Overlay diagram showing the* ***S-*** *and* ***l-*** *types of syn-anti-syn conformers of the 5-methyl aminothiazole unit in the two polymorphs of* ***6.2*** *(drawn by fixing the phenylene units in one plane). (e) Numbering of molecules to describe C-N bond rotations to change of orientation of the thiazole ring.*

Figure 6.24: Crystal packing pattern along the ab-crystallographic plane (a) polymorph ***6.2a*** *and (b) polymorph* ***6.2b****.*

Assemblies of ***S***-shaped molecules are interesting for helical constructions.[11] There are examples of molecules having two methylene groups held across a rigid unit, which show conformational adjustments[1]. For example, the molecule 6,6'-(1,4-phenylenebis(methylene))bis(1,3,4-trimethylpiperazine-2,5-dione crystallizes with a stable folded conformer (*C*-shaped) in which the two ends of the molecule interact through favorable intramolecular interactions (dispersion and electrostatics) and a metastable unfolded conformer (***S***-shaped) as shown in Figure 6.25 in which the increased distance precludes such interactions.[12]

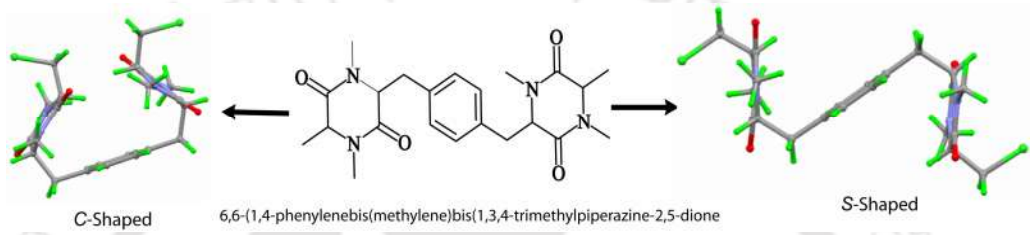

Figure 6.25: C- and S-shaped geometry of 6,6'-(1,4-phenylenebis(methylene))bis(1,3,4-trimethylpiperazine-2,5-dione).

6.7.2: DFT study of polymorphs of 6.2

A gas phase geometry optimization as well as energy calculated based on B3LYP/6-31++g (d,p) and B97-D/ccpVTZ level showed that **6.2b** has a lower energy than **6.2a**. The respective energy differences of the polymorphs at these levels of calculation are –7.119 and –1.204 kJ/mol. In this particular case, the gas phase energy optimizations of geometry and the calculation of optimized energy of the two forms correspond to two optimum energies calculated independently at B3LYP/6-31++g (d,p) and B97-D/ccpVTZ level. These calculations showed the differences in dihedral angles between the two forms are 90.41 and 99.81º. The experimentally observed difference between the two dihedral angles is 100.56º which is close to a stable conformer. As the geometries observed are very close to stable conformations, the two forms are conformational polymorphs.[1] The two polymorphs possess very low energy differences ~7 kJ/mol but **6.1a**, the lesser stable form is easily crystallizable from solutions in number of solvents. This suggests that the stability difference being very small they can adopt either of the forms based on the interactions with different solvents involving weak interactions which also falls in the range of the range of ~10-100 kJ/mol. The torsion angles as per numbering of atoms shown in the Figure 6.23e,

(Θ^1= C4-N2-C5-C6) obtained from the crystal data as well as gas-phase geometry optimizations at different levels of calculations are listed in Table 6.4.

Table 6.4: Torsion angle[#] (Θ^1= C4-N2-C5-C6) for polymorphs **6.2a** and **6.2b**.

	Polymorph **6.2a**	Polymorph **6.2b**
	Θ^1= C4-N2-C5-C6	Θ^1= C4-N2-C5-C6
X-ray crystal data	71.0°	171.6°
B3LYP/6-31++g (d,p)	82.4°	172.8°
B97-D/ccp-VTZ	76.9°	175.7°

= Numbering of atoms as in Figure 6.23e.

6.7.3: IR- study and Hersfield surface analysis of polymorphs of 6.2

The IR spectra of the polymorphs shown in Figures 6.26a and Figure 6.26b have distinguishable features. The polymorph **6.2a** has a sharp and broad N-H stretching 3440 cm^{-1} suggesting them to be hydrogen bonded, whereas the polymorph **6.2b** shows two N-H stretching at 3447 cm^{-1} 3220 cm^{-1}. This difference could be due to the differences in the packing of the two polymorphs, in former case the broad peak is unresolved due to more ordered distribution of molecules as linear chain-like arrangements, whereas in **6.2b** the assembly is two dimensional due to the presence of weak CH**…**π interactions between the molecules.

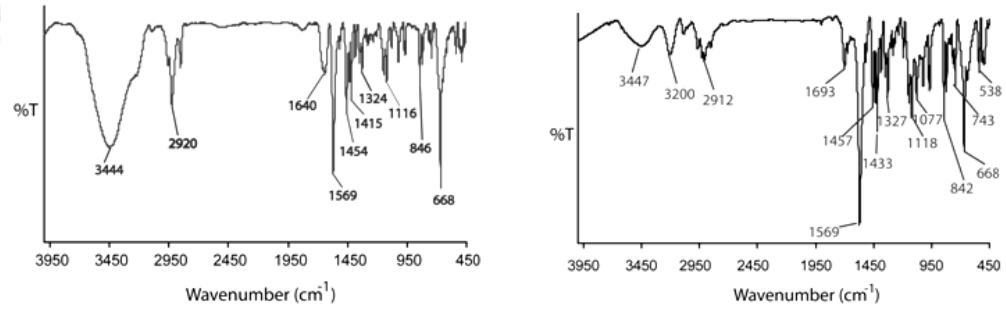

(a) (b)

Figure 6.26: IR (KBr) spectrum of (a) ***6.2a****, (b)* ***6.2b****.*

Differences in the extent of different weak interactions in the self-assemblies were determined by Hersfield surface analysis.[13,14] 2D-Fingerprint plots for polymorphs **6.2a** and **6.2b** as shown in the Figure 6.27. The C-H**…**π interactions in **6.2b** are seen as wings in 2D- fingerprint plot ($d_{C\text{-}H...\pi}$ = 3.729 Å). But the wings are not prominent for the polymorph **6.2b** molecule because the interaction is long and weak. The absence of C-H**…**π interactions in the polymorph **6.2a** means that the wings are

absent in its fingerprint 2D plot (Figure 6.27a). Thus the polymorphism in this compound may be attributed to have a significant contribution from C-H**…**π interactions. The C-H**…**π interactions guide many self-assemblies and influence their physical properties.[15,16] The weak interactions other than the C-H**…**π interactions are comparable in the two polymorphs of **6.1**. The C-H**…**π interactions are relatively weak hence the interplay of all the weak interactions decided the packing pattern to guide the directional organization of the thiazole rings. The relative percentages of the different interactions present in the packing of two polymorphs are shown in bar graph (Figure 6.28). This graph is the collective representation of finger-print plots of each interaction. This comparative bar-diagram suggests that the attractive interactions such C**…**H, N**…**H and S**…**H interactions are slightly higher in the polymorph **6.2a**, whereas H**…**H interactions are slightly higher in polymorph **6.2a**, the role of S**…**S interactions in both the cases are negligible.

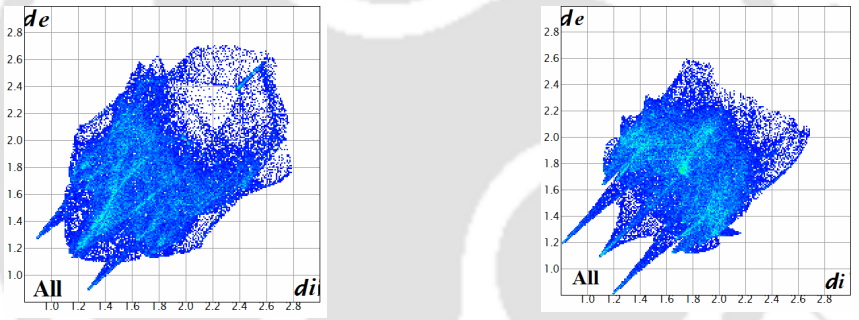

(a) (b)

*Figure 6.27: 2D fingerprint plots of (a) polymorph **6.2a,** (b) polymorph **6.2b**.*

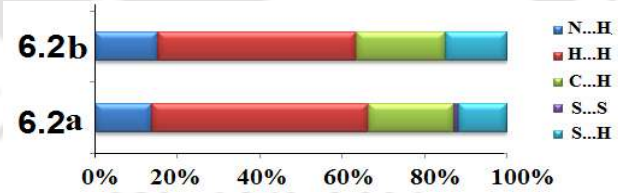

*Figure 6.28: Relative contribution of different interactions to the Hirshfeld surface in **6.2a** and **6.2b**.*

6.7.4: Differential scanning calorimetry study

Thermal properties of the two polymorphs are distinguishable, differential scanning calorimetry showed that polymorph **6.2a** melts at 198.55°C, whereas **6.2b** at 194.55°C (Figure 6.29ab). Melted samples of both the polymorphs on cooling, exhibit a sharp

recrystallization exothermic peak at 162.22 and 148.44°C, respectively. The powder XRD patterns of both the samples after recrystallization from the melt showed them to transform to respective parent form (Figure 6.29c, d). The recrystallization process is cyclic and can be repeated upon both the polymorphs.

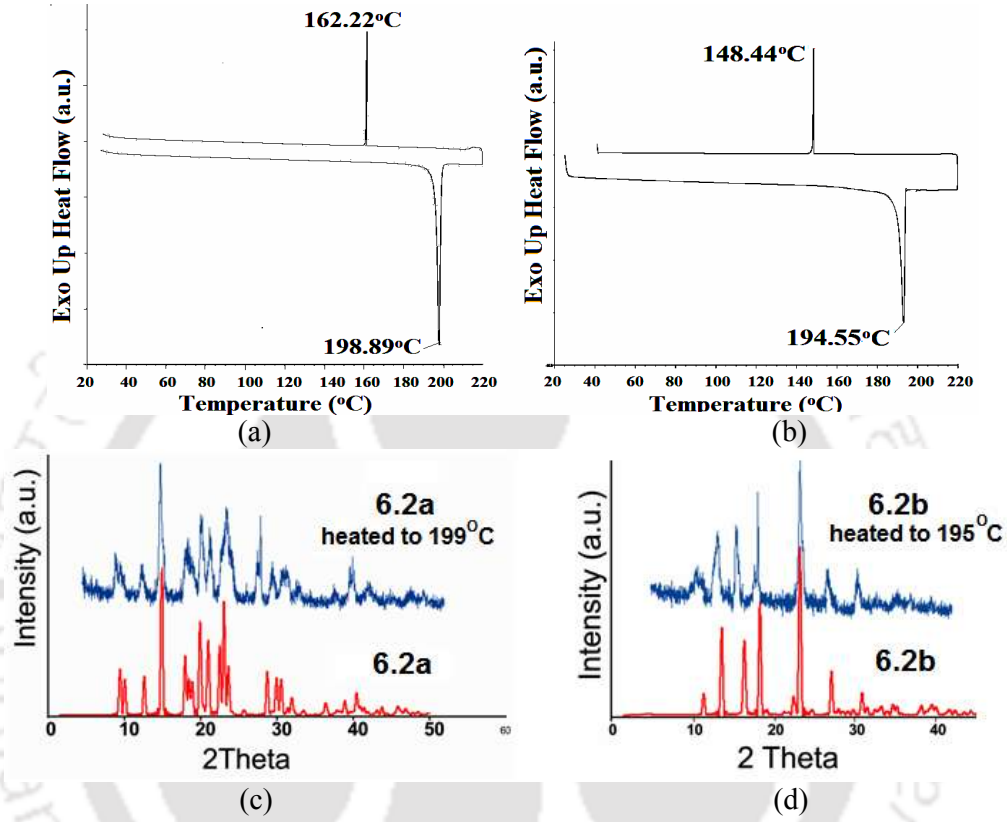

Figure 6.29: Differential scanning calorimetry plots of (cyclic heating and cooling) polymorph (a) ***6.2a*** *and (b)* ***6.2b*** *(heating rate of 5 °C/min and cooling rate of 1 °C/min). Powder XRD patterns of (c)* ***6.2a*** *and (d)* ***6.2b*** *at different temperatures.*

6.8: Anion guided assemblies and conformational adjustment of 6.2

The lone pair of electrons present on the nitrogen atom of the amine -NH is resonance delocalized in the N,N'-(1,4-phenylene*bis*(methylene))-*bis*(5-methylthiazol-2-amine) **6.2**, thus this nitrogen atom is less basic, facilitates the nitrogen on the sp^2 nitrogen of thiazole rings to be prone towards protonation. Hence, a set of salts with HBr, HNO_3, and H_3PO_4 were prepared by protonating the later site as shown in Scheme 6.2.

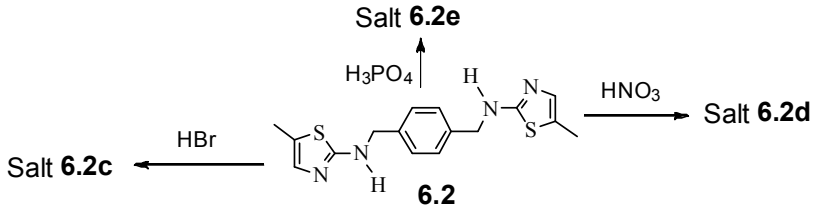

*Scheme 6.2: Synthesis of salts of **6.2**.*

Generally conformational flexible pre-organized cationic host molecules undergo reorganisation to provide a platform for anion, [17-19] Due to presence of intervening hydrophobic phenylene unit flanked by hydrophilic amionothiazole in **6.2**, the salts of **6.2** should be able to form robust hydrogen bonded synthons. Such robust synthons guided by strong hydrogen bonds will have extra stability than a self-assembly of neutral molecules. Generally robust synthons originating from weak hydrogen bonds between neutral molecules are less stable. As anticipated the three salts **6.1a-6.1c** have shown robust hydrogen bonded synthons and prominent cyclic synthons.

6.8.1: Bromide assisted assembly of 6.2

The crystalline salts **6.2c** have doubly protonated cationic form $[H_2(\mathbf{6.2})]^{2+}$ within its crystal lattice. Within the self-assembly **6.2c**, the spherical Br^- ions were hydrated by forming anionic hydrogen-bonded cluster $[Br_2(H_2O)_2]^{2-}$. These clusters have two water molecules proving four O-H bond as hydrogen bond donors to hydrogen bond with two bromide ions forming synthons with R_2^4 (8) graph-set notation.[20] These cyclic synthons held two ***S***-shaped of cations through N-H**…**Br and N^+-H**…**Br interactions to form $R_3^2(8)$ type hydrogen bonded synthons at each end of the $[H_2(\mathbf{6.2})]^{2+}$.

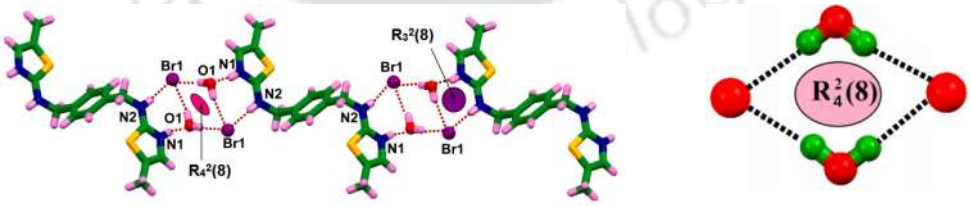

(a) (b)

*Figure 6.30: (a) 1D H-bonded chain pattern in salt **6.2c** showing various hydrogen bonding interactions to hold syn-anti-syn conformer (view along the c crystallographic axis). (b) Bromide-water tetrameric $[(H_2O)_2Br_2]^{2-}$ cluster in **6.2c**.*

Thus the cationic counterpart is assembled through the intervening bromide-water cluster as shown in Figure 6.30a. $[Br_2(H_2O)_2]^{2-}$ cluster has a rectangle-like geometry (Figure 6.30b). This result can be added to our earlier study on bromide salt of another thiazole derivative, where an octameric bromide-water $[Br_2(H_2O)_6]^{2-}$ cluster was found described in Chapter 2.

6.8.2: Nitrate assisted assembly of 6.2

Structural analysis of nitrate salt **6.2d** revealed that each NO_3^- ion interacts with two $[H_2(\mathbf{6.2})]^{2+}$ cations via strong N-H**…**O bonds, and with additional $[H_2(\mathbf{6.2})]^{2+}$ blocks via weak C-H**…**O bonds as shown in Figure 6.31a. One of the nitrate ion is anchored to a $N_{(amine)}$-H bond of $[H_2(\mathbf{6.2})]^{2+}$ through bifurcated hydrogen bond $R_1^2(5)$ synthon and another form a $R_2^2(7)$ synthons involving $C_{(thiazole)}$-H**…**$O_{(nitrate)}$ and $N^+_{(thiazole)}$-H**…**$O_{(nitrate)}$ bonds as shown in Figure 6.31b. Two oxygen atoms of such $R_2^2(7)$ synthons further involves in formation of C-H**…**O bonds of phenylene ring to make a robust $R_4^4(14)$ synthons. To reduce the repulsive interactions in tight packed structures between the oxygen atoms of nitrates and also due to inherent planarity of nitrate ions, ***l***-shaped structures of the cations are stabilized in crystal lattice.

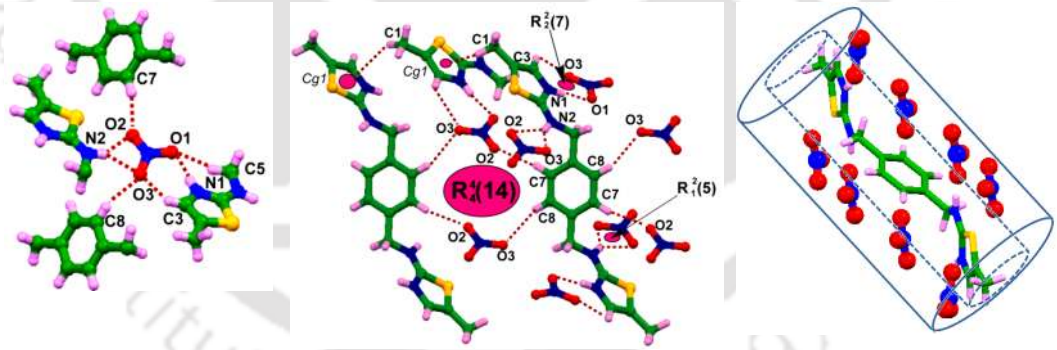

(a) (b) (c)

*Figure 6.31: (a) Environment around nitrate ion in lattice of **6.2d**, (b) Hydrogen bonds of $[H_2(\mathbf{6.2})]^{2+}$ with nitrate anion in **6.2d**. (c) Nitrate anion-induced molecular barrel having anti-anti-anti conformer of cationic host at the center.*

Thus, the nitrate ions weakly interacts with both aromatic and aliphatic -CH protons having $d_{D\ldots A}$ distance ranging from 3.212 to 3.572 Å and ∠D-H**…**A ranging from 115º to 167º. This shows that there are a set of very weak C-H**…**O bonds[21,22] that contribute to overall stabilization of the orientation of the thiazolium cationic parts. In

the packing pattern all together eight nitrate anions surround one $[H_2(\mathbf{6.2})]^{2+}$ block, generating a molecular barrel type structure (Figure 6.31b) with a width of ~12.6 Å. Although nitrate anions typically participate in anion-π interactions with aromatic counterparts,[23,24] such interactions are absent in the present example. On the other hand, nitrate ions in self-assemblies of the salts of organic amines occur in pairs,[25] but in **6.2d** we observe them as independent anion interactions with cations that are rather uncommon.[26,27]

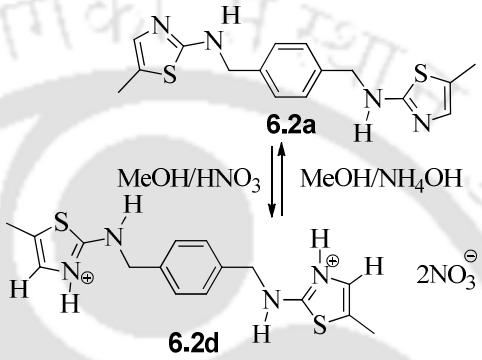

Scheme 6.3: Conformational change from syn-anti-syn to anti-anti-anti of $[H_2(\mathbf{6.2})]^{2+}$

Intriguing aspect of the nitrate salt is the orientation of the amino-thiazolinium cations, which are *anti-anti-anti* of Figure 6.31b. The reversal of the conformer is due to the participation of the $-N^+-H$ in hydrogen bonds with nitrate anions. To check reversal of the conformation to parent conformer of **6.2a**, we recrystallized the salt by adjusting pH to a neutral condition, using a methanol solution of **6.2d** and adding ammonium hydroxide. Needle shaped crystals of **6.2a** could be obtained; the process is represented in Scheme 6.3. This information clearly indicated that the inter-conversion of conformational changes from *syn-anti-syn* to *anti-anti-anti* conformer by crystallization from solution with nitric acid and subsequent neutralization.

6.8.3: Dihydrogenphosphate assisted assembly of 6.2

The reaction of **6.2** with phosphoric acid yielded $[H_2(\mathbf{6.2})](H_2PO_4)_2{\cdot}2H_3PO_4$ (**6.2e**). This salt comprises of $[H_2(\mathbf{6.2})]^{2+}$ cation, two dihydrogen phosphate anion ($H_2PO_4^-$) and two phosphoric acid molecule (H_3PO_4) molecules. The thiazole $-N^+-H$ and amine -NH groups are held by N-H**…**O and N^+-H**…**O hydrogen bonds with $H_2PO_4^-$ anion (Figure 6.32a). The adjacent $H_2PO_4^-$ anions are hydrogen bonded via strong O-H**…**O bonds, thereby forming a 1D chain-like arrangements, which is sandwiched between

arrays of protonated hosts $[H_2(\mathbf{6.2})]^2$ as shown in Figure 6.32a. Interestingly, each $H_2PO_4^-$ anion interacts concurrently with another $H_2PO_4^-$ anion and one H_3PO_4 molecule which, in turn, interacts with another H_3PO_4 moiety generating an infinite tetrameric anion-acid $[(H_2PO_4^-{\cdot}H_3PO_4)_2]_n$ cluster with a tetragonal planar arrangement (Figure 6.32b). The biphosphate and phosphoric acids assemblies can be described by repeat cyclic $R_3^3(12)$ synthon, where two biphosphate held by one phosphoric acid. In this cluster there are two biphosphate anions, one biphosphate provides two P=O bonds as hydrogen bond acceptor and another provides one O-H as donor and one P=O as acceptor, whereas the phosphoric acid molecule provides two O-H bonds as donors to bridge two biphosphates as shown in Figure 6.32b. The $R_3^3(12)$ synthon is held by a $R_3^2(10)$ synthon formed with a phosphoric acid molecule which provides one O-H as donor and one P=O as hydrogen bond acceptor. These synthons extend infinitely and help to form a layered structure. The biphosphate anions at alternate positions of the chain are linked to aminothiazole through $R_2^2(8)$ hydrogen bonded synthons. These $R_2^2(8)$ synthons have $N_{(amine)}$-H**…**$O_{(biphosphate)}$ and $N_{(thiazole)}^+$-H**…**$O_{(biphosphate)}$ bonds.

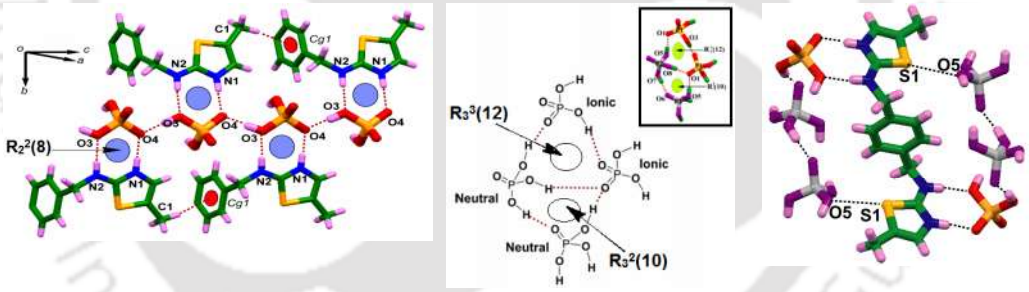

(a) (b) (c)

*Figure 6.32: (a) Hydrogen bonds between cationic host and $H_2PO_4^-$ [N1**…**O4 = 2.760 Å, N2**…**O3 = 2.817 Å, O3**…**O4 = 2.480 Å], (b) Hydrogen bonded synthon within the $(H_2PO_4^-{\cdot}H_3PO_4)_2$ cluster, inset: phosphate mixed cluster in ball and stick model. (c) Assembly of salt **6.2e**.*

The layers of $[H_2(\mathbf{6.2})]^{2+}$ are formed by cations connected to one another through C-H**…**π interactions ($d_{C\text{-}H\ldots\pi}$ = 3.678Å) between C-H bond of -CH_3 group with the π-cloud of aromatic ring of the phenylene unit of neighboring molecule. In the overall tight packed structure each $[H_2(\mathbf{6.2})]^{2+}$ ion is surrounded by phosphoric acid and biphosphate anions as shown in Figure 3.32c. Different types of polyamines that are

capable of generating distinct assemblies of phosphate structures were elegantly analyzed by Steed and coworkers.[28] Literature on the self-assemblies of $H_2PO_4^-$ anions analyzed by Custelcean's group revealed that distribution of 1D and 2D tetrameric hydrogen bonded assemblies and 9% and 0.4% respectively.[29] Here, we have isolated a mixed $(H_2PO_4^-\cdot H_3PO_4)_2$ cluster. This type of clusters is rare in chemistry.

6.9: Conclusion

Two conformational polymorphs having close energy difference adopting ***S***- and ***l***-shaped geometry of N,N'-(1,4-phenylene*bis*(methylene))-*bis*(5-methylthiazol-2-amine) **6.2** were established. The conformation adjustment occurs through C-N bonds rotations which are guided by anions in respective salt. The extent of changes by solvents and anions is different as shown in Figure 6.33.

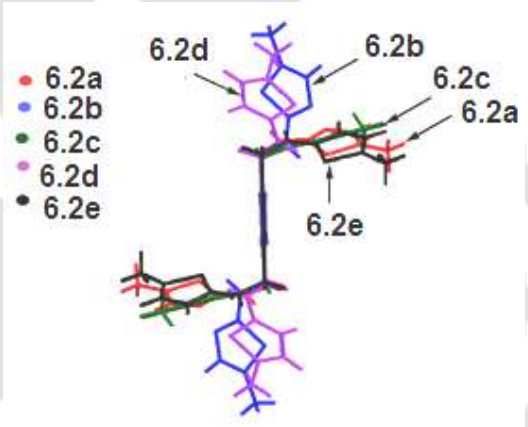

Figure 6.33: Overlaid diagram of the structures of ***6.2*** *and* $[H_2(\mathbf{6.2})]^{2+}$ *drawn by fixing the phenylene units in one plane.*

The conformation adjustments have three fold major impacts on these structures of **6.2**:

a) To modify the orientation of the aminothiazole ring across the phenylene unit
b) To rotate the thiazole ring and to assist in formation of robust hydrogen bonded cyclic synthon. The change from *syn-anti-syn* to *anti-anti-anti* was observed when the nitrate salt was formed whereas *syn-anti-syn* conformer was observed in all other cases. Thus, the planar nitrate ion is capable of stabilizing the *anti* form of aminothiazole.

c) The anionic clusters $[Br_2(H_2O)_2]^{2-}$ and $[(H_2PO_4^{-}\cdot H_3PO_4)_2]_n$ cause conformational adjustments of the host cation retaining *syn-anti-syn* form. Formation of robust hydrogen bonded cyclic synthons, anion clusters and hydrated anion clusters within the assemblies of the salts are the special feature of the anion guided assemblies of the diprotonated **6.2**. Extra stability conferred to robust synthon in assemblies of salts enforced by strong electro-statistically guided hydrogen bonds caused a synergic *syn* to *anti* conversions of the same molecule at two ends.

6.10: Experimental Section

Synthesis of N,N'-(1,4-phenylene*bis*(methylene))-*bis*(5-methylthiazol-2-amine) (6.2): 5-Methylthiazol-2-yl-amine (0.229 g, 2 mmol) and terephthalaldehyde (0.13 mg, 1 mmol) were dissolved in dry methanol (20 mL) and the solution was refluxed for 6 hrs. The resulting mixture was evaporated, and the precipitate was dried in vacuum. A yellow colored precipitate was obtained, which was dissolved in dry methanol (30 mL). To this solution sodium borohydride (37 mg, 10 mmol) was added in small portions and stirred for 2 hrs keeping the reaction mixture over an ice bath. The solvent was evaporated from the reaction mixture, and the precipitate was extracted with ethyl acetate. Yield, 80 %. HRMS : calcd for $(\mathbf{6.2} + H)^+$: $C_{16}H_{19}N_4S_2$ 331.1053, found 331.1072. ^{1}H-NMR (400 MHz, $CDCl_3$): δ 7.33 (s, 4H), 6.74 (s, 2H), 5.39 (s, 2H), 4.43 (s, 4H), 2.27 (s, 6H). IR (KBr, cm^{-1}): 3447 (w), 3444 (w), 3200 (m), 2920 (s), 1693 (m), 1640 (m), 1569 (s), 1454 (m), 1415 (m), 1324 (m), 1116 (m), 668 (s). The polymorph **6.2a** was crystallized from N,N-dimethylformamide/chloroform (3:1), whereas **6.2b** crystallized from methanol.

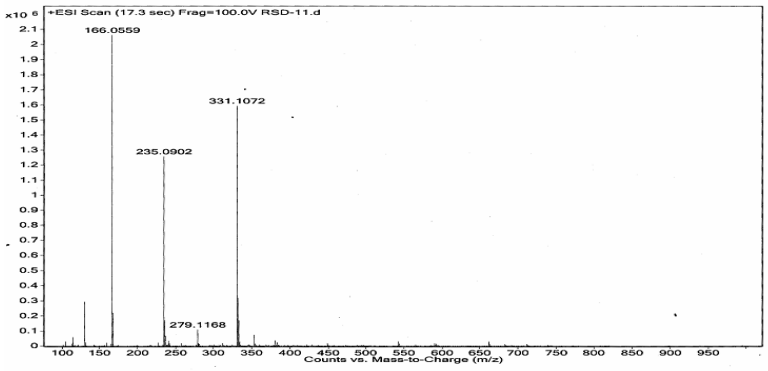

*Figure 6.34: ESI mass spectrum of **6.2**.*

$[H_2(\mathbf{6.2})]Br_2 \cdot 2H_2O$ (**6.2c**): This salt was obtained by adding 0.4 mL 37 % hydrobromic acid to methanol solution of **6.2** (124 mg, 0.5 mmol in 5 mL). The solution was stirred at room temperature for 30 mins and filtered. The filtrate was allowed to crystallize at room temperature to yield colorless crystals after three days. Yield: 82 %. Melting point 220° C. HRMS: calcd for $(\mathbf{6.2})^+$: $C_{16}H_{19}N_4S_2$ 331.1053, found 331.1051.^{1}H-NMR ($CDCl_3$, 400 MHz): δ 7.38 (s, 4H), 7.08 (s, 2H), 4.60 (s, 4H), 2.23 (s, 6H). IR (KBr, cm^{-1}): 3421 (w), 2923 (m), 1615 (s), 1043 (m), 669 (s).

$[H_2(\mathbf{6.2})](NO_3)_2$ (**6.2d**): A solution of **6.2** (124 mg, 0.5 mmol) and nitric acid in methanol/DMF (10 mL, 1:1) yielded colorless crystals of **2** after three days. Yield: 85 %; Melting point 185° C. HRMS: calcd for $(\mathbf{6.2})^+$: $C_{16}H_{19}N_4S_2$ 331.1053, found 331.1059. ^{1}H-NMR ($CDCl_3$, 400 MHz): δ 7.55 (s, 4H), 6.89 (s, 2H), 4.41 (s, 4H), 2.25 (s, 6H). IR (KBr, cm^{-1}): 3433 (w), 2924 (s), 2853 (m), 1624 (w), 1457 (m), 1384 (m), 1019 (w), 668 (s).

$[H_2(\mathbf{6.2})](H_2PO_4)_2 \cdot 2H_3PO_4$ (**6.2e**): To a suspension of compound **6.2** (25 mg) in methanol (10 mL) orthophosphoric acid (0.3 mL) were added and stirred for 30 mins, a clear solution was formed. This solution on slow evaporation resulted in colorless crystals after a week. Yield 82 %; Melting point 191° C. HRMS: calcd for $(\mathbf{6.2})^+$: $C_{16}H_{19}N_4S_2$ 331.1053, found 331.1047. ^{1}H-NMR ($CDCl_3$, 400 MHz): δ 7.25 (s, 4H), 6.65 (s, 2H), 4.39 (s, 4H), 4.03 (s, 8H), 2.17 (s, 6H). IR (KBr, cm^{-1}): 3441 (w), 3239 (s), 2848 (m), 1617 (s), 1449 (m), 1254 (m), 1082 (m), 997 (s), 668 (s), 498 (m).

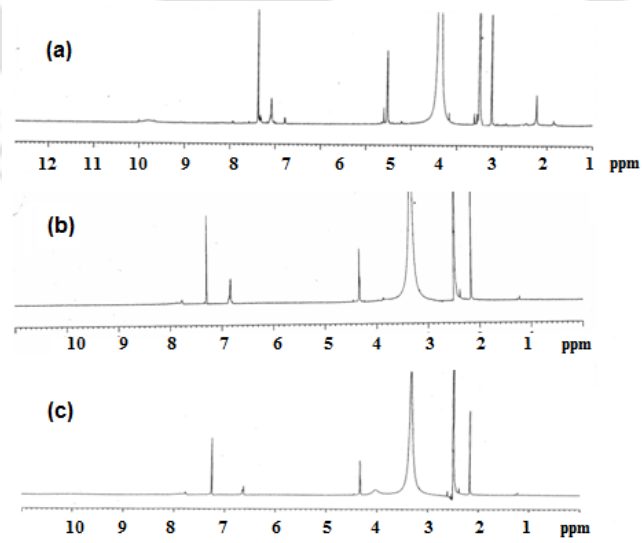

Figure 6.35: ^{1}H-NMR (DMSO-d_6) spectrum of salt (a) ***6.2c****, (b)* ***6.2d*** *and (c)* ***6.2e****.*

6.11: References

1. A. J. Cruz-Cabeza, J. Bersntein, *Chem. Rev.,* 2014, **114**, 2170.
2. F. Hof, C. Nuckolls, S. L. Craig, T. Martin, J. Rebek, Jr. *J. Am. Chem. Soc.,* 2000, **122***,* 10991.
3. M. de Wild, S. Berner, H. Suzuki, L. Ramoino, A. Baratoff, T. A. Jung, *Ann. N.Y. Acad. Sci.,* 2003, **1006**, 291.
4. W. Auwarter, A. Weber-Bargioni, A. Riemann, A. Schiffrin, O. Groning, R. Fasel, J. V. Barth, *J. Chem. Phys.,* 2006, **124,** 194708.
5. J.-P. Brog, C.-L. Chanez, A. Crochet, K. M. Fromm, *RSC Adv.,* 2013, **3**, 16905.
6. J. Bernstein, A. T. Hagler, *J. Am. Chem. Soc.* 1978, **100,** 673.
7. J.-R. Wang, B. Zhu, Q. Yu, X. Mei, *CrystEngComm*, 2016, **18**, 1101.
8. N. Phukan, J.B. Baruah, *ChemistrySelect*, 2016, **3**, 440.
9. M. S. Vickers, P. D. Beer, *Chem. Soc. Rev.*, 2007, **36**, 211.
10. J. -M. Lehn, Supramolecular Chemistry, Wiley-VCH Verlag GmbH, Weinheim, 1995.
11. Y. Kervella, E. Shilova, S. Latil, B. Jousselme, F. Silly *Langmuir*, 2015, **31**, 13420.
12. N. W. Polaske, G. S. Nichol, B. Olenyuk, *Acta Crystallogr. C: Cryst. Struct. Commun*., 2009, **65,** o381.
13. M. A. Spackman, D. Jayatilaka, *CrystEngComm*, 2009, **11,** 19.
14. J. J. McKinnon, D. Jayatilaka, M. A. Spackman, *Chem. Commun.*, 2007, 3814.
15. M. Nishio, M. Hirota, Y. Umezawa, The CH/π interaction. Evidence, Nature and Consequences, Wiley, New York, 1998.
16. M. Nishio, *CrystEngComm,* 2004, 130.
17. C. Wang, H. Luo, D. -E. Jiang, H. Li, S. Dai, *Angew. Chem., Int. Ed.,* 2010, **49**, 5978.
18. C. Wang, X. Luo, H. Luo, D. -E. Jiang, H. Li, S. Dai, *Angew. Chem., Int. Ed.,* 2011, **50,** 4918.
19. P. D. Beer, P. A. Gale, *Angew. Chem., Int. Ed.,* 2001, **40**, 486.
20. M. C. Etter, *Acc. Chem. Res.*, 1990, **23,** 120.

21. G. R. Desiraju, *Angew. Chem., Int. Ed.*, 1995, **34**, 2311.
22. M. C. Etter, J. C. McDonald, J. Bernstein, *Acta Crystallogr.*, 1990, **B46**, 256
23. H. Casellas, C. Massera, F. Buda, P. Gamez, J. Reedjik, *New. J. Chem.*, 2006, **30**, 1561.
24. D. -X. Wang, M. -X. Wang, *J. Am.Chem. Soc.*, 2013, **135**, 892.
25. L. Vlaencia, R. Bastda, E. Gracia-Espana, J. V. de Julian-Ortiz, J. M. Llinares, A. Macias, P. P. Lourido, *Cryst. Growth Des*., 2010, **10**, 3418.
26. P. Khakhlary, J. B. Baruah, *J. Chem. Sci.*, 2015, **127**, 95.
27. S. Marivel, M. Arunachalam, P. Ghosh, *Cryst. Growth Des*., 2011, **11**, 1642.
28. C. A. Ilioudis, D. G. Georganopoulou, J. W. Steed, *J. Mater. Chem.,* 2002, **4,** 26.
29. A. Rajbanshi, S. Wan, R. Custelcean, *Cryst. Growth Des*., 2013,**13,** 2233.

Conclusion

Based on free rotation of C-N bond over intramolecularly hydrogen bonded six-membered synthon of a phenyl thiourea tethered thiazole derivative, three polymorphs were isolated. Each polymorph was obtained by crystallization from different solvent systems. Highly ordered structures was observed in each case, comprising of molecules with different orientation arranged in their respective lattice. But in case of the respective positional isomer, no polymorphs were observed, due to intermolecular locking of orientations over hydrogen bonded six-membered ring. Each polymorph as well as the monomorph adopts *syn-anti* orientation across the thiourea moiety. By protonating thiazole nitrogen, various salts of the two positional isomeric thiourea tethered thiazole derivative were prepared. Each salt adopt *syn-syn* orientation across the thiourea moiety. Formation of hydrated anion assembly and deprotonation of a polyacid to form crystalline salt is host-specific. Novel clusters of hydrated bromide ions, cyclic assemblies of dihydrogen phosphate, and chainlike structure of assemblies of bisulphate-water were established by stabilizing them in cationic hosts.

Polymorphism by rotation over intramolecular hydrogen bonded synthon of thiourea derivatives has been extended to another system, comprising of two positional isomers of naphthyl thiourea tethered thiazole derivative. Due to the free rotation of naphthyl group over intramolecular hydrogen bonded six-membered synthon, two polymorphs were isolated in each case. *Anti*-centrosymmetric homodimeric synthons guided the assembly of each polymorph. No polymorphs were obtained in case of respective urea derivatives, but their assembly also guided by *anti*-centrosymmetric homodimeric synthons. Anion guided the *anti*-conformation of the parent form to *syn*-form in the cationic host of the salts of urea derivatives. Neutral multi-component crystals of urea derivative with tetrabutylammonium chloride were isolated. In multi-component crystals the conformational adjustment over hetero synthons took place due to local environment change and through interplay of weak supramolecular interactions.

Imine form of two positional isomers of thiourea tethered thiazole derivative, having nitro-substituent is isolated in solid state. Different solvents solvate the two isomers. Polymorphic solvates was observed in one case. Conformational adjustments on a particular host of polymorphic solvates with respect to parent molecule done by the

same solvent. Unsolvated crystals of the two isomers differ in number of molecules in their respective asymmetric units. The position of the methyl-substituent contributed different hydrolytic stability of the two positional isomers. Mercuric ions catalysed hydrolysis of the thiourea derivatives to urea derivatives, caused chemodosimetric signal transductions that reflected in UV-visible absorptions. Fluoride could be detected through naked eye. A ring-opened adduct of 1,8-diazabicyclo [5.4.0] undec-7-ene was isolated. A highly selective bromination reaction differentiates the two positional isomers through their chemical reactivities.

Two imines derived from *ortho*-hydroxyaromatic carbonyl compounds show polymorphism due to different orientations of the thiazole ring via C-N bond rotation over the intramolecularly hydrogen bonded six-membered ring. The differential scanning calorimetry analysis established, polymorphs of one of the imine derivative are interconvertible. Stable polymorph converted to the metastable form, which on crystallization from melt reforms both polymorphs. Other imine applied to detect toxic Al^{3+} ions in the presence of various metal ions.

An uncommon form of conformation of a thiazole derivative in absence of intramolecular hydrogen bond in solid state is isolated. Anion guided conformational adjustment of the cationic host takes place by forming salts. Conformational adjustment by nitrate anion leads to reversal of conformation.

Two polymorphs having ***S***- and ***l***- shaped geometry were isolated from a thiazole derivative, where two $-CH_2-$ and two -NH groups can orient the methyl-thiazole rings across a rigid phenylene unit. The conformation adjustment occurs through C-N bonds rotations which are guided by anions in respective salt. Novel bromide water cluster as well as mixed dihydrogen phosphate cluster caused conformational adjustments of the host cation retaining parental *syn-anti-syn* form. The change from *syn-anti-syn* to *anti-anti-anti* was observed with nitrate anion.

All these conformational results suggested that the analysis of supramolecular assemblies based on orientation of different functional groups is an important issue.

Appendix

Details of the analytical instruments

X-Ray Crystallography

X-ray diffraction data were collected on Bruker 3-circle diffractometer with CCD area detectors ProteumM APEX or SMART 6000 or Bruker Nonius Apex 2, using graphite-monochromated Mo-Kα radiation (λ= 0.71073Å) from a 60W micro-focus Bede Microsourse® with glass polycapillary optics or sealed tube.

X-ray diffraction data for all crystals were collected using Bruker SMART software. This software is also used for indexing and determination of the unit cell parameters. Some data were also collected in Oxford SuperNova diffractometer and data refinement refinement and cell reductions were carried out by CrysAlisPro.

Cell structures were solved by direct method and refined by full-matrix least squares against F2 of all data, using SHELXTL software. The CIF of all the compounds synthesized and characterised are included in the soft copy.

All the non H-atoms were refined by full-matrix least squares in anisotropic, all H-atoms in isotropic approximation, against F^2 of all reflections. All non H-atoms were refined by full matrix least squares in anisotropic approximation and the hydrogen atoms attached to these atoms were treated as 'riding' in calculated positions and in some of the cases the hydrogen atoms have been located on the difference Fourier maps. In all the cases the H-atoms attached to the polar atoms such as O and N were located on the difference Fourier maps and refined in the final structure in isotropic approximation. The crystallographic tables for all the compounds are given at the end of this section, which includes the crystal parameters and the refinement factor.

Powder X-ray Diffraction data were collected on Bruker D2 phaser diffractometer in Bragg- Brentano Θ-Θ geometry with CuKα source (λ = 154 Å) on a glass surface of air dried sample using a secondary curved graphite monochromator. Diffraction patterns were collected over a 2Θ range of 5-45°C at a scan rate of 2° per molecule.

UV-visible Spectroscopy, emission and IR Spectroscopy

UV-vis absorption spectra were recorded using Perkin-Elmer Lambda 750 spectrophotometer equipped with double cell compartments. All the chemicals and solvents used were as obtained from the satndard suppliers such as E.Merck Germany, Sigma Aldrich USA, Ranbaxy India. The solvents for spectroscopic were of HPLC grade (Aldrich or Merck) and used as obtained. The fluorescence spectra were recorded in Fluoromax-4, spectrofluorometer. The FT-IR spectra were recorded on Perkin-Elmer spectrum one spectrometer in the range 4000-400 cm^{-1}.

NMR Spectroscopy

The NMR spectra were recorded in a Bruker 400 MHz and 600 MHz spectrometer. The chemical shifts in the NMR spectra are all given in ppm and tetramethylsilane as the internal standard.

Thermogravimetric Studies and Hot Stage Microscopy:

The thermogravimetric studies were performed using a Mettlar Toledo TGA/ STDA 851^e and Mettlar Toledo DSC^e thermal analyser. Typically about 4-6 mg of the samples were mounted on platinum crucibles and the TG/ DSC profiles recorded at the heating rate of 5˚C/min and under nitrogen atmosphere. Hot-stage microscopic study was performed by using a Metler Toledo FP82HT hot-stage microscope.

Crystallographic data and refinement parameters for the compounds

Compound No.	**Polymprph I**	**Polymprph II**	**Polymprph III**	**2.2**
Formulae	$C_{11}H_{11}N_3S_2$	$C_{11}H_{11}N_3S_2$	$C_{11}H_{11}N_3S_2$	$C_{11}H_{11}N_3S_2$
CCDC No.	967973	967974	967975	967976
Mol. wt.	249.37	249.35	249.35	249.35
Crystal system	Monoclinic	Triclinic	Monoclinic	Triclinic
Space group	*P 21/c*	*P1¯*	*C2/c*	*P1¯*
Temperature (K)	296(2)	296(2)	296(2)	296(2)
Wavelength (Å)	0.71073	0.71073	0.71073	0.71073
a (Å)	11.3183(4)	8.941(3)	16.8654(10)	5.7601(7)
b (Å)	5.7063(2)	10.074(3)	6.1269(3)	8.8710(10)
c (Å)	20.5287(6)	13.822(4)	24.5611(14)	12.0970(14)
α (°)	90.00	92.594(18)	90.00	103.779(6)
β (°)	113.537(2)	95.21(2)	108.596(7)	96.286(6)
γ (°)	90.00	105.985(17)	90.00	95.705(6)
V ($Å^3$)	1215.55(7)	1188.7(6)	2405.5(2)	591.67(12)
Z	4	4	8	2
Density/Mgm^{-3}	1.363	1.393	1.377	1.400
Abs. Coeff. /mm^{-1}	0.413	0.423	0.418	0.425
Abs. correction	multi-scan	multi-scan	multi-scan	multi-scan
F(000)	520	520	1040	260
Total reflections	2299	4147	2174	2132
Reflections, $I > 2\sigma(I)$	1811	3239	1564	1502
Max. θ/°	25.75	25.00	25.24	25.25
Ranges (h, k, l)	$-13 \le h \le 12$ $-6 \le k \le 6$ $-23 \le l \le 23$	$-8 \le h \le 9$ $-11 \le k \le 11$ $-16 \le l \le 15$	$-20 \le h \le 18$ $-7 \le k \le 7$ $-28 \le l \le 29$	$-6 \le h \le 6$ $-10 \le k \le 10$ $-14 \le l \le 14$
Complete to 2θ (%)	99.3	98.9	1.00	99.3
Data/ restrain/ parameter	2299/ 0/ 146	4147/ 0/ 291	2174/ 0/ 146	2111/0/146
Goof(F^2)	1.095	1.087	0.908	1.079
R indices [$I > 2\sigma(I)$]	0.0375	0.0480	0.0384	0.0971
R indices (all data)	0.0447	0.0822	0.0617	0.1117

Compound No.	**2.1a**	**2.1b**	**2.1c**	**2.1.1c**
Formulae	$C_{11}H_{12}ClN_3S_2$	$C_{11}H_{12}BrN_3S_2$	$C_{22}H_{26}N_8O_7S_4$	$C_{11}H_{12}N_4O_3S_2$
CCDC No.	967983	967982	967987	967986
Mol. wt.	285.83	330.27	642.79	312.39
Crystal system	Triclinic	Monoclinic	Triclinic	Monoclinic
Space group	$P\bar{1}$	$I\,2/c$	$P\bar{1}$	$P2_1/n$
Temperature (K)	296(2)	296(2)	296(2)	296(2)
Wavelength (Å)	0.71073	0.71073	0.71073	0.71073
a (Å)	9.6400 (6)	23.7103(11)	10.551(3)	19.502(3)
b (Å)	15.4273 (9)	4.45641(17)	10.6973(19)	6.1168(7)
c (Å)	19.1760 (11)	25.3321(7)	13.648(3)	23.967(3)
α (°)	73.592 (5)	90.00	108.804(9)	90.00
β (°)	86.432(5)	95.947(3)	96.519(11)	105.989(16)
γ (°)	89.798(5)	90.00	91.481(8)	90.00
V (Å^3)	2730.1(3)	2662.26(17)	1445.6(5)	2748.5(6)
Z	8	8	2	8
Density/Mgm^{-3}	1.391	1.648	1.477	1.510
Abs. Coeff. /mm^{-1}	0.567	3.383	0.385	0.400
Abs. correction	multi-scan	multi-scan	multi-scan	multi-scan
F(000)	1184.0	1328	668	1296
Total reflections	10111	2410	5155	4839
Reflections, I > 2σ(I)	6880	1855	3214	2483
Max. θ/°	25.50	25.24	25.25	25.00
Ranges (h, k, l)	$-8 \le h \le 11$ $-18 \le k \le 18$ $-22 \le l \le 23$	$-28 \le h \le 22$ $-4 \le k \le 5$ $-22 \le l \le 30$	$-12 \le h \le 10$ $-12 \le k \le 12$ $-16 \le l \le 16$	$-23 \le h \le 23$ $-6 \le k \le 7$ $-15 \le l \le 28$
Complete to 2θ (%)	99.0	99.8	98.2	99.9
Data/ restrain/ parameter	9999 / 0 / 617	2410/3/167	5320/3/400	4839/0/363
Goof(F^2)	0.998	0.969	1.060	1.213
R indices [I > 2σ(I)]	0.0454	0.0358	0.0464	0.0859
R indices (all data)	0.0716	0.0540	0.0767	0.1640

Compound No.	**2.1d**	**2.1e**	**2.1f**	**2.2a**
CCDC No.	967984	967988	967985	967978
Formulae	$C_{11}H_{16}ClN_3O_6S_2$	$C_{22}H_{24}N_6O_4S_5$	$C_{11}H_{14}N_3O_4PS_2$	$C_{11}H_{12}ClN_3S_2$
Mol. wt.	385.84	596.82	347.34	285.83
Crystal system	Monoclinic	Triclinic	Monoclinic	Triclinic
Space group	$P\,2_1/a$	$P\bar{1}$	C_2/c	$P\bar{1}$
Temperature (K)	296(2)	296(2)	296(2)	296(2)
Wavelength (Å)	0.71073	0.71073	0.71073	0.71073
a (Å)	14.6126(4)	11.1939(13)	11.6810(19)	8.6544(9)
b (Å)	7.3778(2)	11.8157(16)	8.5182(19)	9.2851(9)
c (Å)	15.9027(4)	12.0646(17)	30.608(6)	10.0278(12)
α (°)	90.00	110.959(13)	90.00	65.682(5)
β (°)	95.712(2)	106.648(11)	100.777(13)	75.992(5)
γ (°)	90.00	104.205(11)	90.00	64.045(4)
V (Å^3)	1705.94(8)	1315.3(3)	2991.8(10)	658.36(12)
Z	4	2	8	2
Density/Mgm^{-3}	1.502	1.507	1.542	1.442
Abs. Coeff. /mm^{-1}	0.500	0.483	0.481	0.588
Abs. correction	multi-scan	multi-scan	multi-scan	multi-scan
F(000)	800	620.0	1440	296
Total reflections	3078	4894	2666	2299
Reflections, I > 2σ(I)	2501	3092	1434	1625
Max. θ/°	25.25	25.49	25.24	25.00
Ranges (h, k, l)	$-15 \le h \le 17$ $-7 \le k \le 8$ $-18 \le l \le 19$	$-13 \le h \le 12$ $-14 \le k \le 14$ $-14 \le l \le 13$	$-9 \le h \le 14$ $-8 \le k \le 10$ $-35 \le l \le 36$	$-9 \le h \le 10$ $-10 \le k \le 10$ $-11 \le l \le 10$
Complete to 2θ (%)	99.9	99.8	98.4	99.2
Data/ restrain/ parameter	3078/ 6/ 225	4894/0/336	2666/5/208	2299 /0/155
Goof(F^2)	1.019	1.013	1.012	1.087
R indices [I > 2σ(I)]	0.0401	0.0606	0.0469	0.0337
R indices (all data)	0.0509	0.0951	0.0812	0.0413

Compound No.	**2.2b**	**2.2c**	**2.2d**	**2.2e**
CCDC No.	967977	967980	967979	967981
Formulae	$C_{11}H_{18}BrN_3O_3S_2$	$C_{11}H_{12}N_4O_3S_2$	$C_{11}H_{14}ClN_3O_5S_2$	$C_{11}H_{15}N_3O_5S_3$
Mol. wt.	384.31	312.37	367.84	365.47
Crystal system	Monoclinic	Monoclinic	Triclinic	Triclinic
Space group	$P2_1/n$	$P2_1/n$	$P\bar{1}$	$P\bar{1}$
Temperature (K)	296(2)	296(2)	296(2)	296(2)
Wavelength (Å)	0.71073	0.71073	0.71073	0.71073
a (Å)	14.3819(10)	11.2755(8)	7.5147(5)	7.0435(5)
b (Å)	7.2911(4)	18.3129(14)	9.0185(8)	9.4168(9)
c (Å)	31.790(2)	14.0015(10)	12.1146(7)	12.3566(10)
α (°)	90.00	90.00	90.801(6)	85.815(7)
β (°)	94.778(6)	103.005(4)	98.642(5)	88.897(7)
γ (°)	90.00	90.00	109.424(7)	71.023(8)
V ($Å^3$)	3321.9(4)	2817.0(4)	763.70(10)	772.96(11)
Z	8	8	2	2
Density/Mgm^{-3}	1.537	1.473	1.586	1.570
Abs. Coeff. /mm^{-1}	2.735	0.390	0.549	0.505
Abs. correction	multi-scan	multi-scan	multi-scan	multi-scan
F(000)	1568	1296	380.0	380.0
Total reflections	6180	4899	2752	2884
Reflections, $I > 2\sigma(I)$	3744	3235	1948	2053
Max. θ/°	25.50	25.00	25.25	25.50
Ranges (h, k, l)	$-15 \le h \le 17$ $-8 \le k \le 8$ $-24 \le l \le 38$	$-13 \le h \le 11$ $-21 \le k \le 20$ $-16 \le l \le 16$	$-9 \le h \le 8$ $-10 \le k \le 10$ $-14 \le l \le 14$	$-8 \le h \le 8$ $-11 \le k \le 11$ $-14 \le l \le 14$
Complete to 2θ (%)	99.9	98.4	99.8	99.9
Data/ restrain/ parameter	6180/12/411	4899 /0/363	2752/2/208	2884/2/ 209
Goof(F^2)	0.959	0.998	1. 008	1.023
R indices [$I > 2\sigma(I)$]	0.0587	0.0567	0.0538	0.0613
R indices (all data)	0.1564	0.1486	0.0794	0.0820

Compound No.	**3.1a**	**3.1b**	**3.2a**	**3.2b**
Formulae	$C_{15}H_{13}N_3S_2$	$C_{15}H_{13}N_3S_2$	$C_{15}H_{13}N_3S_2$	$C_{15}H_{13}N_3S_2$
CCDC No.	1453057	1453058	1453059	1453060
Mol. wt.	299.40	299.40	299.40	299.40
Crystal system	Monoclinic	Monoclinic	Triclinic	Triclinic
Space group	$P2_1/n$	$C\,2/c$	$P\bar{1}$	$P\bar{1}$
Temperature (K)	296(2)	296(2)	296(2)	296(2)
Wavelength (Å)	0.71073	0.71073	0.71073	0.71073
a (Å)	10.5847(6)	22.884(3)	7.6645(6)	7.6357(5)
b (Å)	8.8751(5)	8.3045(6)	7.8706(7)	8.2456(8)
c (Å)	16.2063(9)	15.2009(12)	12.6909(12)	11.8464(6)
α (°)	90.00	90.00	107.745(6)	97.352(6)
β (°)	106.210(6)	101.047(8)	99.244(7)	104.485(5)
γ (°)	90.00	90.00	97.038(6)	96.981(7)
V (Å^3)	1461.91(14)	2835.3(5)	707.60(11)	707.00(9)
Z	4	8	2	2
Density/Mgm^{-3}	1.360	1.403	1.405	1.406
Abs. Coeff. /mm^{-1}	0.357	0.368	0.368	0.369
Abs. correction	multi-scan	multi-scan	multi-scan	multi-scan
F(000)	624	1248	312	312
Total reflections	2645	2511	2531	2553
Reflections, I > 2σ(I)	1928	1696	1890	2052
Max. θ/°	25.25	25.25	98.8	25.25
Ranges (h, k, l)	$-12 \le h \le 11$ $-8 \le k \le 10$ $-11 \le l \le 19$	$-28 \le h \le 27$ $-5 \le k \le 5$ $-28 \le l \le 17$	$-9 \le h \le 9$ $-9 \le k \le 9$ $-15 \le l \le 14$	$-9 \le h \le 9$ $-9 \le k \le 9$ $-14 \le l \le 14$
Complete to 2θ (%)	99.8	98.0	98.8	99.8
Data/ restrain/ parameter	2645/0/190	2511/0/190	2531/0/182	2553 /0/190
Goof(F^2)	1.017	1.092	1.061	1.077
R indices [I > 2σ(I)]	0.0531	0.0360	0.0363	0.0382
R indices (all data)	0.0757	0.0432	0.0527	0.0500

Compound No.	**3.3**	**3.4**	**3.5**	**3.3a**
Formulae	$C_{15}H_{13}N_3OS$	$C_{15}H_{13}N_3OS$	$C_{15}H_{11}N_3S_2$	$C_{15}H_{16}ClN_3O_6S$
CCDC No.	1453062	1479504	1453061	1453064
Mol. wt.	283.34	283.34	297.39	401.82
Crystal system	Triclinic	Monoclinic	Monoclinic	Monoclinic
Space group	$P\bar{1}$	$P\,2_1/c$	$P\,2_1/c$	$P\,2_1$
Temperature (K)	296(2)	296(2)	296(2)	296(2)
Wavelength (Å)	0.71073	0.71073	0.71073	0.71073
a (Å)	8.079(5)	8.4428(8)	12.4078(12)	8.3350(16)
b (Å)	9.344(6)	22.3348(19)	15.0565(12)	7.3210(18)
c (Å)	9.702(6)	7.7119(7)	15.0342(11)	14.859(3)
α (°)	100.825(13)	90.00	90.00	90.00
β (°)	94.448(13)	106.990(6)	97.887(8)	91.577(13)
γ (°)	105.221(12)	90.00	90.00	90.00
V (Å^3)	687.9(7)	1390.8(2)	2782.1(4)	906.4(3)
Z	2	4	8	2
Density/Mgm^{-3}	1.368	1.353	1.420	1.472
Abs. Coeff. /mm^{-1}	0.234	0.231	0.374	0.363
Abs. correction	multi-scan	none	multi-scan	multi-scan
F(000)	296	592.0	1232	416
Total reflections	2461	2490	5028	2731
Reflections, I > 2σ(I)	1552	1604	3054	1889
Max. θ/°	25.25	25.25	25.25	25.50
Ranges (h, k, l)	$-9 \le h \le 9$ $-11 \le k \le 11$ $-11 \le l \le 11$	$-10 \le h \le 9$ $-26 \le k \le 26$ $-8 \le l \le 8$	$-13 \le h \le 14$ $-17 \le k \le 18$ $-18 \le l \le 13$	$-10 \le h \le 10$ $-8 \le k \le 8$ $-17 \le l \le 16$
Complete to 2θ (%)	98.4	98.5	99.8	96.2
Data/ restrain/ parameter	2461/0/190	2490/0/233	5028/0/363	2731/3/249
Goof(F^2)	1.078	1.071	1.099	1.057
R indices [I > 2σ(I)]	0.0394	0.0439	0.0957	0.0626
R indices (all data)	0.0621	0.0718	0.1436	0.0960

Compound No.	**3.3b**	**3.3c**	**3.3d**	**3.3e**
Formulae	$C_{15}H_{16}ClN_3O_2S$	$C_{31}H_{49}ClN_4OS$	$C_{31}H_{51}ClN_4O_2S$	$C_{31}H_{51}ClN_4O_2S$
CCDC No.	1453063	1453065	1453066	1453067
Mol. wt.	337.82	561.25	579.27	579.27
Crystal system	Orthorhombic	Monoclinic	Triclinic	Monoclinic
Space group	*Pbca*	*P* $2_1/c$	$P\bar{1}$	$P2_1/c$
Temperature (K)	296(2)	296(2)	296(2)	296(2)
Wavelength (Å)	0.71073	0.71073	0.71073	0.71073
a (Å)	15.4084(8)	8.3706(12)	8.4037(12)	11.5868(16)
b (Å)	7.7845(4)	18.536(2)	10.2399(15)	15.626(2)
c (Å)	27.4631(14)	21.658(3)	19.874(3)	19.065(2)
α (°)	90.00	90.00	97.051(7)	90.00
β (°)	90.00	99.199(10)	95.211(7)	98.020(9)
γ (°)	90.00	90.00	94.056(7)	90.00
V (Å3)	3294.1(3)	3317.2(8)	1684.5(4)	3418.2(8)
Z	8	4	2	4
Density/Mgm-3	1.362	1.124	1.142	1.126
Abs. Coeff. /mm-1	0.368	0.206	0.207	0.204
Abs. correction	multi-scan	none	none	none
F(000)	1408	1216	628	1256
Total reflections	2999	5996	5710	6171
Reflections, I > 2σ(I)	1639	3181	2871	2605
Max. θ/°	25.50	25.25	96.4	25.25
Ranges (h, k, l)	$-18 \le h \le 18$ $-7 \le k \le 8$ $-33 \le l \le 31$	$-10 \le h \le 9$ $-22 \le k \le 22$ $-25 \le l \le 16$	$-8 \le h \le 8$ $-10 \le k \le 10$ $-20 \le l \le 21$	$-13 \le h \le 13$ $-18 \le k \le 18$ $-21 \le l \le 22$
Complete to 2θ (%)	97.5	1.000	96.4	99.7
Data/ restrain/ parameter	2999/10/216	5996/12/356	5710/11/373	6171/23/365
Goof(F2)	1.085	1.094	1.055	1.096
R indices [I > 2σ(I)]	0.0397	0.0609	0.0497	0.0902
R indices (all data)	0.0866	0.1229	0.0738	0.1919

Compound No.	**4.1**	**4.2**	**4.1a**	**4.1b**
Formulae	$C_{11}H_{10}N_4O_2S_2$	$C_{11}H_{10}N_4O_2S_2$	$C_{13}H_{16}N_4O_3S_3$	$C_{15}H_{19}N_5O_3S_2$
CCDC No.	1436503	1445143	1436502	1436501
Mol. wt.	294.35	294.35	372.48	381.47
Crystal system	Triclinic	Monoclinic	Triclinic	Triclinic
Space group	$P\bar{1}$	C 2/c	$P\bar{1}$	$P\bar{1}$
Temperature (K)	296(2)	296(2)	296(2)	296(2)
Wavelength (Å)	0.71073	0.71073	0.71073	0.71073
a (Å)	10.6976(8)	24.0180(18)	7.8556(4)	8.5882(6)
b (Å)	12.5934(9)	4.9616(2)	10.5492(5)	9.0566(7)
c (Å)	14.4096(9)	23.5481(18)	11.5009(6)	13.2569(9)
α (°)	87.490(5)	90.00	91.605(3)	93.909(4)
β (°)	85.965(5)	112.834(9)	102.511(3)	107.379(4)
γ (°)	83.479(5)	90.00	110.839(2)	107.982(4)
V (Å^3)	1922.7(2)	2586.3(3)	863.80(8)	921.26(11)
Z	6	8	2	2
Density/Mgm^{-3}	1.525	1.512	1.432	1.375
Abs. Coeff. /mm^{-1}	0.418	0.415	0.447	0.313
Abs. correction	multi-scan	multi-scan	multi-scan	multi-scan
F(000)	912	1216	388	400
Total reflections	6199	2324	3058	3152
Reflections, I > 2σ(I)	3099	1834	2624	2348
Max. θ/°	25.00	25.25	97.6	25.00
Ranges (h, k, l)	$-8 \le h \le 11$ $-14 \le k \le 14$ $-17 \le l \le 16$	$-28 \le h \le 27$ $-5 \le k \le 5$ $-28 \le l \le 17$	$-9 \le h \le 9$ $-12 \le k \le 12$ $-13 \le l \le 13$	$-10 \le h \le 10$ $-9 \le k \le 10$ $-15 \le l \le 15$
Complete to 2θ (%)	97.5	99.8	97.6	97.3
Data/ restrain/ parameter	6599/0/525	2324/0/181	3058/0/250	3152/0/234
Goof(F^2)	1.003	0.999	1.037	1.036
R indices [I > 2σ(I)]	0.0577	0.0415	0.0339	0.0398
R indices (all data)	0.1077	0.0572	0.0393	0.0590

Compound No.	**4.1.1b**	**4.1c**	**4.3**	**4.2a**
Formulae	$C_{15}\,H_{19}\,N_5\,O_3\,S_2$	$C_{20}\,H_{26}\,N_6\,O_3\,S$	$C_{27.60}\,H_{31.60}\,N_{10}\,O_6\,S_4\,Zn$	$C_{13}\,H_{15}\,Br\,N_4\,O_4\,S_2$
CCDC No.	1445144	1436500	1436503	1436505
Mol. wt.	381.47	430.53	793.06	435.31
Crystal system	Triclinic	Monoclinic	Monoclinic	Triclinic
Space group	$P\bar{1}$	$P\,2_1/n$	$C2/c$	$P\bar{1}$
Temperature (K)	296(2)	296(2)	296(2)	296(2)
Wavelength (Å)	0.71073	0.71073	0.71073	0.71073
a (Å)	8.6923(2)	12.7147(16)	35.437(2)	9.2653(7)
b (Å)	9.6622(2)	6.2855(9)	5.1812(3)	10.2683(7)
c (Å)	11.9422(3)	27.243(3)	19.7021(10)	11.4407(8)
α (°)	106.3890(10)	90.00	90.00	66.570(4)
β (°)	91.6680(10)	100.679(9)	94.827(5)	80.387(5)
γ (°)	107.4030(10)	90.00	90.00	65.245(5)
V ($Å^3$)	911.10(4)	2139.5(5	3604.7(4)	906.93(11)
Z	2	4	4	2
Density/Mgm^{-3}	1.390	1.337	1.461	1.594
Abs. Coeff. /mm^{-1}	0.317	0.186	0.967	2.521
Abs. Correction	multi-scan	multi-scan	multi-scan	multi-scan
F(000)	400	912	1636.8	440
Total reflections	3258	3862	3271	3255
Reflections, $I > 2\sigma(I)$	2775	1513	2266	1699
Max. θ/°	98.5	25.25	25.25	25.25
Ranges (h, k, l)	$-10 \leq h \leq 10$ $-11 \leq k \leq 11$ $-14 \leq l \leq 14$	$-15 \leq h \leq 14$ $-7 \leq k \leq 7$ $-32 \leq l \leq 32$	$-42 \leq h \leq 42$ $-6 \leq k \leq 4$ $-23 \leq l \leq 12$	$-11 \leq h \leq 11$ $-12 \leq k \leq 11$ $-13 \leq l \leq 13$
Complete to 2θ (%)	98.5	99.4	99.8	99.1
Data/ restrain/ parameter	3258/0/289	3862/0/280	3271/0/225	3255 /6/208
Goof(F^2)	1.005	0.817	1.034	1.004
R indices [$I > 2\sigma(I)$]	0.0384	0.0509	0.0571	0.0516
R indices (all data)	0.0444	0.1320	0.0844	0.1286

Compound No.	**4.2b**
Formulae	$C_{11}H_{12}N_4O_4S$
CCDC No.	1445145
Mol. wt.	296.31
Crystal system	triclinic
Space group	$P\bar{1}$
Temperature (K)	296(2)
Wavelength (Å)	0.71073
a (Å)	6.557(2)
b (Å)	8.595(2)
c (Å)	12.225(3)
α (°)	92.35(2)
β (°)	91.90(2)
γ (°)	98.16(2)
V ($Å^3$)	680.9(3)
Z	2
Density/Mgm^{-3}	1.445
Abs. Coeff. /mm^{-1}	0.257
Abs. Correction	multi-scan
F(000)	308
Total reflections	2399
Reflections, $I > 2\sigma(I)$	1122
Max. θ/°	25.25
Ranges (h, k, l)	$-15 \leq h \leq 17$ $-8 \leq k \leq 8$ $-24 \leq l \leq 38$
Complete to 2θ (%)	97.3
Data/ restrain/ parameter	2399 /8/190
Goof(F^2)	1.097
R indices [$I > 2\sigma(I)$]	0.1164
R indices (all data)	0.2901

Compound No.	**5.1a**	**5.1b**	**5.2a**	**5.2b**
Formulae	$C_{11}H_{10}N_2OS$	$C_{11}H_{10}N_2OS$	$C_{15}H_{12}N_2OS$	$C_{15}H_{12}N_2OS$
CCDC No.	1003313	1017945	1003311	1003312
Mol. wt.	218.28	218.28	268.33	268.33
Crystal system	Orthorhombic	Monoclinic	Triclinic	Orthorhombic
Space group	*Pbca*	$P\,2_1/n$	$P\bar{1}$	$P\,2_1\,2_1\,2_1$
Temperature (K)	296(2)	296(2)	296(2)	296(2)
Wavelength (Å)	0.71073	0.71073	0.71073	0.71073
a (Å)	12.2113(6)	13.9955(8)	4.1718(2)	5.7381(3)
b (Å)	8.9422(5)	5.0754(3)	10.9716(4)	16.0080(7)
c (Å)	19.5495(11)	15.7830(9)	14.1852(5)	28.0274(13)
α (°)	90.00	90.00	88.491(3)	90.00
β (°)	90.00	110.209(4)	86.540(3)	90.00
γ (°)	90.00	90.00	81.432(2)	90.00
V ($Å^3$)	2134.7(2)	1052.09(11)	640.76(4)	2574.5(2)
Z	8	4	2	8
Density/$g.cm^{-3}$	1.358	1.378	1.391	1.385
Abs. Coeff. /mm^{-1}	0.276	0.280	0.245	0.244
Abs. Correction	multi-scan	multi-scan	multi-scan	multi-scan
F(000)	912	456	280	1120
Total reflections	1916	1888	2277	4592
Reflections, I > 2σ(I)	1210	952	1634	3766
Max. θ/°	25.25	25.25	25.25	25.75
Ranges (h, k, l)	$-14 \le h \le 14$ $-10 \le k \le 9$ $-23 \le l \le 23$	$-16 \le h \le 15$ $-5 \le k \le 6$ $-18 \le l \le 18$	$-4 \le h \le 4$ $-13 \le k \le 13$ $-16 \le l \le 16$	$-7 \le h \le 5$ $-19 \le k \le 19$ $-34 \le l \le 27$
Complete to 2θ (%)	99.1	99.5	99.0	99.7
Data/ restrain/ parameter	1916/ 0/ 165	1888/0/138	2277/0/209	4592/ 9 /417
Goof(F^2)	1.039	1.019	1.035	1.093
R indices [I > 2σ(I)]	0.0400	0.0362	0.0380	0.0460
R indices (all data)	0.0665	0.0822	0.0549	0.0595

Compound No.	**6.1**	**6.1a**	**6.1b**	**6.1c**
Formulae	$C_{11}H_{12}N_2OS$	$C_{11}H_{13}ClN_2OS$	$C_{11}H_{13}BrN_2OS$	$C_{11}H_{13}N_3O_4S$
CCDC No.	1003307	1003309	1003308	1003310
Mol. wt.	220.29	256.74	301.20	283.31
Crystal system	Monoclinic	Monoclinic	Monoclinic	Monoclinic
Space group	*P 2$_1$/c*	*P 2$_1$/c*	*P2$_1$/c*	*P 2$_1$/n*
Temperature (K)	296(2)	296(2)	296(2)	296(2)
Wavelength (Å)	0.71073	0.71073	0.71073	0.71073
a (Å)	9.8547(7)	13.6186(5)	13.7012(10)	7.2459(5)
b (Å)	9.3128(6)	7.5391(2)	7.7944(5)	14.6900(10)
c (Å)	12.1257(8)	13.1804(4)	13.4039(10)	12.4554(9)
α (°)	90.00	90.00	90.00	90.00
β (°)	98.164(5)	118.179(2)	119.191(3)	98.650(4)
γ (°)	90.00	90.00	119.191(3)	90.00
V (Å^3)	1101.56(13)	1192.86(7)	1249.64(15)	1310.70(16)
Z	4	4	4	4
Density/g.cm^{-3}	1.328	1.430	1.601	1.436
Abs. Coeff. /mm^{-1}	0.268	0.475	3.437	0.261
Abs. Correction	multi-scan	multi-scan	multi-scan	multi-scan
F(000)	464	536	608	592
Total reflections	1990	2142	2232	2349
Reflections, I > 2σ(I)	1525	1869	1859	1306
Max. θ/°	25.25	25.24	25.25	25.25
Ranges (h, k, l)	-11 ≤ h ≤ 11 -11 ≤ k ≤11 -14 ≤ l ≤14	-16 ≤ h ≤ 15 -9 ≤ k ≤9 -15 ≤ l ≤15	-16 ≤ h ≤ 13 -9 ≤ k ≤9 -14 ≤ l ≤16	-8 ≤ h ≤ 8 -17 ≤ k ≤17 -14 ≤ l ≤13
Complete to 2θ (%)	99.8	99.6	98.6	99.2
Data/ restrain/ parameter	1990/0/173	2142/0/ 151	2232/0/147	2349/3/213
Goof(F^2)	1.058	1.066	1.070	1.033
R indices [I > 2σ(I)]	0.0368	0.0311	0.0290	0.0547
R indices (all data)	0.0559	0.0354	0.0396	0.1063

Compound No.	**6.2a**	**6.2b**	**6.2c**	**6.2d**
Formule	$C_{16}H_{18}N_4S_2$	$C_{16}H_{18}N_4S_2$	$C_{16}H_{24}Br_2N_4O_2S_2$	$C_{16}H_{20}N_6O_6S_2$
CCDC No.	1420844	1420845	1420846	1420847
Mol. wt.	330.46	330.46	528.31	456.50
Crystal system	Monoclinic	monoclinic	Triclinic	monoclinic
Space group	*C 2/c*	*C 2/c*	$P\bar{1}$	$P\,2_1/n$
Temperature (K)	296(2)	296(2)	296(2)	296(2)
Wavelength (Å)	0.71073	0.71073	0.71073	0.71073
a (Å)	19.017(2)	16.2875(16)	7.5072(6)	7.0178(17)
b (Å)	5.1090(5)	9.6657(10)	8.4305(7)	16.125(4)
c (Å)	17.805(2)	13.4747(13)	9.1386(7)	9.208(2)
α (°)	90.00	90.00	73.216(4)	90.00
β (°)	99.507(12)	127.121(8)	85.375(5)	104.814(15)
γ (°)	90.00	90.00	74.943(5)	90.00
V (Å3)	1706.2(3)	1691.5(3)	534.72(7)	1007.4(4)
Z	4	4	1	2
Density/Mgm^{-3}	1.287	1.298	1.641	1.505
Abs. Coeff. /mm^{-1}	0.314	0.316	4.003	0.312
Abs. Correction	multi-scan	multi-scan	multi-scan	multi-scan
F(000)	696	696	266	476
Total reflections	1522	1518	1900	1812
Reflections, $I > 2\sigma(I)$	1217	1273	1593	1298
Max. θ/°	25.24	25.23	25.24	25.24
Ranges (h, k, l)	$-20 \le h \le 22$ $-6 \le k \le 6$ $-19 \le l \le 20$	$-19 \le h \le 19$ $-11 \le k \le 11$ $-14 \le l \le 16$	$-9 \le h \le 9$ $-6 \le k \le 10$ $-10 \le l \le 10$	$-7 \le h \le 8$ $-19 \le k \le 19$ $-10 \le l \le 11$
Complete to 2θ (%)	98.4	99.0	98.4	99.7
Data/ restrain/ parameter	1522/0/ 101	1518/0/101	1900/2/127	1812/0/137
Goof(F2)	1.062	1.089	1.083	1.058
R indices [$I > 2\sigma(I)$]	0.0659	0.0380	0.0303	0.0678
R indices (all data)	0.0765	0.0451	0.0386	0.0906

Compound No.	**6.2e**
Formule	$C_{16}\ H_{30}\ N_4\ O_{16}\ P_4\ S_2$
CCDC No.	1420848
Mol. wt.	722.44
Crystal system	monoclinic
Space group	*P* $2_1/c$
Temperature (K)	296(2)
Wavelength (Å)	0.71073
a (Å)	8.0722(8)
b (Å)	19.8911(19)
c (Å)	9.3871(9)
α (°)	90.00
β (°)	98.293(4)
γ (°)	90.00
V (Å3)	1491.5(3)
Z	2
Density/Mgm^{-3}	1.609
Abs. Coeff. /mm^{-1}	0.470
Abs. Correction	none
F(000)	748
Total reflections	2691
Reflections, $I > 2\sigma(I)$	2473
Max. θ/°	25.24
Ranges (h, k, l)	$-9 \leq h \leq 8$ $-23 \leq k \leq 23$ $-11 \leq l \leq 11$
Complete to 2θ (%)	99.3
Data/ restrain/ parameter	2691/15/211
Goof(F2)	1.024
R indices [$I > 2\sigma(I)$]	0.0298
R indices (all data)	0.0331

List of Publication

1) N. Phukan, J. B. Baruah, Polymorphs of 1-(5-Methylthiazol-2-yl)-3-phenylthiourea and Various Anion-Assisted Assemblies of Two Positional Isomers.
   Cryst. Growth Des., 2014, **14**, 2640.
2) N. Phukan, J. B. Baruah, Polymorphs of Thiazole-Derived Imines Connected to Hydroxyaromatics.
   Cryst. Growth Des., 2015, **15**, 1843.
3) N. Phukan, J. B. Baruah, Imine-tautomers of Aminothiazole Derivatives: Intriguing aspects of Chemical Reactivities.
   CrystEngComm, 2016, **18**, 3877.
4) N. Phukan, J. B. Baruah, Anion Guided Conformational Adjustments by Protonation Leading to Conformation Reversal.
   ChemistrySelect, 2016, **3**, 440.
5) N. Phukan, J. B. Baruah, Solvent and anion facilitated conformational changes in benzylamine substituted thiazolamine.
   New J. Chem., 2016, **40**, 6899.
6) N. Phukan, J. B. Baruah, Detection of Al^{3+} and Zn^{2+} ions by 2-(5-methylthiazol-2-yliminomethyl)phenol.
   Inorg. Chem. Comm., 2013, **37**, 89.
7) N. Phukan, J. B. Baruah, Conformational adjustments over Hydrogen bonded synthons of urea and thiourea based assemblies.
   CrystEngComm., 2016, DOI: 10.1039/C6CE01326K